EXPERIMENTAL EVALUATION OF MONOTONIC AND CYCLIC FRACTURE BEHAVIOR USING DISK-SHAPED COMPACT TENSION TEST AND RELEASED ENERGY APPROACH

BY

CHAIWAT NA CHIANGMAI

DISSERTATION

Submitted in partial fulfillment of the requirements
for the degree of Doctor of Philosophy in Civil Engineering
in the Graduate College of the
University of Illinois at Urbana-Champaign, 2014

Urbana, Illinois

Doctoral Committee:
Professor William G. Buttlar, Chair
Professor Imad L. Al-Qadi
Professor Marshall R. Thompson
Associate Professor Eshan V. Dave

Abstract

This thesis involves the evaluation of fracture behavior of asphalt concrete under monotonic and cyclic loading using the disk-shaped compact tension (DC(T)) test and a released-energy based approach. The standard DC(T) test was revised to facilitate both monotonic and cyclic loading tests, including some modifications of the test geometry and testing modes. The research was motivated to explore possible extensions of the DC(T) test device to consider cyclic fracture phenomena such as cyclic thermal cracking, block cracking and reflective cracking. Five different asphalt concrete mixtures were tested for both loading mechanisms across four test temperatures (-12, 0, 10, and 20^{o}C). After an extensive exploratory stage, the load-controlled testing mode utilizing a sine waveform and a frequency of 0.5 Hz with no rest period were selected as the main testing parameters for this study. In addition, peak load obtained from the monotonic DC(T) test was used as a reference value for determining loading magnitudes of the cyclic DC(T) test for a given mixture and test temperature. For data analysis, the released energy approach was introduced as a key concept to characterize the cyclic fracture data generated in this study. Stemming from this approach, a released energy rate parameter, R2, was identified with the characteristic of mixture and temperature independence. By correlating a fracture energy parameter (G_f) to released energy rate (R2), cyclic loading behavior could be predicted based upon three different data sets deriving from the DC(T) test: one involving a comprehensive cyclic loading testing suite; a slightly simpler method involving a limited number of required cyclic tests, and; a highly simplified approach where cyclic fracture behavior was predicted form monotonic fracture test results alone (standard DC(T) fracture energy). All three prediction methods were shown to be plausible, but as expected, the more rigorous the testing suite, the more accurate the prediction. Furthermore, monotonic and cyclic fracture behaviors were monitored using a webcam-based imaging technique to investigate fracture processes at a macro-scale level. As a result, each stage of cracking, including crack initiation and crack propagation, could be potentially predicted based on the cyclic test data through a relation of the crack initiation to number of cycles to a failure and crack propagation ratios, respectively.

Table of Contents

Chapter 1 Introduction

Pavement cracking continues to be a critical challenge in pavement engineering, particularly as higher recycling rates of materials containing aged/oxidized asphalt products are being motivated by the desire increase pavement sustainability. Numerous studies have been conducted to evaluate fracture mechanisms of asphalt concrete (AC) pavements by Schapery (1975), Majidzadeh et al. (1971), Van Dijk and Chomton (1972), Monismith et al. (1973), Kim and Buttlar (2002), Shen and Carpenter (2006), Wagoner and Buttlar (2006). In these studies, several prevalent types of pavement cracking are often described, including, reflective cracking, fatigue cracking, thermal cracking, and block cracking,. These fracture mechanisms were influenced by many factors, such as type of material, pavement structure and layer bonding condition, environmental conditions, and loading history. Based upon effects of loading, fracture can be generated by single heavy loading, such as an aircraft on a runways where an asphalt overlay is placed over a PCC pavement with low load transfer efficiency, or by repeated loading from vehicles on roadways. Effects of loading have been simulated in the laboratory, for example, using monotonic and cyclic loading tests, to study underlying fracture mechanisms. Therefore, to gain better understanding of the fracture mechanisms, this study was primarily conducted experimentation on both monotonic and cyclic loading to evaluate fracture mechanisms of modern asphalt concrete mixtures.

1.1 Fracture mechanism of asphalt concrete pavement

In flexible pavements, different types of cracking have been signified by a specific mechanism occurring within a pavement structure, for instance, reflective cracking within overlay pavements, a new layer of hot mix asphalt (HMA) paved on top of an existing pavement, which is commonly placed on Portland cement concrete (PCC) slabs. The overlay was very popular and extensively used because it saved construction time and money, while improving pavement surface characteristics and profile and possibility increasing load carrying capacity. However, a major deficiency in these systems stems from the fact that a crack can be initiated in the overlay layer and reflected through to the new surface of the HMA layer; hence referred to as ‘reflective cracking’. Another example of a major cracking form in AC pavements is fatigue cracking. This fracture mechanism sometimes arises when a pavement is subjected to repeated loading from vehicles, while material properties change with age, leading to the damage accumulation which is generally

attributed to fatigue. Wheel path cracking patterns result from this form of pavement deterioration. These two examples of fracture in asphalt pavement layers are related to repeated loading; therefore, it was deemed important to study intrinsic fracture behavior in asphalt under cyclic loading.

Several tests were used to evaluate fracture behavior of asphalt concrete (AC) mixes. Regarding loading application, both monotonic and cyclic loading tests can be used to evaluate fracture mechanisms. In early studies, in an attempt to physically portray field loading conditions, a flexural beam test was most commonly used to study cyclic loading behavior of AC mixes. However, this test had the disadvantages of requiring large specimens, time consuming, and highly variable. Alternatively, a monotonic loading test can also be utilized to evaluate fracture behaviors of AC materials. However, monotonic loading does not directly simulate repeated loading behavior; therefore, the burden of proof remains to evaluate is this simpler and more repeatable testing can be used to reliably predict fracture mechanisms. Regardless of loading type, the stages of fracture to consider in any test and/or modeling system include crack nucleation, initiation, propagation, and ultimate failure. Although all of these stages are generally present in both monotonic and cyclic fracture tests, the fracture processes associated with these stages under different loading forms is an open question and an important consideration when linking monotonic and cyclic fracture tests.

Many approaches were proposed to analyze fracture behavior of the AC mixes. Concepts involving released energy (i.e., energy release rate) have been extensively employed to study cracking behavior in asphalt concrete materials. This approach was employed to evaluate material performance of both monotonic and cyclic loading tests. For the monotonic loading test, the released energy was represented by an area surrounded by a unique plot of the load-displacement curve divided by a fracture area, defined as fracture energy (Hillerborg et al., 1976). Conversely, for a cyclic loading test, energy-based approaches examine how material properties change or degrade under cyclic loading (Van Dijk, 1972). More details of the released energy approach were provided in the literature review (Chapter 2).

In this study, a modified DC(T) test geometry and released-energy based approach for data analysis were developed as a step towards a better understanding of this important phenomenon. Additionally, to provide a deeper understanding of the fracture mechanisms under both loading mechanisms, cracking processes of crack initiation and crack

propagation were investigated at the macro-scale using a digital imaging technique. Further details of the study are provided in the following sections and chapters.

1.2 Problem statement

Cracking mechanisms in asphalt concrete pavements is an important research topic for pavement engineers, as better understanding of the underlying mechanism can aid in improving material and pavement system designs. Regarding current tests and analytical approaches, several failure criteria have been introduced to evaluate fracture behaviors in AC mixtures, such as those used in traditional stress or strain-based fatigue tests, those developed in fracture-mechanics-based approaches, and those used in dissipated energy-based approaches; however, these approaches have been typically focused on a particular stage of fracture.

Regarding cyclic loading testing, a flexural bending beam test is the most reliable and extensively used to evaluate fatigue cracking or cyclic fracture behavior. However, some disadvantages of the test are found, such as

(1) It requires a significant amount of materials and time to complete an evaluation of the cyclic loading behavior,

(2) A beam geometry is very difficult to extract from the field,

(3) Potential damage could occur at where a test specimen was clamped because of viscoelastic material response, especially at intermediate to high test temperatures. This makes interpretation of test results difficult.

Test configurations, which have been typically used to perform monotonic fracture tests, for example, disk-shaped compact tension (DC(T)), semi-circular beam (SC(B)), and fenix test, as shown in Figure 1.1, have also been employed to study fracture mechanisms of the AC under cyclic loading. These tests are more convenient than the flexural beam fatigue tests, as they utilize specimens that can be obtained from cylindrical geometries, such as lab-compacted specimens and field cores.

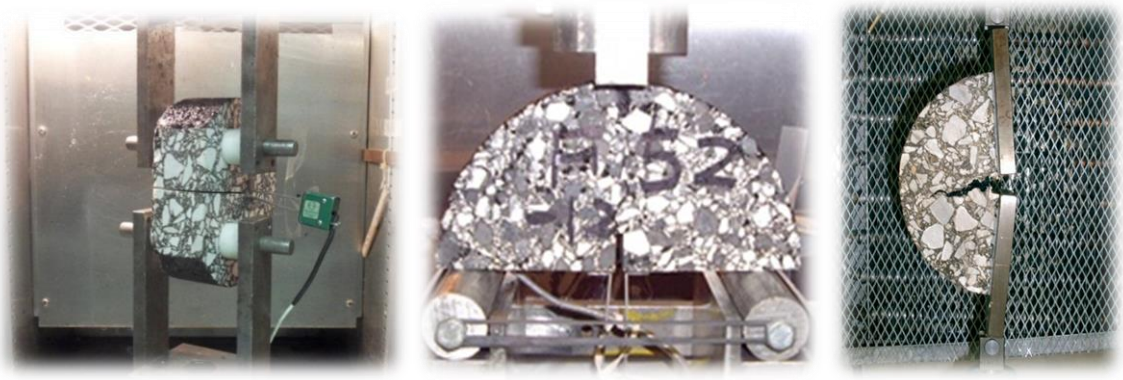

Figure 1.1 DC(T) test (left), SC(B) test (middle), and fenix test (right).

Although these tests have proven to be convenient, some drawbacks with regards to cycling fracture testing were identified at the onset of this study:

(1) The SC(B) configuration can only be loaded in one direction (load cannot be reversed). As a result, creep damage is mixed with damage and fracture,

(2) Stress distribution within the fenix test is influenced by the presence of the loading platens, which creates a fairly uniform tensile field ahead of the crack tip and more abrupt/unstable failure once the crack propagates.

(3) The standard DC(T) geometry was not designed to handle repeated loading, resulting in potential breakage at the loading holes. In addition, measurement of the material separation at the CMOD location may not be ideal for the closed-loop control variable in cyclic fracture testing, especially at intermediate to high test temperatures due to compliance effects. Further details are provided in chapter 3.

In terms of analytical approaches for data interpretation, for traditional or phenomenological fatigue approaches, some issues were found:

(1) In the case of the strain-controlled mode, the fatigue criterion was arbitrarily defined as a 50-percent reduction in stiffness because a true failure or rupture of the material rarely existed under typical strain-controlled testing [Pell (1967), Monismith et al. (1964), Ramsamooj (1991) and Ghuzlan and Carpenter (2000)]. The dissipated or released energy-based concept to describe fracture behaviors of AC mixes has evolved steadily over time, for instance as described by Chomton (1972) and Van Dijk (1975). The released energy approach provided a seemingly more fundamental approach to understanding material degradation under cyclic loading by evaluating energy parameters extracted from the load-displacement or stress-strain relationship. Recently, Carpenter and his colleagures [Carpenter, S. H., and M. Jansen (1997), Ghuzlan, K., and Carpenter, S.H. (2000), and

Shen, S., and Carpenter, S. H. (2005)] employed this released energy approach by introducing a ratio change of the dissipated energy (RCDE) and a plateau value (PV) as a new fatigue criterion to evaluate cyclic fracture behaviors of the AC mixes. However, some problems were reported by Na chiangmai (2010) and Kim et al. (2004), with respect to variability associated with test precision combined with the small numerical value associated with the plateau value (in the range of 10^{-5} to 10^{-30} (Carpenter et al, 2007).

(3) A computation of the PV values remained based on a number of cycles to failure of the traditional fatigue approach as arbitrarily defined by a 50-percent reduction in stiffness (N_{f50}), which did not represent an intrinsic fracture mechanism of the materials.

Other approaches have been introduced to study fatigue and fracture behavior in asphalt mixtures by Majidzadeh et al. (1971) and Birgisson and Roque (2002); some based on complex, continuum-damage-mechanics based approaches by Kim et al. (1997 and 2004) and Kutay (2011). However, the aforementioned approaches were not directed at studying cyclic fracture behaviors such as those present in reflective cracking at studying cyclic thermal cracking phenomena, which is the subject of this investigation.

1.3 Objectives of study

Objectives of the study are follows:

(1) To conduct experimentation on both monotonic and cyclic loading tests using the disk-shaped compacted tension (DC(T)) configuration for evaluating fracture behaviors of both loading mechanisms.

(2) To evaluate monotonic fracture behavior at intermediate test temperatures of 10^{o}C and 20^{o}C, as well as different loading rates for different types of AC mixtures,

(3) To examine a new cyclic fracture criterion by employing a released-energy based approach,

(4) To determine a correlation between monotonic and cyclic fracture mechanisms through a potential relationship among their released energy parameters,

(5) To construct prediction models of cyclic loading behavior for three different scenarios: (1) using a full suite of cyclic DC(T) tests; (2) using monotonic plus several cyclic DC(T) tests, or; (3) using monotonic DC(T) test results alone.

(6) To investigate the fracture processes of crack initiation and crack propagation at a macro-scale level using an inexpensive digital imaging technique.

In order to accomplish the objectives, the following tasks were developed:

(1) The disk-shaped compact tension (DC(T)) test geometry was used to evaluate fracture behaviors of the AC mixtures under monotonic loading. However, the standard DC(T) geometry had to be modified because of potential breakage at loading holes under repeated loading.

(2) To enable cyclic loading, standard test procedures for the DC(T) were modified. Cyclic loading test parameters, such as mode of loading, waveform, and magnitude of loading, were considered in this study.

(3) The current released energy criteria approaches represented only a particular stage in the entire cyclic loading mechanism. For example, plateau value (PV) of ratio of dissipated energy change (RDEC) was defined as a value corresponding to a specific number of cycles where an initial stiffness decreased by 50%. Therefore, a new cyclic fracture criterion was developed using a released energy-based concept. Then, relationships between monotonic and cyclic loading test results were investigated. Prediction of cyclic loading behavior was undertaken by developing analytical relationships using data sets including a full suite of cyclic DC(T) tests, a limited number of cyclic test results, and monotonic DC(T) test results alone.

(4) Fracture processes of crack initiation and propagation at the macro-scale level was monitored using the webcam. This was pursued to provide better understanding of the cracking process and an estimate of crack length during cyclic loading using an inexpensive measurement system.

1.4 Organization of Dissertation

This dissertation is composed of six chapters. Motivation, problem statement, and objectives were provided in this introductory chapter. Chapter 2 recalls historical studies and important concepts used to evaluate both monotonic and cyclic fracture testing of asphalt concrete. Then, Chapter 3 and 4 provide experimental evaluations and test results for monotonically and cyclic fracture testing campaigns, respectively. The development of predictive systems to relate monotonic and cyclic fracture behavior were investigated in Chapter 5. Finally, summary, conclusions, and recommendations derived from this study are provided in Chapter 6.

Chapter 2 Literature Review

Fracture mechanisms of asphalt concrete (AC) materials can be evaluated under both monotonic and cyclic testing. Regardless of loading type mechanisms, similar fracture processes of crack initiation, crack propagation, and failure are observed. In order to develop an appropriate framework and starting point for the study, historical works on fracture mechanics and mechanisms of the AC materials were reviewed, as summarized in this chapter. Monotonic fracture tests are first reviewed, followed by cyclic fatigue and fracture studies.

2.1 Studies of monotonic fracture behavior

In the early 1900's, testing under monotonic loading was the simplest approach to evaluate fracture mechanisms in materials and structures. A theory of classic fracture mechanics was introduced to solve complex fracture problems which were simplified into three local fracture modes: Mode I (tensile opening), Mode II (in-plane shearing), and Mode III (anti-plane shearing). Based upon application of fracture mechanics to AC materials, two primary concepts were used to characterize fracture behaviors, including linear elastic fracture mechanics and viscoelastic fracture mechanics.

2.1.1 Application of linear elastic fracture mechanics

Linear elastic fracture mechanics (LEFM) was extensively used to describe fracture problems for many materials because analysis was relatively simple. According to the concept of the LEFM, two approaches were proposed to solve fracture problems, including energy-based and stress intensity factor (SIF) approaches. Interestingly, solutions of both approaches were proven to be equivalent (Irwin, 1957).

Energy-based Approach

Griffith (1920) introduced an energy concept based upon the first law of thermodynamics: "When a system goes from non-equilibrium to equilibrium, there is a net decrease in energy." He proposed energy balance for an incremental increase of the crack area, dA, under an equilibrium condition which was derived as

$$\frac{dE}{dA} = \frac{d\prod}{dA} + \frac{dW_s}{dA} = 0$$

where E is total energy, $\prod$ is potential energy supplied by the internal strain energy and external forces, and W_s is work required to create new surfaces. Regarding to the

expression, the potential energy must be greater than required energy in order to create a new surface. Such an increase of energy was transferred to a vicinity of a crack tip, where the stress concentration greatly presented in order to maintain a balance of the energy.

Irwin (1956) extended Griffith's energy balance concept to simplify fracture problems. An energy release rate (*G)* was a rate of change in potential energy within a crack area. The potential energy was composed of the crack driving force or strain energy and the external force (Anderson, 1995). The energy release rate was defined as

$$G = \frac{-d\Pi}{dA} = \frac{-d(U-F)}{dA}$$

where *U* is the strain energy stored in the body and *F* is the work done by the external force.

For experimentation, two different modes of loading: fixed load and fixed displacement could be used to determine released energy rate. In case of the fixed load, the energy release rate was consisted of strain energy and work done by external forces that the displacement increased by the material compliance. On the other hand, the energy release rate was only induced by strain energy in case of the fixed displacement because the external work did not exist as the displacement was fixed. A released energy of both tests are graphically presented in Figure 2.1.

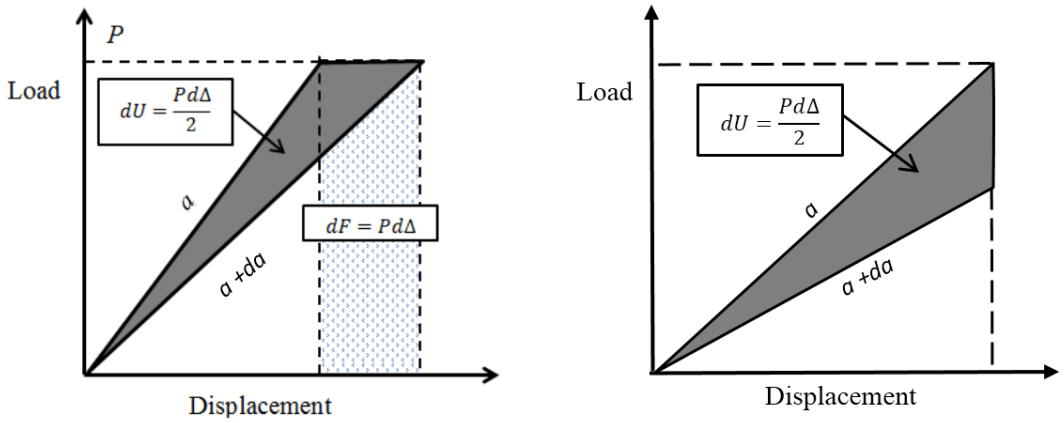

(a) fixed load (b) fixed displacement

Figure 2.1 Load-displacement relations of LEFM energy approach (Irwin, 1956).

Stress-based approach

Intuitively, a crack was typically formed in the area of concentrated stress, for example, adjacent to a void or fabricated hole in a solid. According to Westergaard's study (1939), there was an attempt to compute stress and strain distributions near a crack tip. However, the problem was very complicated to solve because of the many variables in the three-dimensional (3D) analysis. Thus, some assumptions were made to simplify the

analysis, for example, a material was assumed to be an isotropic linear elastic behavior, and the analysis was also done on a two-dimensional (2D) basis. Irwin (1952) used the Westergaard's approach to show that stresses and displacements ahead of the mathematically shaped crack were described by a single constant of the stress intensity factor (SIF). Based on asymptotic solutions, each stress component was proportional to a single constant (K) as

$$\sigma_{ij} = \frac{K}{\sqrt{2\pi r}} f_{ij}(\theta) + Higher\ order\ terms\ (H.O.T.)$$

Based on the equation, stresses were proportional to $1/\sqrt{r}$, regardless of specimen geometries which were denoted by a term of $f_{ij}(\theta)$. As the r value became zero, a value of stress was infinity that the stress was singularity at the crack tip. Interestingly, the SIF was a very powerful fracture parameter to solve fracture problems because if such a constant K was known, stresses and strains at any other locations on an object could be determined. Also, a fracture criterion of the crack initiation was defined as the K value was greater than the critical stress intensity factor (K_{IC}) or toughness of the materials.

However, both approaches of the LFEM were not suitable to analyze fracture problems of the AC materials because the AC exhibited the nonlinearly viscoelastic behavior. Moreover, the mix was heterogeneous, composing of two different materials of asphalt binder and aggregates, and the K-field dominance of LEFM barely existed since a plastic zone and fracture process zone were relatively large.

2.1.2 Application of viscoelastic fracture mechanics

Because of nonlinear behavior of AC materials, application of the LEFM might not be appropriate to evaluate fracture behaviors of the AC. As a result, both linear energy release rate, G and stress intensity factor, *K*, approaches were invalid for such a nonlinearly time-dependent material.

The J-Integral approach

The J-integral by J. Rice (1968) was successfully used to characterize nonlinear elastic and elastic-plastic materials. According to Rice's work, nonlinear energy release rate was derived as a path-independent integral of the closed boundary in an object under an equilibrium condition. By considering an arbitrary counterclockwise path (Γ) as presented in Figure 2.2 around a crack tip, the *J* integral was given as

$$J_i = \int_{\Gamma}(wdy - T_i \frac{du_i}{dx} ds) = 0$$

where w is strain energy density which is defined as $w = \int_0^{\varepsilon_{ij}} \sigma_{ij} d\varepsilon_{ij}$, T_i is components of traction vectors which is given by $T_i = \sigma_{ij} n_j$, u_i is displacement vector components, and ds is length increment along the contour Γ. He proved that the J-integral was equal to zero in any closed-loop boundaries because the traction term was derived to be identical to a term of the strain energy of the energy-balanced concept.

Furthermore, the released energy concept of LEFM was used to obtain energy released in nonlinear materials, replacing linear energy release rate (G) by the J term as

$$J = -\frac{d\Pi}{dA} = -\frac{d(U - F)}{dA}$$

where Π is the potential energy, U is the strain energy stored in the body, F is the work done by external forces, and A is the crack area as showed in Figure 2.2. Moreover, Rice proved that the nonlinear released energy expression was identical to a solution of the J-integral.

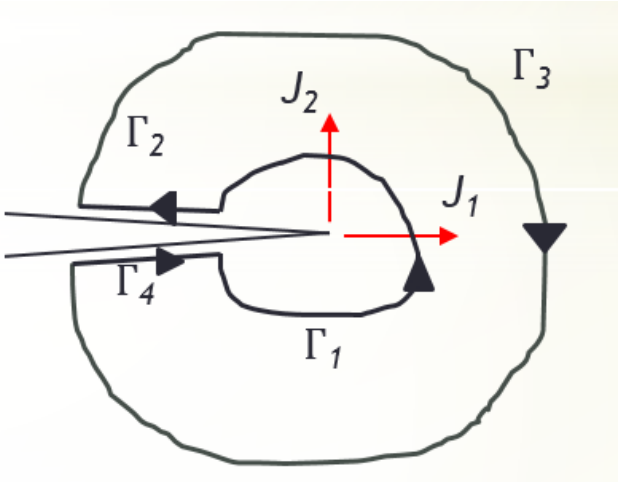

Figure 2.2 Integration path of J-integral definition (Rice, 1968).

An analysis of the fracture mechanics for AC materials was more complicated than linear elastic fracture mechanics due to a non-linear behavior of the material, which was claimed to be either viscoelastic or visco-elastic-plastic behavior. Consequently, fracture mechanics theories of the nonlinear behavior were relatively new, and also practical applications were scarcely available. Nevertheless, Schapery (1975) completed the most theoretical works on viscoelastic fracture mechanics of the AC materials. He employed the J-integral to the viscoelastic problems and assumed that a non-linear viscoelastic constitutive equation was in a form of the hereditary integral as

$$\varepsilon(t) = E_R \int_0^t D(t - \tau, t) \frac{d\varepsilon_{ij}^e(\tau)}{d\tau} d\tau$$

where pseudo-elastic strain (ε_{ij}^e) is related to stress through linear or nonlinear elastic constitutive laws. This pseudo strain was used to convert a viscoelastic to elastic problem using correspondence principle. Therefore, a generalized time-dependent *J* integral of the non-linear elastic materials is

$$J_v = \int_\Gamma (w^e dy - T_i \frac{du_i^e}{dx} ds)$$

where w^e is pseudo-strain energy density, and a material behaves with steady-state creep at $t > t_o$. The displacement or strain is replaced by $\varepsilon_{ij}^e = \dot{\varepsilon}_{ij}$.

Disadvantages of the *J*-integral approach were found that a J_{22} term, which was perpendicular to a direction of the crack-tip orientation as illustrated in Figure 2.2, was assumed to be zero, but the J22 was non-zero for heterogeneous materials. As a result, the total J integral was composed of the J_{11} and J_{22} terms. Also, regarding to a definition of the J-integral, it was supposed to be assumed that no frictions presented on crack lips, so-called traction free. However, an effect of bridging stress and crack shielding behind the crack tip of the AC materials was predominated which the traction of the crack lips were not negligible. Moreover, some analytical assumptions were violated, for instance, the mathematically shaped crack barely existed in experimentation because a notch tip of the test sample was typically bunted. Also, crack path was not straight and branch cracking was observed.

Fracture energy approach

Regarding to the monotonic loading test, a unique load-displacement response of quasi-brittle materials, such as Portland cement concrete (PCC) and the AC mixtures, was found after peak load was reached, known as a softening behavior, as illustrated in Figure 2.3. The softening behavior was used to explain the ability of a material to carry loading after reaching peak load, based upon aggregate interlocking and viscoelastic properties of the bituminous material.

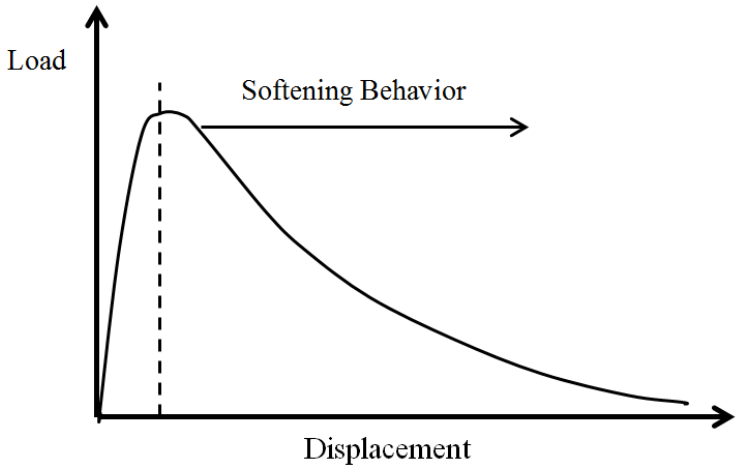

Figure 2.3 Load-displacement curve of quasi-brittle material (Bazant and Planas, 1998).

Hillerborg and his colleagues (1976) introduced fracture energy to describe the softening behavior of the quasi-brittle materials. By the definition, fracture energy described the required energy per unit area to complete fracture processes of crack initiation, crack propagation, and failure, which was mathematically defined as an area surrounding the load-displacement curve divided by a fracture area as

$$G_f = \frac{A_f}{BL}$$

where G_f is fracture energy (J/m^2), A_f is an area under load-displacement curve, B is a thickness of a test specimen, and L is a ligament length of a test specimen.

Wagoner and Buttlar (2006) developed a disk-shaped compact tension (DC(T)) test to determine fracture energy for AC mixtures to evaluate low temperature cracking. According to their study, fracture energy was depended on type of mixtures, test temperatures, loading rates, and specimen geometries. The DC(T) test and the concept of fracture energy provided an alternative to describe fracture behaviors of the AC. Practically, the DC(T) test is one of the simplest tools to examine fracture properties of AC materials. Therefore, this particular study proposed to employ the DC(T) configuration to perform a monotonic loading test, as well as a cyclic loading test. In-depth details of the research, including a revision of the standard DC(T) test, analytical procedures, and test results of both loading mechanisms, were provided in the following chapters.

2.2 Studies of cyclic fracture behavior

In reality, pavements are predominately subjected to repeated loading from vehicles and temperature cycles. As a result, performance of the pavements are dictated by such

repeated loading. Regarding to a deterioration of the AC pavements, reflective cracking and fatigue cracking were two major failures driven by the repeated loading. In term of experimentation, a cyclic loading test was promised to be the closest test setup to simulate repeated loading happening in the field. Considerable studies were conducted to evaluate these two major fracture mechanisms. Consequently, following sections provided a summary of historical works of the cyclically-loaded fracture studies of the AC materials.

2.2.1 Reflective cracking mechanism and laboratory evaluation

In the late 1900's, rehabilitation of deteriorated pavements was considered because of economic concerns. One of the efficient techniques to rejuvenate a pavement structure was to place an AC layer on top of an existing layer, such as Portland concrete cement (PCC) or AC layer, which was known as an overlay. The overlay improved structural capacity and waterproofing benefits, and also it was cost-effective and required less time for lane closures. However, a classic problem of the overlay was when a crack in an existing layer subjected to severe loading from loading of vehicles and temperature variations, the crack initiated and propagated as a reflection on the new surface of the HMA overlay, so called reflective cracking.

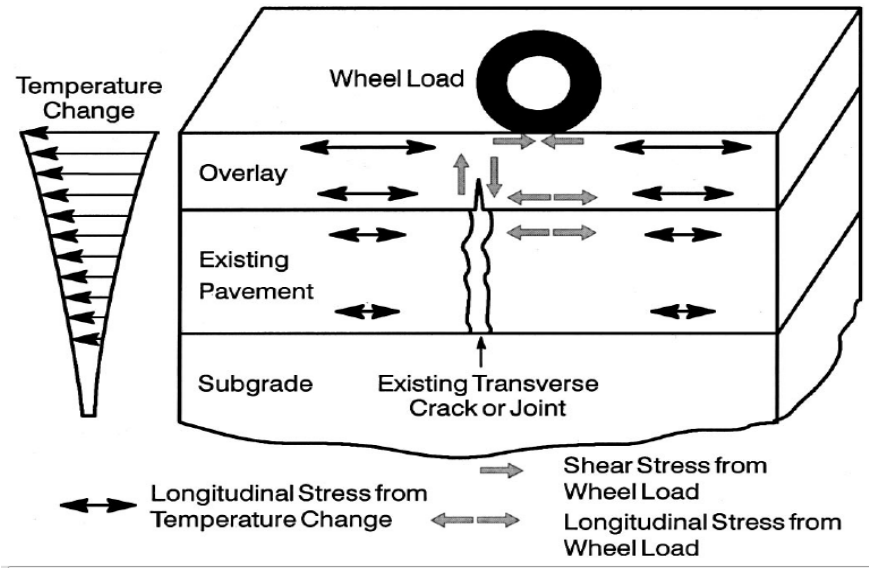

Figure 2.4 Reflective cracking mechanism (Kim and Buttlar 2002).

Nunn (1989) identified two major driving forces causing reflective cracking: thermal expansion and contraction due to temperature variations, and vertical and horizontal movements due to traffic loading as illustrated in Figure 2.4. The first driving force involved to daily temperature variations resulting thermal expansions and contractions. This phenomenon was almost exclusively linked to an opening mechanism of

the pure mode I cracking. The other driving force was an applied loading from vehicles resulted in bending of the discontinuous PCC slabs and contributed to high stress and strain levels in the overlay structure. If the stress state exceeded the fracture resistance, a crack initiated and propagated into the new layer. Especially, during the winter, a magnitude of both traffic and thermal loading stresses was significantly high because the AC material became stiffer and more brittle at lower temperatures.

Many test devices were invented to evaluate the reflective cracking mechanism. Figure 2.5 shows small Texas overlay tester introduced by Zhon et al (2003) which was the most extensively used to study reflective cracking in a laboratory. A test sample was applied cyclic loading along with other test variables, such as test frequencies, test temperatures, magnitudes of loading, and mode of loading, either load-controlled or displacement-controlled. Regarding to test results, a number of cycles to failure (N_f) was typically used to indicate an allowable number of cycles for the pavement service life. However, drawbacks of the test was that special equipment was used to extract a rectangular shape of a test specimen from the field, and a large amount of material required to produce a specimen in a laboratory. Moreover, the test device was relatively expensive and only used for this particular purpose of testing. In another word, the test device could not be utilized to perform other tests.

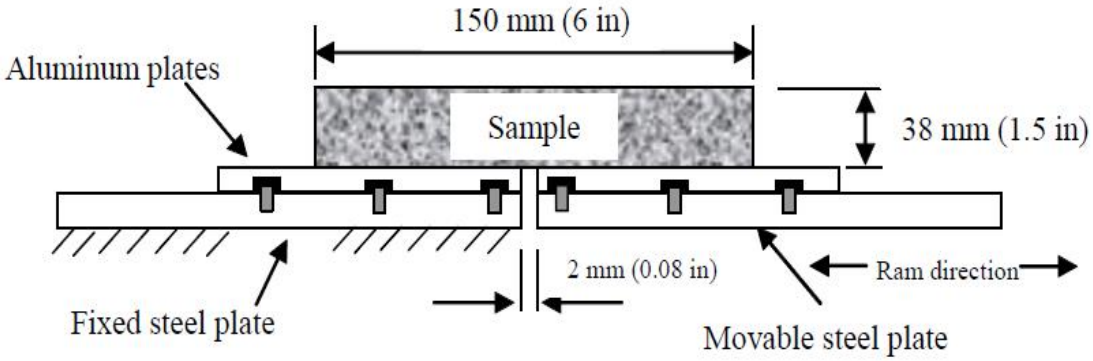

Figure 2.5 Small Texas Overlay Tester (Zhou et al, 2003).

2.2.2 Fatigue cracking mechanism and analytical approach

In transportation engineering, the study of fatigue was first noticed, regarding to a railway accident, reported in The Times of London on May 11, 1843. Wohler (1860) conducted a systematic investigation to examine strength, bending, torsion, and axial loading of steel railway axles that subjected to cyclic loading on a full-scale railway test.

According to his study, the stress amplitude to fatigue life was introduced to characterize fatigue of railway axles, known as Wohler's S-N curve (Figure 2.6).

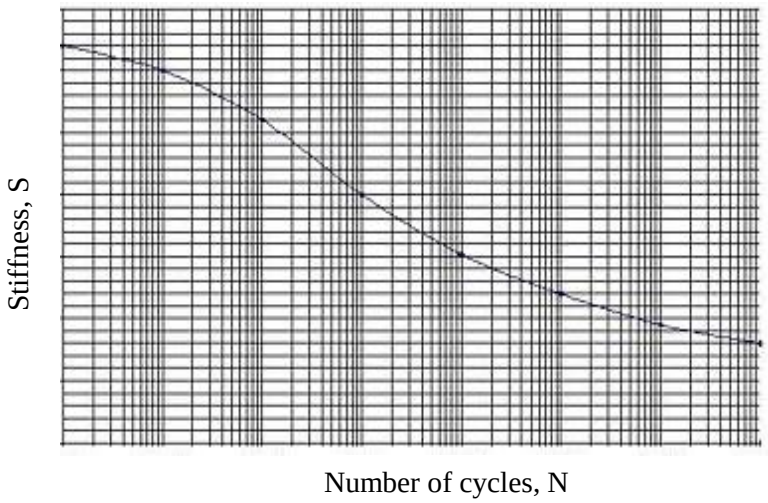

Figure 2.6 Stiffness and number of cycle relation as S-N curve (Wohler, 1860).

In the United States, fatigue of the AC pavements was recognized by Hveem and Carmany (1948). The fatigue mechanism was explained by when a pavement subjected to repeated loading from vehicles, material properties were degraded, leading to an accumulation of damages within a pavement structure. Eventually, a crack formed due to lack of load carrying capacity. The fracture process was mainly divided into three stages of crack initiation, crack propagation, and failure. Suresh (1990) explained that crack initiation started at the micro-scale level, which it was very difficult to characterize each state of the cracking process. Stress distribution of this stage was extremely small and it was difficult to distinguish between the stages of crack initiation and propagation. Typically, crack propagation started when small cracks became larger and connected to other cracks nearby. Finally, pavement was terminated as the end of the service life.

Many analytical approaches were proposed to evaluate fatigue behaviors of the AC mixtures. The followings presented some approaches that were extensively used to evaluate cyclic fracture behavior of the AC mixes, including traditional approach, fracture mechanics approach, and energy-based approach.

Traditional approach

The traditional approach was first introduced by Wohler (1860) based on the fatal railway incident. Two cyclic loading applications were involved in this empirical study. First, high-cyclic fatigue (HCF) test, where the low-amplitude cyclic stresses primarily induced to elastic deformations, was designed for longer life. Second, low-cycle fatigue

(LCF), where high-amplitude cyclic stresses were concentrated, was typically applied to consider plastic deformations. The traditional approach was employed by Pell (1967) to represent a relation of stress or strain to a number of cycles to failure occurring within the AC materials as presented by

$$N_f = a(\frac{1}{\varepsilon_t})^b \quad \text{or} \quad N_f = c(\frac{1}{\sigma_t})^d$$

where N_f is a total number of cycles to failure. ε_t and σ_t are magnitudes of tensile strain and stress respectively, and *a, b, c, d* are material coefficients obtained from a laboratory test. Monismith et al. (1985) claimed that not only repeatedly applied stress or strain, but also stiffness of mixtures did influence to fatigue life. As a result, a stiffness term was added to the equation as

$$N_f = a\left(\frac{1}{\varepsilon_t}\right)^b \left(\frac{1}{S}\right)^c$$

where S is mixture stiffness, and a, b, c are material coefficients.

Because of a simplicity of the analysis, this approach has been extensively used up to the present. However, this model did not represent a true cyclic loading mechanism from a damage accumulation point of view. Ghuzlan and Carpenter (2003) presented that such a relation of strain and fatigue life was not exhibit linearly at low strain levels. Moreover, the traditional approach did not account for complex mechanisms, such as stress redistributions and healing effects.

Fracture mechanics approach

Fracture mechanics was employed to study fatigue cracking in metallic materials by Paris, Gomez and Anderson (1961). They introduced empirical crack growth law ($\frac{da}{dN}$) to characterize a crack propagation stage, related to a number of cycle at different stages of cracking in a conjunction with linear elastic fracture parameter of the stress intensity factor (K) as illustrated in Figure 2.7, known as Paris's law as

$$\frac{da}{dN} = C(\Delta K)^m$$

where $\frac{da}{dN}$ is a rate of crack growth, a is the crack length, N is the number of load replications, ΔK is a range of the stress intensity factor defined as, $\Delta K = K_{max} - K_{min}$, where K_{max} and K_{min}, are the maximum and minimum stress intensity factors corresponding

to maximum and minimum loading, respectively, and *C* and *m* are empirical constants of a material, mode of loading, test frequencies, and test temperatures.

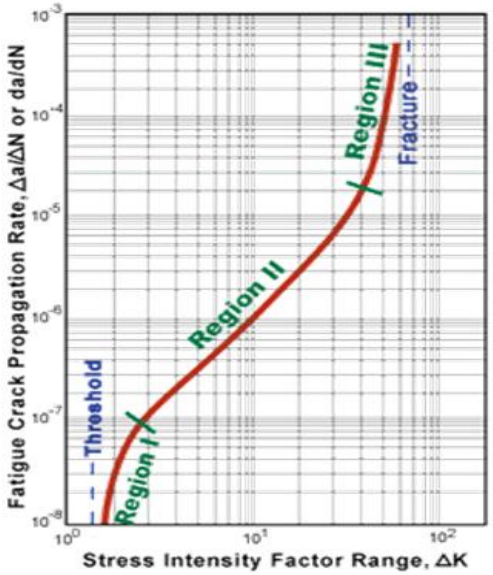

Figure 2.7 Crack propagation model of Paris' law (1961).

This concept was extended to pavement engineering by Majidzadeh et al. (1971), and Monismith et al. (1973). They used the Paris's law to predict crack growth of fatigue cracking in AC mixes. Based upon cracking stages (Figure 2.7), it was assumed that the second phase of the stable cracking occupied most of the fatigue life. Moreover, the size of plastic zone around a crack tip was crucial in the analysis during the crack propagation phase. If the plastic zone was relatively small compared to the crack size, the LEFM was valid. However, for the AC materials, an application of stress intensity factor (K) was invalid because of nonlinear material behaviors of the AC mixes, which the *K* field was greatly influenced by a large size of the plastic zone, especially at high temperatures.

In 2009, the J-integral concept of the classic fracture mechanics, which was used to account for nonlinear behaviors, was introduced to characterize the crack propagation of fatigue mechanisms of the AC mixes by Kuai et al as

$$\frac{da}{dN} = A(\Delta J)^m$$

where ΔJ is a range of the path-independent J-integral, *a* is the crack length, *A* and m are a material constant, and *N* is a number of cycles at crack length, a. However, a crack growth rate of the da/dN was relatively difficult to extract from the cyclic loading test because a crack path was not straight and branch cracking existed. Moreover, the J definition was strictly assumed to be valid for the outset of crack growth.

Released or dissipated energy approach

An idea behind this concept was when a material subjected to loading, the material was induced to deformation. If the applied load was removed, the deformation was supposed to be fully recovered. However, if not, it was assumed to be a damage created by a source of the released energy within the material. This phenomenon was graphically presented by a stress-strain plot, as shown in Figure 2.8. Energy lost or the released energy was defined by an area surrounded by a loaded-unloaded path, which was also called a hysteresis loop, as described by

$$DE_i = \pi \sigma_i \varepsilon_i \sin \emptyset_i$$

where DE_i is dissipated energy at loading cycle i, σ_i and ε_i are stress and strain amplitude at load cycle i, respectively, and $\emptyset_i$ is phase angle between stress and strain wave signals.

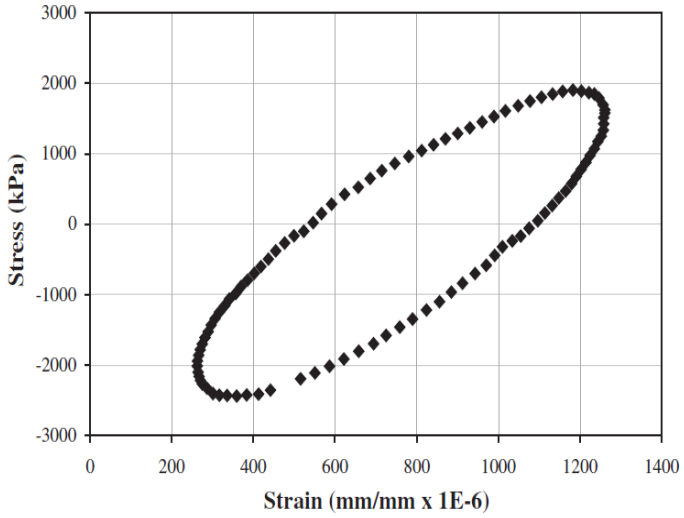

Figure 2.8 Hysteresis loop of AC mix (Ghuzlan, 2000).

Regarding to the released energy-based concept, three different approaches were introduced to characterize cyclic loading behaviors of the AC mixtures, including Initial Dissipated Energy (IDE), Total Dissipated Energy (TDE), and Ratio of Dissipated Energy Change (RDEC).

(1) Initial dissipated energy (IDE) approach was to relate a total number of cycles to failure (N_f) and dissipated energy (DE) at an initial stage of loading cycles, which was defined by an occurrence of the 50th cycle in cyclic loading mechanisms (Rowe, 1993, and SHRP, 1994). Such a relation was presented by

$$N_f = 6.72e^{0.049(VFB)}(W_o)^{-2.047}$$

where N_f is fatigue life, *VFB* is percentage of voids filled with bitumen, and W_o is initial dissipated energy. However, a major disadvantage of the IDE approach was that an initial DE did not truly represent an entire cyclic loading mechanism and other complexities, such as crack growth and healing effect.

(2) Total dissipated energy (TDE) was defined as a summation of all dissipated energy within a material, associating to a total number of cycles to failure. As a result, a unique relation between a total number of cycles to failure (N_f) and TDE was found by SHRP (1944), Van Dijk and Chomton (1972), and Tayebali et al (1992) as

$$N_f = a(TDE)^b$$

where TDE is total dissipated energy (J/m^2), and a and b mixture constants. However, similar to IDE approach, the TDE approach did not represent the entire loading mechanism.

(3) Ratio of Dissipated Energy Change (RDEC) was introduced by Shen and Carpenter (2006). The RDEC was defined by

$$RDEC_a = \frac{DE_a - DE_b}{DE_a(b-a)}$$

where $RDEC_a$ is a ratio of dissipated energy change at cycle a, compared with the next cycle b, and DE_a and DE_b are dissipated energy in load cycle a and b, respectively.

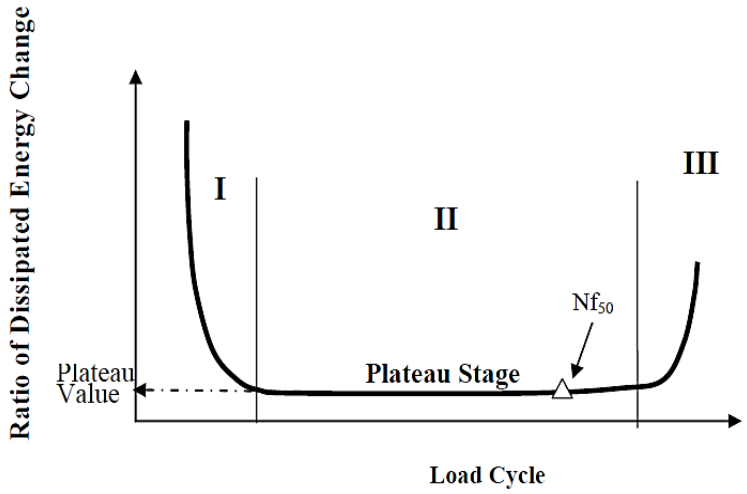

Figure 2.9 Schematic plot of RDEC versus Load Cycle (Shen and Carpenter, 2006).

By plotting the RDEC against a number of loading cycles to failure, three different regions were classified, as shown in Figure 2.9, composing of stage I: rapid decrease of dissipated energy ratio, stage II: constant change of the RDEC as a plateau value (PV) which was defined as the proposed fatigue criterion, and stage III, rapid increase of the RDEC to failure. Then, a fatigue model was obtained by plotting the PV values against a

number of cycles to failure (N_f) for each stress or strain level. This model was suggested to represent a fundamental approach fatigue damage modeling.

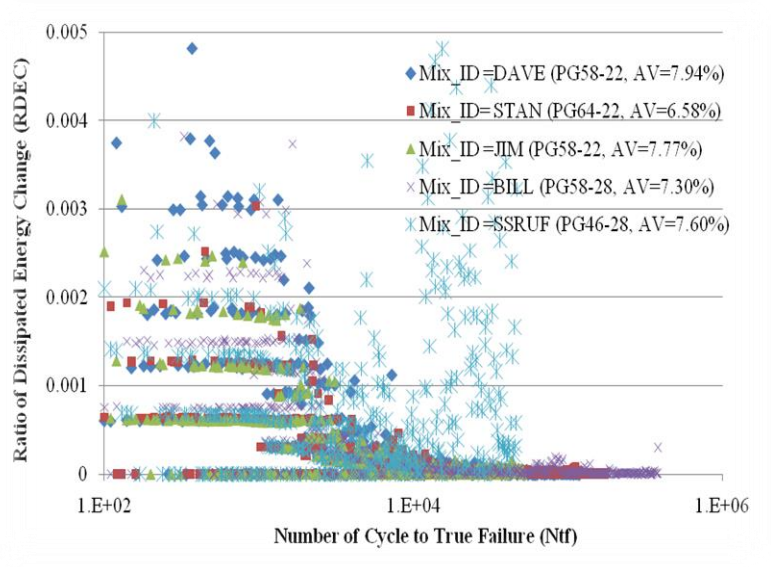

Figure 2.10 Scattering data on plot of RDEC versus cycles.

However, Na chiangmai (2010) evaluated the RDEC approach and reported that the plateau stage was difficult to accurately characterize because of scattering of data plot as presented in Figure 2.10 (also confirmed by Kim et al, 2004) and PV values were relatively small, within a range of 10^{-5} to 10^{-30}, which the PV value was easily miscalculated. Moreover, the calculation of the PV was based on the number of cycles to failure in the traditional fatigue approach, which was arbitrarily defined by a 50-percent reduction in stiffness (N_{f50}). Therefore, the PV criterion was not found to be an intrinsic cyclic fracture criterion.

Chapter 3 Fracture Behavior Under Monotonic Loading

3.1 Introduction

A Disk-shaped Compact Tension (DC(T)) test was successfully developed to study fracture behaviors of asphalt concrete (AC) mixtures under monotonic loading by Wagoner and Buttlar (2006). The DC(T) test was proposed to determine fracture properties of the AC mixes at low temperatures, for instance, sub-zero Celsius, which the AC was considered as a quasi-brittle material. According to the standard DC(T) test procedures, monotonically tensile loading was applied to a specimen with a constant loading rate of 1 mm/min. Then, a separation of the specimen was measured corresponding to the applied loading. Fracture properties, such as fracture strength, fracture toughness, and fracture energy, were then obtained based upon a load-displacement response and dimensions of the DC(T) geometry. Moreover, the fracture energy was used to describe the total amount of required energy to complete the fracture processes of crack initiation, crack propagation, and failure of a test sample.

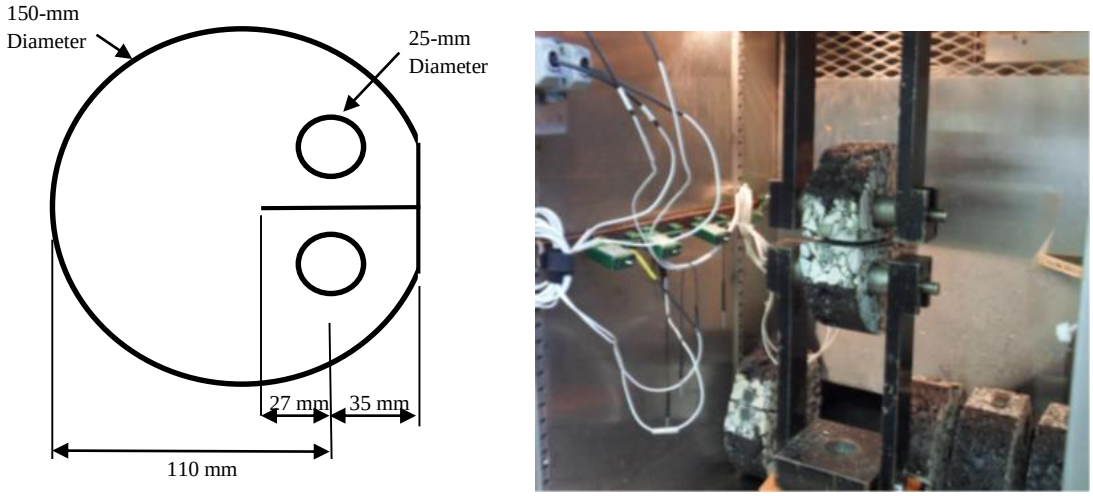

Figure 3.1 Standard DC(T) geometry and test setup.

Figure 3.1 shows dimensions of the standard DC(T) geometry and test setup. Advantages of the DC(T) geometry were that test samples were easily extracted from the field using a core bit, and it required less amount of materials to make a test specimen in a laboratory, comparing with a beam geometry of the standard flexural beam test. Moreover, there was a possibility to use the DC(T) configuration to perform a cyclic loading test because the geometry could potentially handle repeated tensile and compressive loading. This concept was important because in reality a pavement was typically subjected to both tensile and compressive loading from vehicles.

Figure 3.2 Breakage of standard DC(T) specimens at loading hole when subjected to repeated loading for certain mixes tested.

According to the scope of the study, the ultimate goal was to evaluate monotonic and cyclic fracture behaviors of AC mixes using an identical DC(T) geometry. However, a problem was found when the standard DC(T) geometry was utilized to perform the cyclic loading test. The geometry could not handle repeated compressive loading in some types of mixtures, for example, stone matrix aggregate (SMA) and 19-mm nominal maximum aggregate size (NMAS) or larger NMAS mixes. As a result, an undesirable breakage of the test specimens at a loading hole existed as shown in Figure 3.2. Due to such a geometric issue, therefore, this chapter presents a revision of the standard DC(T) test which included a modification of the DC(T) geometry, a comparison of test results between standard and modified configuration, and a movement of the test control location. Furthermore, since the DC(T) test was typically conducted at test temperatures of sub-zero Celsius, the study also proposed to evaluate monotonic fracture behaviors at intermediate test temperatures of 10^{o}C and 20^{o}C.

3.2 Test setup

The ASTM D7313-07 specification provided the standard test protocol of "Determining Fracture Energy (G_f) of Asphalt-Aggregate Mixtures Using the Disk-shaped Compact Tension (DC(T)) Geometry". Based upon the study, the standard DC(T) geometry was proposed to perform a cyclic loading test in order to find potential correlations or interpretations between these two loading mechanisms using the identical test geometry. However, as previously presented, the standard DC(T) geometry was not able to carry repeated loading, resulting the undesirable breakage at the loading hole. Therefore, the following section presents some adjustments of the standard DC(T) test which includes a

modification of the DC(T) geometry, specimen preparation and test procedures, and consideration of the test control location.

3.2.1 Modification of standard DC(T) geometry

Because of the undesirable breakage at the loading hole of the standard DC(T) geometry subjected to cyclic loading, the geometry was modified to be able to perform both monotonic and cyclic loading tests. Several DC(T) geometries were attempted to accommodate repeated loading. For example, loading holes were located near the notch tip in a perpendicular orientation to the notch as shown in Figure 3.3 (a), and the other trial was to increase a standard notch length as illustrated in Figure 3.3 (b). This notch length of 92.5 mm was successfully used to perform the DC(T) test for Portland cement concrete (PCC) mixtures (Armen and Roesler, 2012). However, a breakage at the loading hole still persisted in both cases.

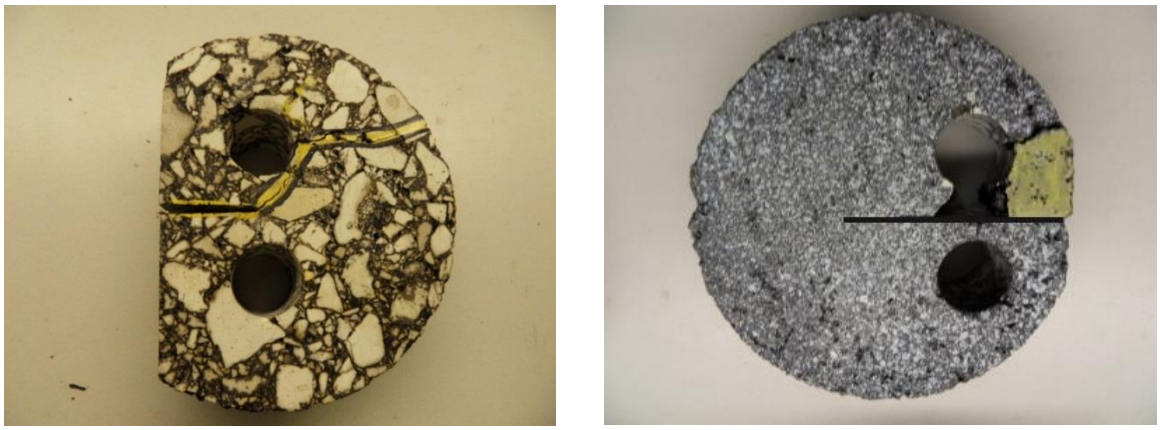

(a) Loading holes by notch tip (b) 92.5-mm notch used on PPC DC(T)

Figure 3.3 Examples of unsuccessful trials of geometric modifications to accommodate repeated loading.

The newly proposed DC(T) geometry and dimensions are presented in Figure 3.4. This was the most robust DC(T) geometry, resistant to repeated loading in the cyclic DC(T) test without any breakages. Approximately 22-mm of clearance is provided in a perimeter around the loading holes. This configuration appears to reduce bending moment at the crack tip. In addition, tight fitting, Teflon-coated loading pins were used to facilitate load reversal.

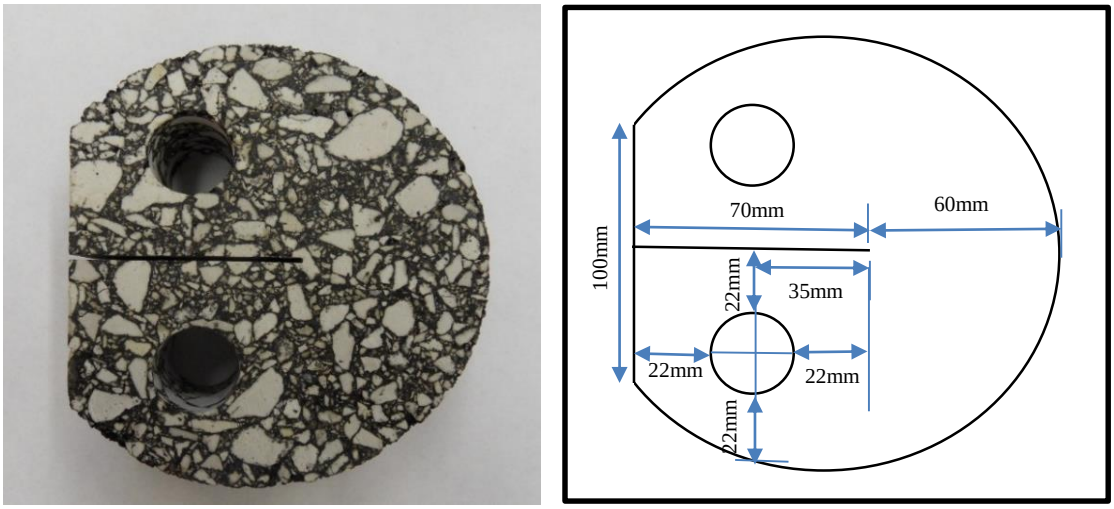

Figure 3.4 Proposed robust DC(T) geometry and dimensions.

Figure 3.5 presents a comparison of load-displacement curves between the standard and modified DC(T) geometry of three mixes, coarse-graded and two fined-graded mixes, tested at a temperature of -12ºC. Additionally, similar plots for other two test temperatures of 0ºC and 10ºC were presented in Figure A.1 and Figure A.2 in the appendix A.

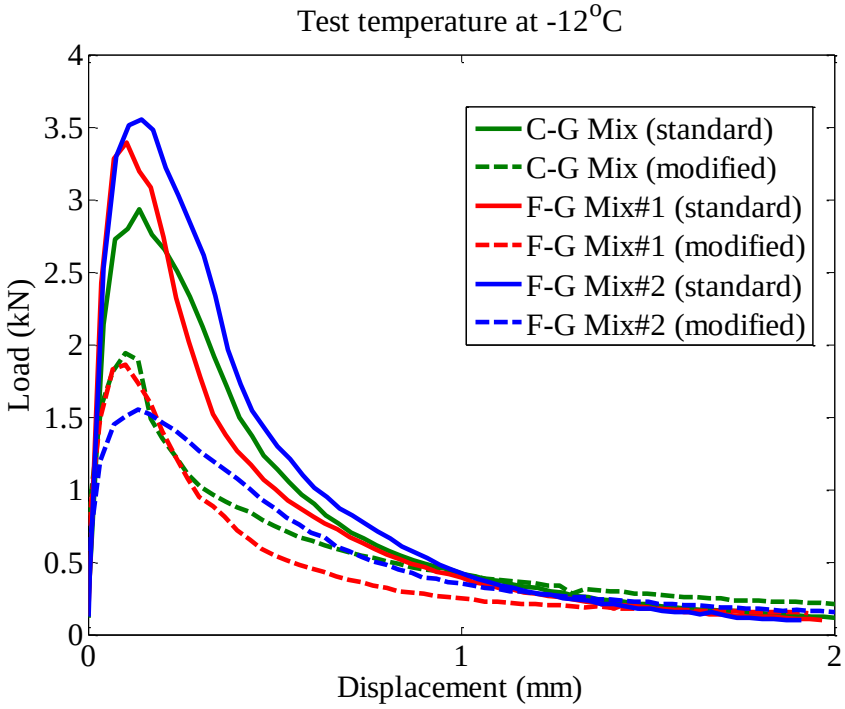

Figure 3.5 Comparison of load-displacement curves between standard and modified DC(T) geometry for three different mixes tested at -12ºC.

Table 3.1 Comparison of fracture energy between standard and modified DC(T) geometries.

Temp (°C)	Mix ID	Standard DC(T)		Modified DC(T)		Difference (%)
		G_f (J/m^2)	CV (%)	G_f (J/m^2)	CV (%)	
+10	C-G Mix	1,978	13.2	1,164	12.1	41
	F-G Mix#1	1,639	8.5	964	12.3	41
	F-G Mix#2	1,687	8.7	843	4.5	44
0	C-G Mix	707	6.5	425	8.8	40
	F-G Mix#1	635	8.3	375	13.7	40
	F-G Mix#2	632	24.1	386	6.9	39
-12	C-G Mix	415	5.2	354	18.4	15
	F-G Mix#1	427	16.4	375	17.4	13
	F-G Mix#2	429	13.0	366	11.2	13

Based on the graphical illustration of load-displacement curves (Figure 3.5) and a comparison of fracture energy (Table 3.1) between the standard and modified DC(T) geometries, it was found that peak load and fracture energy of the standard DC(T) geometry is greater than that of the modified geometry. Also, a difference of fracture energy varied with test temperatures as the warmer the temperature, the greater the difference in fracture energy.

3.2.2 Preparation of specimen and test procedures

Fabrication procedures of the test specimen were relatively straightforward, which had similar steps as the standard DC(T) fabrication, except that a location of loading holes and a notch length were changed. Figure 3.6 presents the steps of the fabrication of modified DC(T) test specimens. The first step was to cut a sample into the standard thickness of 50 mm using a water-cooled masonry saw as shown in step 1. Locations of loading holes, flat edge of the mouth, and alignment of the notch length were marked using a template as shown in step 2. Then, loading holes were drilled using a core bit of the 25-mm outside diameter with water as shown in step 3. Finally, a notch was made using a tile saw with a blade width of 1.5 mm as illustrated in the step 4.

Step 1: Cut specimen to 50-mm thickness

Step 2: Mark holes and notch using template

Step 3: Drill loading holes using core bit

Step 4: Make notch using tile saw

Figure 3.6 Steps for fabricating DC(T) specimen.

Besides the test specimen preparation, the test apparatus, such as loading frame, loading figure, displacement gage, and data acquisition device, were the same as specified by the standard DC(T) test of ASTM D7313-07. For the monotonic DC(T) test procedures, steps were remained similar to those of the standard test specification. Test samples were placed in a temperature controlled chamber for a minimum of 2 hours. The specimen was set in the loading fixtures and applied a seating load of no greater than 0.2 kN. Then, a test was performed with a constant displacement rate and completed when the post-peak loading has reduced to 0.1 kN. However, since the study proposed to evaluate a fracture behavior at intermediate temperatures of 10^{o}C and 20^{o}C. Some issues were raised, such as a test-controlled location of the crack mouth opening displacement (CMOD) and the standard loading rate of 1 mm/min may not suitable for the intermediate to high temperatures because an effect of viscoelastic properties of the AC mixes was great influent to test results that did not represent the intrinsic fracture behavior. Therefore, the following

section presents a consideration of the test-controlled location and effects of temperature and loading rate at the temperatures of 10ºC and 20ºC.

3.2.3 Consideration of test-controlled location

A crack mouth opening displacement (CMOD) location, physically located at a distance of 70 mm from the notch tip of the DC(T) geometry, was typically used to control and measure separation of the specimen with a clip-on gage of Epsilon Model 3541-0020-250-ST that has a gage length of 5 mm and travel range of 6.35 mm. According to Wagoner's dissertation (2006), the tests were performed under different loading rates at different test temperatures of 0, -10, -20, and -30ºC. The separation of the specimens was measured at locations of CMOD and δ25 gages, which were placed by the notch tip and being attached 25 mm apart from each other introducing a measurement of the crack tip opening displacement (CTOD) under the CMOD-controlled loading (Figure 3.7).

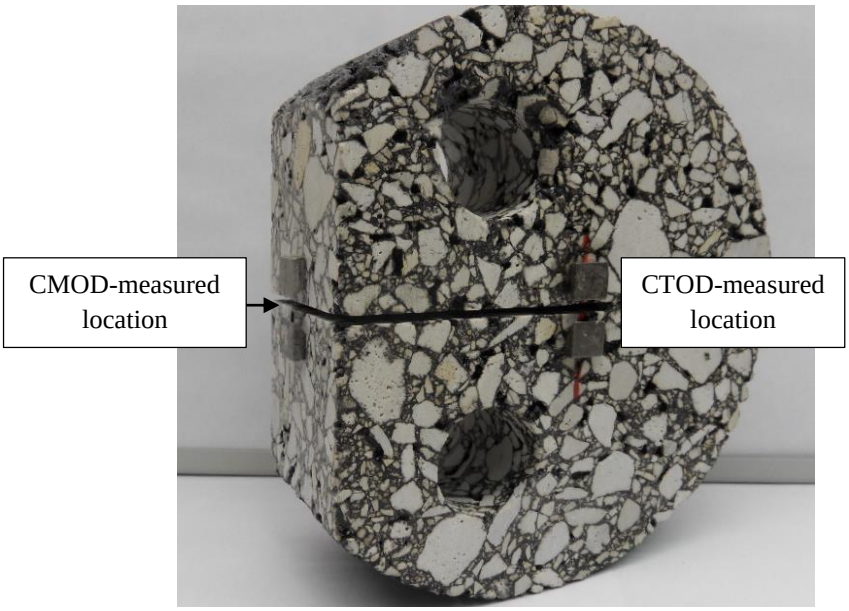

Figure 3.7 Locations for CMOD and CTOD or δ25 measurements.

Since, the study proposed to evaluate fracture behavior at low and intermediate test temperatures as high as 20ºC, significant effects of material compliance were anticipated in the CMOD measurement. Wagoner presented that a trend of the test results of fracture energy obtained from both CMOD and CTOD were the same; therefore, the CMOD measurement was acceptable to be used to compare performance of different mixtures in practice. However, fracture energy computed from the CMOD measurement was not an intrinsic fracture property because a magnitude of the displacement was integrated with the material compliance. Such an effect of the material compliance was acceptable if the test

was done at low temperatures as the AC became brittle, which the material compliance was relatively small. However, the compliance effect was influent to a test result when intermediate to high test temperatures performed.

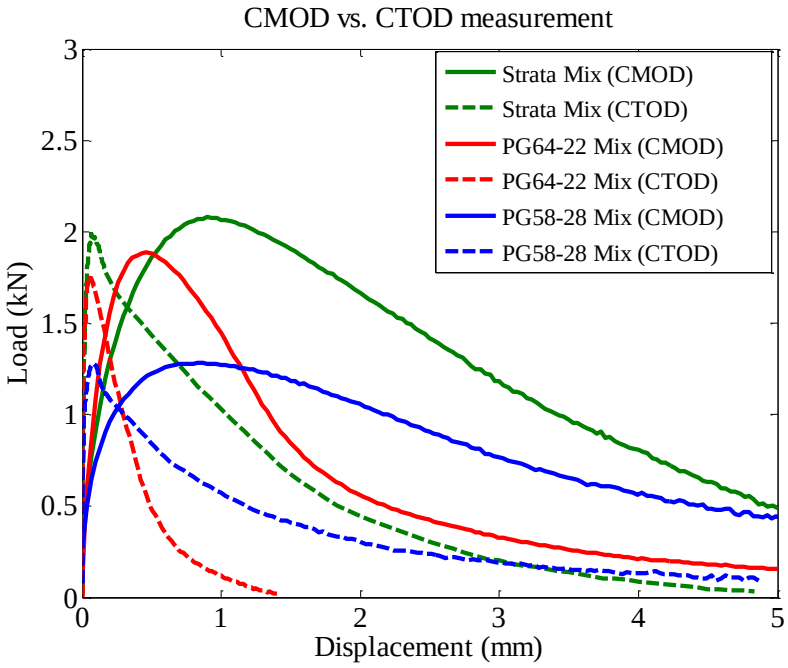

Figure 3.8 Load-displacement curves of CMOD vs. CTOD measurement tested at 10ºC.

Figure 3.8 presents load-displacement curves of CMOD and CTOD measurements of three different mixtures: 4.75-mm NMAS PG70-28, 9.5-mm NMAS PG64-22, and 19-mm NMAS 58-28 tested at 10ºC under the CMOD-controlled mode of loading. Based on the plot, the most noticeable difference between the CMOD and CTOD measurements was the pre-peak portion of the curves that a magnitude of the CMOD was integrated with the material compliance. As a result, the CTOD location should be used to control and measure a test to provide an intrinsic fracture behavior.

Table 3.2 Test results of CMOD and CTOD measurements.

Mixtures	Fracture Energy (J/m^2)		Diff(1)	Peak-Load Location (mm)		Diff(1)
	CMOD	CTOD	(%)	CMOD	CTOD	(%)
Strata Mix	1,523	877	42	0.93	0.07	92
PG64-22 Mix	1,050	238	77	0.56	0.06	82
PG58-28 Mix	1,283	518	60	0.86	0.07	92

Note: (1) is percent decrease in a value obtained from CMOD measurement.

Table 3.2 presents a summary of fracture energy and peak-load locations from the CMOD and CTOD measurements. Based on the results, fracture energy computed from the CMOD was approximately 40-80 percent greater than that of the CTOD measurement. Apparently, the compliance effect played an important role, which provided larger area underneath the load-CMOD curve, resulting the calculation of fracture energy was overestimated. Thus, in order to describe a real fracture behavior under monotonically loading scenarios, it was believed that separation of the material as characterized at the crack tip opening displacement (CTOD) was a more suitable approach to studying fracture mechanisms in the proposed application. However, the CTOD measurement was done under the CMOD-controlled loading that an additional clip-on gage was required, which was relatively expensive. Also, another benefit of measuring a separation at the CTOD location was a maximum opening displacement of the test specimen could be fully captured within a travel range of the clip-on gage of 6.35 mm until the test completed, which an applied load decreased to 0.1 kN. So, an extrapolation of test results was not required for fracture energy calculation. Therefore, the CTOD-controlled location was investigated to perform the DC(T) test.

Effect of loading rate on CTOD-controlled location

According to the standard DC(T) test procedures, a loading rate of 1-mm/min was standardized to perform the DC(T) test. However, when this loading rate was directly applied at the CTOD-controlled location, a softening curve barely existed for some types of the AC mixtures, for example, stone mastic aggregate (SMA) and 19-mm NMAS mixes, especially at low test temperatures as the AC became brittle. As a result, an effect of different loading rates was investigated to determine a proper loading rate for a variety of mixes and temperatures using the CTOD-controlled location.

Figure 3.9 and Figure 3.10 present test results with different loading rates of the 19-mm NMAS coarse-graded mix performed at 20^{o}C and -12^{o}C, respectively. Regardless of test temperatures and loading rates, they have showed that a post portion of the load-displacement curves or softening curves was not clear as an existence of two-peak phenomenon. A possible assumption was that a coarse-graded mix contained less contacted surfaces between aggregate particles and mastic phase. So, it was insufficient to distribute stresses from the notch tip to a vicinity of the notch tip, especially at -12^{o}C as an appearance of a two peak phenomenon on the load-displacement curves, which was possibly produced by aggressive tensile loading resulting an instability of the closed-loop system of the test

machine. Therefore, a relocation of the test-controlled location was considered in order to compromise both effects of the material compliance at the CMOD-controlled location and the aggressive tensile loading at the CTOD-controlled location.

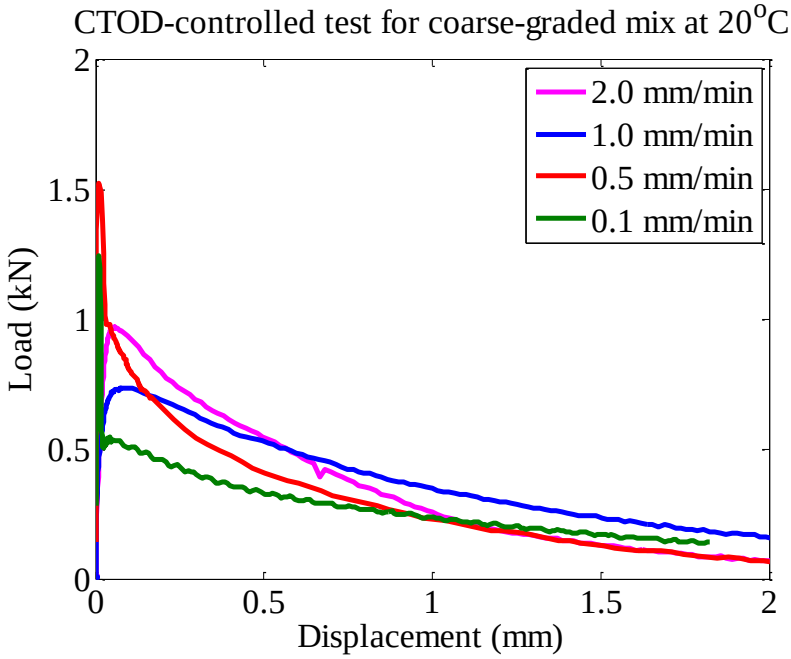

Figure 3.9 Loading rate effect of CTOD-controlled location for coarse-graded mix, performed at 20°C.

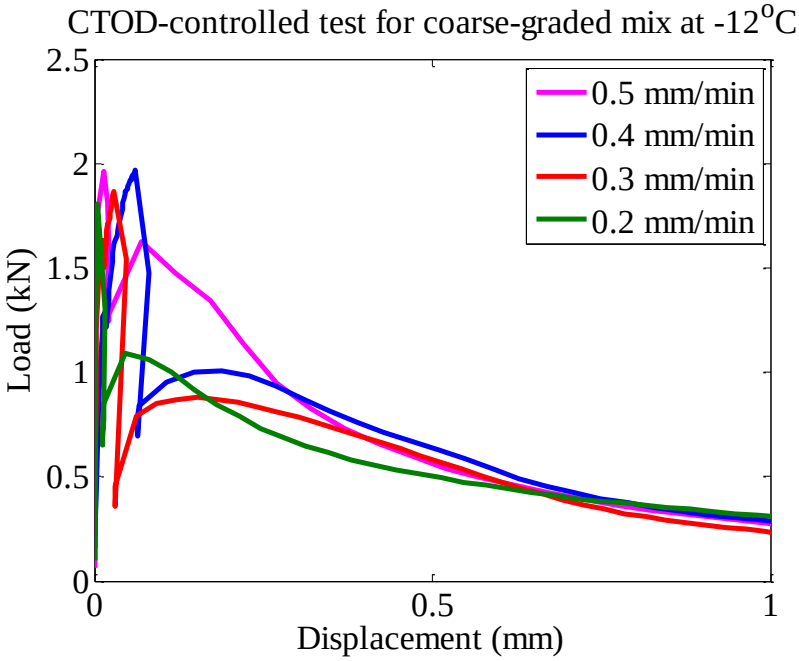

Figure 3.10 Loading rate effect of CTOD-controlled location for coarse-graded mix, performed at -12°C.

Proposal of 1-cm offset CTOD

Conceptually, a measurement of the crack tip opening displacement (CTOD) was more suitable to study fracture behavior because it directly measured fracture properties by a crack or notch tip; however, as presented in the above section that unstable test results occurred when the CTOD test control was attempted, which resulted lack of the softening curve for examining fracture properties. As a compromise, a new test-control gauge location for attaching a clip-on gage was examined; 1-cm offset from the notch tip, so-called the 1-cm offset CTOD, was used to control the test, as illustrated in Figure 3.11. This location was found to strike a reasonable balance between material compliance issues and unstable test control.

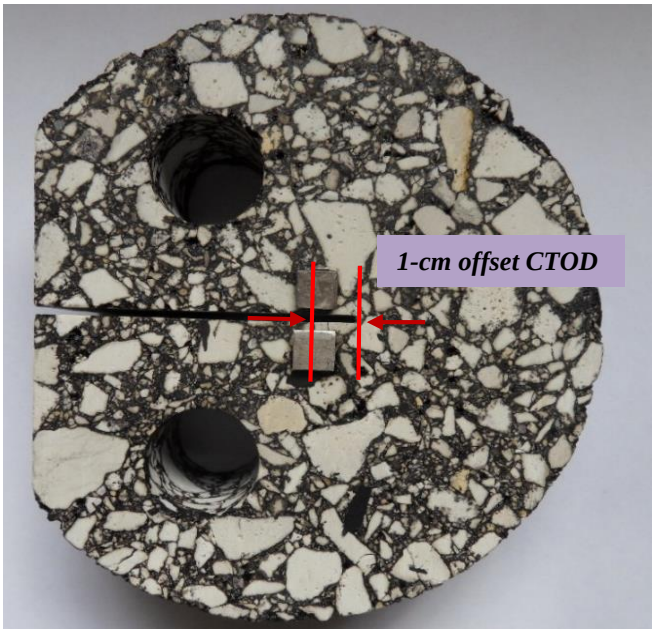

Figure 3.11 1-cm offset CTOD location, shifted toward loading holes, as proposed for new test-controlled location.

Figure 3.12 presents load-displacement curves of the DC(T) test results for the coarse-graded mix using the 1-cm offset CTOD location. The temperature of -12^{o}C was selected to verify the new setup because it provided the most unacceptable test results as presented in the previous section. Three different loading rates of 0.3, 0.5, and 1.0 mm/min were conducted. Regardless of the loading rates, the modified, 1-cm offset CTOD location appeared to produce desired test control and material response. As a result, this setup was proposed to perform both monotonic and cyclic loading tests for the remainder of this study.

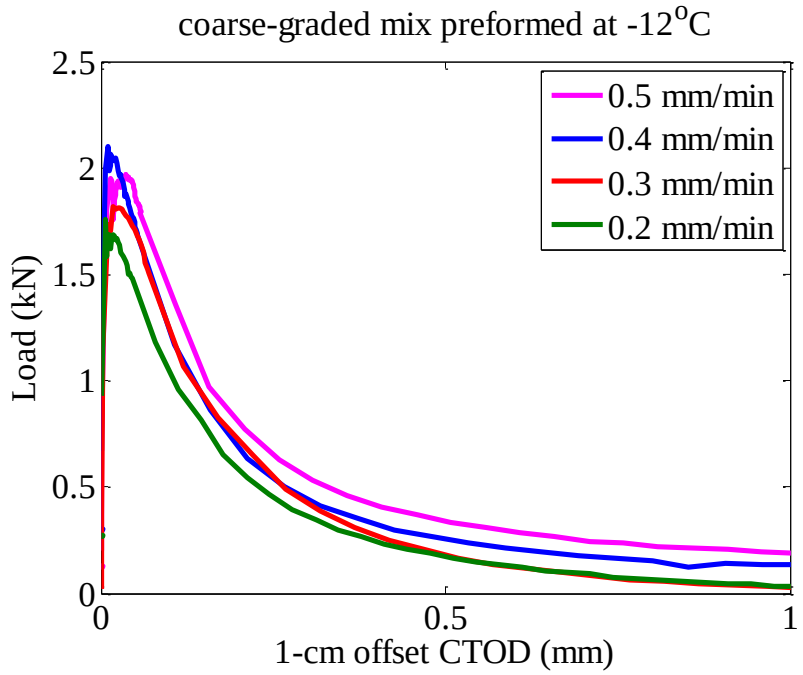

Figure 3.12 Validation of 1-cm offset CTOD location at -12°C.

3.3 Materials and experimental design

Five different AC mixtures were used in the study. These mixtures represented a range of nominal maximum aggregate size (NMAS) and used different types of asphalt binder and recycled materials, including:

- Mix A: 4.75-mm NMAS Strata
- Mix B: 9.5-mm NMAS PG64-22
- Mix C: 19-mm NMAS PG58-28
- Mix D: 9.5-mm NMAS recycled asphalt shingles (RAS)
- Mix E: 19-mm NMAS foamed bituminous with PG64-22

Mix A, B, and E were received as plant-produced, loose mixes. Whereas, mix C was mixed and compacted in a laboratory, and mix D involved core samples obtained in the field. Table 3-3 provides gradations of a blended aggregate structure on standard sieve size and volumetric properties. Also, Figure 3.13 presents a plot of gradations of all five mixtures based upon the 0.45 power chart.

Table 3.3 Blended aggregate structures and volumetric properties of mixtures.

Material Code	Mix A	Mix B	Mix C	Mix D	Mix E
Sieve Size	% Passing Sieve				
1" (25.0 mm)	100	100	100	100	100
3/4" (19.0 mm)	100	100	95.9	100	96.5
1/2" (12.5 mm)	100	100	83.6	100	77.0
3/8" (9.5 mm)	100	99.6	76.2	99	66.8
No.4 (4.75 mm)	97.8	88.7	58.5	73	34.5
No.8 (2.36 mm)	77.4	62.5	40.8	48	18.8
No.16 (1.18 mm)	56.9	40.4	25.4	35	11.8
No.30 (600 µm)	38.5	23.4	15.6	26	7.7
No.50 (300 µm)	21.5	13.3	8.6	16	6.5
No.100 (150 µm)	11.9	7.9	5.6	10	5.5
No.200 (75 µm)	9.9	6.0	4.7	6.7	4.8
Volumetric Properties					
Asphalt Content, AC (%)	6.9	7.0	5.5	6.8	5.2
Specific Gravity of AC, G_b	1.025	1.025	1.036	1.034	1.031
Specific gravity of blended agg.	2.611	2.619	2.616	2.633	2.659
G_{mm}	2.457	2.466	2.528	2.423	2.504
G_{mb}	2.361	2.367	2.326	2.350	2.335
Percent VMA (%)	15.8	15.9	13.6	16.8	16.7
Percent VFA (%)	78.7	74.8	69.9	82.2	80.5
Dust-binder (D/B) ratio	1.9	1.1	0.9	1.0	0.9

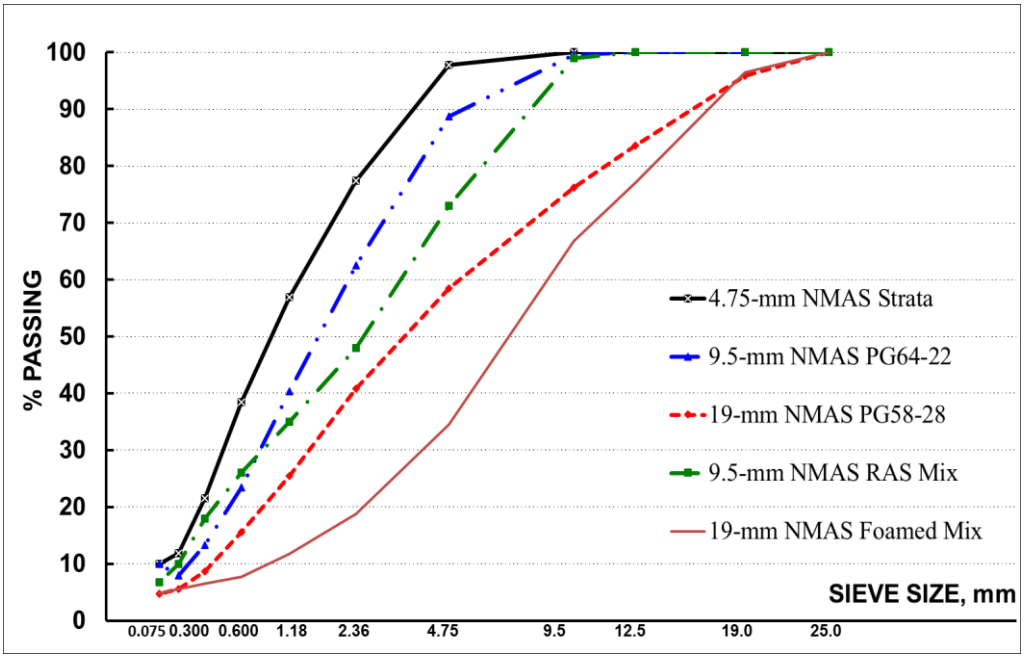

Figure 3.13 Gradations of the five study mixtures on 0.45-power chart.

For the experimental design, mix A, B, and C, which were proposed as the base mixtures, were conducted on all test temperatures of -12, 0, 10, and 20°C. Mix D and E were used only at test temperatures of -12°C and 20°C. So, all of the five mixtures were performed at the lowest and highest test temperatures of -12°C and 20°C in order to ensure that all of the methodologies proposed in the study was valid for different types of AC mixtures in two distinct test temperature ranges. In addition, test samples were compacted to 7 percent air voids using a Superpave gyratory compactor.

For the monotonic DC(T) test setup, a modified DC(T) geometry with the 1-cm offset CTOD location was used to perform all tests in the study. Initially, a loading rate of 0.5 mm/min was used to perform the monotonic DC(T) test. However, limited fracture studies have been conducted at temperatures higher than 0°C. Thus, this study also proposed to evaluate fracture behavior at intermediate test temperatures of 10°C and 20°C, which included an effect of temperatures on fracture properties and effect of loading rate at intermediate temperatures.

3.4 Test results

For the monotonic DC(T) test results, four fracture parameters were extracted from test data, including total fracture energy (G_f), pre-peak load fracture energy, post-peak load fracture energy, and fracture strength (S_f). A definition and mathematical expression of each parameter is provided as follows:

o ***Total fracture energy*** was used to describe total amount of released (or dissipated) energy within a material to complete fracture processes of crack initiation, crack propagation, and failure of the material. The total fracture energy can be mathematically defined as the area under a load-displacement curve divided by the fractured area as

$$G_f = \frac{A_f}{(BxL)}$$

where G_f is fracture energy (J/m^2), A_f is an area under load-CMOD curve (kN-m), B and L are a thickness and ligament length of the specimen (m), respectively.

o ***Pre-peak fracture energy*** uses data from the pre-peak portion of the load-displacement curve. It was defined as the consumed energy prior to reaching peak load, which is taken as the area beneath the load-displacement curve from the beginning of the test to the point where peak load is reached.

o ***Post-peak fracture energy***, was computed by subtracting the pre-peak fracture energy from the total fracture energy. This parameter characterizes the fracture energy associated with post-peak or softening response.

o ***Fracture strength*** is a parameter associated with peak load. It can be calculated using the standard formula for computing a plane-strain fracture strength of metallic materials using a DC(T) test configuration, which expressed as

$$S_f = \frac{2P(2W + a)}{B(W - a)^2}$$

where S_f is fracture strength (MPa), P is a maximum load sustained by a sample, B is thickness of specimen, and W and a are geometric dimensions defined by ASTM E399-90. Based on a proposal of the modified DC(T) geometry in this study, B, W, and a are taken as 50, 95, and 35 mm, respectively.

For this particular study, however, only load-displacement curve, peak load, and total fracture energy (G_f) were used for data analysis.

3.4.1 Effect of temperature on fracture properties

According to the standard DC(T) test procedures, a test is recommended to perform at a temperature of 10 degree warmer than the low temperature performance grade (PG) of the bituminous material, for example, the test is conducted at the -12^{o}C for PG XX-22. Based on Wagoner's study (2006), the DC(T) tests were only evaluated at temperatures less than 0^{o}C. However, it is very important to understand fracture behaviors at other higher

temperatures because pavements exposed to a wide range of temperatures all year round in the field.

In this study, all based mixtures of the mix A, B, and C were tested at all proposed temperatures of -12, 0, 10 and 20°C. Based on the new setup of the DC(T) test, a loading rate of 0.5 mm/min was initially used at the 1-cm offset CTOD location to study temperature effects. As a result, Figure 3.14 presents a plot of the load-displacement curves of the PG64-22 mix for all test temperatures. Additionally, similar plots of the load-displacement curves for the other based mixes of Strata and PG58-28 mixes were presented in Figure A.3 and Figure A.4 in the appendix A. Regardless of mixtures, a trend of the curves was similar that the warmer test temperature, the lower peak load and the greater maximum opening of the displacement to complete a failure. Interestingly, the peak load of all mixtures tested at 20°C significantly decreased, comparing with the other temperatures.

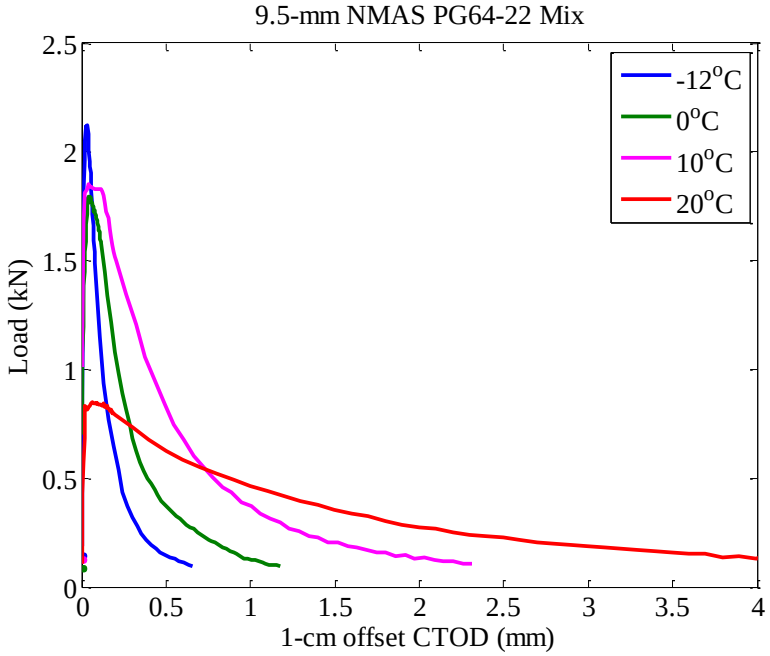

Figure 3.14 Load-displacement plots of PG64-22 with loading rate of 0.5 mm/min.

Table A.1 in the appendix A provided a summary of fracture energy and peak load for all mixes and temperatures. Additionally, test results of the RAS and foamed mixes were provided for the temperatures of -12°C and 20°C. Based on the test results, RAS mix, which was made of the recycled materials, provided the highest coefficient of variation (CV) for both peak load and fracture energy (G_f). Similar to the standard DC(T) test, the modified DC(T) geometry presented well repeatability of the test results.

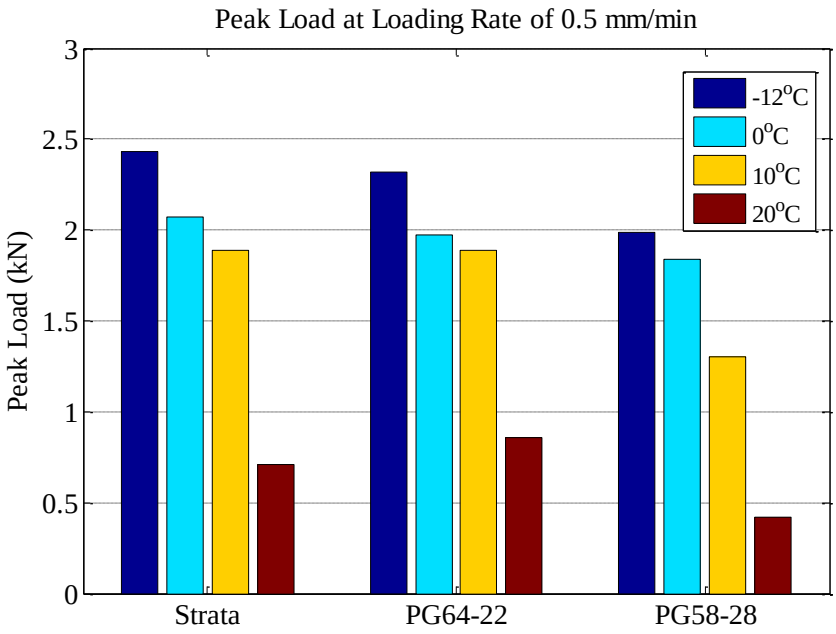

Figure 3.15 Comparison of peak load of mixtures for all temperatures.

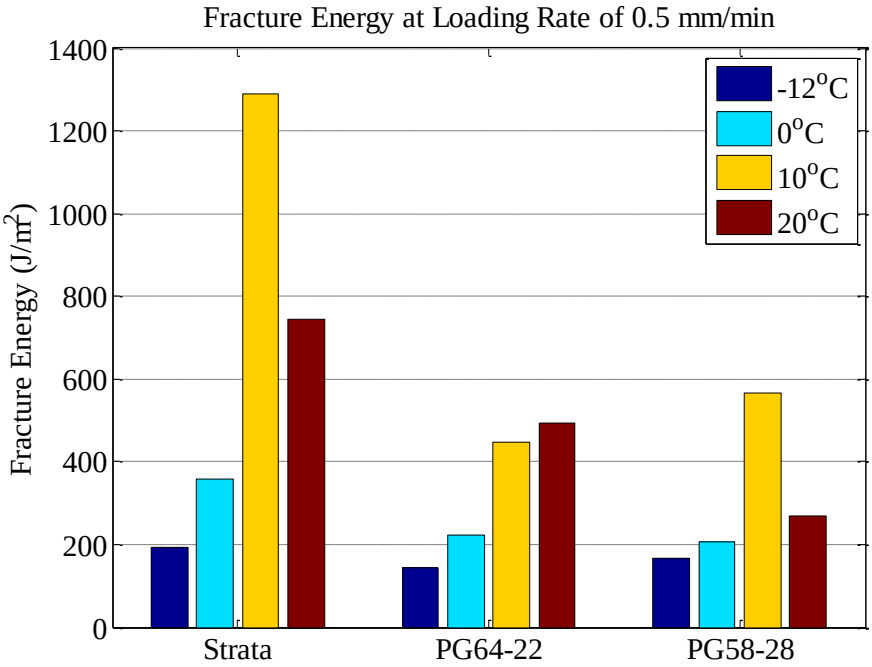

Figure 3.16 Comparison of fracture energy of mixtures for all temperatures.

Figure 3.15 and Figure 3.16 provide a comparison of the peak load and fracture energy of the based mixes for all temperatures, respectively. In terms of peak load, a peak load decreased with an increase of the test temperature for all mixtures. At higher temperature, the AC mixture became more ductile which required a less amount of loading to initiate a crack, comparing to a test done at lower test temperatures as the asphalt was more brittle. Moreover, at a low temperature, a load rapidly decreased after reaching the

peak load because the mixture was lack of the load carrying capacity. Conversely, a load gradually decreased when the peak load reached for a higher temperature because the asphalt binder was more ductile which provided well-bonded aggregate particles, resisting to the applied loading. As a result, the G_f increased when the test temperature increased. However, fracture energy significantly decreased when a test was performed at 20^{o}C because an effect of viscoelastic properties exhibited the relatively low peak load. Moreover, a lower coefficient of variance (CV) presented in the test result, where a mixture was tested at low temperature due to effect of time and temperature dependency.

It was noteworthy that all tests were conducted using a loading rate of 0.5 mm/min to study the temperature effect. However, a single loading rate might not be suitable for intermediate test temperatures of 10^{o}C and 20^{o}C because of the relatively small magnitude of the peak load, and also a test required a significant time to complete. Therefore, an effect of loading rates was evaluated to determine a proper loading rate for intermediate test temperatures of 10^{o}C and 20^{o}C, which test results were presented in the following section.

3.4.2 Effect of loading rate at intermediate temperature

According to Wagoner's study (2006), an effect of loading rates between 0.1 and 10 mm/min was evaluated at sub-zero test temperatures of 0, -10, -20 and -30^{o}C. The test results showed that fracture behavior was not only depended on the test temperature, but also loading rates. However, both peak load and fracture energy values were within a small range, for example, fracture energy was within a range of 100 to 500 J/m^2, and a difference between maximum and minimum values of the peak load was less than 0.5 kN. Therefore, a loading rate of 1-mm/min was used for the DC(T) test which was the most practical for low test temperatures. For this study, the loading rate of 0.5 mm/min was initially used to perform the DC(T) test for all temperatures. This particular loading rate was arbitrarily selected based on an evaluation of the test-controlled location. However, when such a single loading rate was used, the peak load decreased with an increase of the temperature, especially at 20^{o}C a significant decrease of both peak load and fracture energy. Therefore, this section presents an effect of loading rates for intermediate temperatures of 10^{o}C and 20^{o}C.

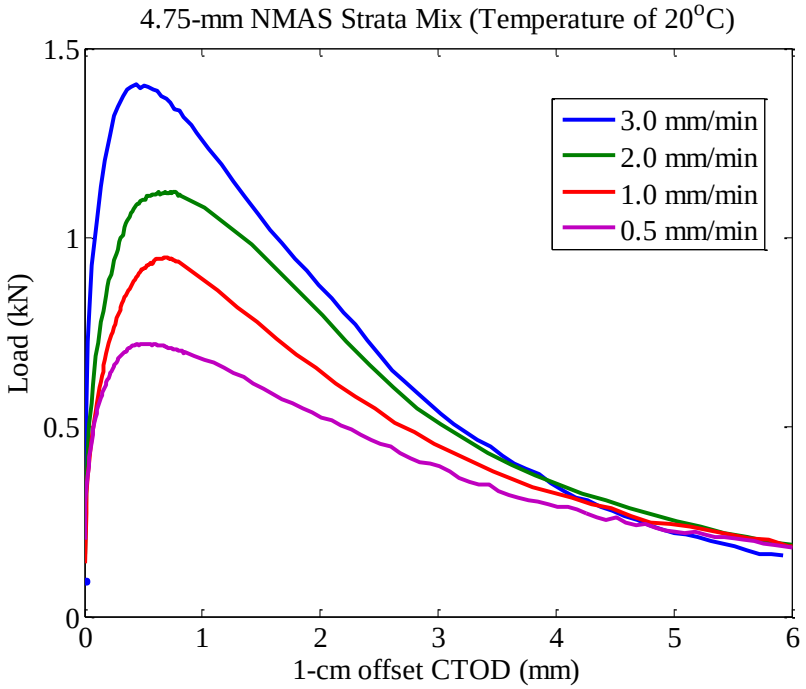

Figure 3.17 Load-displacement curves of Strata mix with different loading rates at 20°C.

Figure 3.17 illustrates a plot of load-displacement curves for the strata mix tested at 20°C with different loading rates between 0.5 and 3.0 min/mm. Additionally, similar plots for PG64-22 and PG58-28 tested at 10°C and 20°C were presented in Figure A.5 to Figure A.10 in the appendix A. Regardless of mixtures and temperatures, a peak load increased with an increase of the loading rate, but a maximum opening displacement approximately remained the same for all different loading rates, for example, Figure 3.17 showed that the maximum 1-cm offset CTOD was about 6 mm for all loading rates.

Figure 3.18 presents a comparison of peak load values of all based mixes tested at 20°C. It showed that a peak load increased with an increase of the loading rate. In addition, a similar plot of the peak load comparison for 10°C was provided in the Figure A.11. Also, Figure 3.19 presents a comparison of fracture energy for the mixtures tested at 20°C with different loading rates, and a similar plot for a test temperature of 10°C was provided in Figure A.12. As shown in the plots, fracture energy increased with an increase of the loading rate, which had the same trend as that of the peak load because the fracture energy was directly computed by an area encompassed by the load-displacement curve as a function of the peak load.

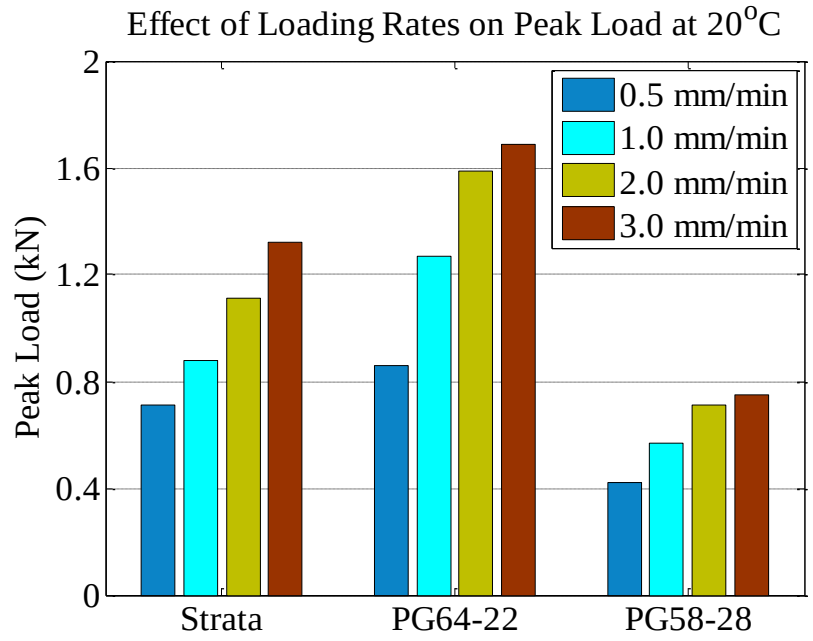

Figure 3.18 Peak load values of mixtures for different loading rates at 20°C.

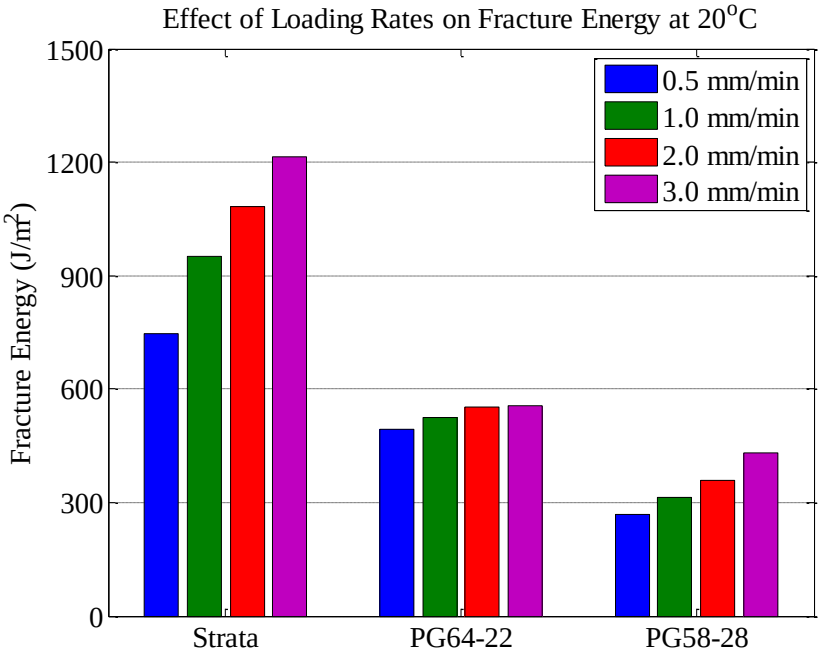

Figure 3.19 Fracture energy of mixtures for different loading rates at 20°C.

Table 3.4 presents a summary of fracture energy and peak load of all mixtures at a temperature of 20°C for different loading rates. It has shown that the coefficient of variation (CV) of the peak loads were mostly less than 10 percent, except for the RAS mix. Also, in terms of fracture energy, test results had the same trend as that of the peak load which a fracture energy increased with an increase of the loading rate. However, the CV values of fracture energy were higher than that of the peak load because a wide range of fracture

energy values was found at the intermediate test temperatures, resulted from a variation of the post-peak or softening curve behavior, which were influent to a computation of the fracture energy. In addition, a summary of fracture energy and peak load for a test temperature of 10°C was provided in Table A.2 in the appendix A.

Table 3.4 Fracture properties of mixes performed at 20°C with different loading rates.

Mix	Loading Rate	Peak Load		Fracture Energy (G_f)	
	(mm/min)	Avg. (kN)	CV (%)	Avg. (J/m^2)	CV (%)
4.75-mm Strata (polymer binder)	0.5	0.71	1.1	746	9.6
	1.0	0.88	7.4	951	6.5
	2.0	1.11	3.6	1,084	9.0
	3.0	1.32	6.0	1,215	1.6
9.5-mm PG64-22	0.5	0.86	1.2	494	3.3
	1.0	1.27	3.4	526	15.5
	2.0	1.59	1.5	552	5.2
	3.0	1.69	2.1	556	17.4
19-mm PG58-28	0.5	0.42	8.3	270	13.8
	1.0	0.57	5.9	313	7.2
	2.0	0.71	2.3	357	3.9
	3.0	0.75	5.4	432	10.7
RAS Mix	2.0	1.30	18.9	343	8.3
Foamed Mix	2.0	1.60	5.2	504	3.7

3.4.3 Selection of loading rate for different test temperatures

Generally, a single loading rate was used to perform monotonic DC(T) tests for different temperatures. For example, the loading rates of 1.0 mm/min and 0.7 mm/min were standardized for DC(T) and SC(B) test, respectively. However, these single rates of loading were arbitrarily selected. From Wagoner's thesis (2006) of the DC(T) proposal showed that

the 1 mm/min was the most practical for test temperatures of sub-zero Celsius. However, based upon this study, the effect of intermediate temperatures and loading rates on fracture properties were evaluated. As a result, using a single loading rate for different temperatures produced in a significant decrease of the peak load, and also required a great amount of time to complete a test at a higher test temperature. Moreover, within the same test temperatures of 10^{o}C and 20^{o}C, the higher loading rate applied, the greater peak load presented. Therefore, using a single rate of loading for a wide range of test temperatures may not be suitable.

- A question was raised which level of a loading rate should be used to perform the DC(T) test for a variety of mixtures and temperatures. As proposed, a peak load of the monotonic DC(T) test was used as a reference value for determining magnitudes of loading for the cyclic DC(T) test, which further details were presented in the next chapter. So, a selection of the loading rate for the monotonic DC(T) test was decided based on test results of the cyclic DC(T) test. Consequently, if a loading magnitude of the cyclic test, which was about 85-90% to the reference peak load, provided an approximate number of cycles to a failure (N_f) between 100 and 300 cycles, the loading rate associating to the reference peak load was chosen to perform the monotonic test for a given test temperature. As a result, As a result, the loading rates for the monotonic DC(T) test in this particular study are:

A loading rate of 0.5 mm/min was used for temperatures of -12^{o}C and 0^{o}C,

A loading rate of 1.0 mm/min was used for temperatures of 10^{o}C, and

A loading rate of 2.0 mm/min was used for temperatures of 20^{o}C.

Figure 3.20 and Figure 3.21 present a summary of the peak load and fracture energy of all mixtures regarding to the proposed loading rates. In addition, Figure A.13 in the appendix A provided the summary plots of the load-displacement curves of the mixes corresponding the proposed loading rates for the monotonic DC(T) test. The peak load was used to be a reference value for determining loading magnitudes of the cyclic DC(T) test and fracture energy was used to investigate potential correlations between monotonic and cyclic fracture behaviors, as well as prediction models, which they all were provided in the chapter 4 and chapter 5.

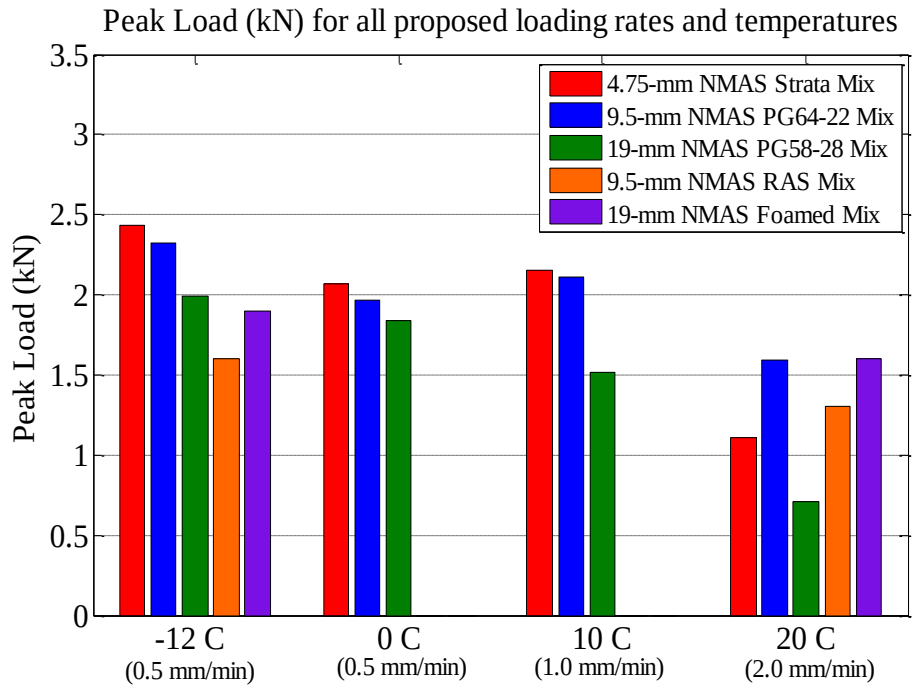

Figure 3.20 Summary of peak loads of all mixtures associated to proposed loading rates of all test temperatures.

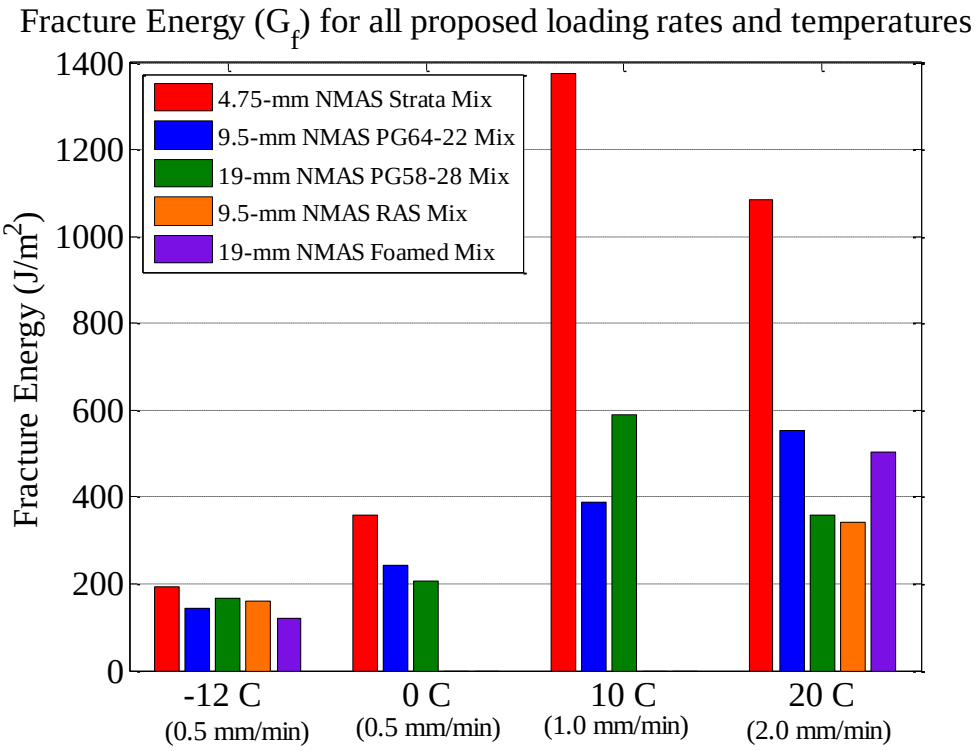

Figure 3.21 Summary of fracture energy (G_f) of all mixtures associated to proposed loading rates of all test temperatures.

3.5 Summary

The disk-shaped compact tension (DC(T)) test was first introduced by Wagoner et al (2005) to evaluate the low temperature fracture behavior of the asphalt concrete (AC) mixtures. The fracture energy was the used to describe the amount of required energy to complete fracture processes of crack initiation, crack propagation and failure under monotonic loading phenomena. In addition, the DC(T) test utilizes cylindrical specimens, which are more readily available as compared to flexural beams.

Monotonic and cyclic fracture behavior of asphalt mixtures was evaluated using an identical test configuration in order to investigate potential correlations between specimen responses under these two distinct load types. However, some issues were found when conducting cyclic tests with the standard sample configuration and test setup, resulting in a revision of the standard DC(T) test. This can be summarized as follows:

- Due to possible fracture near loading holes using the standard DC(T) test under cyclic loading for some types of mixes, such as stone mastic aggregate (SMA) or 19-mm or larger NMAS mixes, the standard geometry was modified. As a result, a far more robust DC(T) geometry was made to be able to handle repeated loading. By comparing test results between the standard and modified DC(T) geometries, both peak load and fracture energy of the standard DC(T) geometry were slightly larger than those of the modified geometry (due to reduced ligament area). Also, differences in fracture energy between the two geometries varied with test temperatures (warmer temperatures were associated with greater differences in the fracture energy.

- The study also proposed to evaluate fracture behavior not only at low temperatures, but also in the intermediate temperature range by testing at 10ºC and 20ºC. However, the crack mouth opening displacement (CMOD) measurement, which is part of the standardized DC(T) test for the sake of simplicity, was combined with the effect the material compliance that would potentially mask the intrinsic fracture behavior. Thus, the crack tip opening displacement (CTOD) location, which theoretically provided true fracture parameters as directly measured at a crack or notch tip, was considered.

- Unstable test results occurred when true CTOD test control was attempted, such that inexistence of the softening curve and two peak-load phenomenon were found. Therefore, a relocation of the 1-cm offset CTOD, shifted toward the loading holes, was proposed to perform the DC(T) test. A major goal of this setup was to strike a reasonable balance between material compliance issues at CMOD location and unstable test control at

CTOD location. Moreover, another benefit was that separation was fully captured by standard clip gages such that extrapolation of test result was not required to compute fracture energy.

- Effect of temperature on fracture properties was evaluated. Peak load and peak fracture energy were both found to occur in the middle of the temperature range considered in this study.

- Due to the fracture behavior of the AC mixtures at intermediate test temperatures, a single loading rate may not be suitable to conduct the DC(T) test for a wide range of test temperatures. Hence, the effect of loading rates was evaluated. Regarding the test result, it showed that the higher loading rate, the greater peak load, as well as fracture energy. So, a question was raised as to which level of the loading rate should be used to perform the monotonic DC(T) test.

- A selection of the loading rate for different test temperatures was examined. The decision was made based upon test results of the cyclic DC(T) test. If a loading magnitude of 85-90% to a peak load producing a number of cycles to failure (N_f) of around 100-300 cycles, the loading rate associated to that particular peak load was chosen. As a result, the loading rates for the monotonic DC(T) test in this particular study are:

A loading rate of 0.5 mm/min was used for temperatures of -12^{o}C and 0^{o}C,

A loading rate of 1.0 mm/min was used for temperatures of 10^{o}C, and

A loading rate of 2.0 mm/min was used for temperatures of 20^{o}C

- Peak load from the monotonic DC(T) test results was used as a reference value to determine loading magnitudes of the cyclic DC(T) test, and fracture energy was analyzed with test results of the cyclic DC(T) test to investigate prediction models of cyclic loading mechanisms, where details are presented in Chapters 4 and 5.

Chapter 4 Fracture Behavior Under Cyclical Loading

4.1 Introduction

Pavements are generally subjected to repeated loading from vehicles and thermal loading. As a result, pavement performance is strongly linked to the material's ability to withstand these repeated loading forms. In addition to traditional fatigue cracking, thermal, block, and reflective cracking involve large, discrete crack patterns in pavements induced by repeated loading which are costly to repair and maintain. Unlike traditional fatigue studies, discrete cracking modes generally require a traditional fracture testing geometry to elicit realistic pavement fracture behavior.

Experimentally, discrete fracture tests such as the disk-shaped compact tension test (Wagoner et al., 2005) are now standardized and being implemented in the United States to control low temperature cracking. However, dealing with cyclic, discrete cracking is a more complex endeavor, yet to be completely understood let alone standardized. Regarding to the objectives of the study, the cyclic fracture behavior of the AC was evaluated using the disk-shaped compact tension (DC(T)) test geometry and the released-energy based approach for data analysis. Because of some drawbacks of the current analytical approaches, as discussed in Chapter 2, a new cyclic fracture criterion was examined using a concept of the released energy that indicated damage occurring within a material, evaluated through the load-displacement relation. Therefore, this chapter primarily presents the experimental evaluation of cyclic fracture behavior.

Concept of released energy

A released energy concept of fracture mechanics was extensively employed to study fracture behaviors of the AC materials because it provided a fundamental concept of how material properties changed or degraded after being subjected to cyclic loading (Van Dijk, 1972). This has been done by considering a relationship between load and displacement or stress and strain of the cyclic loading. Currently, approaches of initial dissipated energy (IDE) by Rowe (1993) and SHRP (1994), total dissipated energy (TDE) by Chomton (1972) and Tayabali et al (1992), and ratio of dissipated energy change (RDEC) by Carpenter et al. from 1997 to 2007, were utilized the released-energy concept to evaluate cyclic fracture behaviors of the AC. However, these approaches did not describe true fracture mechanisms of the AC mixtures. For example, a total number of cycles to failure

(N_f) was related to an initial dissipated energy of the first 50 cycle for the IDE approach and the N_f was correlated to a summation of all dissipated energy for the TDE approach, which these criteria only represented a particular stage of the entire loading mechanism. Also, a ratio change of dissipate energy (RCDE), which was the latest approach, was claimed to be a fundamental property being in charge of the cyclic loading behavior of the AC mixes. Nevertheless, a fracture criterion of the plateau value (PV) was obtained from a partial stage of the entire loading regions. Also, the PV value was difficult to be determined due to scattering data on the RCDE plot. In addition, a PV computation remained based on the traditional fatigue approach of the number of cycle to failure (N_{f50}) which was arbitrarily defined by a 50-percent reduction in an initial stiffness.

Conceptually, when an external loading was removed from an object, if a deformation is fully recovered, no damage occurred within the material. Conversely, if not, the damage was created via energy released into the material. The released energy can be evaluated through a relation between load and displacement which is commonly presented in the form of loaded and unloaded paths, so-called a hysteresis loops, as shown in Figure 4.1. The area encompassed by the hysteresis loop was considered as the released energy. By studying a nature of the released energy of cyclic loading, this fundamental concept provided a promising tool to evaluate AC performance.

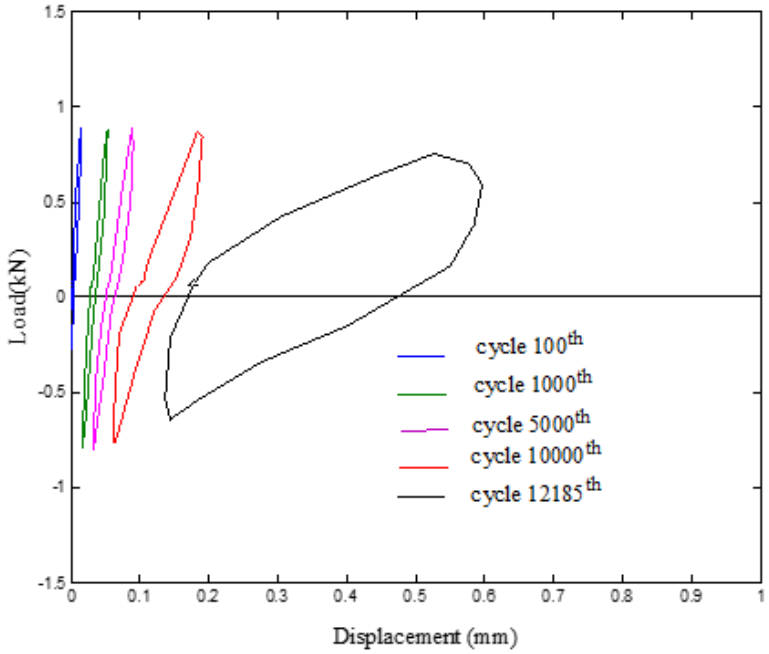

Figure 4.1 Loaded and unloaded paths or hysteresis loops of cyclic loading.

To complete the objectives of the study, a development of practical test procedures for the cyclic loading test, a test setup of the cyclic DC(T) test, materials and experimental

design, and an examination of the new cyclic fracture criterion were provided and discussed in the following sections.

4.2 Test setup

Currently, standard test procedures of the cyclic DC(T) test were not available. As a result, the cyclic DC(T) test was developed based on the monotonic DC(T) test; therefore, this section presents some adjustments of the standard DC(T) test (ASTM D7313-07), including modification of loading fixture, selection of test variables, and test procedures for cyclic DC(T) test. Also, some contents were referred to the monotonic DC(T) test, which was presented in the chapter 3.

4.2.1 Modification of loading fixture

Regardless of loading mechanisms, the identical test setup of DC(T) geometry, loading fixture, and other test apparatus used for the monotonic DC(T) test was also employed for the cyclic loading test. However, a problem was found on test results of the cyclic loading test using the monotonic test setup. Figure 4.2 presents data acquisition of the applied load and measured displacement from the cyclic DC(T) test. This trial was conducted under a load-controlled mode with an amplitude of the 1-kN sine waveform.

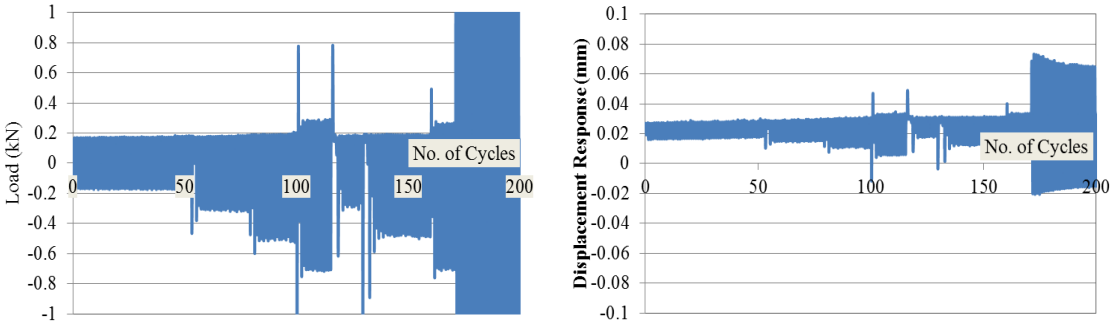

Figure 4.2 Applied load (left) and measured displacement (right) resulting from standard loading bars.

Based on the data acquisition, a loading magnitude of 1 kN was not able to be controlled as assigned as shown in Figure 4.2 (left), resulting an inaccurately response of measured displacement as presented in Figure 4.2 (right). Several tests were tried with other loading magnitudes and test variables, but similar test results were found. Regarding to the test machine, a test was vertically loaded so that a gravitational force was associated to the test. As a result, such a problem was created by an unstable movement or “rocking” of the

test specimen inside a gap between the loading holes and bars due to a transition phase between tensile and compressive loading. In order to solve the problem, modified loading bars were invented. Figure 4.3 illustrates pictures of standard loading bars (left) and the modified loading bars (right).

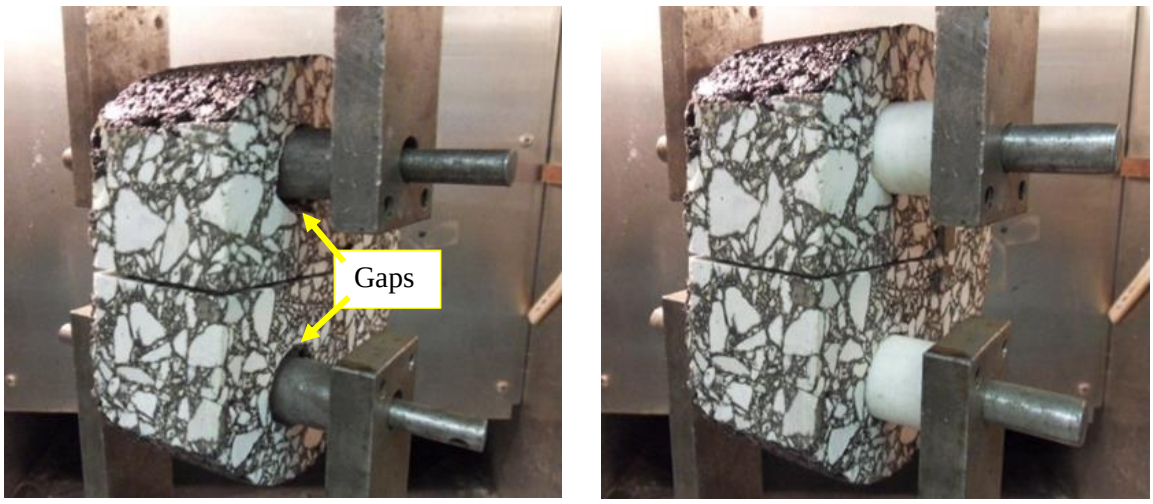

Figure 4.3 Standard loading bars (left), and modified loading bars (right).

The modified loading bars were made of a Teflon tube embedding on the original loading bars. A major purpose was to reduce a gap between a loading bar and a hole of the specimen in order to minimize unstable movement while testing. In addition, Teflon was used for easily inserting the bars into a specimen to provide frictionless and also to reduce bending moment at the notch tip.

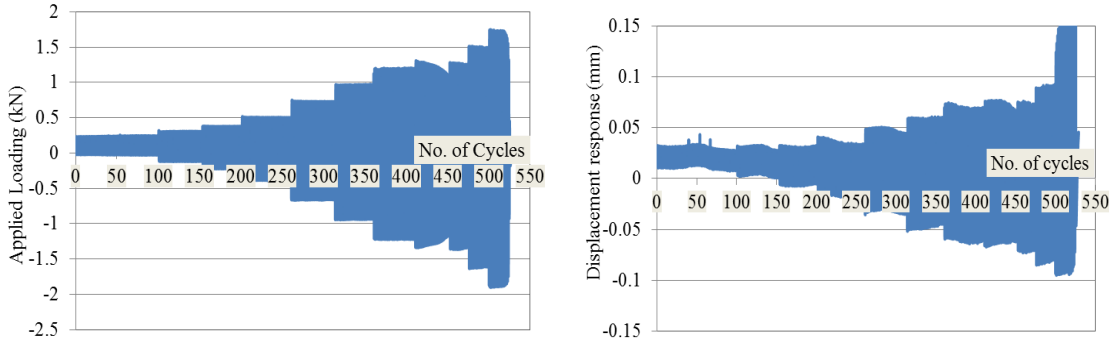

Figure 4.4 Load-controlled (left) and measured CMOD (right) using modified bars.

For a verification of the modified loading bars, as presented in Figure 4.4, the trial was conducted on several magnitudes of loading in order to ensure that loading was precisely applied to the test. So, an amplitude of 0.2 kN was initially applied for the first 100 cycles. Then, an increase of 0.1 kN was added for next 50 cycles up to a cycle of 250.

Next, another 0.5 kN was assigned for the next 50 cycles until a test specimen failed. Based on the data acquisition of using the modified loading bars, cyclic loading was accurately controlled as assigned as presented in Figure 4.4 (left). Also, a measured opening displacement increased corresponding to an increase of the applied loading as illustrated in Figure 4.4 (right). It was noteworthy that the modified loading bar was fit to a hole when the test started, but it was slightly loosen while testing because a deformation of materials around the hole existed due to the viscoelastic effect of AC mixes, especially for intermediate test temperatures of 10^{o}C and 20^{o}C.

4.2.2 Selection of test variables

Regarding to the literature review, pavement performance under cyclic loading is influenced by many factors. Experimentally, these factors or test variables for the cyclic loading tests typically include mode of loading (either load-controlled or displacement-controlled), shape of waveform, magnitude of loading, frequency of test, and rest period. Hence, this particular section provides a summary of the test variables selected to perform the cyclic DC(T) test in the study.

Pattern of loading

Two modes of loading are commonly used in cyclic loading tests: load- or stress-controlled and displacement- or strain-controlled. According to the current fatigue tests, for example, four-point bending beam and push-pull tests, the strain-controlled mode was preferably selected to perform a test because of accommodating the stress-stage consideration and stability of cracking. However, a major concern was that, in the displacement-controlled case, a true failure or rupture of test specimens barely existed due to a decrease of the applied load, resulted from a material degradation. As a result, a fatigue criterion was arbitrarily defined relating to a specific level of damage. Conversely, for the load-controlled mode, a test was closer to what happened in the field because a pavement was typically subjected to loading of vehicles, regardless of different loading magnitudes. To evaluate such effects of the test variables, four cases were examined to verify which case was most suitable for performing the cyclic DC(T) test. These cases included (1) strain-controlled with haversine waveform, (2) strain-controlled with sine waveform, (3) stress-controlled with haversine waveform, and (4) stress-controlled with sine waveform. The results and discussions are follows.

Case 1: strain-controlled mode with shifted sine waveform. Based on the result shown in Figure 4.5, an applied load of the next cycle required less than that of the previous cycle because of a need of less energy to produce the same amount of an opening displacement. Consequently, a crack initiation barely existed, especially in cases of low strain levels. Moreover, the shifted sine waveform only provided tensile loading that accelerated a rate of creep compliance.

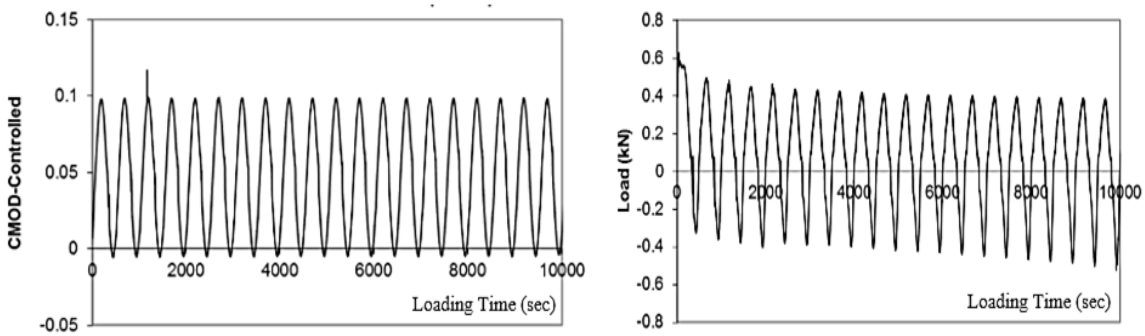

Figure 4.5 Case 1: strain-controlled with shifted sine waveform.

Case 2: strain-controlled mode with reversing sine waveform, the result of this case had the same trend as case 1 that required loading of the next cycle was less than that of the previous cycle as a function of the material degradation (Figure 4.6). However, a difference was the reversing sine waveform was applied that both tensile and compressive loading presented which the creep effect was minimized as the creep rate decreased due to an application of the compressive loading.

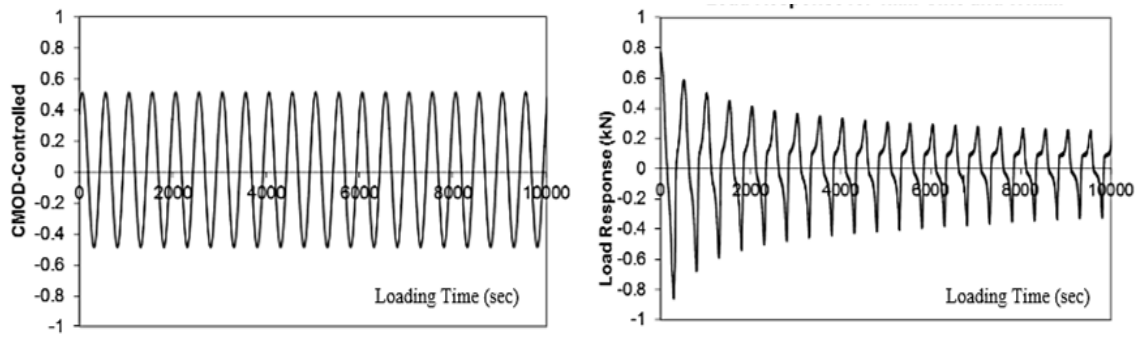

Figure 4.6 Case 2: strain-controlled with sine waveform.

Case 3: load-controlled mode with shifted sine waveform. Similar to case 1, the shifted sine waveform was used where only tensile loading was applied to the specimen. However, the load-controlled mode was used in this case. As a result, the measured displacement or a separation of the specimen increased with loading time because more energy released under the load-controlled mode (Figure 4.7). Therefore, to study true

fracture behavior, the load-controlled mode is better than the displacement-controlled mode as an existence of cracking processes of crack initiation, crack propagation, and true failure.

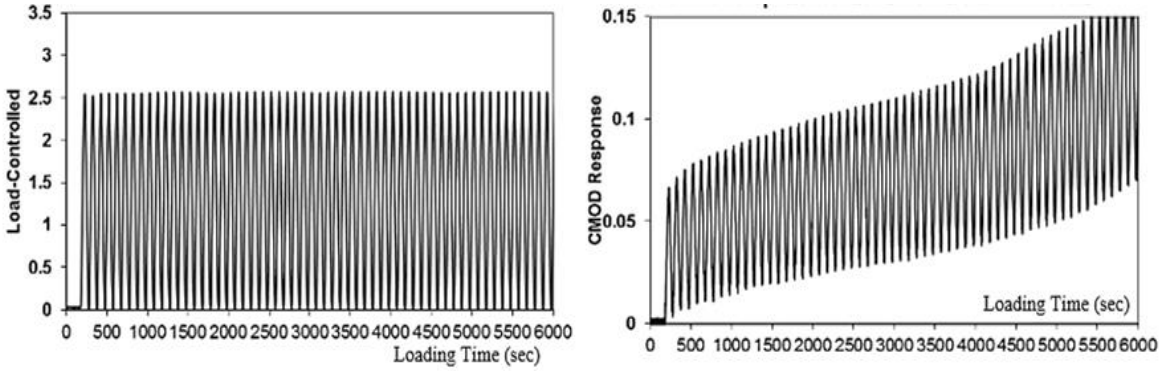

Figure 4.7 Case 3: Load-controlled with haversine waveform.

Case 4: load-controlled mode with reversed sine waveform (Figure 4.8). This case provided the most suitable test parameters to study cyclic loading behavior. Firstly, the load-controlled mode was the closest simulation to the field as a pavement was more likely to be controlled by loading from vehicles. Also, a rupture or true failure was presented. Secondly, both tensile and compressive loading were applied under the sinusoidal waveform which in the reality a pavement was subjected to both types of loading. Additionally, the rate of creep compliance decreased as the application of the compressive loading.

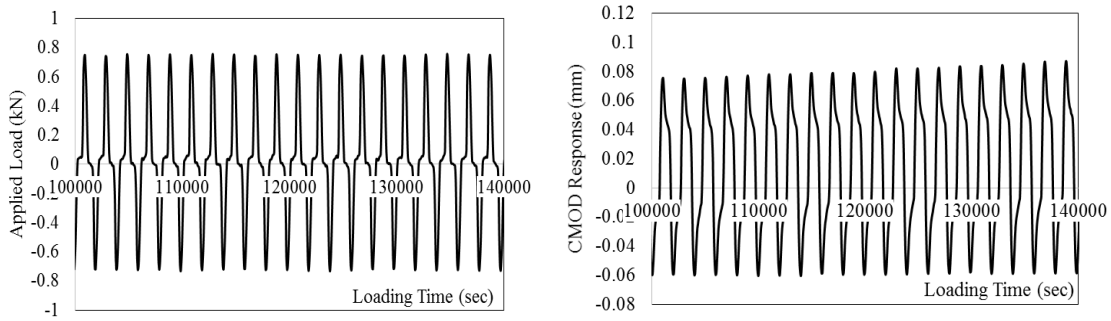

(a) Case 4: Load-controlled with sine waveform.

Figure 4.8 Effects of different mode of loading and loading waveforms**.**

For this study, a load-controlled, reversing, sinusoidal waveform was selected for the cyclic DC(T) test, using the modified DC(T) geometry and 1-cm offset CTOD location previously described. Ultimately this testing mode was selected based on practical considerations and robustness of data produced. The load control mode produced stable crack growth across a broad range of load levels, whereas CMOD control did not lead to significant crack growth except for high initial CMOD levels, which sometimes produced

rapid failure. In addition, load control is a much simpler mode for cyclic test control and more desirable for a practitioner-friendly test. Reversing loads were selected in order to negate creep behavior, which would otherwise be present if only tensile loads were applied. This is a distinct advantage of the DC(T) over other proposed cyclic tests, such as the cyclic indirect tensile (IDT) or semi-circular bend test (SC(B)), which cannot be practically subjected to reversing load forms.

Magnitude of loading

Cyclic fracture behavior is obviously strongly related to the magnitude of repeated loading, where repeated loads of higher magnitude are associated with relatively lower number of cycles to failure (N_f), and vice-versa. In this study, magnitudes of loading for the cyclic DC(T) test were determined based upon peak loads measured in the monotonic DC(T) test, using the modified DC(T) geometry presented herein. Peak load of monotonic DC(T) test result, associating to the same mixture and test temperature for a cyclic loading test, was used to establish the upper limit or 100% loading (tension and compression) amplitude levels for the sinusoidal waveform. For example, Figure 4.9 presents the loading waveform for 60% case. With the same procedure, other loading magnitudes were determined as different percentages to peak load.

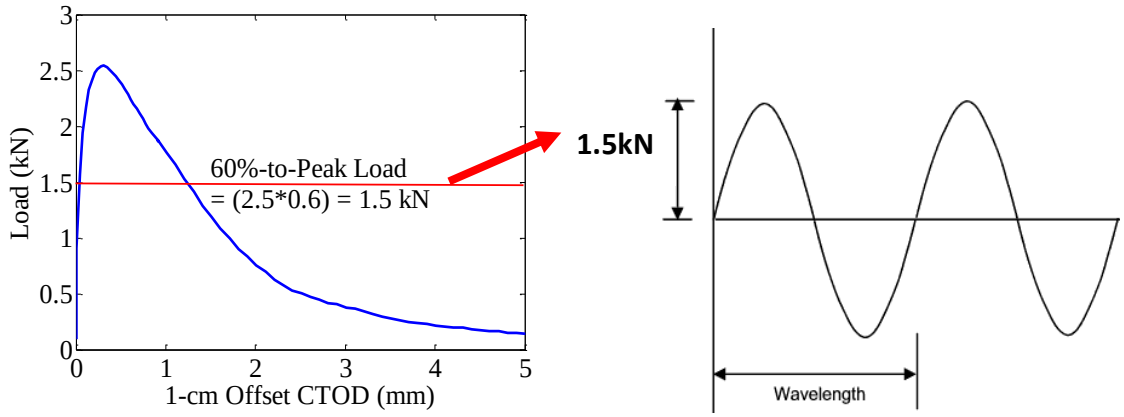

Figure 4.9 Example of loading magnitude definition for cyclic DC(T) test.

4.2.3 Test procedures

Similar to the monotonic DC(T) test, all cyclic loading tests was conducted using an Instron 8500 with a capability of 100 kN load frame. An environmental chamber had a capable to control a temperature of -30 to 30°C. A 10-kN load cell was used to perform a cyclic loading test. To study intrinsic fracture behavior of both monotonic and cyclic loading mechanisms, the new adjustment was proposed for the modified DC(T) geometry

and relocation of the 1-cm offset CTOD as shown in Figure 4.10. The adjustment was to address issues of the compliance effect at CMOD location and the high stress concentration at a notch tip or the CTOD location, which previously discussed in the chapter 3.

Unlike the monotonic DC(T) test, a series of cyclic loading was applied on the cyclic DC(T) test, which currently test procedures were not specified. Therefore, to be able to perform the cyclic DC(T) test, steps are provided as follows:

1. Conditioning – the fabricated specimens shall be placed in the temperature controlled chamber for a minimum of 2 hours.

2. After conditioning, insert a specimen into loading fixtures using the modified loading bars. No seating load is applied on the specimen, which the initial loading shall be started at 0 kN. Also, a strain channel was zeroed, which this step is the same as what has done for the monotonic DC(T) test.

3. For cyclic test parameters, on the control panel of the test machine, the sinusoidal (sine) waveform was selected with a frequency of 0.5 Hz, and no a rest period of time was applied.

4. Magnitudes of loading were designed based on a value of the peak load obtained from the monotonic DC(T) test that the maximum loading would be equal to the peak load. In order to evaluate cyclic loading behavior, an amplitude of loading waveform shall be less than the peak load as the maximum load carrying capacity of the material. A test was also recommended to perform high cyclic loading first, which an approximate 85-90% to the peak load was used as a half amplitude of the sine waveform. Then, a decrease of about 5-10 percent of the loading magnitude was recommended for the next specimen, depending on an availability of the test samples.

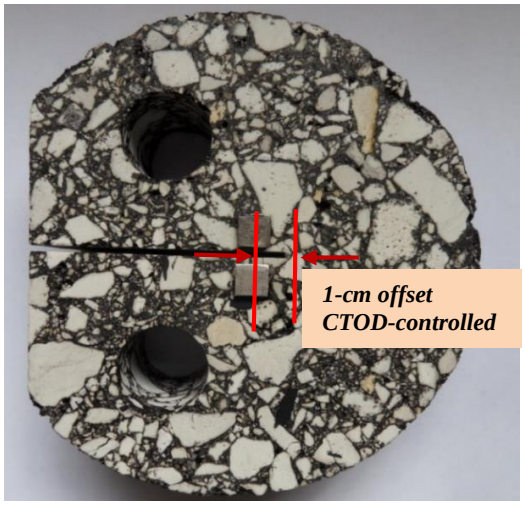

Figure 4.10 Modified DC(T) geometry with 1-cm offset CTOD.

4.3 Materials and experimental design

For the materials, five identical asphalt concrete mixtures, which were used to study the monotonic fracture behavior, were also used for the cyclic DC(T) test. To sum up, these mixes include Strata, PG64-22, PG58-28, RAS, and foamed mixes. Similar to the monotonic test, the based mixes of the Strata, PG64-22, and PG58-28 mixes were conducted on all proposed temperatures of -12, 0, 10, and 20^{o}C. However, RAS and foamed mixes were only conducted on temperatures of -12^{o}C and 20^{o}C for a verification at test temperatures of -12^{o}C and 20^{o}C, representing scenarios of thermal cracking and fatigue cracking, respectively. The gradations and volumetric properties of the mixes were presented in the material section of the chapter 3.

In terms of the experimental program for the cyclic DC(T) test, the following test parameters were used:

- Mode of loading: load-controlled
- Wave shape: sinusoidal, reversing
- Frequency: 0.5 Hz
- Number of replicates: 10-13 reps per mixture for each test temperature
- Magnitude of loading: different percentages of peak load of monotonic peak load for a given same mixture and test temperature. The highest magnitude used was in the range of 85-90% of the peak monotonic fracture load, based on experience. Lower load levels at intervals in the range of 5-10% were used, until more than 50,000 cycles were required to fail the specimen (after which, no tests with further reduction in loading was attempted)
- The subjects of fatigue endurance limit, rest periods, and healing were not considered in this stage of the study, but are certainly important directions to consider in future research.

4.4 Test results

Applied load and measured CTOD was obtained from the modified DC(T) test, producing the expected hysteresis loops when plotted. Figure 4.11 illustrates an example of a graphical comparison of the load-displacement relation between the monotonic and cyclic DC(T) test results. Note that the monotonic DC(T) test was controlled in the normal fashion with constant opening rate of the displacement, whereas a load-controlled mode of loading was used for the cyclic DC(T) test. Both loading approaches created an existence

of fracture processes of crack initiation, crack propagation, and complete failure of the test specimen, as shown in Figure 4.11 that a material separation increased along the x-axis of the displacement until the specimen failed.

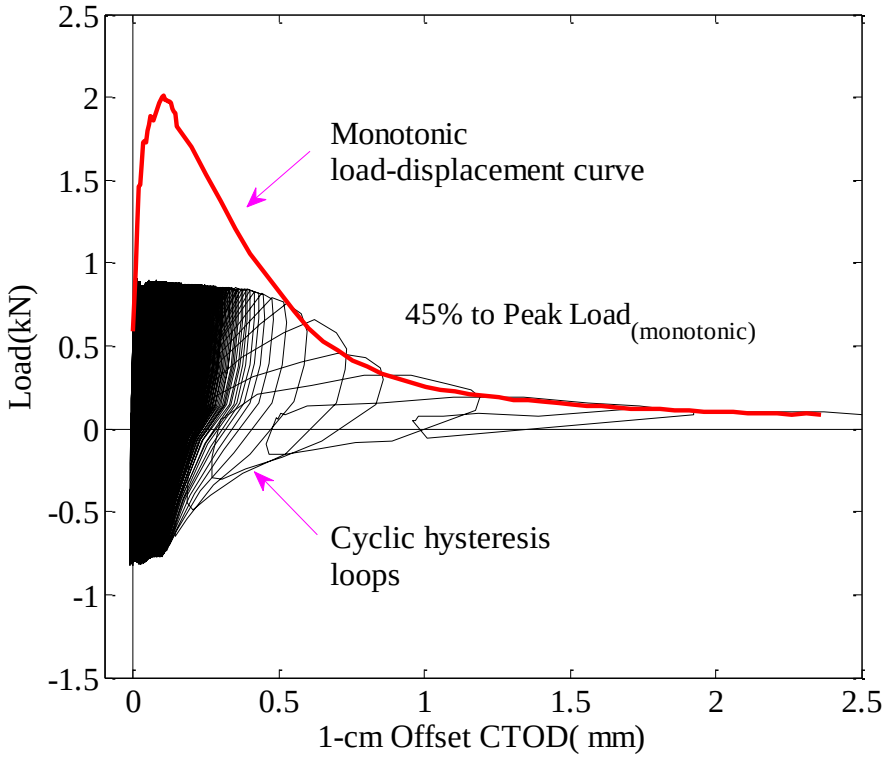

Figure 4.11 Example of comparison of load and displacement relation between monotonic and cyclic DC(T) test results.

Interestingly, when average monotonic test results were plotted against a typical cyclic test result, the monotonic test result appears as a failure envelope for the cyclic test on the tension side of response (Figure 4.11), This phenomenon happened to all of the other test conditions, which examples of the plots for other mixes and temperatures were presented in appendix D. This suggests a unique relationship in the load-separation behavior of asphlat mixtures tested in a similar geometry regardless of monotonic vs. cyclic loading. This in turn suggests that pavement models involving progressive fracture under varied load levels may possibly be simplified based on this observed fracture behavior. An interesting observation in this behavior is that the machine control loop was unable to 'close the loop' in the final load cycles, as the material behaved according to the failure envelope, which eventually dropped below the prescribed repeated load level.

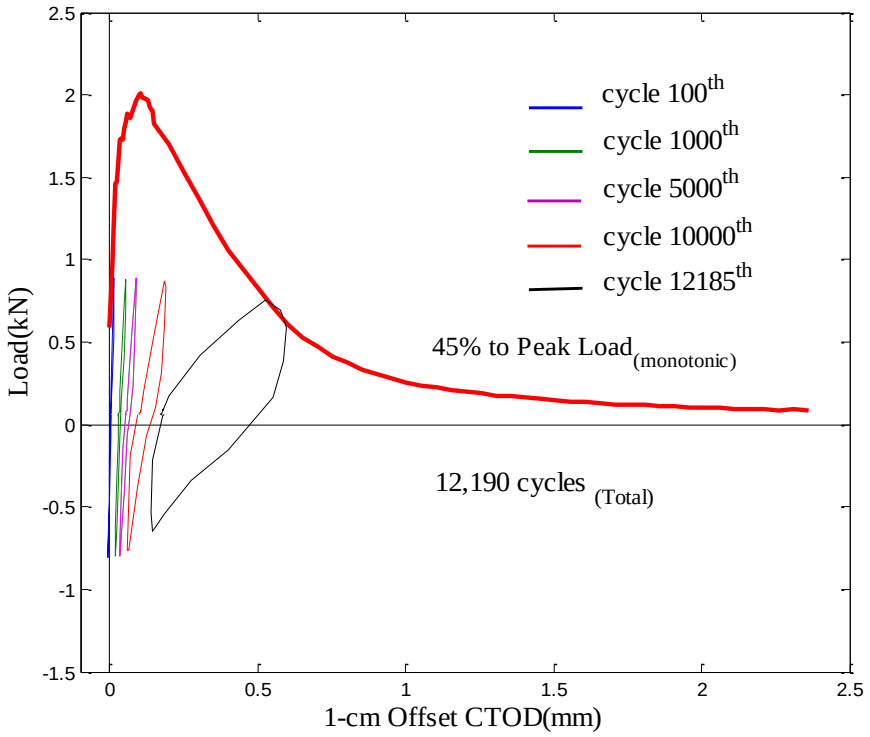

Figure 4.12 Development of hysteresis loops throughout cyclic loading mechanism.

To provide a general idea how cyclic loading exhibited throughout the test, Figure 4.12 presents a development of the hysteresis loops of some loading cycles between the beginning and the end of the test. Hysteresis loops were relatively small in the early stage of loading. Then, it became larger and larger until the specimen failed. According to a concept of the released energy, this event was explained as each hysteresis loop represented an amount of the energy released into the material. At the initial stage of loading, a small amount of released energy as minor damage occurred within the material. Then, the larger loop, the more damage created as a function of a material degradation. In addition, regarding to the comparison plot of the load-displacement curves between the monotonic and cyclic tests, an approximate half of the total number of cycles to failure (N_f) existed in the pre-peak region of the monotonic load-displacement curve for most cases.

4.4.1 Released Energy Development (RED) Model

A key aspect of data analysis was to determine cyclic fracture parameters and to attempt to develop prediction models to describe fracture behavior of the AC mixes under cyclic loading for eventual use in simplified design approaches considering cyclic fracture. As proposed, the released energy approach was employed to characterize a behavior of the

material that the concept provided how damage occurred within the material after being subjected to repeated loading.

Based upon the released energy concept, the released energy occurring during each loading cycle, which was defined as the surrounding area within the hysteresis loop in a full loading cycle, was plotted against number of the cycles. Figure 4.13 presents plots of released energy versus a number of cycles (right), associated with a given the load-displacement plot (left) for two different loading magnitudes: high cyclic fracture (HCF) and low cyclic fracture (LCF) tests for the 9.5-mm NMAS PG64-22 mix performed at 20°C. Similarly, the same procedures were employed for the other mixtures and test temperatures to evaluate cyclic loading behaviors of the AC mixes. As results, similar plots to Figure 4.13 for other test variables, such as different mixes, test temperatures, and loading magnitudes, were presented in the appendix D.

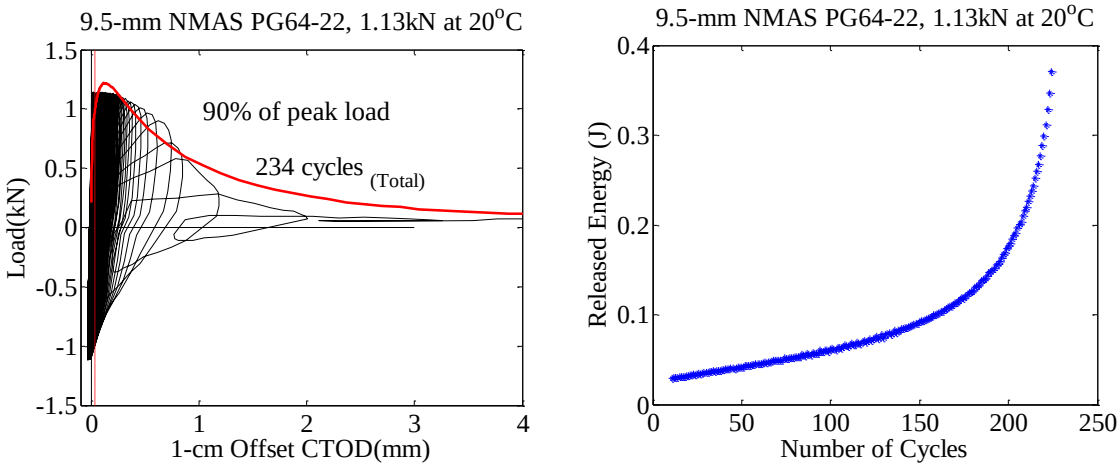

Case 1: Low cyclic Fracture (LCF) test.

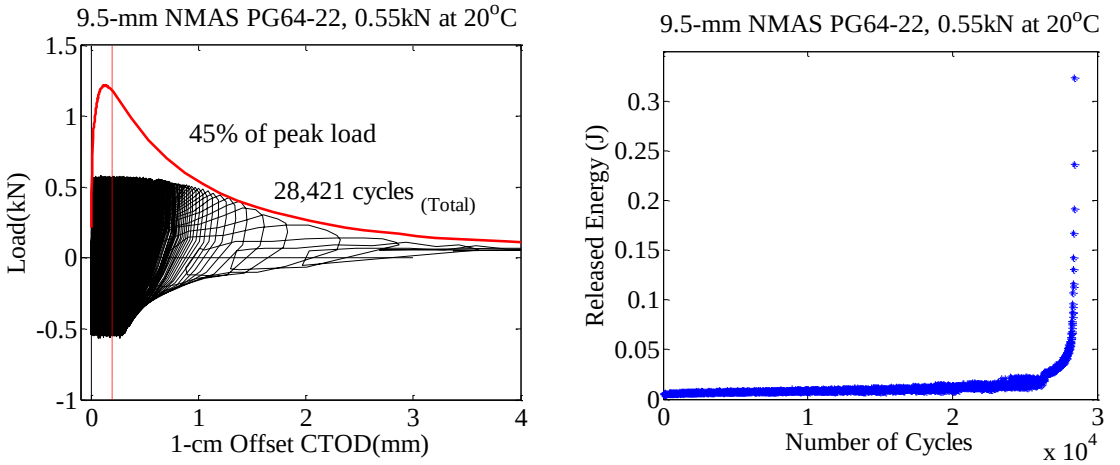

Case 2: High Cyclic Fracture (HCF) test.

Figure 4.13 Development of released energy (right) corresponding to load-displacement relations (left) for LCF and HCF cases of PG64-22 mix performed at 20°C.

Regarding the released energy (RE) versus number of cycles to fracture (N_c) relation, a unique characteristic of the curve was found. The behavior was very accurately captured using a simple exponential function (Figure 4.14), which the exponentials are often used when a rate of change of a quantity is proportional to the initial amount of the quantity. Based on such a unique feature of the RE-N_c plots, the two-term exponential function was required to fit a model as an existence of two different growth rates in the RE-N_c curve.

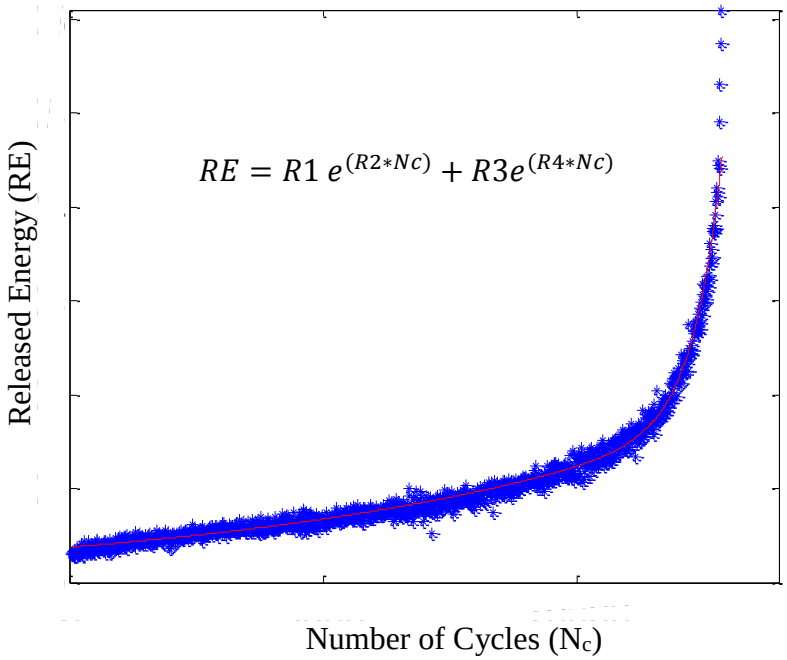

Figure 4.14 Typical released energy development (RED) curve of describing cyclic fracture behavior of an asphalt concrete mixture.

As a result, a two-term exponential function, termed herein as the released energy development (RED) model is given as

$$Released\ Energy\ (RE) = R1e^{(R2*N_c)} + R3e^{(R4*N_c)}$$

where N_C presents cycle number, and R1, R2, R3, and R4 are material coefficients defined as released energy factors or parameters.

In order to verify that the second term of the exponential function was necessary to fit the RED model. Figure 4.15 presents comparisons of two different exponential fitting models for two loading magnitudes: low cyclic fracture (LCF) and high cyclic fracture (HCF) tests.

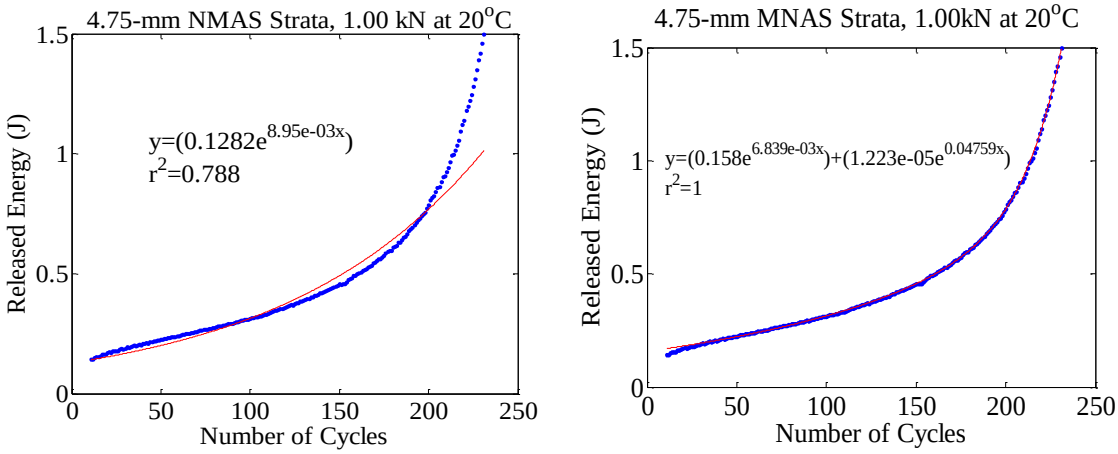

Case 1: Low Cyclic Fracture (LCF) test.

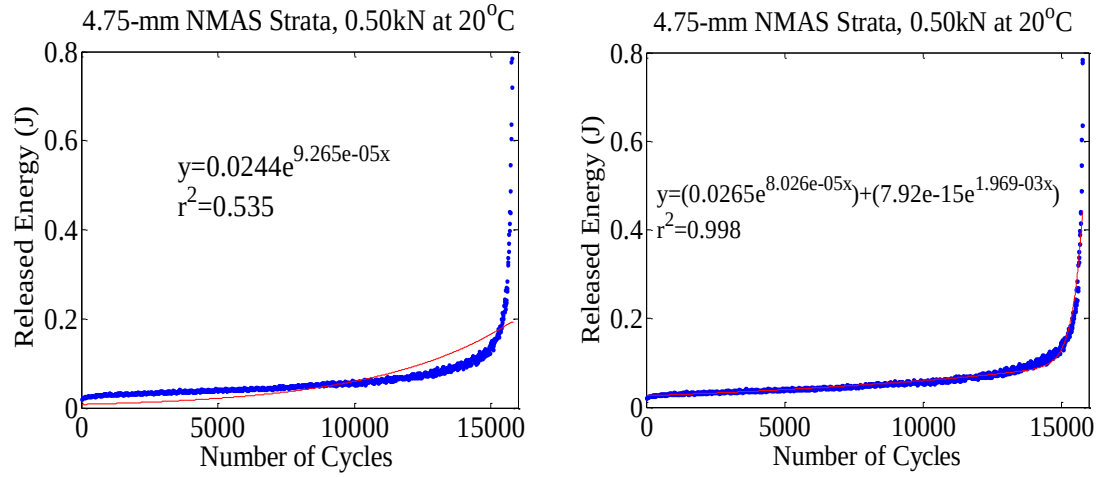

Case 2: High Cyclic Fracture (HCF) test.

Figure 4.15 Comparison of fitting models for LCF and HCF tests.

Table 4.1 Comparison of R1 and R2 coefficients for different models.

Case	N_f (cycles)	# of Terms (1)	R1	R2	R^2
LCF	243	1	0.1282	8.95E-03	0.788
		2	0.1580	6.84E-03	1
Difference			0.0298	0.0021	0.212
HCF	15,785	1	0.0244	9.27E-05	0.535
		2	0.0265	8.03E-05	0.998
Difference			0.0021	1.24E-05	0.463

Note: (1) numbers of exponential terms for the fitting model.

Figure 4.15 presents a comparison of the R1 and R2 coefficients obtained from the two different exponential fitting models: with and without the second term of the exponentials. As a result, the R1 was greatly influenced by the second term of the exponentials for the LCF test. Also, using two terms of the exponentials provided better statistical values of the R-square comparing with that of the one-term exponential fitting model, especially in case of HCF test as the R^2 significantly increased by 46 percent. Therefore, the RED model was essentially comprised of two terms of the exponentials with the material coefficients of the R1, R2, R3, and R4 as the existence of two growth rates in the RE-N_C curve.

To accommodate the data analysis, a computer program of Matlab was used to fit such a complicated exponential function, which an example was shown in Figure 4.16. A command of the curve fitting tool or 'cftool' was used to fit the RE-N_c relation as proposed of the RED model. Regarding to the cftool command window, after feeding X and Y data, an exponential fitting curve was selected from a drop box with a number of terms of two. In order to use actually x and y values, instead of x and y mean values, a check box of the center and scale was not supposed to be selected. In addition, to provide a better correlation of the RED model, the fit options command was used for the nonlinear least square fitting. The robust of LAR and the algorithm of Levenberg-Marquardt were recommended.

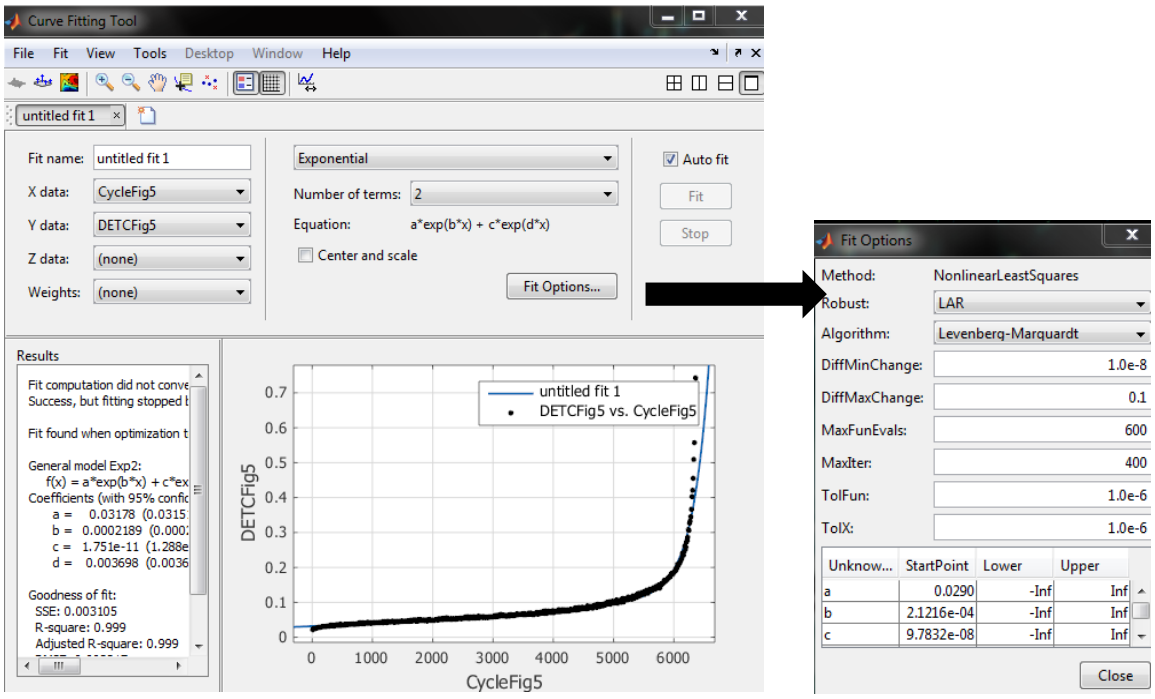

Figure 4.16 Curve fitting tool window in Matlab employed to determine RED model.

Based upon the Matlab data analysis, plots of the RE-N_c curve and RED model of all mixes and test temperatures were derived as presented in the appendix D. Also, a summary of the total numbers of cycles to failure (N_f) and released energy factors, R1, R2, R3, and R4, of the RED model for the temperatures of -12, 0, 10, and 20^{o}C was provided in the Table B.1 in the appendix B.

According to the scope of the study, another goal was to investigate whether high cyclic fracture (HCF) behavior could be predicted based upon test results of the low cyclic fracture (LCD) tests. To accomplish this particular objective, potential correlations of the released energy factors among different loading magnitudes, resulting in different numbers of cycles to failure (N_f), were investigated. As a result, none of correlations was found on the R3 and R4 material coefficients. Even though, the R3 value, which was in a range of 10^{-5} to 10^{-20}, was significantly less than the R1 value, the second-term exponentials could not be eliminated because it essentially provided better fitting for the RED model as an existence of the two growth rates on the RE-N_c relation as early presented. Therefore, the cyclic fracture behavior was assumed to be predominantly dictated by the R1 and R2 material coefficients of the first term exponential function. As a result, potential correlations between a number of cycles to failure (N_f) and the released energy factors of the R1 and R2 were examined, which presented in the following sections.

4.4.2 Characteristic N_f -R1 relation

The released energy factor, R1 was examined for different loading magnitudes for the same mixture and temperature. The R1 coefficient, mathematically explained an initial value of the exponentials, describes the initial released energy during testing. For a given mix and test temperature, by plotting the R1 versus N_f on the semi-logarithm scale, the initial released energy (R1) values for different loading magnitudes was found to be correlated to a total number of cycles to failure (N_f). As a result, Figure 4.17 and Figure 4.18 present the N_f-R1 relation for all study mixtures performed at -12^{o}C and 20^{o}C, respectively. In addition, the similar plots for 0^{o}C and 10^{o}C were presented in Figure B.1 and Figure B.2 in the appendix B, respectively. Regarding to plots of the N_f-R1 relations, a relationship between N_f and R1 was then captured using a power-law function as follows:

$$N_f = C1\left(\frac{1}{R1}\right)^{C2}$$

where N_f is total number of cycles to failure, R1 is the released energy factor obtained from the RED model, and C1and C2 are material coefficients. A summary of the C1 and C2 material coefficients and R^2 of all test temperatures were provided in Table B.2 in the appendix B. A purpose of the Nf-R1 relation is to rank mixture performance, relating to service life. For example, within the same R1, a clear ranking of study mixes was observed as the strata mixture requiring more numbers of cycles to produce complete fracture than that of RAS mixture.

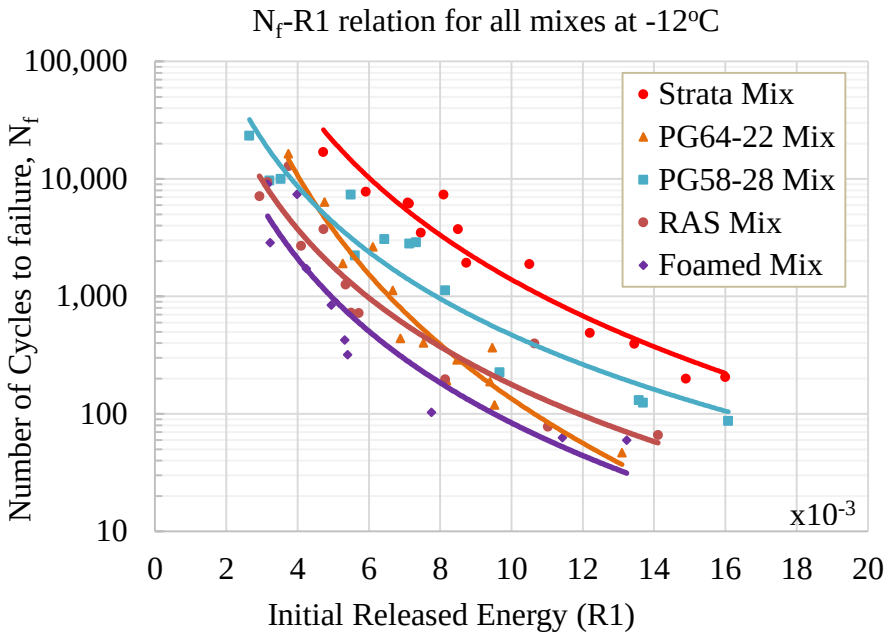

Figure 4.17 N_f-R1 relation of all mixes at test temperature of -12ºC.

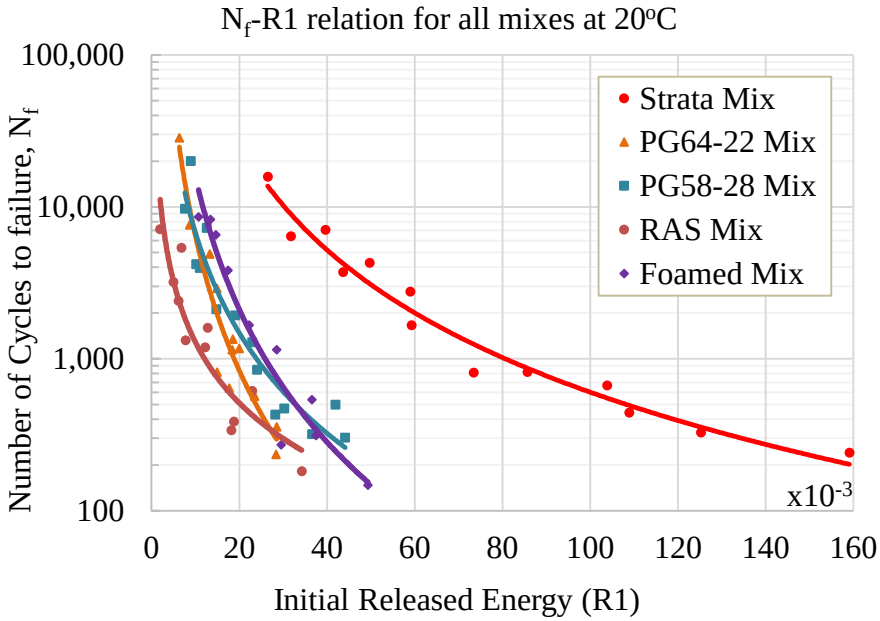

Figure 4.18 N_f-R1 relation of all mixes at test temperature of 20ºC.

Effect of mixtures on N_f-R1 relation

Figure 4.17 and Figure 4.18 demonstrate that the N_f-R1 relationship is mix-depended. A comparison of the material coefficients of the C1 and C2 for each study mixture is presented in Figure 4.19 and Figure 4.20, respectively.

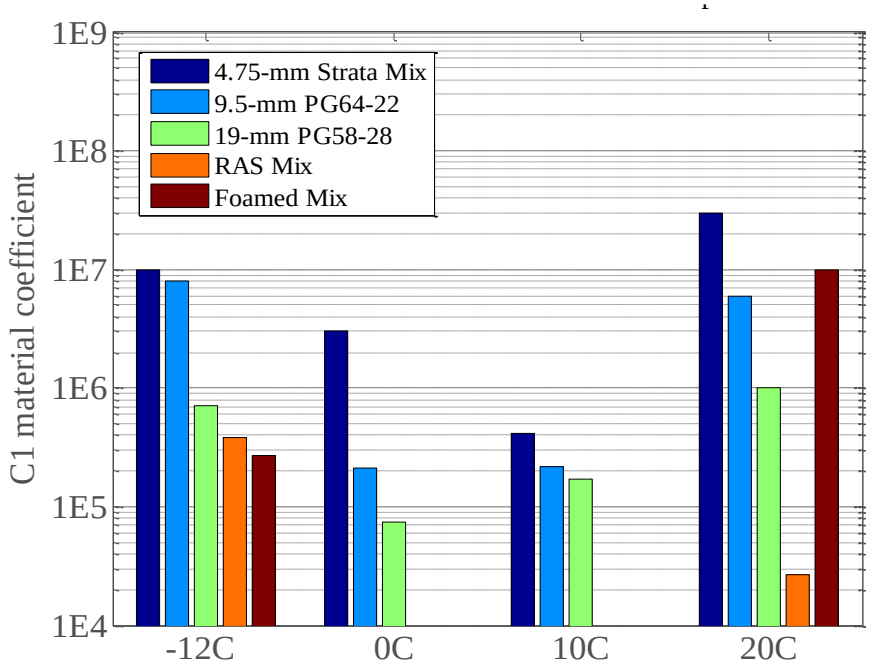

Figure 4.19 Comparison of C1 of mixes for all test temperatures.

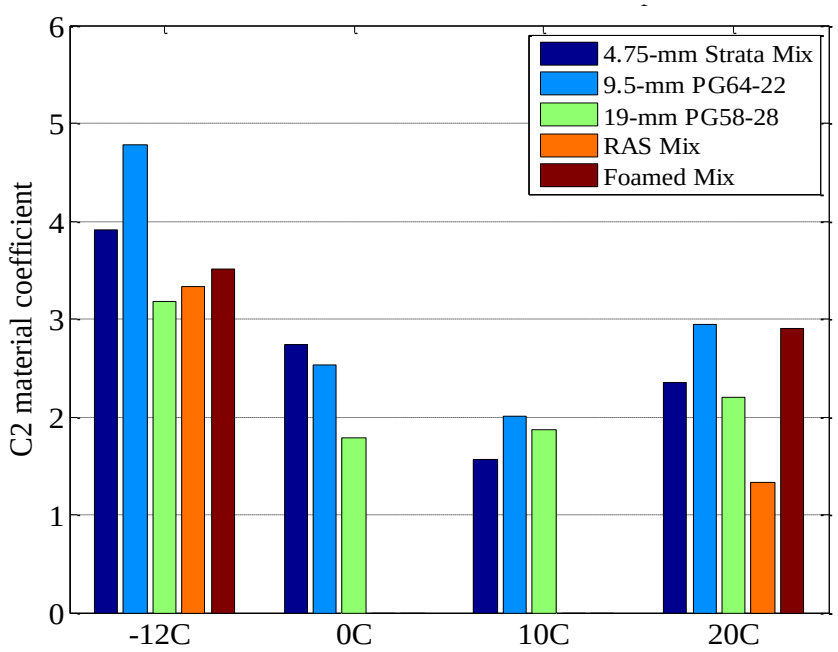

Figure 4.20 Comparison of C2 of mixes for all test temperatures.

The material coefficient C1 appears to be related to the relative fracture resistance of the study mixes. By considering the same level of the initial released energy factor (R1), the C1 values were highly correlated to a number of cycles to failure (N_f), where the higher C1, the longer the service life. As a result, Table 4.2 presents a rank of the mixtures in terms of service life, associated with the C1 values. However, the material coefficient C2, which was in a range of 1 to 5 as presented in Figure 4.20, did not appear to be related to expected relative to performance, except that a trend of the C2 for different temperatures was similar to that of the C1 as decreased with an increase of the temperature, but both C1 and C2 increased when the test temperature conducted at 20°C.

Table 4.2 Ranking of mixture performance associated with C1 coefficient.

Mixture	Temperature			
	-12°C	0°C	10°C	20°C
4.75-mm NMAS Strata	1	1	1	1
9.5-mm NMAS PG64-22	2	2	2	3
19-mm NMAS PG58-28	3	3	3	4
9.5-mm RAS with Eco-binder	4	n/a	n/a	5
19-mm NMAS Foamed mix	5	n/a	n/a	2

Note: lower numbers represent better performance (longer service life).

Effect of temperatures on N_f-R1 relation

The N_f-R1 relation was also influenced by test temperatures. By considering a comparison of the C1 and C2 coefficients of the same mix across different test temperatures, as presented in Figure 4.19 and Figure 4.20, it was found that the C1 and C2 values decreased with decreasing temperatures. Figure 4.21 showed the comparison plot of the N_f-R1 curves of the PG58-28 mix for all test temperatures. Additionally, similar comparisons for other based mixes were provided in Figure B.3 in the appendix B. A disadvantage of the N_f-R1 relationship, from the standpoint of test simplification, is that the model depends on mix type and test temperature. Also, a problem was found for a case of high loading magnitude or HCF tests which yielded the total number of cycles to failure (N_f) less than 100 cycles. The R1 value of the HCF test was not correlated to other loading magnitudes. As a final note, selection of testing load such that a practical minimum N_f of 100 cycles is recommended to maintain a stable N_f-R1 relationship.

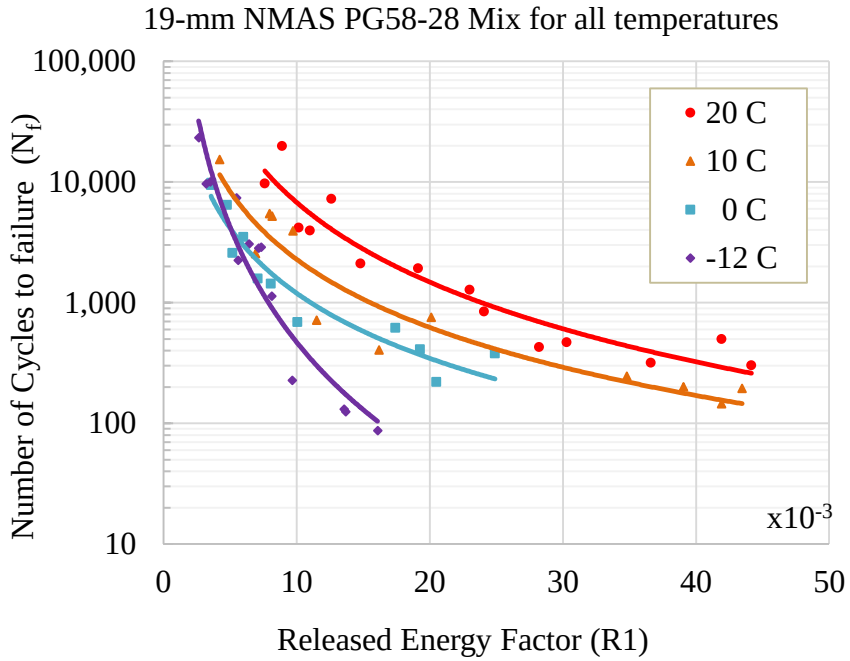

Figure 4.21 Comparison of N_f-R1 curves of PG58-28 mix for all temperatures.

4.4.3 Unique characteristic of N_f –R2 relation

Similar to the other released energy factors of the RED model, a relation between the R2 coefficient and the total number of cycles to failure (N_f) was investigated to evaluate cyclic fracture behavior and possible means towards test simplifications. By definition, the R2 exponential coefficient indicates the growth rate of the released energy, which respected to the initial quantity or the initial released energy of the R1. Figure 4.22 presents a plot of the N_f versus the R2 parameter on a log-log scale. Interestingly, a unique N_f-R2 relationship was found for all study mixtures and test temperatures. As a result, the R2 parameter is proposed as anew cyclic fracture criterion. The apparently unique N_f-R2 relation was mathematically described using the power-law function:

$$N_f = 1.18\left(\frac{1}{R2}\right)^{0.977}$$

where N_f and R2 are as defined earlier.

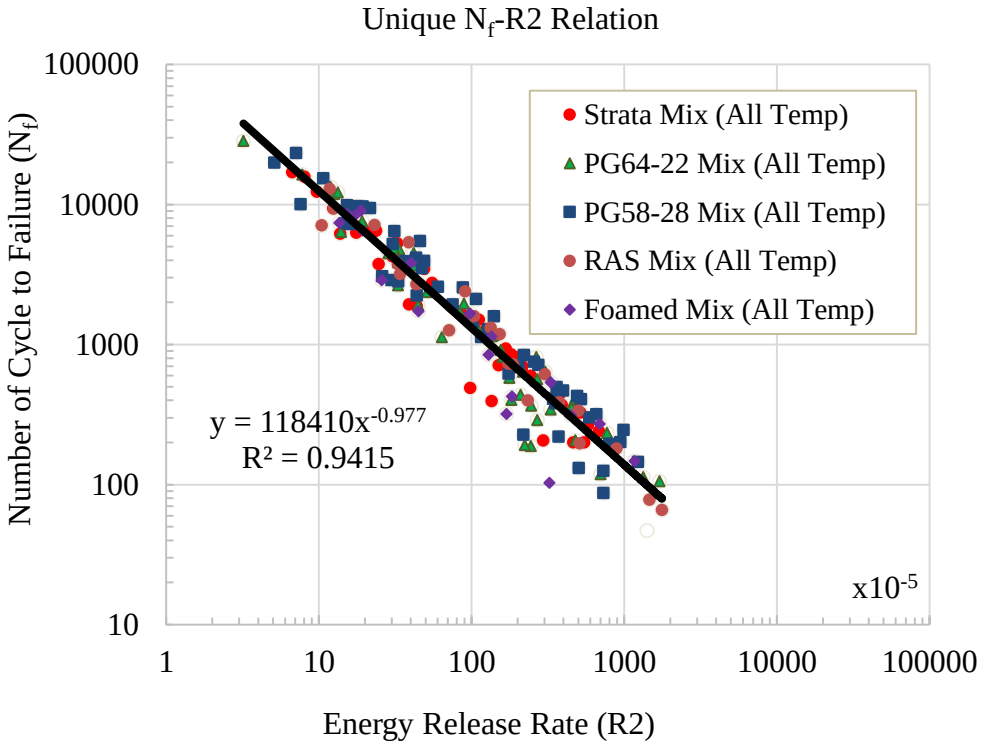

Figure 4.22 Unique N_f - R2 relation for all study mixtures and temperatures.

Using the proposed model, number of cycle to failure (N_f) can be predicted by the energy release rate, R2. However, this particular model was constructed based on a total number of 188 cyclic fracture tests, conducted on the five study mixes at four test temperatures and several loading levels. Since both power-law coefficients were found to be close to 1, the particular model of the N_f-R2 relation can be simplified as:

$$N_f \approx \frac{1}{R2}$$

In this approximation, N_f is slightly under-predicted, which is conservative. Furthermore, it is believed that the N_f-R2 model could be used to predict a cyclic fracture type 'endurance limit.' Note that tests taking less than 100 cycles were not included in the formation of the N_f-R2 relation as the R1 at this particular loading level does not relate to the other higher loading magnitudes.

4.4.4 Repeatability of test results

Regarding to cyclic loading test results, a coefficient of variation (CV) of numbers of cycles to failure (N_f) , statistically showing an extent of variability in relation to mean of the population, was relatively high, which indicated that test results were not repeatability.

Traditionally, The N_f values were correlated to either stress or strain level, associating to the load-controlled and displacement-controlled mode of loading, respectively.

Based upon the analysis of this study, Figure 4.23 provides a plot of all CV values of the N_f, corresponding to loading magnitudes (percentages of peak load of the monotonic test results), which relates to different stress levels for all mixtures and temperatures. Also, Figure 4.24 presents a plot of all CV values of the N_f, associating to the energy released rate (R2). As a result, they have shown that a half of the populations regarding to loading magnitudes (or stress levels) provided CV values higher than 40%, whereas 62% of the population regarding to the released energy rate (R2) provided CV values lower than 40%. Therefore, by considering repeatability of test results, associating to a new cyclic fracture criterion of the released energy rate (R2) provided better the statistical CV value than that of the traditional stress- or strain-based fatigue approach. Consequently, a number of cycles to failure (N_f) was dictated by the released energy rate, rather than the traditional fatigue criterion.

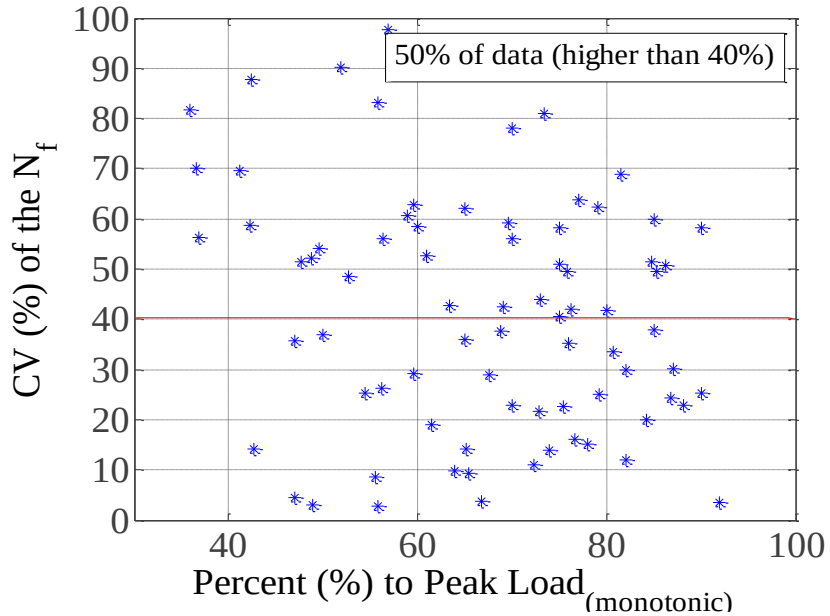

Figure 4.23 Plot of CV values of N_f associating to loading magnitudes.

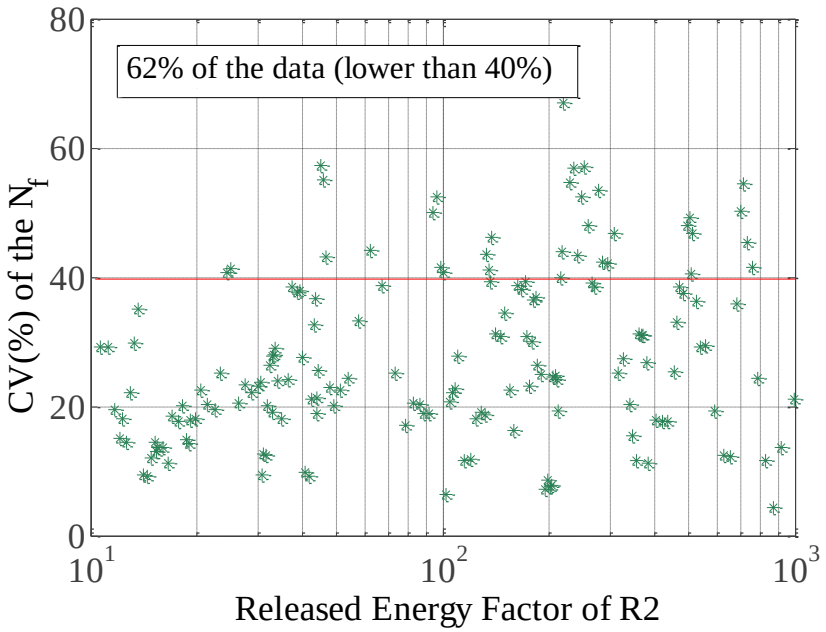

Figure 4.24 Plots of CV values of N_f associating to energy release rate (R2).

4.4.5 Experience of endurance limit

Even though the scope of this study did not involve a comprehensive investigation of the fatigue endurance limit (FEL), this section provides brief discussion of the FEL based upon observations made in the course of analyzing the study data. By definition, the FEL was defined as a significantly low loading level applied to a material, resulting an inexistence of damage. According to the latest publication of national cooperative highway research program, NCHRP in 2013, entitled "laboratory validation of an endurance limit of asphalt pavements", the FEL of the AC mixtures was dependent to several test variables, such as mix types, test temperatures, and loading period.

Based on the experimental observations and data analysis of the cyclic DC(T) test in the study, some tests were conducted at loading levels akin to reaching the FEL. Regardless of different mixtures, the endurance limit was met when a test performed at loading magnitudes less than 45, 40, 35, and 30 percentage of a peak load of the monotonic test results for the test temperatures of -12°C, 0°C, 10°C, and 20°C, respectively. So, a conclusion could be initially drawn that the FEL of the AC mixtures under the load-controlled mode of the cyclic DC(T) test depended on test temperatures which the warmer test temperature, the lower level of loading magnitudes experienced with endurance limit. However, more research needs to be performed to evaluate such an endurance limit of the AC materials using the cyclic DC(T) test.

4.5 Summary

Pavements are typically subjected to repeated loading from both vehicular and thermal loading; therefore, pavement performance is related to the material's resistance to cyclic loads. This study proposed an alternative way to evaluate cyclic loading behavior using the DC(T) test and also to examine a new cyclic fracture criterion by employing a released-energy based approach. This approach examines how material properties change or degrade after being subjected to cyclic loading. This method is generally based on cyclic loading data expressed in terms of load and displacement or stress and strain curves, which exhibit changing hysteresis loops. Cyclic DC(T) test procedures were developed based results of the monotonic DC(T) test as an input (peak load). For this study, a load-controlled, reversing, sinusoidal waveform was selected for the cyclic DC(T) test, using the modified DC(T) geometry and 1-cm offset CTOD location previously described. This testing mode was selected based on practical considerations and robustness of data produced. In addition, load control is a much simpler mode for cyclic test control and more desirable for a practitioner-friendly test. In the study, five mixtures and four temperatures (-12, 0, 10, and 20^{o}C) were performed on the cyclic DC(T) test. Based upon the test results, key findings are as follows:

- A unique relationship between released energy (RE) and a number of the cycles (N_c) appears to exist, which forms the basis for a released energy development (RED) model to characterize cyclic loading behavior. The RED model was mathematically described by using two-term exponentials, consisting of four material coefficients of R1, R2, R3, and R4 as the released energy factors because of an existence of two different growth rates.

- Potential correlations between the total number of cycles to failure (N_f) and the released energy factors were examined among different loading magnitudes. As a result, no clear correlations were found for the material coefficients R3 and R4. However, the R3 and R4 coefficients were non-negligible because they influenced to the other coefficients - R1 and R2, especially for cases of low cyclic fracture (LCF) test. Thus, cyclic fracture behavior was assumed to be dictated by the released energy factors R1 and R2.

- The R1 coefficient in the RED model was linked to initial released energy, and found to be related to a number of cycles to failure among different loading magnitudes for the same mixture and test temperature. Also, the N_f-R1 relation was related to performance

of the AC in terms of service life. By considering the C1 power-law coefficient, the greater value of the C1, the longer the service life.

- The N_f-R1 relation, however, was dependent on material type and temperature. In the case of the LCF tests where N_f was measured to be less than 100 cycle, the R1 parameter was not correlated to other levels of loading magnitudes. As a result, selection of testing load such that a practical minimum N_f of 100 cycles is recommended to maintain a stable N_f-R1 relationship.

- By definition, the R2 coefficient (exponent) is linked to the rate of growth of the released energy. Interestingly, the unique N_f-R2 relationship was found to exist in the five distinct mixtures investigated, and was also independent of test temperature. Therefore, the released energy rate (R2) formed the basis of a new cyclic fracture criterion. This led the way to development of cyclic fracture prediction models from various subsets of DC(T) cyclic and monotonic fracture test data. In-depth details of the prediction models were provided in Chapter 5.

- In terms of repeatability of test results, the energy release rate (R2) provided better correlation to a total number of cycles to failure than that of the traditional stress- or strain-based fatigue approach.

- Even though this study did not include an in-depth evaluation of fatigue endurance limit (FEL), based on the experimental observation and data analysis, as a general trend the FEL was found to depend on temperatures. At warmer test temperatures, lower loading level thresholds were associated with reaching the FEL. However, more research is needed to evaluate FEL of AC materials using the cyclic DC(T) test.

Chapter 5 Prediction of Cyclic Loading and Fracture Behavior

5.1 Introduction

The main objectives of the study were not only to evaluate monotonic and cyclic fracture behaviors of asphalt concrete mixtures, but to also to attempt to develop a prediction model for cyclic fracture behavior from reduced cyclic testing data sets, or ideally, from monotonic fracture results alone. An expected outcome of the monotonic-cyclic relation was to provide an alternative way to predict cyclic loading behavior based upon monotonic and/or cyclic test results. Consequently, prediction models for the cyclic loading behavior were attempted based on three potential scenarios: (1) a full suite of cyclic DC(T) tests; (2) monotonic plus several cyclic DC(T) tests limit numbers of test samples, or; (3) monotonic test result alone.

Another objective was to investigate fracture behaviors of both loading mechanisms. Generally, fracture mechanisms of the pavements were very sophisticated. It has been always a question where a crack started, how it behaved or propagated, and how long it required to fail a material as considered to be the end of service life. Therefore, prediction models of cyclic loading and fracture behaviors were examined in this chapter, and the findings are follows.

5.2 Prediction of cyclic loading behavior

A prediction model of cyclic loading behavior was investigated based upon test results of the monotonic and cyclic DC(T) tests. As a starting point for simplified model development, Chapter 3 and chapter 4 provided all details of the experimental and analytical procedures and test results of both loading mechanisms. To sum up, regardless of different loading mechanisms, the disk-shaped compact tension DC(T) test with a geometric modification and the analytical methodology of the released energy approach were employed to evaluate monotonic and cyclic loading behaviors. As a result, the fracture criteria of both mechanisms were obtained.

Based on the test results, several fracture parameters were determined from the monotonic and cyclic DC(T) tests. In order to investigate prediction models, the most likely useful fracture parameters of each mechanisms were employed. Fracture energy which was commonly used to describe monotonic fracture behavior was selected, and a summary of fracture energy all mixes and temperatures in the study is presented in Figure 5.1. Whereas, the released energy rate (R2) of the released energy development (RED) model was

proposed as the new cyclic failure criterion because of the unique relation between a number of cycles to failure (N_f) and the R2 on mix types and temperatures, as illustrated in Figure 5.2. Thus, these fracture criteria of both mechanisms were used to investigate prediction models of the cyclic loading behaviors.

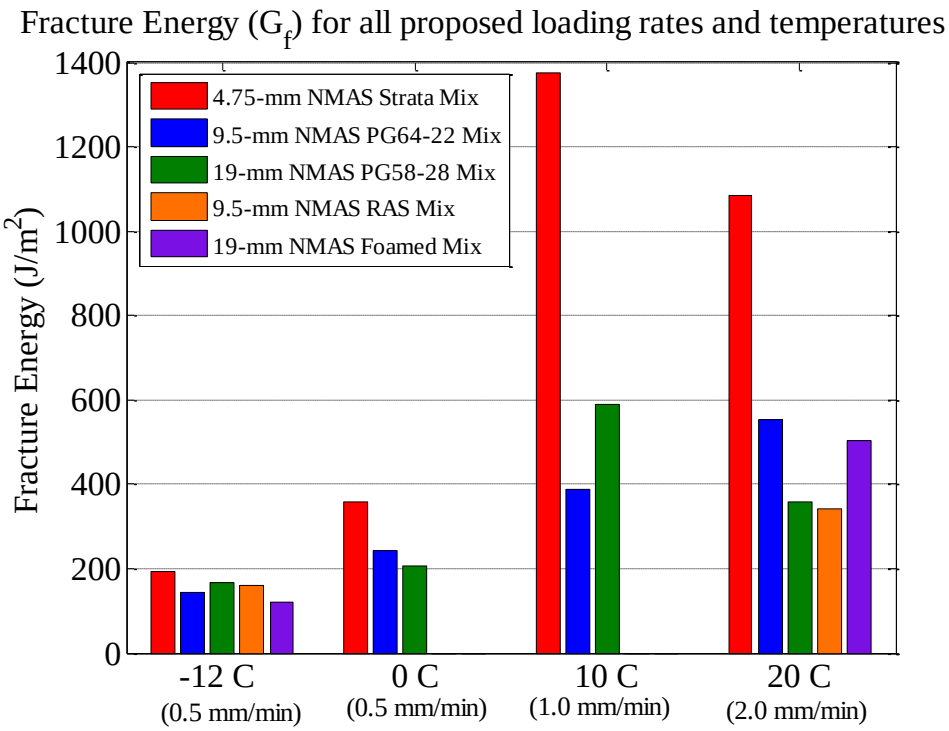

Figure 5.1 Summary of fracture energy as monotonic fracture parameter.

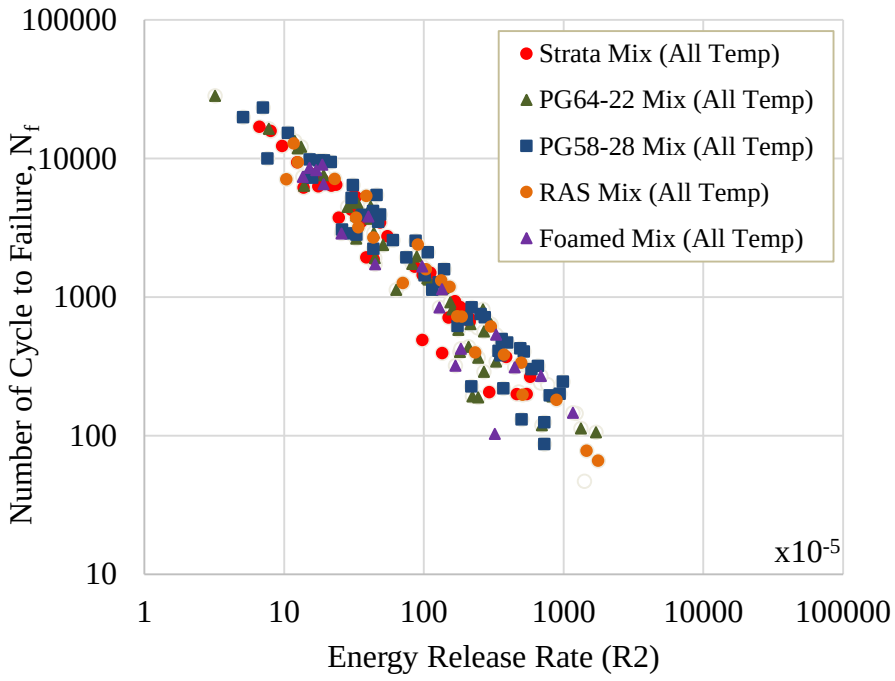

Figure 5.2 Unique N_f-R2 relation as cyclic fracture criterion.

5.2.1 Cyclic Loading Prediction with full suite of cyclic DC(T) test

Regarding to the unique characteristic of the N_f-R2 relation, the energy release rate of R2 was independent to mixture types and test temperatures. So, there was a potential to predict a fatigue life (N_f) of the mixtures by determining the R2 value through such a unique relation. However, because the N_f-R2 relation was independent to a type of the mixes, fracture energy of the monotonic test results was employed to differentiate performances of the AC mixtures. According to the experimentation, approximately 10-13 replicates of each mix were tested at each test temperature with different loading magnitudes, which was considered as the full suite test. Consequently, a predicting model of each mixture at a particular temperature was constructed based upon the full suite test. Regarding to the same mixture and temperature, by considering a ratio of the released energy parameters of fracture energy (G_f) to energy release rate (R2), a predicting model of the cyclic loading behavior was set.

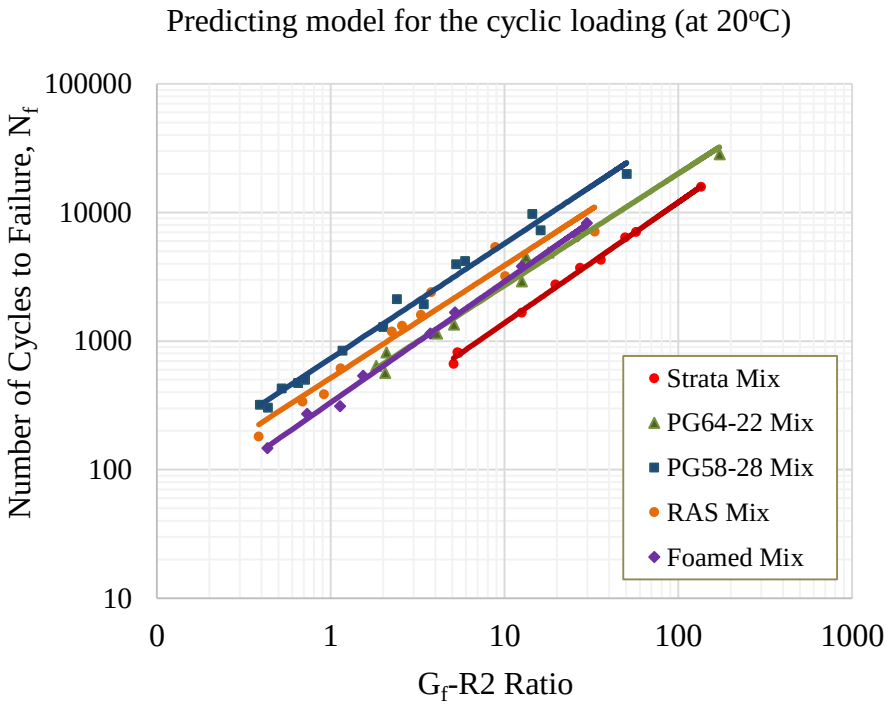

Figure 5.3 Plot of N_f versus G_f-R2 ratio for mixes tested at 20°C.

By plotting N_f versus G_f-R2 ratio as the released energy ratio, a cyclic fracture prediction model was developed. For example, Figure 5.3 presents a plot of the prediction model of the mixes, conducted at a test temperature of 20°C. Additionally, similar plots of other test temperatures were provided in Figure C.1 to Figure C.4 in the appendix C. As a

result, a correlation between N_f and released energy ratio can be mathematically described using a power-law equation given as:

$$\text{Model A:} \quad N_f = A\left(\frac{G_f}{R2}\right)^B$$

where N_f is number of cycles, G_f and R2 are fracture energy and energy release rate for the same mixture and temperature, and A and B are material coefficients. From the cyclic DC(T) test, values of R2 can be derived from the RED model. Then, the predicted N_f can be computed using the prediction model of the N_f and released energy ratio relation, as presented by Model A. As a result, a summary of the A and B values of all test temperatures is provided in Table 5.1.

Table 5.1 Summary of A and B coefficients based up full-scale cyclic DC(T) test.

Temp (^{o}C)	Mixture	A	B	R^2
-12^{o}C	4.75-mm NMAS Strata	351.92	1.153	0.965
	9.5-mm NMAS PG64-22	526.91	1.099	0.978
	19-mm NMAS PG58-28	489.28	1.123	0.972
	9.5-mm NMAS RAS mix	732.71	1.044	0.992
	19-mm NMAS Foamed mix	461.65	1.352	0.964
0^{o}C	4.75-mm NMAS Strata	374.79	1.024	0.979
	9.5-mm NMAS PG64-22	601.68	1.065	0.989
	19-mm NMAS PG58-28	533.33	1.114	0.964
10^{o}C	4.75-mm NMAS Strata	117.06	0.976	0.992
	9.5-mm NMAS PG64-22	356.43	1.028	0.991
	19-mm NMAS PG58-28	332.98	0.972	0.972
20^{o}C	4.75-mm NMAS Strata	159.22	0.939	0.997
	9.5-mm NMAS PG64-22	364.11	0.871	0.986
	19-mm NMAS PG58-28	732.84	0.893	0.987
	9.5-mm NMAS RAS mix	516.98	0.875	0.949
	19-mm NMAS Foamed mix	332.75	0.941	0.996

Based upon the A and B values of the model A for the full-suite test, they showed that these coefficients depend on mixture type and test temperature. Moreover, for the same mixture, a trend was not found on the A coefficient across different temperatures. However, the warmer test temperature, the lower value of the B coefficient.

Statistically, the root-mean-square error (RMSE) and normalized root-mean-square error (NRMSE) are commonly used to measure differences between predicted values by a model and actual or observed values from experimentation.

$$RMSE = \sqrt{\frac{\sum_{t=1}^{n}(\hat{y}_t - y_t)^2}{n}}$$

$$NRMSE\ (\%) = \left(\frac{RMSE}{y_{max} - y_{min}}\right) x100$$

Where $\hat{y}_t$ is a predicted value, $y_t$is measured value, and n is a number of test data.

Based on the analysis of study data, Figure 5.4 presents a plot of the predicted N_f from model A versus the measured N_f directly obtained from the experimentation. The result shows that the RMSE is 1,103 and the NRMSE of the test data is 2.92%, which statistically represent relatively low residual variance of test data.

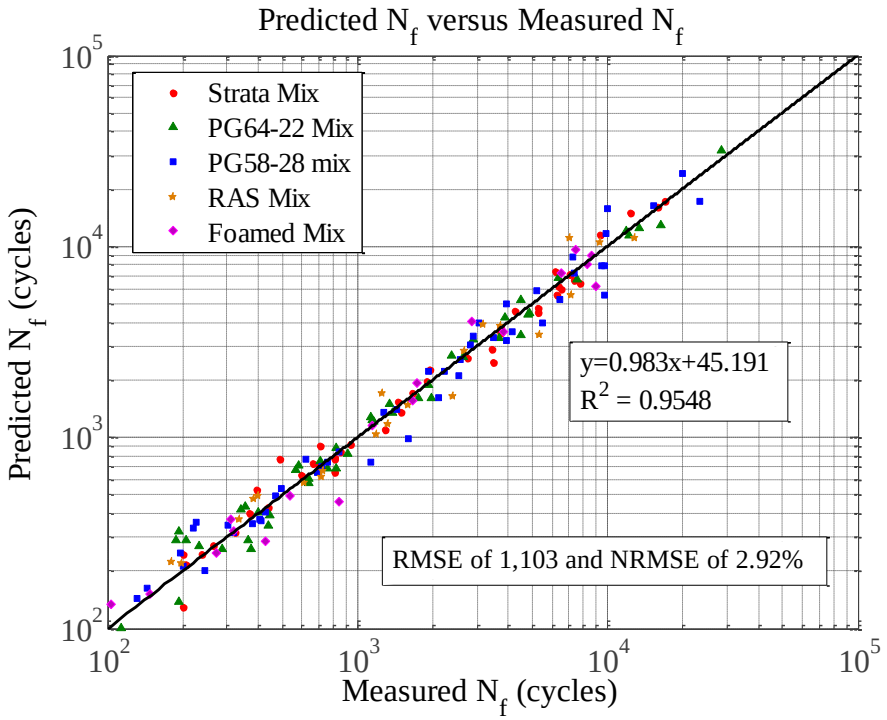

Figure 5.4 Predicted N_f using model A versus measured N_f across all temperatures.

5.2.2 Cyclic loading Prediction with limited number of cyclic DC(T) tests

The Prediction model of the cyclic loading behavior presented in the previous section was constructed based on a total number of test specimens in a range of 10-13 replicates for each mixture at a specific test temperature. Similar to the traditional fatigue testing, it requires a significant amount of materials and time to complete the evaluation.

However, this study proposed to evaluate the cyclic loading performance based on limited numbers of test samples for a less costly option.

A reduced number of test replicates, six and three replicates, were next considered (again at a single test temperature but multiple load levels). When using six replicates, a single replicate at each of the six different loading magnitudes were used to establish the prediction model. In a case of three replicates, test results for the highest, medium, and lowest loading magnitudes were selected. As a result, similar to the model A of the full-scale test, a summary of the A and B coefficients and R^2 of the prediction models of both cases were provided in Table C.1 the appendix C.

Figure 5.5 and Figure 5.6 plot a comparison between predicted N_f and the measured N_f, for the cases of six and three replicates, respectively. Regarding to the plots, a difference in the normalized root-mean-square errors (NRMSE) for the case with six and three replicates was quite small (less than 1%), and both RMSE and NRMSE are only slightly higher than the prediction made using the full data set. Therefore, it appears that cyclic fracture behavior can be predicted with reasonable accuracy by testing at a single temperature, with one replicate at each of three different load levels.

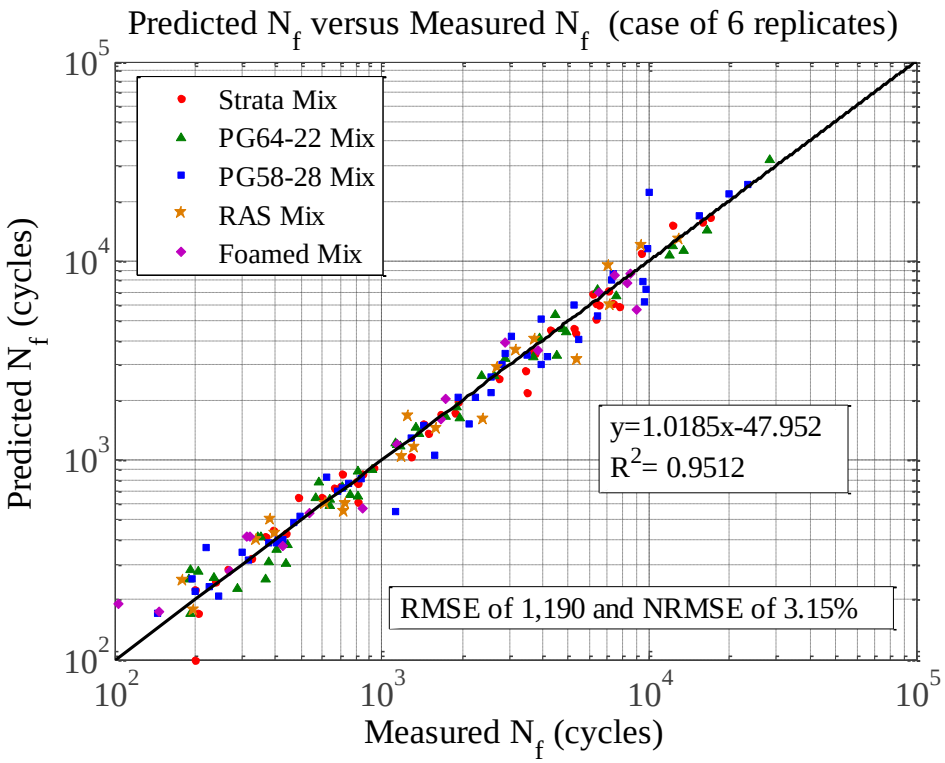

Figure 5.5 Predicted N_f versus measured N_f for 6 replicates.

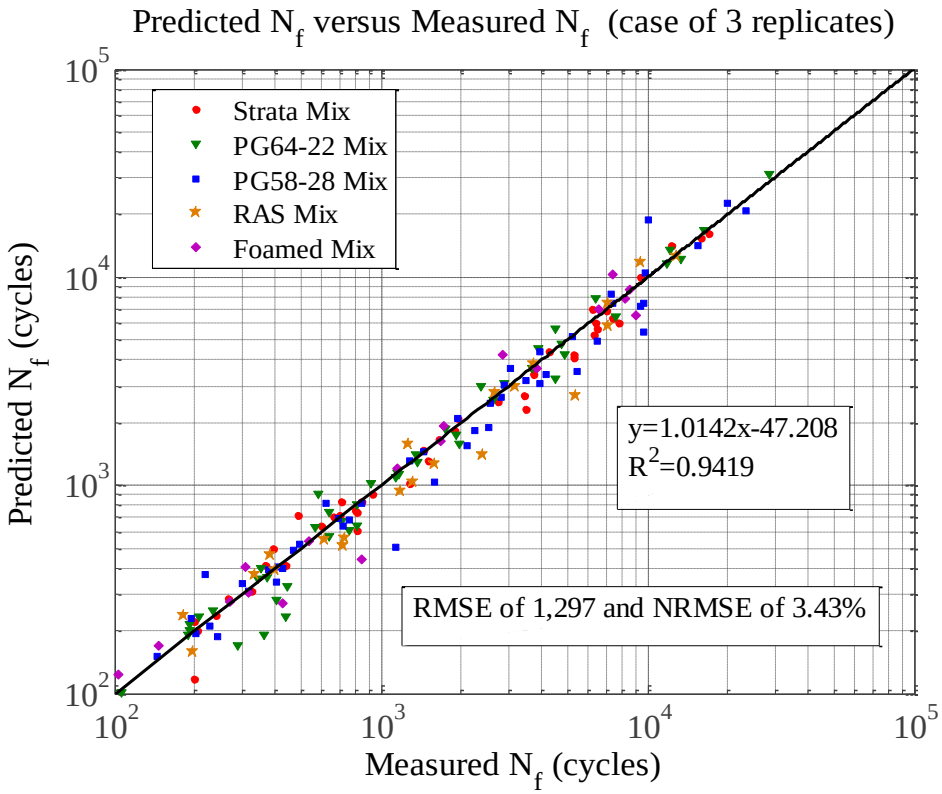

Figure 5.6 Predicted N_f versus measured N_f for 3 replicates.

5.2.3 Cyclic Loading Prediction without cyclic DC(T) test

The study was also to examine whether a prediction of the cyclic loading behavior could be made based on a test result of the monotonic DC(T) test alone. Referring back to the unique N_f-R2 relation, a single fitting model could be derived for all mixtures and test temperatures. For this study, such a unique relation was established based on the total number of 188 test samples that a predicting model between the N_f and released energy ratio was expressed as model B.

$$\text{Model B:} \quad N_f = 1.18\left(\frac{Gf}{R2}\right)^{0.977}$$

Apparently, coefficients of this specific model would be varied with a change in a number of test samples. The more test specimens conducted, the more stability of the model as larger data base used to construct the model. In this model, fracture energy and released energy rate are needed in order to determine a predicted N_f. Fracture energy is simply obtained from the monotonic DC(T) test. However, unlike the other prediction models that the energy release rate (R2) was directly obtained from a cyclic loading test, this prediction was proposed to be done without a cyclic DC(T) test or based on the monotonic DC(T) test alone. As a result, the R2 term was not available from the cyclic DC(T) test. In order to

determine the R2 term, a relation between energy release rate (R2) and loading magnitudes, as presented by percentages to a peak load value of the monotonic test results, was found using an exponential function, as shown in Figure 5.7. Therefore, such a relation was used to examine a R2 value of the model B, corresponding to different loading magnitudes.

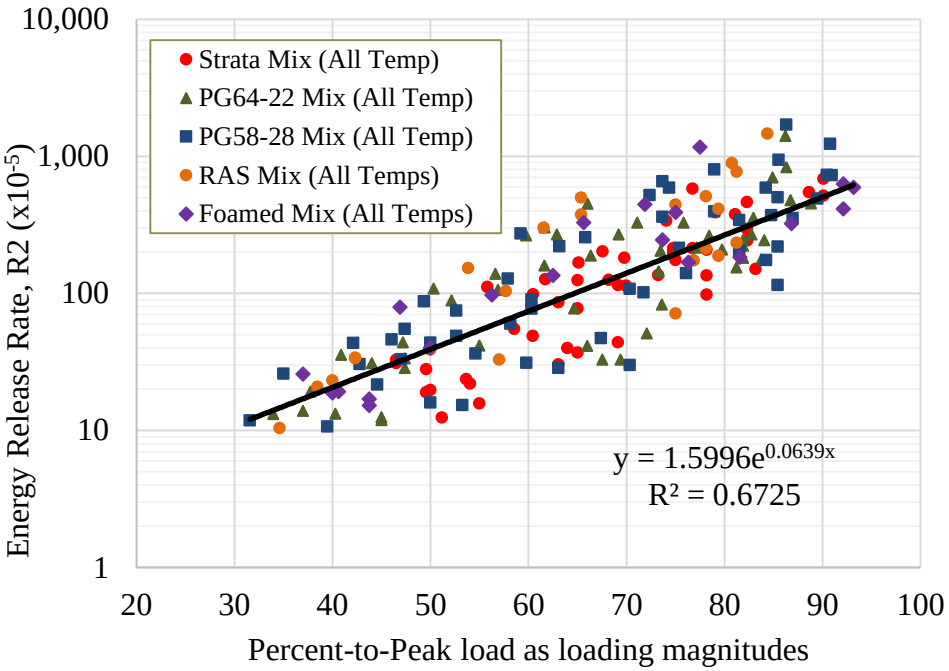

Figure 5.7 Relation of released energy rate (R2) and magnitudes of loading.

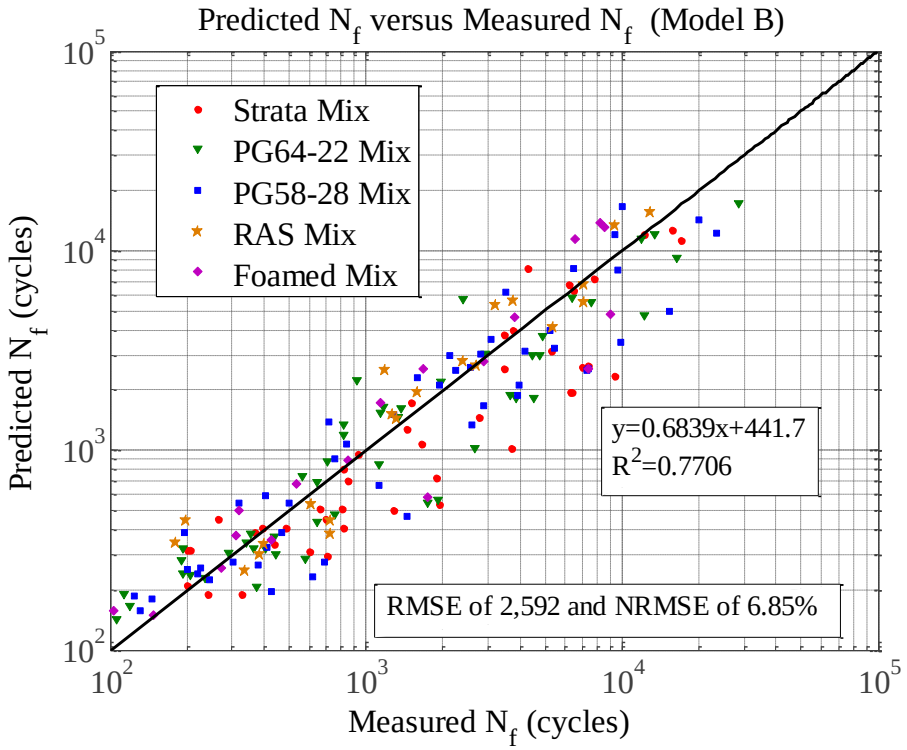

Figure 5.8 Predicted N_f of model B versus measured N_f all test temperatures.

Figure 5.8 presents a comparison plot of the predicted N_f versus the measured N_f obtained from model B. As expected, both RMSE and NRMSE of the predicted values were approximately 50% higher than the previous methods. Furthermore, regarding to the model B, as both of the power-law coefficients were approximately close to 1, the model B could be simplified as a quick tool to evaluate cyclic loading behaviors, as presented in the model C. This approximation was proposed to be used as a rule of thumb for practitioners in the field.

$$\text{Model C:} \quad N_f \cong \frac{Gf}{R2}$$

Figure 5.9 presents comparison plots of the predicted N_f versus the measured N_f that was made based on the model C. As a result, this model provides the NRMSE of 6.68% which a difference between NRMSE of model B and C is less than 1%.

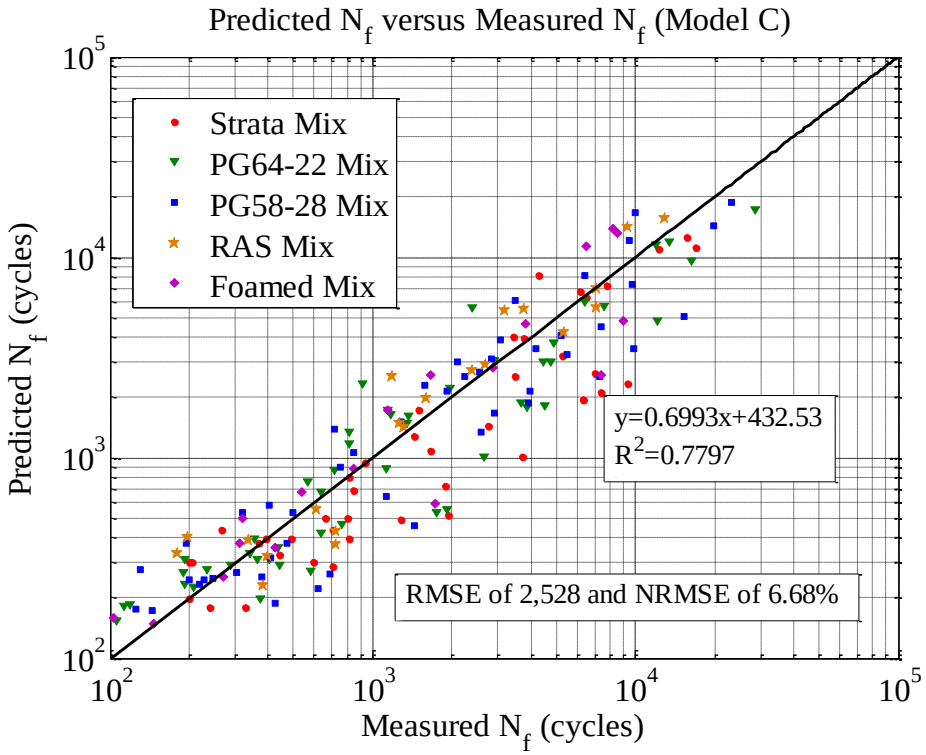

Figure 5.9 Predicted N_f of model C versus measured N_f all test temperatures.

Based on the results of both model B and model C, there was a potential to use these models to predict cyclic loading behaviors regarding to monotonic DC(T) test results alone. However, since the RMSE and NRMSE's of the models were relatively high, these models should be only employed for a rough evaluation of cyclic fracture behavior, or if comprehensive field validation of the simplified method is conducted and found to produce acceptable accuracy.

5.3 Prediction of fracture behavior

Fracture behavior in AC pavements are very complicated. Cracks can be initiated in one of many locations, such as in the mastic phase, within an aggregate particle, or at the interface of mastic and aggregate. Typically, damage and micro-cracking exist, and can coalesce into one or more larger, discrete cracks, propagating under mixed fracture modes (tension, shearing, and/or tearing). Also, fracture behaviors at a micro-scale or atomic level was very difficult to detect, which required expensive equipment and special knowledge, such as digital image correlation (DIC) or acoustic emission (AE).

This study was proposed to investigate fracture behaviors at a macro-scale level to provide how fracture behaved within asphalt concrete mixtures. A webcam-based imaging technique was used to monitor fracture processes. Unlike other high technology techniques, for example, DIC and AE, using the webcam does not require special knowledge to operate the device. Also, the device is affordable, which the price of the webcam used in this study is less than 50 dollars. A setup of the webcam with the cyclic DC(T) test is shown in Figure 5.10. An approximate area of the1.5x1.5 square inches was focused ahead of the notch tip to monitor fracture processes. However, only one side of the specimen was captured because the other side was used to attach gage points for the 1-cm offset CTOD control location. Figure 5.11 shows an example of capture images of the fracture processes using the webcam, such as crack initiation, crack propagation, and failure of a specimen.

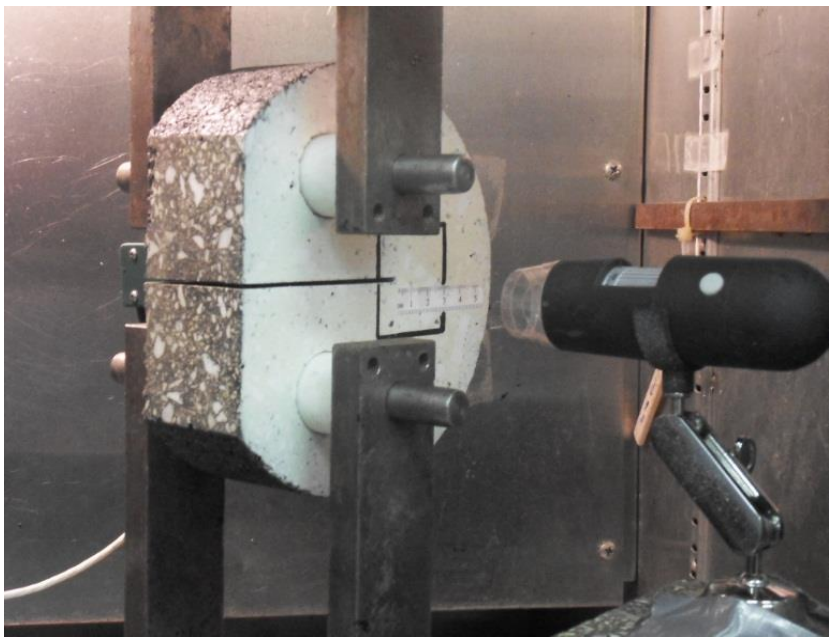

Figure 5.10 Setup of imaging device (or webcam) to capture fracture processes.

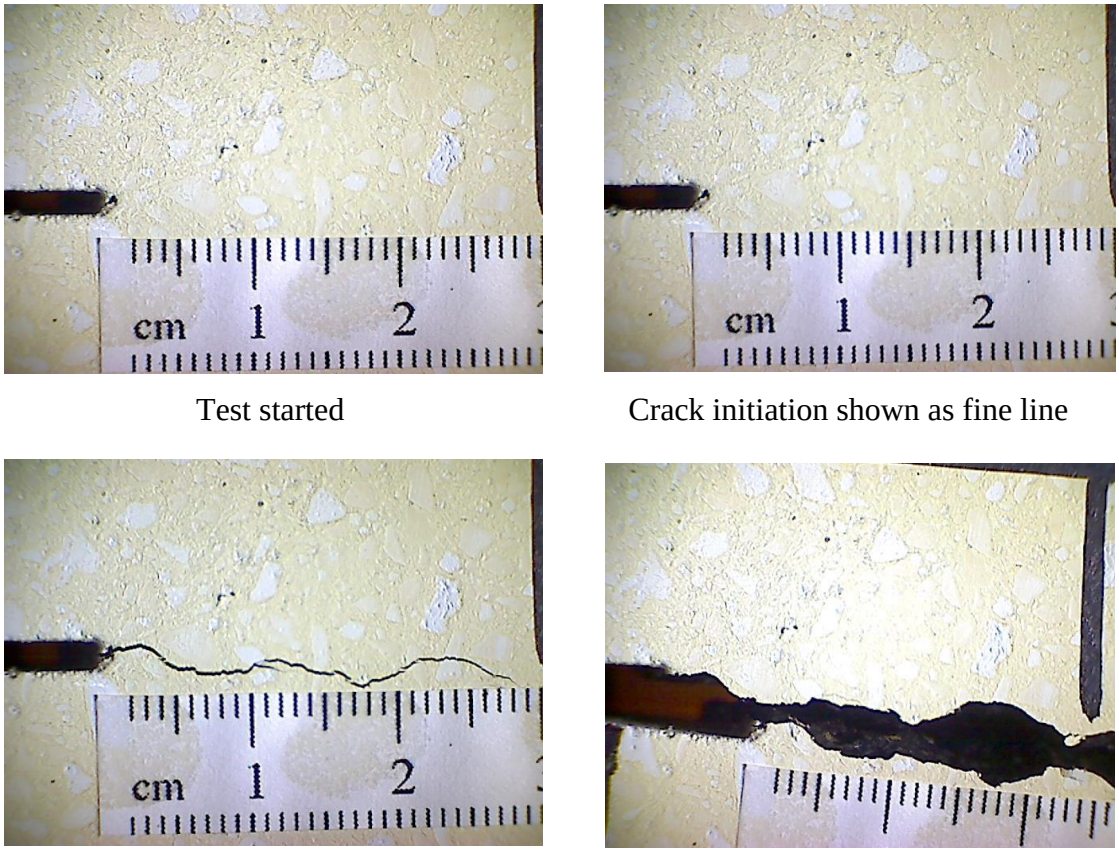

Test started | Crack initiation shown as fine line

Crack propagation | Specimen Failed

Figure 5.11 Captured images of fracture processes using webcam.

5.3.1 Fracture behavior under monotonic loading

From a load-displacement curve of monotonic DC(T) test results, it is assumed that a crack initiated before a peak load reached. In order to prove this assumption, the webcam was used to monitor a crack initiation of the monotonic DC(T) fracture test. As a result, Figure 5.12 illustrates load-displacement curves of the PG58-28 mix with presentation of crack initiation and peak load locations for all test temperatures. In addition, Figure C.5 in the appendix C illustrated a similar presentation of the crack initiation on the load-displacement curves of all based mixtures conducted at -12, 0, 10, and 20^{o}C. Table 5.2 provides a summary of opening displacement locations of crack initiation and peak load for all mixtures and test temperatures in this study.

Therefore, a conclusion is that crack initiated slightly before peak load reached for all test conditions. Moreover, the colder test temperatures, the closer locations between crack initiation and peak load. It is noteworthy that an actual size of the crack is smaller than a size of the notch. Also, a crack path is not straight and sometimes consisted of branch

cracking. As a result, an application of fracture mechanics may not be valid for AC materials due to a violation of some theoretical assumptions.

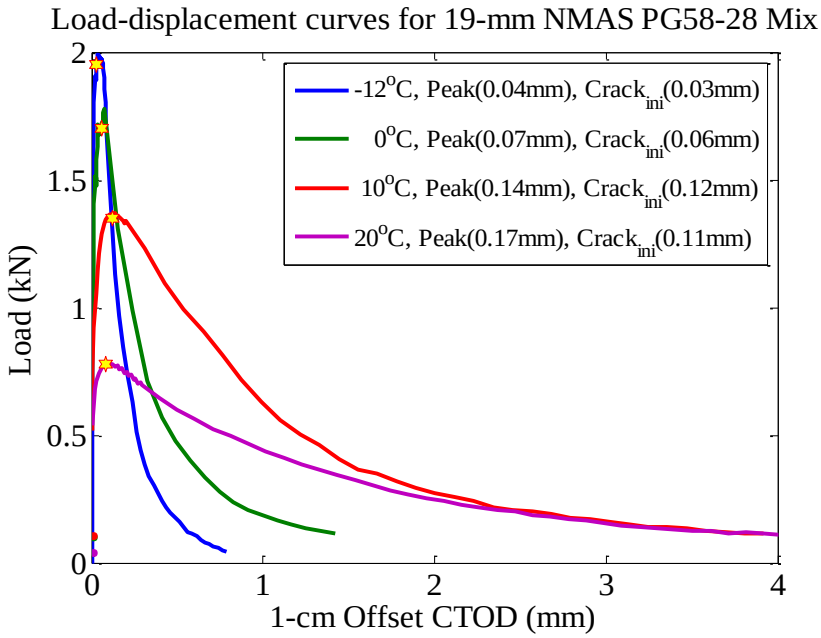

Figure 5.12 Locations of crack initiation and peak load on load and displacement curve.

Table 5.2 Summary of opening locations of peak load and crack initiation.

Temperatures	Mixes	Location of Crack Initiation(1)	Location of Peak Load
		Average(mm)	Average(mm)
-12°C	Strata Mix	0.04	0.05
	PG64-22 Mix	0.03	0.04
	PG58-28 Mix	0.03	0.04
0°C	Strata Mix	0.06	0.08
	PG64-22 Mix	0.05	0.07
	PG58-28 Mix	0.06	0.07
10°C	Strata Mix	0.26	0.30
	PG64-22 Mix	0.10	0.11
	PG58-28 Mix	0.12	0.14
20°C	Strata Mix	0.56	0.61
	PG64-22 Mix	0.09	0.11
	PG58-28 Mix	0.78	0.80
Note: (1) crack initiation was monitored and captured using webcam			

5.3.2 Prediction for crack initiation of cyclic DC(T) test

This section presents an investigation of a potential prediction model of fracture processes based on data collection of the webcam to examine if fracture under cyclic loading is predictable. Regarding to collected data of the webcam, numbers of cycles, corresponding to each stage of fracture processes; crack initiation, crack propagation, and failure, were recorded.

At first, a stage of crack initiation was investigated. Figure 5.13 presents a plot of a relation between the numbers of cycles where a crack initiated (N_i) and the numbers of cycles to failure (N_f) of all mixtures tested at -12°C. Interestingly, a potential correlation between the N_i and N_f was found employing the power-law fitting model as

$$N_i = F1(N_f)^{F2}$$

where N_i is a number of the cycle where a crack initiated, N_f is a total number of the cycles to failure, and F1 and F2 are material coefficients. In addition, N_i-N_f plots and the summaries of F1 and F2 for other test temperatures were provided in Figure C.6 to Figure C.9 and Table C.3 in appendix C, respectively. As a result, by determining a total number of cycles to failure (N_f) from the cyclic DC(T) test, a number of cycles required to initiate a crack can be approximately predicted using the N_i-N_f relation.

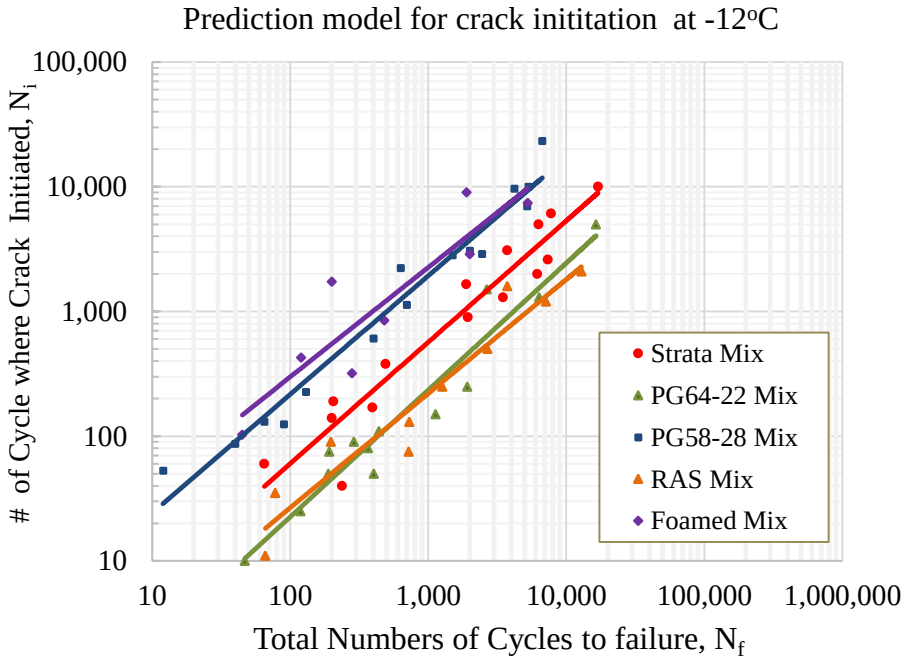

Figure 5.13 N_i-N_f relation at test temperature of -12°C.

5.3.3 Prediction for crack propagation of cyclic DC(T) test

Similar to an investigation of crack initiation, a stage of crack propagation was monitored using the webcam. Numbers of cycles corresponding to specific crack lengths of 0.5, 1.0, 1.5, 2.0, 2.5, 3.0 cm were recorded. Every 0.5 centimeter was proposed because based on visual observation, cracking was not straight (Figure 5.14) and also rapidly propagated at some stages so that a number of cycle was difficult to be precisely determined at some locations. Moreover, the more numbers of the collecting locations, the larger database of test results, which it required significant time to analysis the data.

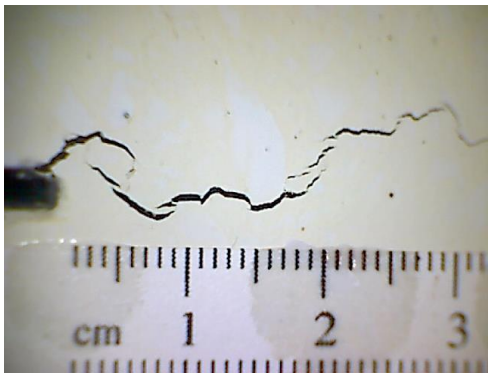

(a) 4.75-mm NMAS Strata Mix

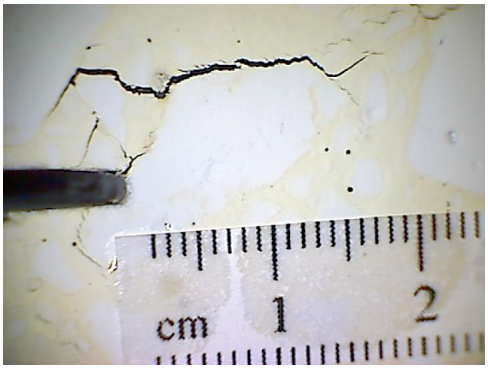

(b) 19-mm NMAS PG58-28 Mix

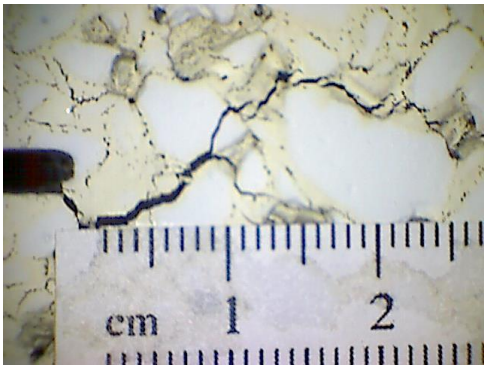

(c) 9.5-mm NMAS RAS Mix

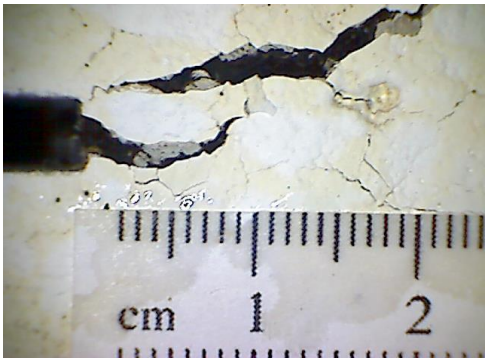

(d) 19-mm NMAS Foamed Mix

Figure 5.14 Branch cracking on different types of mixes from cyclic loading test.

Based upon observation of the captured images, some test samples experienced branch cracking as illustrated in Figure 5.14. Typically, branch cracking was formed to be a large single crack path by connecting at least two individual crack paths. Similar to the monotonic fracture behavior, an actual crack size was relatively smaller than that of a size of the notch. As a result, some assumptions of fracture mechanics were violated, such as mathematically sharped crack tip, and a single crack path. The AC mixes also exhibited as viscoelastic behavior; therefore, an application of the linear elastic fracture mechanics

(LEFM) was invalid. Consequently, the Paris law, which was commonly used to predict a stage of crack propagation as a use of stress intensity factor (K), is invalid as well.

Figure 5.15 presents a plot of loading magnitudes versus crack propagation ratios at the 0.5-cm crack length for all mixtures tested at 20°C. These ratios are a number of cycles where a crack propagated to 0.5 cm ($Np_{0.5cm}$) to a total number of cycles of the entire crack propagation stage (Np_{Total}). The result presents that the stage of crack propagation is not related to loading magnitudes as it required different percentages of the crack propagation ratio for the same loading magnitude in order to propagate a crack at a specific length. Therefore, the crack propagation could not be predicted based upon stress levels or loading magnitudes of the cyclic loading test.

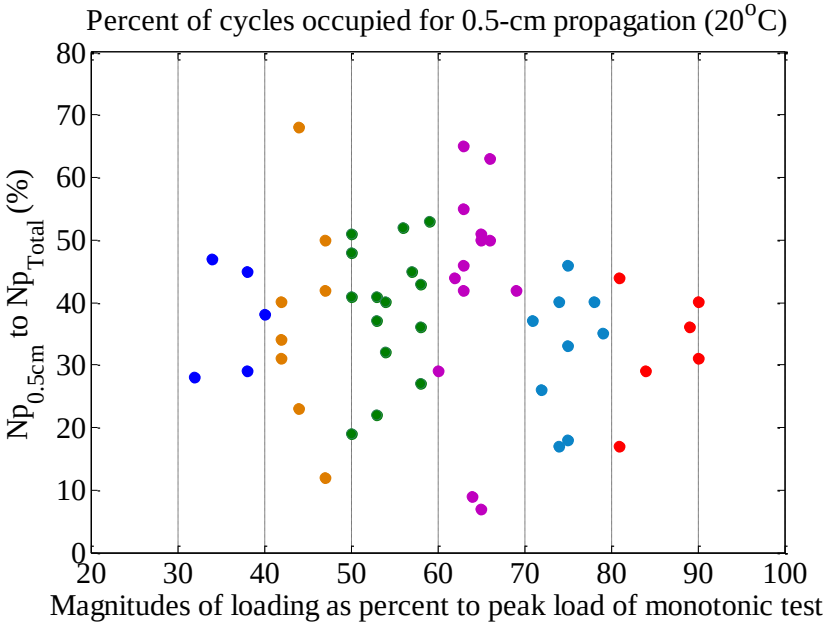

Figure 5.15 Plot of crack propagation ratio at 0.5-cm crack length associating to magnitudes of loading.

From behavior of fracture under cyclic loading, a location and a rate of crack propagation were rarely predictable due to a crack randomly propagated. Also, a wide range of numbers of cycles was found from 10^1 to 10^5 cycles for propagating a crack at a specific crack length, regardless of mixture and test temperature. Therefore, in order to potentially predict the crack propagation stage under cyclic loading, a crack propagation ratio (CPR) was introduced as a ratio of a number of cycles at a specific crack length, for example, at 0.5 cm ($Np_{0.5cm}$) to total numbers of cycles of the entire crack propagation stage (Np_{Total}). Figure 5.16 presents histograms of the crack propagation ratio (CPR) for each crack length of 0.5, 1.0, 1.5, 2.0, 2.5 and 3.0 cm of all mixtures tested at -12°C. These plots have

statistically shown frequencies of the numbers of samples, associating to different percentages or intervals of the crack propagation ratios. Similar plots for other test temperatures of 0ºC, 10ºC, and 20ºC were provided in Figure C-10 to Figure C-13 in appendix C.

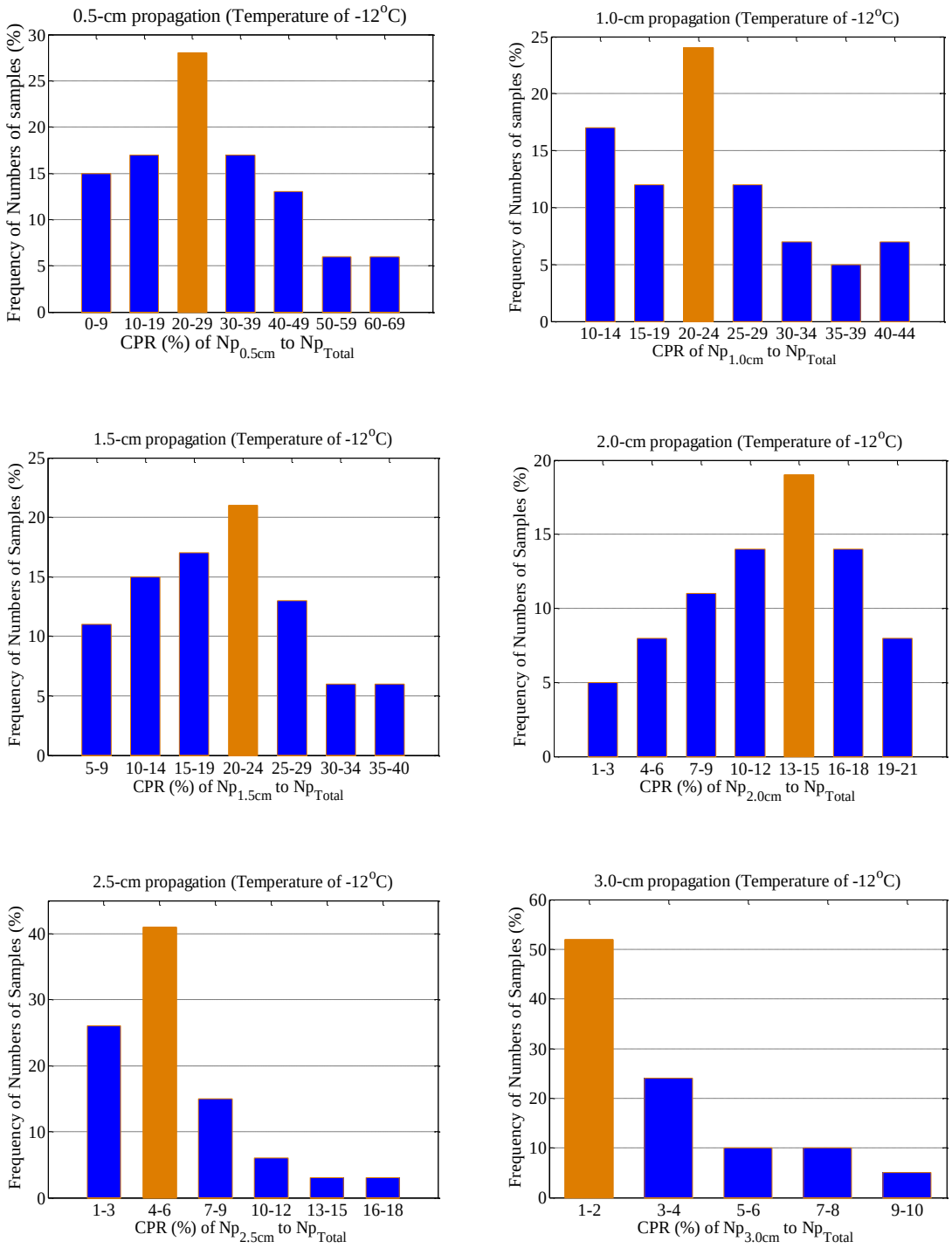

Figure 5.16 Histograms of crack propagation ratio (CPR) at each crack length for all mixtures tested at -12ºC

Based upon the analysis, Figure 5.17 provides a summary of recommended values of the crack propagation ratios (CPR) to predict crack propagation under cyclic loading for a specific crack length and test temperature. These recommended percentages were determined based on the histograms of the crack propagation ratios that a selected CPR (%) was associated to the highest frequency of the numbers of samples for each crack length. In addition, the recommended values were adjusted to have a summation of 100 percent for each test temperature. As a result, a drawback of this model is that a specimen is assumed to fail when a crack propagated by 50% of the ligament length of the DC(T) specimen or by three centimeters; however, this was fairly acceptable because less than 3% of a total number of cycles of the crack propagation stage (Np_{Total}) used to complete a test, as a crack rapidly failed after propagating by a half of the entire crack length.

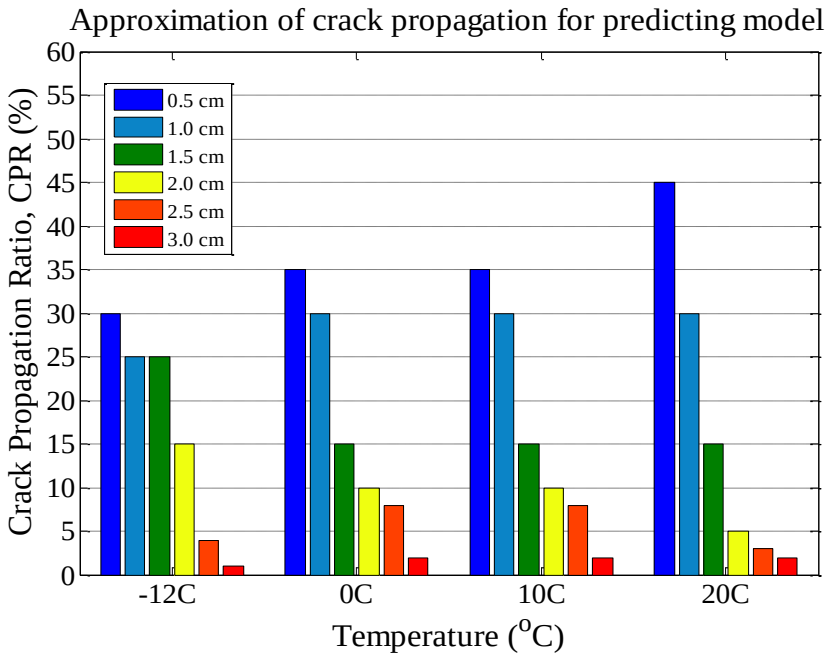

Figure 5.17 Recommended crack propagation ratio (CPR) to predict crack propagation under cyclic loading.

For a prediction of cyclic crack propagation stage, a total number of cycles of the crack propagation stage (N_{pTotal}) was determined using the N_i-N_f relation by substracting N_i from N_f. Then, the recommended crack propagation ratios (CPR) as provided in Figure 5.17 were used to predict required numbers of cycles to propagate a crack at specific crack lengths, associating to each test temperature. For example, the required number of cycles to propagate a crack of 0.5 cm at -12°C is 30% of the total number of cycles within propagation stage. Figure 5.18 to Figure 5.20 present plots of the predicted versus measured numbers of cycles for a crack propagation of 0.5, 1.0, and 1.5 cm, repectively. They have

shown that the highest normalized root-mean-square error (NRMSE) was found at a crack length of 0.5 cm. However, the longer crack length, the less NRMSE of the prediction because a less variation of the crack propagation ratio (CPR) was found for a longer crack length as presented on the histograms of the crack propagation ratios.

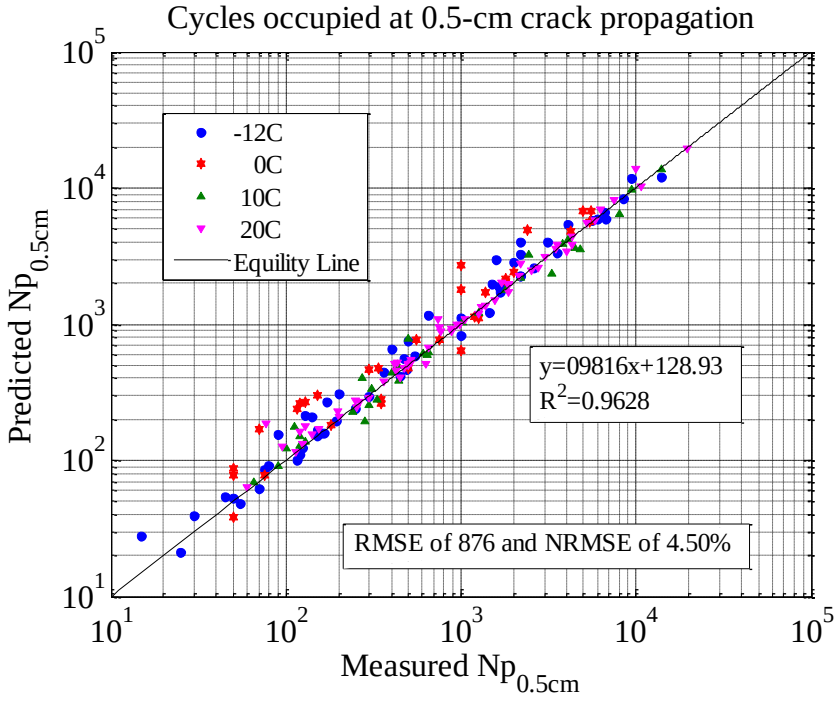

Figure 5.18 Predicted vs. measured numbers of cycles at 0.5-cm crack propagation for all mixtures and temperatures.

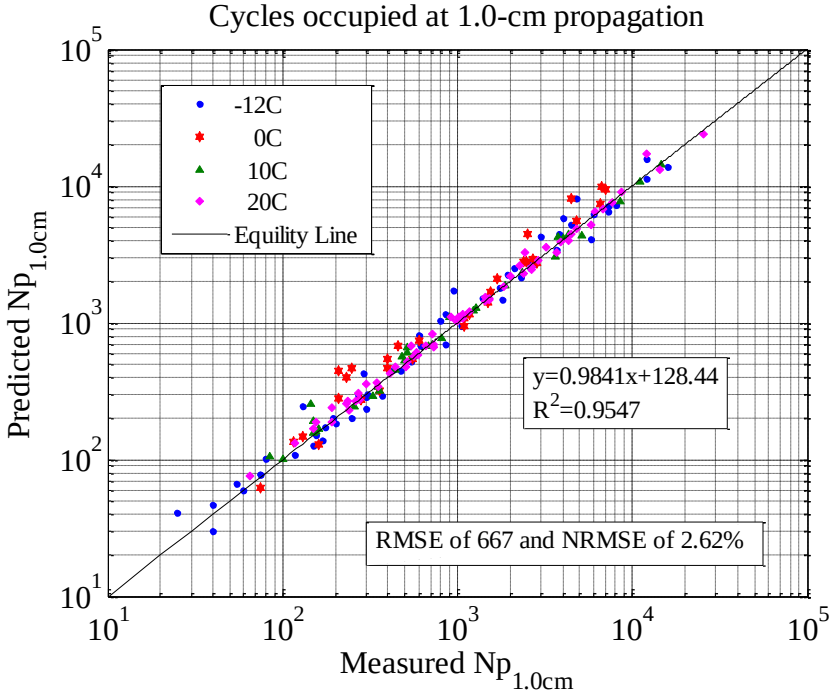

Figure 5.19 Predicted vs. measured numbers of cycles at 1.0-cm crack propagation for all mixtures and temperatures.

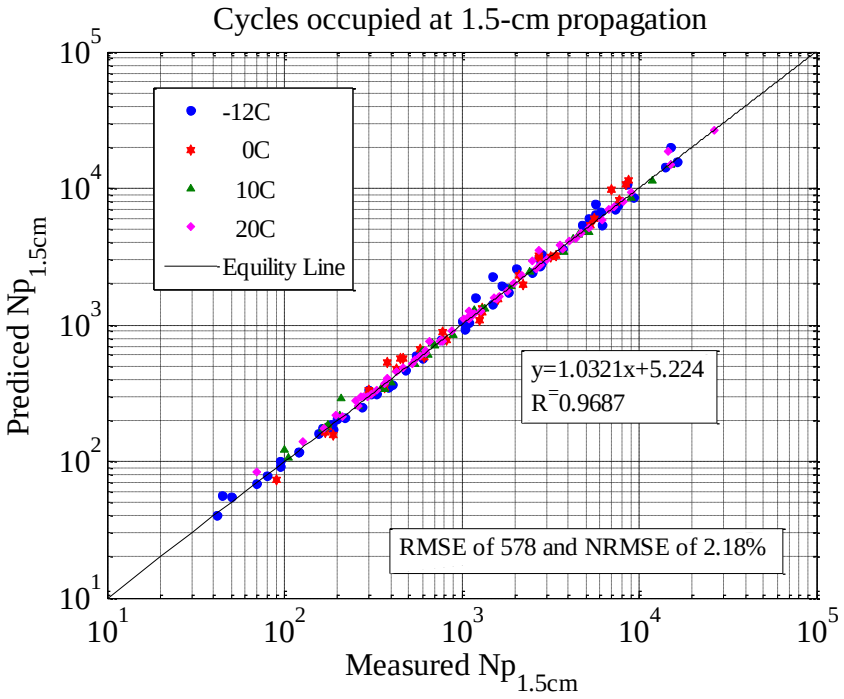

Figure 5.20 Predicted vs. measured numbers of cycles at 1.5-cm crack propagation for all mixtures and temperatures.

5.4 Summary

Models to describe and predict cyclic fracture behavior in asphalt concrete were developed. The noteworthy findings from this analysis can be summarized as follows:

1) Prediction models for cyclic loading behavior were developed using the parameters of fracture energy (G_f) and released energy rate (R2). As a result, by considering the released energy ratio of G_f-to-R2, prediction models were established for three different scenarios; (1) using a full suite of cyclic DC(T) tests; (2) using monotonic plus several cyclic DC(T) tests on a limited number of test samples, and; (3) using monotonic test result alone.

- Based upon the full suite cyclic DC(T) test data set, where a range of 10-13 replicates for a given mixture and test temperature were used, a prediction model was constructed through a relationship between a total number of cycles to failure (N_f) and the released energy ratio (G_f /R2). Similar to the traditional fatigue test, this case requires significant time and materials to complete an evaluation.

- Using a limited number of cyclic DC(T) tests, two cases of six replicates (a single replicate at each of the six different loading magnitudes) and three replicates (highest, medium, and lowest loading magnitudes were) were

considered. The difference in both of RMSE and NEMSE for the cases of six and three replicates were relatively small, and only slightly higher than the model fit error associated with the full data set. This finding suggests that cyclic fracture behavior can be predicted with reasonable accuracy through testing at a single temperature with one replicate at three different load levels.

- Using the unique N_f-R2 relation, a single prediction model was derived. Thus, there exists the potential to predict cyclic loading behavior using monotonic DC(T) test results alone. However, this model is currently only recommended to for use to arrive at a first-order approximation of cyclic fracture behavior due to the relatively high associated prediction error. Using this approach, a minimum of three replicates is required.

2) Fracture process zone behavior under both monotonic and cyclic loading was investigated using a basic, webcam-based imaging system, which was found to produce useful physical and quantitative data about the induced fracture behavior.

- Crack initiation in notched, asphalt concrete specimens subjected to monotonic loading was found to occur just before the peak load was reached. Additionally, the colder the temperature, the closer the proximity between the onset of crack initiation and subsequent achievement of peak load.

- Under cyclic loading, a correlation between the number of cycles to crack initiation (Ni) and number of cycles to failure (N_f) was found. This suggests that, by obtaining N_f from the cyclic DC(T) test, the number of cycles required to initiate a crack from a pre-fabricated notch can be back-estimated without the need for an imaging system.

- For the crack propagation stage, number of cycles vs. crack length was also obtained using image analysis. Physically, actual crack size was relatively small when compared to notch size. Also, branch cracking was observed in some specimens, and significant crack tortuosity was noted. This suggests that small scale yielding assumptions, which is a prerequisite for linear elastic fracture mechanics validity, are not valid.

- A stage of crack propagation can be potentially predicted using the recommended crack propagation ratios (CPR), regarding to a given test temperature.

Chapter 6 Summary and Conclusions

6.1 Summary

This thesis provided an experimental evaluation of monotonic and cyclic fracture behavior using the disk-shaped compact tension (DC(T)) test and a released-energy based analysis approach. The important findings of the study are summarized as follows:

(1) An identical DC(T) configuration was used to perform both monotonic and cyclic loading tests. Due to the geometric problem associating to a cyclic loading test, a modified DC(T) geometry was developed and used. Since the study was proposed to evaluate fracture behavior of AC mixtures at intermediate test temperatures of 10^{o}C and 20^{o}C, a concern was raised that the current crack mouth opening displacement (CMOD) test-controlled location may not be a suitable approach because test results would be influenced by effects of material compliance. Therefore, a new test control location was considered in this study. A 1-cm offset CTOD location, shifted toward loading holes from the standard location, was used to perform the monotonic and cyclic tests. This location was found to strike a reasonable balance between material compliance issues at the CMOD location and unstable test control at the classic CTOD location.

(2) Monotonic fracture behavior was highly dependent on mixture type and test temperature, as well as loading rate. At the warmest test temperature used, or 20^{o}C, low peak loads under the standard loading rate was observed. To minimize the creep effect, temperature dependent loading rates were recommended for the conduct of monotonic DC(T) tests.

(3) Standard test procedures for the cyclic DC(T) test were not available; therefore, the cyclic DC(T) test was developed based upon the monotonic DC(T) test. After extensive preliminary experimentation, the load control mode, reversing sinusoidal waveform and test frequency of 0.5 Hz with no rest period were selected for the cyclic DC(T) test. The testing mode was chosen based on practical considerations and robustness of data produced in the study. Experimental results were then produced at varying levels of load magnitude, i.e., at cyclic load levels representing varying percentages of the peak load obtained in monotonic testing.

(4) A released-energy based approach was employed to characterize cyclic fracture behavior. A unique relationship between released energy and number of cycles was

observed, which formed that basis of a released energy development (RED) model to describe cyclic loading behavior. Two useful cyclic fracture parameters were obtained from the RED model, including the initial released energy parameter (R1) and the energy release rate parameter (R2). The R1 parameter was found to be mix- and temperature-dependent. Interestingly, a unique relationship between fatigue life and the released energy rate (R1) was found to exist in all of the five distinct mixtures investigated, and was also independent of test temperature, which formed the basis of a new cyclic fracture criterion.

(5) By considering the released energy ratio between fracture energy (G_f) to energy release rate (R2) of the comprehensive cyclic loading testing suite, a prediction model for cyclic loading behavior was established. Unlike traditional fatigue testing, which requires a significant amount of time and materials, the study also proposed to investigate if a more practitioner-friendly cyclic fracture prediction system could be developed. The idea was to develop models based on either a reduced amount of the cyclic testing or, more ideally, using monotonic fracture test results alone (standard DC(T) fracture energy). The results of this investigation suggest that cyclic fracture behavior can be predicted with reasonable accuracy by testing at a single temperature with one replicate at three different load levels. Also, the cyclic loading behavior could be roughly approximated based upon the monotonic DC(T) test result alone, but further test improvements to increase model reliability and a comprehensive field validation will be needed to further this possibility.

(6) Fracture behavior under both monotonic and cyclic loading testing was monitored using an imaging technique involving an inexpensive web camera, which was utilized to achieve better understanding of fracture process zone behavior, including: crack initiation, propagation, and failure at the macro-scale level, and to investigate whether fracture processes under cyclic loading could be predicted. The crack path was found to be tortuous, and branch cracking was observed. This suggests that small-scale yielding assumptions are not valid for crack propagation under these conditions, invalidating the possible use of linear elastic fracture mechanics approaches.

(7) It appears that the threshold of crack initiation from a pre-fabricated notch and crack propagation at a specific crack length can be predicted from the total number of cycles to failure (N_f), without the need for a direct measure of crack length vs. cycles.

6.2 Conclusions

Based on the findings of this study, the following conclusions were drawn:

(1) The DC(T) test apparatus can be used to conduct both monotonic and cyclic fracture tests; however, a slight modification to the standard test geometry and loading fixtures is necessary to obtain reliable results.

(2) A released energy approach was introduced and found to be a key concept for modeling of cyclic fracture data. A four-parameter released energy development (RED) model appeared to be suitable for describing cyclic fracture behavior in the proposed test. The released energy rate (R2) was found to be mixture- and temperature-independent, which suggests its potential use as a cyclic fracture parameter or criterion.

(3) Even though a direct correlation between monotonic and cyclic fracture behavior was not found, a ratio of the fracture energy parameter (G_f) to released rate (R2) was utilized to establish prediction models to describe the cyclic fracture behavior.

(4) Cyclic loading behavior could be predicted based upon three different data sets derived from the DC(T) test: one involving a comprehensive cyclic loading testing suite; a slightly simpler method involving a limited number of required cyclic tests, and; a highly simplified approach where cyclic fracture behavior was predicted form monotonic fracture test results alone (standard DC(T) fracture energy). All three prediction methods were shown to be plausible, but as expected, the more rigorous the testing suite, the more accurate the prediction, as characterized by the root-mean-square error statistic.

(5) According an imaging technique of the webcam, fracture behavior of both monotonic and cyclic DC(T) tests were monitored at the macro-scale level. For monotonic fracture behavior, it was confirmed that the crack initiated slightly before the peak load presented. In terms of the cyclic fracture behavior, each stage of the fracture processes, including crack initiation and crack propagation, could be approximately predicted through a relation of the crack initiation to the total number of cycles to failure and the crack propagation ratio, respectively.

6.3 Recommendations

Of the three predictive models presented, the intermediate level (involving three replicate cyclic fracture test replicates), appears to be the best compromise between test expediency and accuracy. However, the monotonic fracture energy based prediction model might prove to be a useful first-order estimator of cyclic fracture behavior in forensic investigations and other engineering studies.

Modification of commercially available DC(T) apparatus to run the proposed test is recommended as a next step in research implementation. Additionally, application of the proposed test and models to a broader set of asphalt mixtures, and in comprehensive field validation studies are recommended. For instance, forensic investigation of good- and poor-performing asphalt overlays could form the basis for a practitioner-friendly approach to the design and control of asphalt mixtures to withstand reflective cracking. Moreover, this field validation is required to correlate all proposed laboratory test and approach to the field in order to be able to predict service life of asphalt concrete pavement in the field. Similar approaches could be employed in studies of block cracking and thermal fatigue cracking. Finally, studies to investigate effect of rest periods and healing on cyclic fracture behavior should be conducted.

References

Adedimila, A.S. (1976) "Repeated-Load Indirect Tensile Fatigue Characteristics of Asphalt Mixtures", TRR Number 595.

Bazant, Z.P., and Planas, J. (1998), "Fracture and Size Effect in Concrete and Other Quasi-brittle Materials", CRC Press, Boca Raton.

Bazin, P., and Saunier, J.B. (1967), "Deformability, Fatigue and Healing Properties of Asphalt Mixes", Second International Conference on the Structural Design of Asphalt Pavements Proc., Ann Arbor, Michigan.

Bin, Y., et al (2011) "Evaluation of Anti-Reflective Cracking Measures by Laboratory Test", International Journal of Pavement Engineering, pp. 1-8.

Buttlar, W.G., and Bozkurt, D. (2000). "Cost-effectiveness of paving fabrics for reflective crack control." Transportation Research Board, Washington, D.C., in press.

Carpenter, S. H., and M. Jansen, (1997), "Fatigue Behavior under New Aircraft Loading Conditions", Aircraft/Pavement Technology, ASCE.

Chomton, G. and Valayer, P.J. (1972), "Applied Rheology of Asphalt Mixes Practical Application", Proceedings, Third International Conference on the Structural Design of Asphalt Pavements, London.

Cleverland, G.S., J.W. Button, and R.L. Lytton. (2002), "Geosynthetics in Flexible and Rigid Pavement Overlay Systems to Reduce Reflective Cracking", Research Report No. FHWA/TX-06/1777-1, Texas Transportation Institute, Texas A&M University, College Station, Texas.

De Bondt, A. H. (1998). "Anti-reflective cracking design of (reinforced) asphaltic overlays." PhD Thesis, Dept. of Civil Engineering, Delft Univ. of Technology, Delft, Netherlands.

Dempsey, B. J., Herlache, W. A., and Patel, A. J. (1985) "The Climatic-material-structure pavement analysis program." Rep. FHWA-RD-84/115, Federal Highway Administration Washington, D.C.

Eltahan, A.A. and Lytton, R.L. (2000) Mechanistic-empirical approach for modeling reflective cracking. Transportation Research Record: Journal of Transportation Research Board, Washington, D.C., Record No. 173, pp. 132-128.

Germann, F.P. and R.L. Lytton. (1979), "Methodology for Predicting the Reflection Cracking Life of Asphalt Concrete Overlays", Research Report FHWA/TX-

79/09+207-5. Texas Transportation Institute, Texas A&M University, College Station, Texas.

Ghuzlan, K., and Carpenter, S.H. (2000), "An Energy-Derived/Damage-Based Failure Criteria for Fatigue Testing", Transportation Research Record No. 1723, pp. 131-141, Washington D.C.

Griffith, A.A., (1920), "The Phenomena of Rupture and Flow in Solids." Philosophical Transactions, Series A, Vol. 221, pp. 163-198.

Gulden, W., and Brown, D. (1984) "Overlays for plain jointed concrete pavements." Research Project No. 7502, Office of Materials and Research, Georgia Dept. of Transportation, Forest Park, Ga.

Heukelom, W. (1966), "Observations on the Rheology and Fracture of Bitumen's and Asphalt Mixes", Proc. of Asphalt Paving Technologists, Vol. 35.

Hillerborg, A. Modeer, M., and Peterson, P.E. (1976), "Analysis of Crack Formation and Crack Growth in Concrete by Means of Fracture Mechanics and Finite Elements," Cement and Concrete Research, Vol. 6, pp. 773-782.

Huang, Y.H. (1992), Pavement Analysis and Design. Englewood Cliffs, NJ: Prentice-Hall. ISBN 0-13-655275-7.

Hveem, F.N. and Carmany, R.M. (1948), "The Factors Underlying the Rational Design of Pavements, Proceedings, Highway Research Board, Washington, D.C., December 7-10, 1948.

Hveem, F.N. (1955), "Pavement Deflections and Fatigue Failures", Highway Research Board, Bulletin 114, Washington D.C.

Irwin, G.R. (1965), "Onset of Fast Crack Propagation in High Strength Steel and Aluminum Alloys." Sagamore Research Conference Proceedings, Vol.2, pp. 289-305.

Irwin, G.R., (1975), "Analysis of Stresses and Strains near the End of a Crack Traversing a Plate." Journal of Applied Mechanics, Vol. 24, pp. 361-364.

Kachnov, L.M., (1958), "Time to Rupture Process under Creep Conditions", In. Izv. Akad. Nauk, USSR, Oth. Tekh. Nauk., pp. 26-31.

Kim, Y. Richard, and Dallas N. Little (1990), "One-Dimensional Constitutive Modeling of Asphalt Concrete", Journal of Engineering Mechanics, Vol. 116, No.4, APR. 1990.

Kim, Y. Richard, Hyum-Jong Lee, and Dallas N. Little, (1997), "Fatigue Characterization of Asphalt Concrete Using Viscoelasticity and Continuum Damage Theory", Proc. of Asphalt Paving Technologists, Vol. 66.

Kim, Y. Richard, Daniel, J.S., Bisirri William (2004), "Fatigue Evaluation of Asphalt Mixtures Using Dissipated Energy and Viscoelastic Continuum Damage Approaches", Association of Asphalt Paving Technologists, pp. 557-583.

Kim, J., and W. G. Buttlar, 2002 "Analysis of Reflective Crack Control System Involving Reinforcing Grid over Base-Isolating Interlayer Mixture," Journal of Transportation Engineering, American Society of Civil Engineers, Vol. 28, No. 4, pp 375–384.

Kuai, H, Lee H.J., et al (2009), "Application of Generalized J-integral to Crack Propagation Modeling of Asphalt Concrete under Repeated Loading", Transportation Research Record No. 2127, pp. 72-81, Washington D.C..

Lytton, R.L., Uzan, H., Fernado, E.G., Roque, R., Hiltuen, D., and Stoffels, S.M. (1993), "Development and Validation of Performance Prediction Models and Specifications for Asphalt Binders and Paving Mixes," SHRP A-357, Strategic Highway Research Program, Washington, D.C.

Majidzadeh, K., Kauffmann, E.M., and Rasmsamooj, D.V. (1971), "Application of Fracture Mechanics in the Analysis of Pavement Fatigue", Proc. of the Association of the Asphalt Paving Technologists, Vol. 40, p. 227-246.

Majidzadeh, K. (1975), "Application of Fracture Mechanics for Improved Design of Bituminous Concrete, Vol. 2", the Ohio State University Research Foundation.

Miner, M.A. (1945), "Cumulative Damage in Fatigue", Transactions of the American Society of Mechanical Engineers, Vol. 67.

Monismith, C.L., and Deacon, J.A. (1964), "Fatigue of Asphalt Paving Mixtures", Transportation Engineering Journal, Proc. of the American Society of Civil Engineers. Vol. 95, No. TE2.

Monismith, C.L. and Salam, Y.M. (1973), "Distress Characteristics of Asphalt Concrete Mixes", Proceedings, Asphalt Paving Technology, Vol. 42.

Monismith, C.L., Epps, J.A., and Finn F.N. (1985), "Improved Asphalt Mix Design", Proc. of Asphalt Paving Technologists, Vol. 54, San Antonio, Texas.

Monismith, C.L., Tsai, B., Jones, D., (2006) "Reflective Cracking Study: First-Level Report on Laboratory Fatigue Testing".

Myre, J. (1992) "Fatigue of Asphalt Materials for Norwegian Conditions", Seventh International Conference on Asphalt Pavements, Vol.3, Proc., U.K.

Na Chiangmai, C. (2010), "Fatigue-Fracture Relation on Asphalt Concrete Mixtures", M.S. Thesis, University of Illinois at Urbana-Champaign, IL.

Nunn, M.E (1989), Investigation of Reflective Cracking in Composite Pavements in the United Kingdom, Proceedings of the RILEM Conference on Reflective Cracking (Liege). London: E & FN Spoon.

Pais, J.C., Perira, P.A.A. (2000) "Evaluation of reflective cracking resistance in bituminous mixtures" Fourth International RILEM Conference and Exhibition on Reflective Cracking in Pavements, Ottawa, pp. 93-102

Paulino, G.H., Jin, Z.H., Dodds Jr., R.H. (2003), "Failure of Functionally Graded Materials", In B. Karihaloo and W.G. Knauss, Editors, Comprehensive Structural Integrity, Vol. 2, Elsevier Science, pp. 607-644.

Paulino, G.H., Song, S.H., and Buttlar, W.G. (2004), "Cohesive Zone Modeling of Fracture in Asphalt Concrete," Proc. of the Fifth RILEM International Conference on Cracking in Pavements, C. Petite and I. Al-Qadi, Limoges, France.

Paris, P.C., Gomez, M.C., and Anderson, W.E. (1961), "A rational analytic theory of fatigue", the Trend in Engineering 13, pp. 9-14.

Pell, P.S. (1962), "Fatigue Characteristics of Bitumen and Bituminous Mixes", International Conference on the Structural Design of Asphalt Pavements, an Arbor, Michigan, August, 1962.

Pell, P.S. (1965), "Fatigue of Bituminous Materials in Flexible Pavements". Proc., Institution of Civil Engineers, Vol. 31.

Pell, P.S., (1967), "Fatigue of Asphalt Pavement Mixes". Proc., Second International Conference on the Structural Design of Asphalt Pavements, Ann Arbor, Michigan, pp.456-483.

Pronk, A.C., and Hopman, P.C. (1990), "Energy Dissipation: The Leading Factor of Fatigue", Highway Research: Sharing the Benefits, Proc. of the Conference the USSHRP, London.

Ramsamooj, D.V. (1991), "Prediction of Fatigue Life of Asphalt Concrete Beams from Fracture Tests," ASTM Journal of Testing and Evaluation, Vol.19, pp. 231-239.

Rice J.R. (1968), "A Path Independent Integral and Approximate Analysis of Strain Concentration Notches and Cracks", Journal of Applied Mechanics, Vol. 35, pp. 379-386.

Roberts, F.L., et al. (1996). Hot Mix Asphalt Materials, Mixture Design, and Construction. 2nd National Asphalt Pavement Association Research and Education Foundation;

Rowe, G.M. (1993), "Performance of Asphalt Mixtures in the Trapezoidal Fatigue Test", Proc. Association of Asphalt Paving Technologists, Vol. 62, pp. 344-384.

Schapery, R.A., (1975) "A Theory of Crack Initiation and Growth in Viscoelastic Media—III. Analysis of Continuous Growth." International Journal of Fracture, Vol.11, 1975, pp. 549-562.

Schapery, R.A. (1981), "On Viscoelastic Deformation and Failure Behavior of Composite Materials with Distributed Flaws." Advances in Aerospace Structures and Materials, AD-01, ASME, New York, pp. 5-20.

Schapery, R.A. (1984), "Correspondence Principles and a Generalized J Integral For Large Deformation and Fracture Analysis of Viscoelastic Media", International Journal of Fracture Vol.25.

Shen, S., and Carpenter, S. H. (2005), "Application of Dissipated Energy Concept in Fatigue Endurance Limit Testing", Journal of Transportation Research Record: Transportation Research Board, No. 1929, pp. 165-173.

Shimazaki, M. et al. (2010) "Development of High Performance Asphalt for Prevention of Reflective Cracking", Journal of Transportation Research Record: Transportation Research Board, No. 71, pp. 227-245.

SHRP, A-404 (1994), "Fatigue Response of Asphalt-Aggregate Mixes", Strategic Highway Research Program, National Research Council.

Smith, R.A. (1990), the Versailles Railway Accident of 1842 and the First Research into Metal Fatigue. In *Fatigue 90* (eds. H, Kitagawa & T. Tanaka), Vol. IV, pp. 33-41.

Standard Test AASHTO (1994), "Fatigue Life of Compacted Hot Mix Asphalt (HMA) Subjected to Repeated Flexural Bending".

Suresh, S. (1990), Mechanics and Micro mechanisms of Fatigue Crack Growth in Brittle Solids. International Journal of Fracture, pp 41-56.

Tada, H., Paris, P.C., and Irwin, G.R. (1985), "The Stress Analysis of Cracks Handbook, 2nd Ed.," Paris Productions, St. Louis, MO.

Tangella, S.C., Craus, J., Deacon, J.A. and Monismith, C.L. (1990), "Summary Report on Fatigue Response of Asphalt Mixtures", SHRP A-003-A, Strategic Highway Research Program, Washington, D.C.

Tayebali, A.A., Rowe, G.M., and Sousa, J.B. (1992), "Fatigue Response of Asphalt-Aggregate Mixtures", Proc. of Asphalt Paving Technologists, Vol. 61.

Van Dijk, W., Moreaud, H., Quedeville, A, and Uge P. (1972), "The Fatigue of Bitumen and Bituminous Mixes", Proc. Third International Conference of the Structural Design of Asphalt Pavements, London, pp. 354-366.

Van Dijk (1975) “Practical Fatigue Characterization of Bituminous Mixes”, Proc. of Asphalt Paving Technologists, Vol.44.

Van Dijk, and Vesser, W. (1977), “The Energy Approach to Fatigue for Pavement Design. Proc., Association of Asphalt Paving Technologists”, Vo.46, pp. 1-40.

Vyce, J. M. (1983). “Reflection cracking in bituminous overlays on rigid pavements.” Rep. No. 109, New York State Dept. of Transportation Research Board.

Wagoner, M.P., Buttlar, W.G., and Paulino G.H. (2005), “Disk-Shaped Compact Tension Test for Asphalt Concrete Fracture”, Experimental Mechanics, Vol.45, pp.270-277.

Wagoner, M.P., (2006), “Fracture Tests for Bituminous-Aggregate Mixtures: Laboratory and Field Investigations,” Ph.D. dissertation. University of Illinois at Urbana-Champaign.

Wells, A.A., (1963) “Application of Fracture Mechanics at and beyond General Yielding.” British Welding Journal, Vol. 10, pp. 563-570.

Wohler A. (1860), Versuche ber die Festigkeit der Eisenbahn Wagenachsen. Zeitschrift Fur Bauwesen, English Summary.

Zhou, F. and T. Scullion. (2003), “Upgraded Overlay Tester and its Application to Characterize Reflective Cracking Resistance of Asphalt Mixtures. Research Report FHWA/TX-04/4467-1, Texas Transportation Institute, Texas A&M University, College Station, Texas.

Appendix A

Supplementary Figures and Tables for Chapter 3

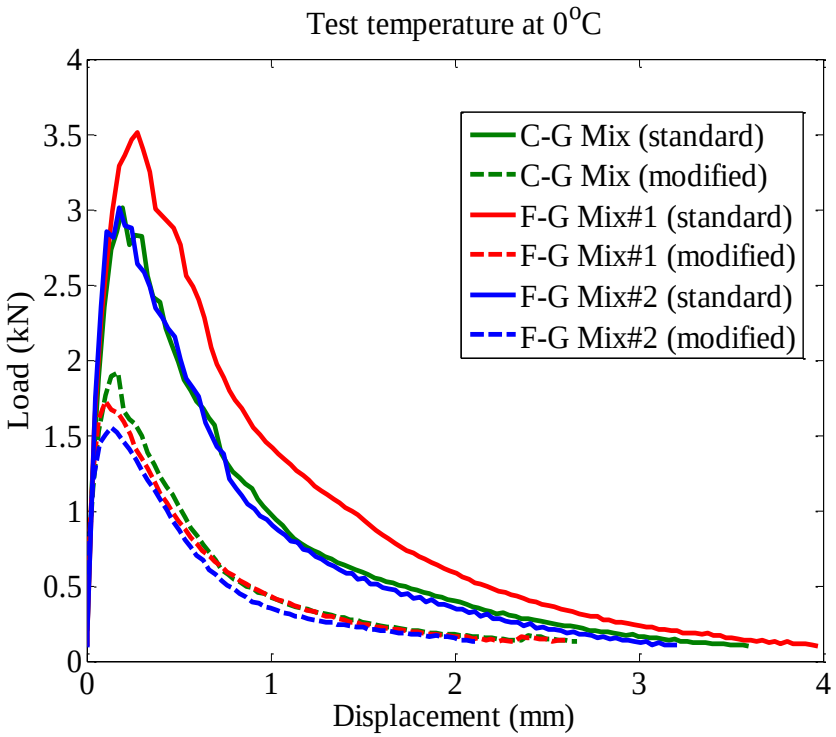

Figure A.1 Comparison of load-displacement curves of standard versus modified DC(T) geometry tested at 10°C.

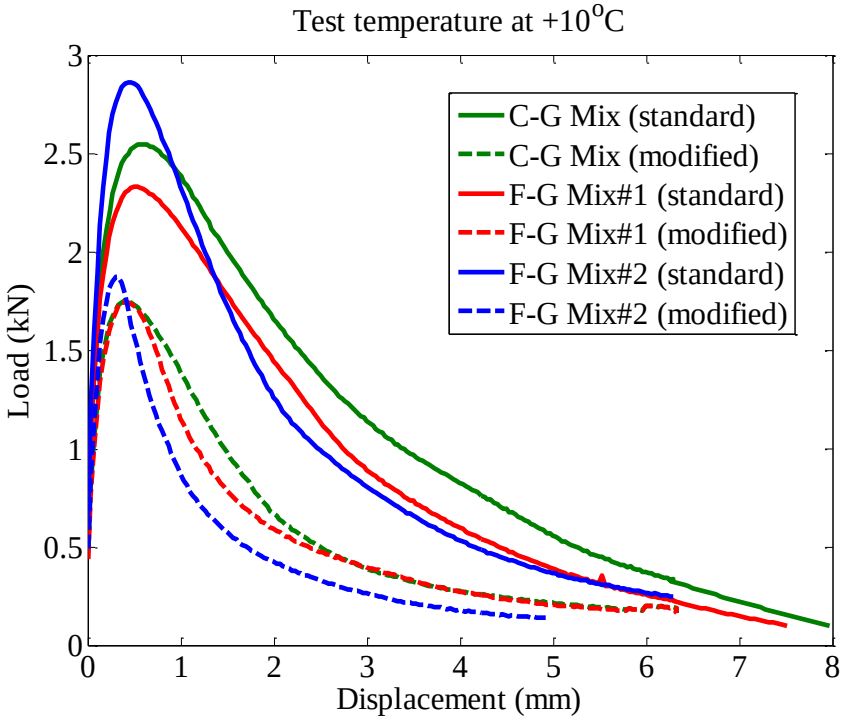

Figure A.2 Comparison of load-displacement curves of standard versus modified DC(T) geometry tested at 0°C.

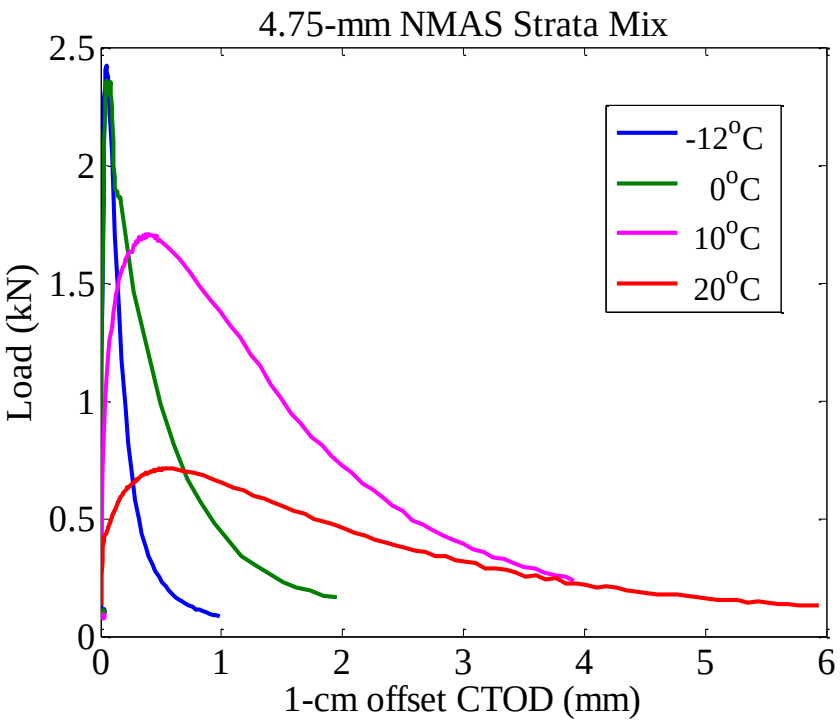

Figure A.3 Load-displacement plots of Strata mix tested at all temperatures with loading rate of 0.5 mm/min.

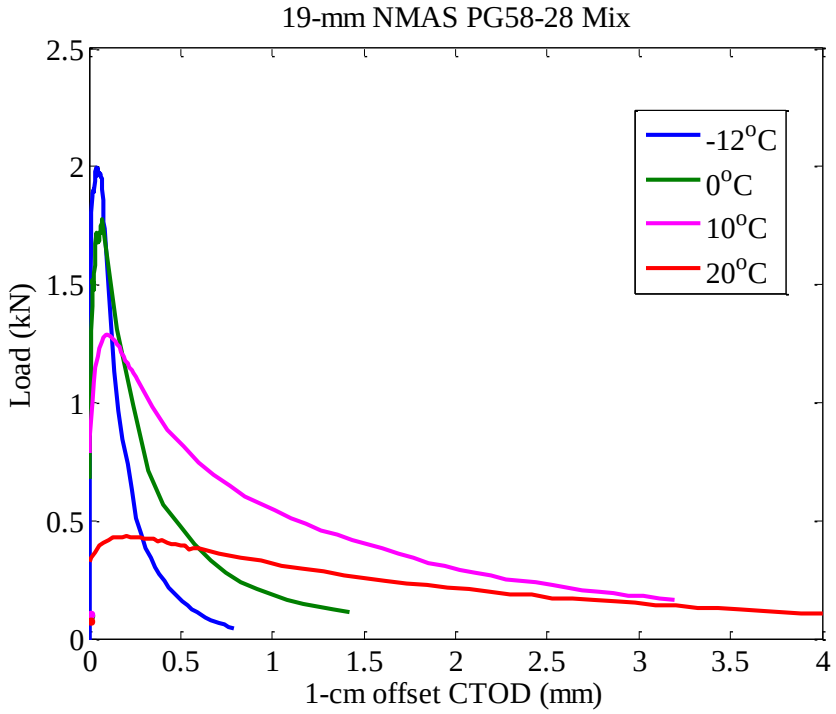

Figure A.4 Load-displacement plots of PG58-28 mix tested at all temperatures with loading rate of 0.5 mm/min.

Table A.1 Fracture properties of mixes for all test temperatures with loading rate of 0.5 mm/min.

Temp	Mix	Peak Load		Fracture Energy (G_f)	
		Avg.(kN)	CV (%)	Avg.(J/m^2)	CV (%)
-12^{o}C	4.75-mm NMAS Strata	2.43	1.7	194	4.2
	9.5-mm NMAS PG64-22	2.32	3.4	143	6.1
	19-mm NMAS PG58-28	1.99	3.9	168	13.5
	9.5-mm NMAS RAS Mix	1.60	13.7	160	14.2
	19-mm NMAS Foamed Mix	1.90	7.5	129	5.6
0^{o}C	4.75-mm NMAS Strata	2.07	4.9	357	13.2
	9.5-mm NMAS PG64-22	1.97	3.5	244	9.3
	19-mm NMAS PG58-28	1.84	3.2	208	1.4
10^{o}C	4.75-mm NMAS Strata	1.89	7.1	1,288	12.0
	9.5-mm NMAS PG64-22	2.10	2.2	448	7.4
	19-mm NMAS PG58-28	1.30	3.9	567	9.0
20^{o}C	4.75-mm NMAS Strata	0.71	1.1	746	9.6
	9.5-mm NMAS PG64-22	0.86	1.2	494	3.3
	19-mm NMAS PG58-28	0.42	10.3	270	13.8

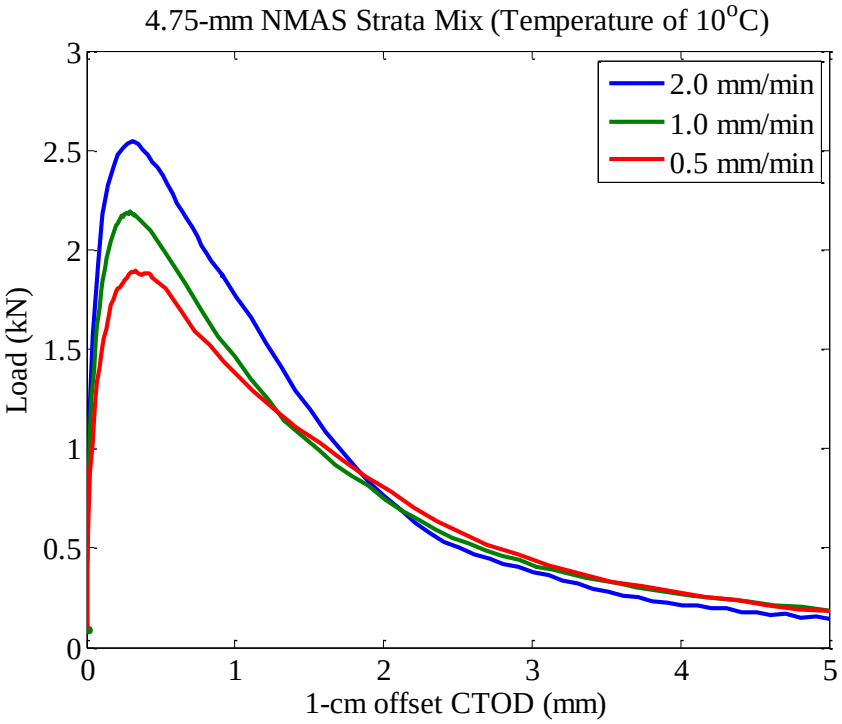

Figure A.5 Load-displacement curves of Strata mix for different loading rates at 10°C.

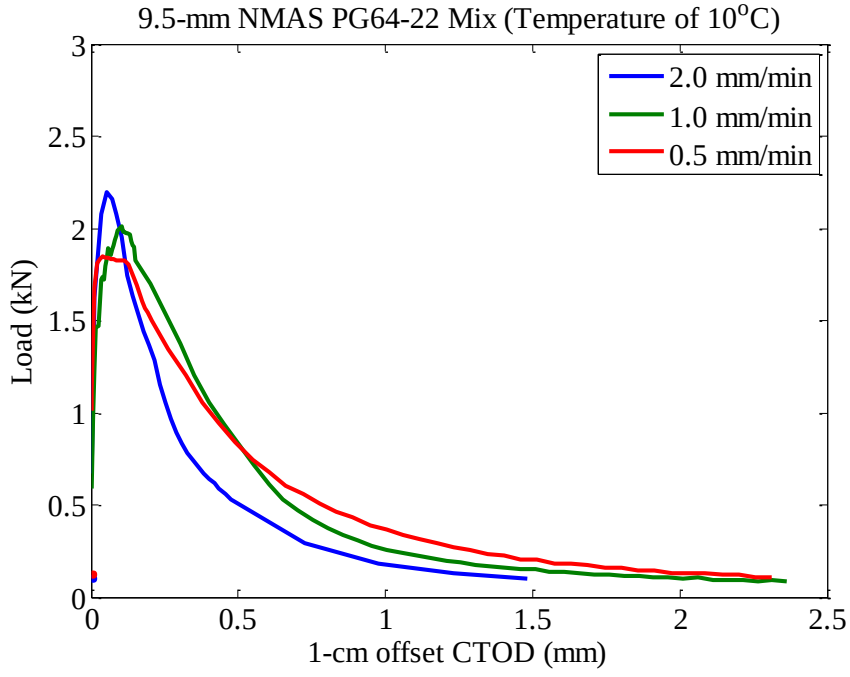

Figure A.6 Load-displacement curves of PG64-22 mix for different loading rates at 10°C.

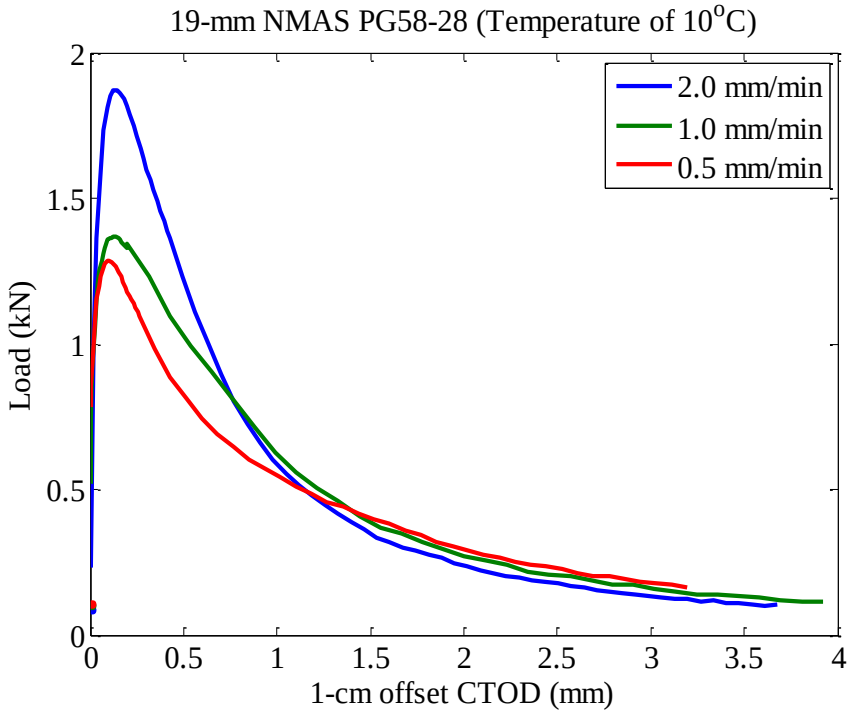

Figure A.7 Load-displacement curves of PG58-28 mix for different loading rates at 10°C.

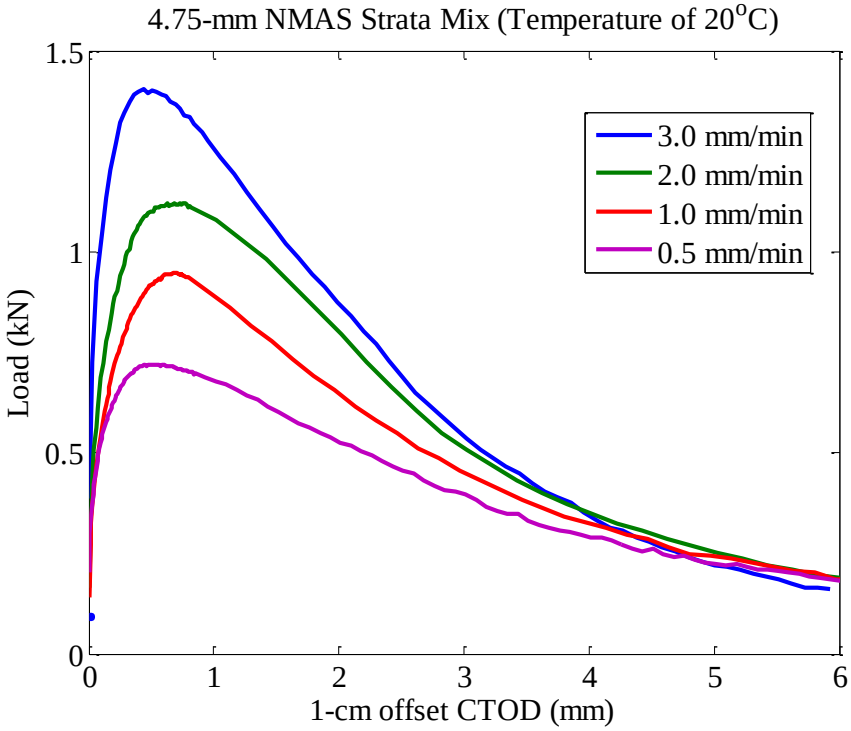

Figure A.8 Load-displacement curves of Strata mix for different loading rates at 20°C.

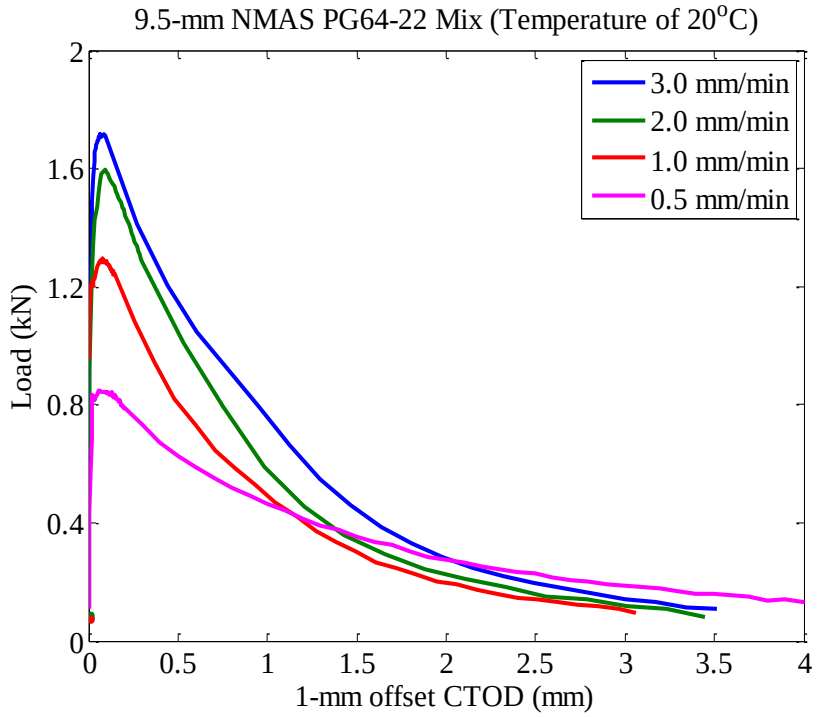

Figure A.9 Load-displacement curves of PG64-22 mix for different loading rates at 20°C.

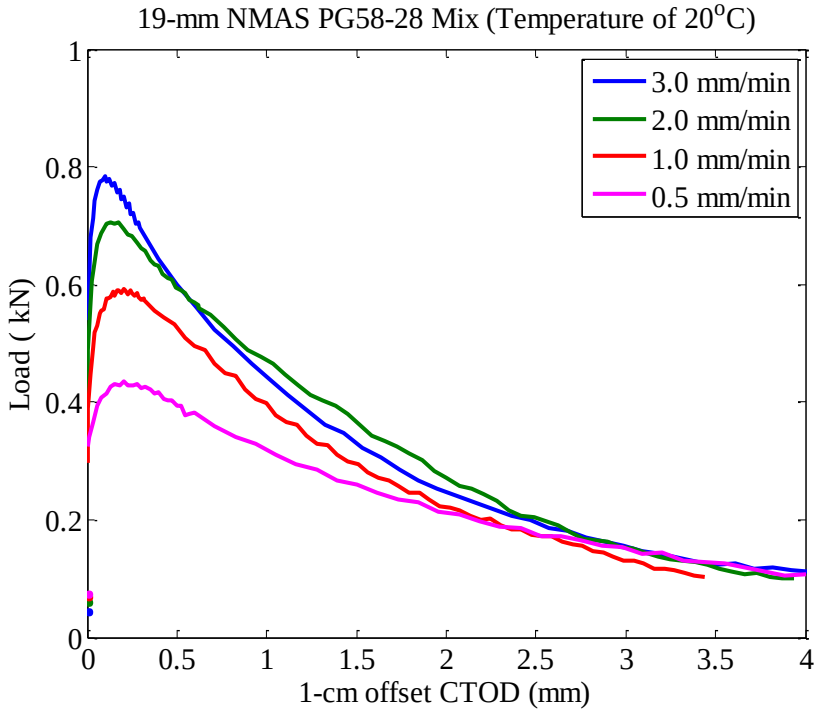

Figure A.10 Load-displacement curves of PG58-28 mix for different loading rates at 20°C.

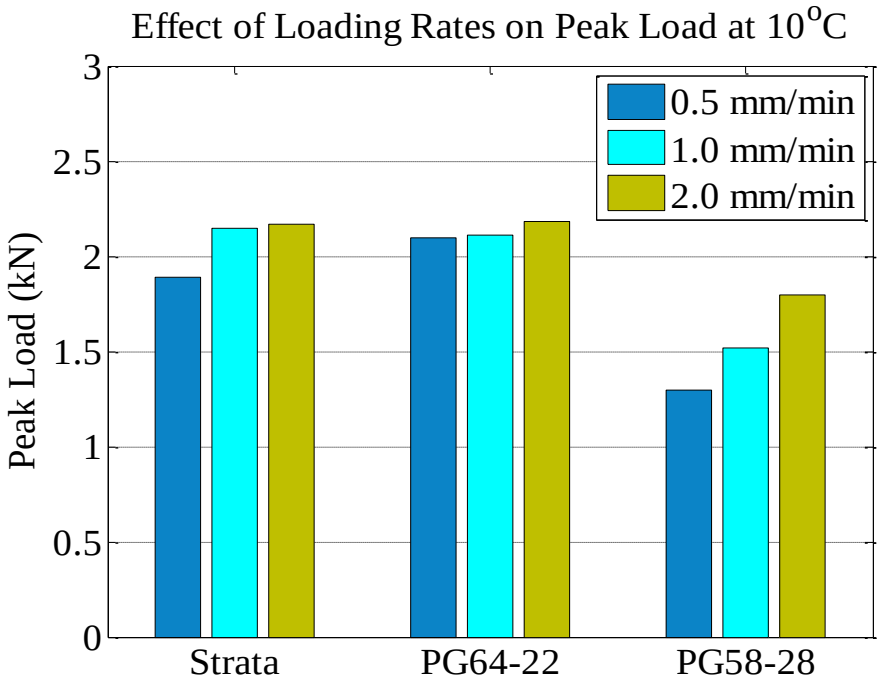

Figure A.11 Peak load values of based mixtures for different loading rate at 10ºC.

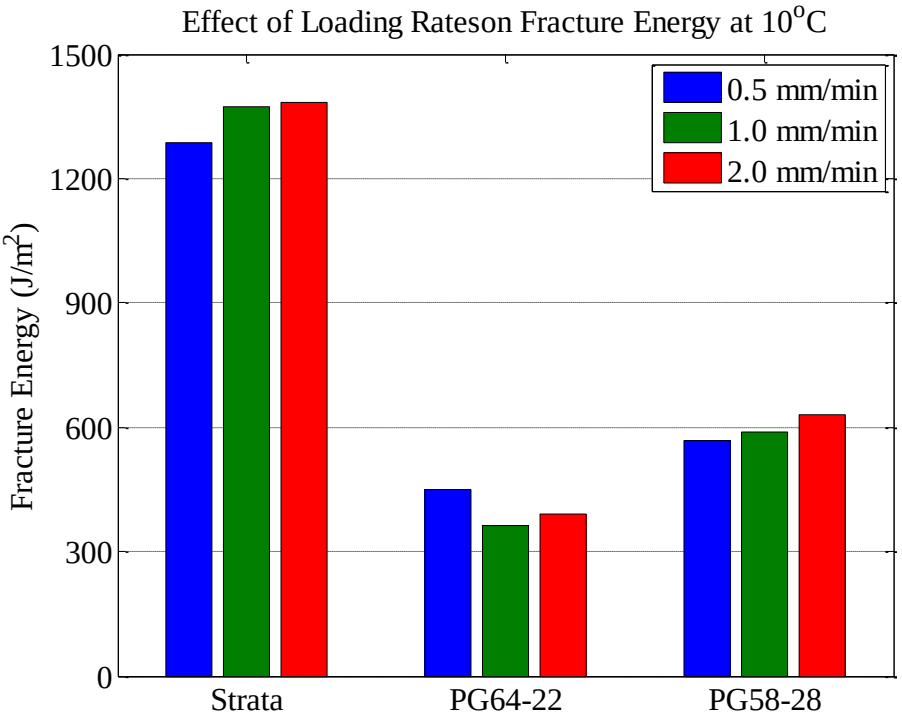

Figure A.12 Fracture energy of the mixtures for different loading rate at 10ºC.

Table A.2 Fracture properties of mixes at 10°C for different loading rates.

Mix	Loading Rate	Peak Load		Fracture Energy (G_f)	
	(mm/min)	Avg. (kN)	CV (%)	Avg. (J/m^2)	CV (%)
4.75-mm Strata (Polymer binder)	0.5	1.89	7.1	1,288	12.0
	1.0	2.15	3.0	1,374	4.6
	2.0	2.17	4.9	1,385	7.1
9.5-mm PG64-22	0.5	2.10	2.2	448	7.4
	1.0	2.11	3.6	364	4.3
	2.0	2.18	5.8	389	5.0
19-mm PG58-28	0.5	1.30	3.9	567	9.0
	1.0	1.52	4.7	588	15.6
	2.0	1.80	3.7	630	10.3

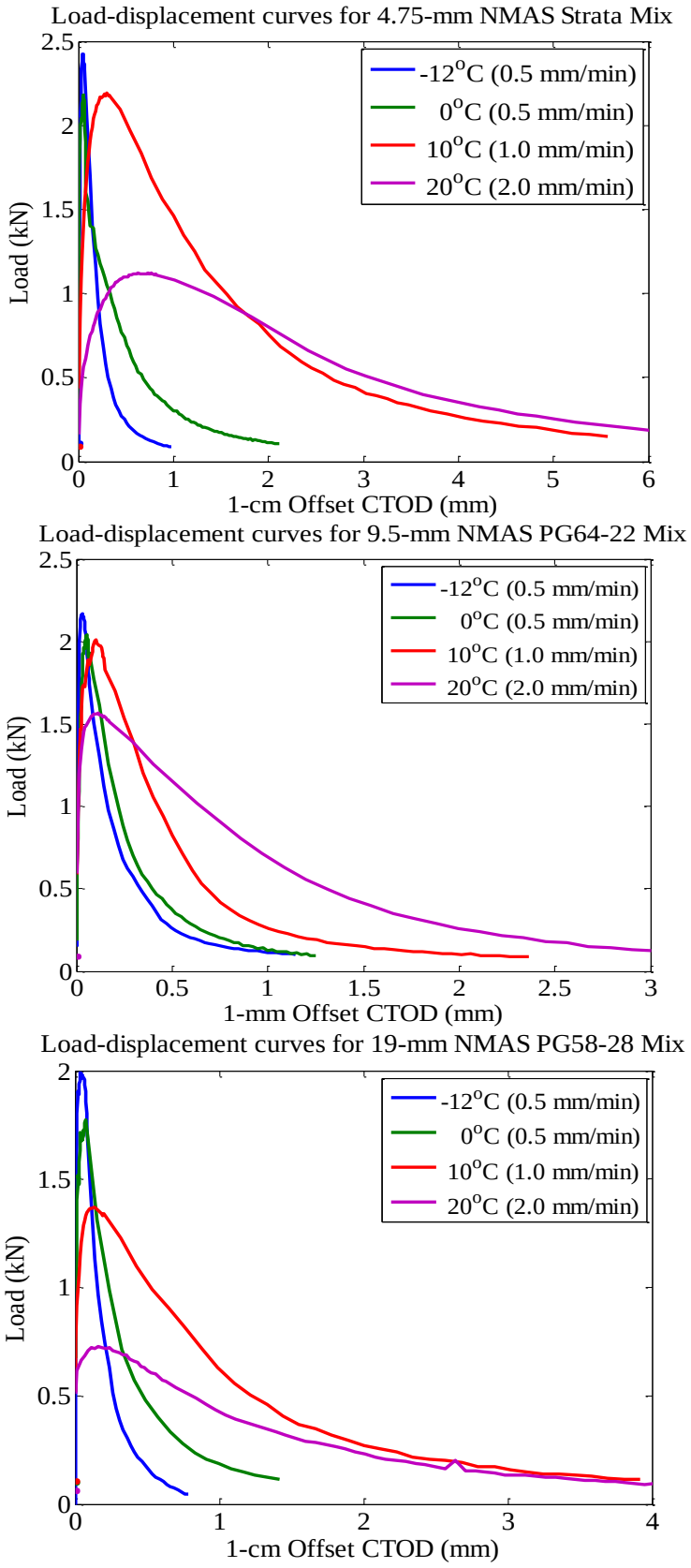

Figure A.13 Summary of load-displacement plots of based mix for proposed loading rates and test temperatures.

Appendix B

Supplemental Figures and Tables for Chapter 4

Table B.1 Summary of released energy parameters of the RED model.

Temp	MIX	Load	Test Data	N_f	Released Energy Parameters				R^2
(°C)		(kN)	%(1)	(cycles)	R1 ($x10^{-03}$)	R2 ($x10^{-05}$)	R3	R4	
-12	4.75-mm NMAS Strata	2.43	100						
		2.00	82	206	16.00	295.30	3.55E-07	5.68E-02	0.9982
		2.00	82	200	14.89	463.10	3.57E-06	4.62E-02	0.9992
		1.90	78	395	13.45	135.40	1.22E-08	3.67E-02	0.9985
		1.90	78	490	12.20	98.07	1.14E-11	4.53E-02	0.9607
		1.80	74	1935	8.73	38.97	2.38E-06	4.30E-03	0.9865
		1.78	73	3488	7.46	35.78	1.74E-11	5.81E-03	0.9994
		1.70	70	6183	7.13	13.83	1.99E-06	1.40E-03	0.9796
		1.68	69	1886	10.50	43.84	1.04E-16	1.75E-02	0.9996
		1.68	69	7368	8.10	15.13	3.50E-10	2.45E-03	0.9990
		1.58	65	3745	8.50	24.66	2.53E-14	7.38E-03	0.9989
		1.58	65	6297	7.09	17.60	7.46E-10	2.65E-03	0.9984
		1.50	62	16983	4.72	6.68	8.02E-10	1.01E-03	0.9918
		1.48	61	7776	5.91	15.72	2.33E-11	2.62E-03	0.9989
-12	9.5-mm NMAS PG64-22	2.32	100						
		2.00	86	47	13.10	1409.00	3.46E-03	3.26E-01	0.9814
		1.97	85	119	9.52	698.90	6.07E-07	9.15E-02	0.9950
		1.95	84	189	9.40	244.40	1.41E-07	6.14E+00	0.9690
		1.92	83	289	8.47	268.70	7.25E-05	2.84E+00	0.9835
		1.90	82	192	8.18	222.90	1.70E-04	2.26E+00	0.8310
		1.90	82	366	9.46	245.10	2.21E-08	3.76E-02	0.9835
		1.90	82	403	7.53	181.70	4.44E-12	5.51E-02	0.9976
		1.85	80	439	6.89	209.00	1.29E-07	2.61E-02	0.9672
		1.82	78	1130	6.67	63.62	1.65E-14	2.44E-02	0.9953
		1.70	73	1912	5.27	44.66	4.59E-15	1.50E-02	0.9950
		1.61	69	2653	6.11	32.92	8.75E-18	1.31E-02	0.9986
		1.55	67	6382	4.75	13.91	2.76E-09	2.42E-03	0.9974
		1.50	65	16400	3.74	7.77	3.68E-15	1.77E-03	0.9977

Note: (1) a percentage to peak-load value of the monotonic test.

Temp	MIX	Load	Test Data	N_f	Released Energy Parameters				R^2
(°C)		(kN)	%(1)	(cycles)	R1 ($x10^{-03}$)	R2 ($x10^{-05}$)	R3	R4	
-12	19-mm NMAS PG58-28	1.99	100						
		1.81	91	87	16.08	728.70	3.98E-05	7.47E-02	0.9980
		1.80	90	125	13.69	731.10	5.93E-04	3.44E-02	0.9956
		1.70	85	1130	8.14	115.20	4.51E-18	3.16E-02	0.9633
		1.70	85	227	9.66	218.90	2.44E-05	3.04E-02	0.9983
		1.70	85	131	13.57	502.40	5.30E-10	1.37E-01	0.9987
		1.60	80	2822	7.14	33.06	2.13E-06	3.47E-03	0.9980
		1.60	80	2238	5.61	43.75	1.35E-13	1.16E-02	0.9986
		1.50	75	3070	6.43	25.99	4.78E-13	8.04E-03	0.9975
		1.50	75	7368	5.50	15.13	3.50E-10	2.45E-03	0.9990
		1.40	70	10039	3.52	7.60	3.35E-14	2.72E-03	0.9988
		1.40	70	2890	7.33	29.92	3.19E-07	3.69E-03	0.9965
		1.20	60	23340	2.65	7.07	1.62E-13	1.10E-03	0.9977
		1.20	60	9685	3.21	19.39	6.87E-10	1.79E-03	0.9988
-12	9.5-mm NAMS RAS	1.60	100						
		1.35	84	78	11.02	1465.00	2.08E-12	3.25E-01	0.9910
		1.30	81	66	14.11	1770.00	2.96E-06	5.13E+00	0.9892
		1.30	81	399	10.65	234.00	9.68E-08	3.15E-02	0.9792
		1.27	79	722	5.71	187.50	6.46E-08	7.34E+00	0.9867
		1.27	79	9375	3.16	12.55	1.55E-10	2.00E-03	0.9976
		1.25	78	12890	3.75	11.75	4.74E-12	1.75E-04	0.9995
		1.25	78	197	8.14	511.00	3.96E-07	5.72E-02	0.9921
		1.23	77	728	5.50	174.00	2.60E-14	3.86E-02	0.9998
		1.20	75	1263	5.35	71.10	4.10E-10	1.39E-02	0.9990
		1.20	75	2690	4.10	43.59	2.68E-14	1.03E-02	0.9975
		1.17	73	3745	4.73	32.86	1.43E-07	3.15E-03	0.9992
		1.17	73	7114	2.93	23.10	3.34E-09	2.26E-02	0.9991
-12	19-mm NMAS FOAMED	1.90	100						
		1.90	100	60	13.23	594.10	1.11E-07	2.04E-01	0.9688
		1.77	93	63	11.43	413.00	1.17E-04	1.06E+00	0.8984
		1.75	92	846	4.94	129.24	7.33E-09	1.65E-02	0.9943
		1.75	92	103	7.75	322.48	7.75E-03	4.62E+00	0.9767
		1.65	87	426	5.32	183.90	1.71E-07	6.16E+00	0.9546
		1.55	82	320	5.41	168.80	4.65E-09	5.69E-02	0.9865
		1.45	76	2879	3.23	25.75	9.42E-16	1.05E-02	0.9868
		1.45	76	1730	4.24	44.90	5.21E-10	6.68E-02	0.9884
		1.40	74	9031	3.16	18.80	4.56E-14	1.78E-04	0.9766
		1.40	74	7405	3.98	13.60	4.23E-18	4.79E-03	0.9909

Note: (1) a percentage to peak-load value of the monotonic test.

Temp	MIX	Load	Test Data	N_f	Released Energy Parameters				R^2
(ºC)		(kN)	%(1)	(cycles)	R1 ($x10^{-03}$)	R2 ($x10^{-05}$)	R3	R4	
0	4.75-mm NMAS Strata	2.20	100						
		1.95	89	200	30.85	545.80	2.11E-06	4.56E-02	0.9893
		1.83	83	710	26.95	150.80	3.93E-09	2.47E-02	0.9984
		1.72	78	815	22.16	207.30	2.81E-10	2.39E-02	0.9920
		1.61	75	1078	13.02		4.72E-07	1.10E-02	0.9999
		1.50	68	1286	16.08	125.10	2.31E-09	1.33E-02	0.9998
		1.33	60	3460	12.35	48.79	5.70E-14	8.09E-03	0.9999
		1.18	54	6481	9.61	23.68	9.98E-11	3.14E-03	0.9998
		1.10	50	12300	8.40	9.69	2.73E-08	5.82E-04	0.9972
0	9.5-mm NMAS PG64-22	1.97	100						
		1.75	89	376	11.79	454.00	4.97E-18	1.02E-01	0.9894
		1.70	86	192	16.03	831.00	3.55E-03	1.46E-02	0.9971
		1.65	84	580	9.64	176.50	1.95E-08	2.43E-02	0.9998
		1.52	77	640	11.31	216.30	6.15E-14	4.27E-02	0.9939
		1.60	81	917	11.10	154.80	4.65E-16	3.56E-02	0.9984
		1.45	74	1743	6.83	82.82	1.10E-14	1.67E-02	0.9992
		1.42	72	2378	6.37	51.15	1.33E-10	7.92E-03	0.9980
		1.33	68	3876	5.60	32.85	7.98E-08	3.56E-03	0.9990
		1.30	66	3675	4.56	41.40	2.18E-09	4.56E-03	0.9992
		1.14	58	11893	2.97	12.50	1.55E-10	1.59E-03	0.9978
		1.05	53	13419	2.79	11.90	3.47E-14	2.05E-03	0.9996
		1.70	86	106	14.14	1702.00	5.02E-04	1.90E+00	0.9858
0	19-mm NMAS PG58-28	1.84	100						
		1.56	85	220	20.50	372.00	2.82E-05	3.00E-02	0.9671
		1.60	87	380	24.90	354.10	1.65E-11	5.64E-02	0.9990
		1.55	84	620	17.40	175.00	4.34E-07	1.88E-02	0.9999
		1.50	82	688	10.05	203.40	1.84E-05	1.10E-02	0.9986
		1.50	82	410	19.27	342.90	2.39E-05	1.94E-02	0.9997
		1.40	76	1588	7.06	140.20	1.59E-08	9.94E-03	0.9997
		1.32	72	1437	8.07	101.60	1.88E-16	7.69E-03	0.9988
		1.24	67	3500	5.98	47.22	4.27E-09	4.83E-03	0.9990
		1.10	60	6450	4.75	31.13	1.96E-17	5.62E-03	0.9845
		1.07	58	2579	5.18	60.10	1.54E-09	6.99E-03	0.9962
		0.98	53	9863	3.59	15.30	2.17E-12	2.44E-03	0.9990
		0.82	45	9435	3.56	21.65	3.34E-13	2.78E-03	0.9990
		1.16	63	3999	8.87	28.54	9.82E-10	4.57E-03	0.9995

Note: (1) a percentage to peak-load value of the monotonic test.

Temp	MIX	Load	Test Data	N_f	Released Energy Parameters				R^2
(ºC)		(kN)	%(1)	(cycles)	R1 ($x10^{-03}$)	R2 ($x10^{-05}$)	R3	R4	
10	4.75-mm NMAS Strata	2.15	100						
		1.77	82	599	45.73	243.50	2.56E-08	2.87E-02	0.9999
		1.70	79	370	87.08	389.60	4.94E-07	3.73E-02	0.9998
		1.65	77	266	101.93	579.70	1.82E-07	5.44E-02	1.0000
		1.65	77	702	80.14	213.90	4.08E-07	1.99E-02	0.9999
		1.50	70	850	58.30	181.90	2.87E-07	2.06E-02	0.9999
		1.40	65	935	44.83	167.60	1.43E-07	1.58E-02	0.9999
		1.30	60	1445	30.30	98.59	2.58E-08	1.15E-02	0.9998
		1.20	56	1501	24.33	111.50	2.79E-11	1.54E-02	0.9999
		1.10	51	9385	12.05	12.43	8.21E-13	2.82E-03	0.9987
		1.00	47	5283	20.38	32.59	3.80E-12	4.75E-03	0.9992
		1.00	47	5278	19.74	31.00	8.03E-11	4.17E-03	0.9991
10	9.5-mm NMAS PG64-22	2.11	100						
		1.75	83	443	21.89	355.40	2.67E-08	3.58E-02	0.9999
		1.83	87	207	39.31	477.30	2.33E-08	4.03E-02	0.9999
		1.60	76	113	38.63	1328.00	5.03E-06	8.33E-02	0.9949
		1.55	73	760	15.88	204.30	5.02E-08	1.95E-02	0.9999
		1.50	71	343	27.33	329.00	8.62E-08	3.92E-02	0.9999
		1.40	66	711	13.66	188.60	1.58E-06	1.53E-02	0.9999
		1.30	62	817	15.20	159.80	8.34E-07	1.40E-02	0.9998
		1.20	57	1371	11.92	105.90	4.30E-10	1.39E-02	0.9997
		1.10	52	1966	9.36	89.00	7.06E-09	8.30E-03	0.9989
		1.00	47	4782	7.13	33.51	2.44E-14	6.05E-03	0.9999
		1.00	47	4487	9.86	28.53	3.81E-12	5.26E-03	0.9993
		0.85	40	12190	4.36	13.26	1.05E-12	1.95E-03	0.9988
10	19-mm NMAS PG58-28	1.52	100						
		1.38	91	145	41.91	1230.00	7.20E-07	9.62E-02	0.9999
		1.30	86	201	39.05	941.60	6.02E-08	8.32E-01	0.9999
		1.20	79	195	43.46	799.80	3.38E-06	6.01E-02	0.9999
		1.13	74	245	34.79	991.20	1.70E-09	7.84E-02	0.9999
		1.10	72	406	16.18	521.50	9.51E-11	5.45E-02	0.9999
		1.00	66	755	20.10	256.10	9.82E-11	2.94E-02	0.9999
		0.90	59	716	11.49	273.60	3.59E-09	2.56E-02	0.9953
		0.83	55	3927	9.73	36.43	2.40E-10	2.51E-02	0.9980
		0.75	49	2550	6.91	87.48	2.27E-14	1.17E-02	0.9997
		0.70	46	5465	7.97	46.02	3.73E-14	5.34E-03	0.9980
		0.65	43	5216	8.15	30.50	1.20E-15	6.23E-03	0.9980
		0.60	39	15350	4.22	10.67	1.11E-12	1.63E-03	0.9984

Note: (1) a percentage to peak-load value of the monotonic test.

Temp	MIX	Load	Test Data	N_f	Released Energy Parameters				R^2
(°C)		(kN)	%(1)	(cycles)	R1 ($x10^{-03}$)	R2 ($x10^{-05}$)	R3	R4	
20	4.75-mm NMAS Strata	1.11	100						
		1.00	90	240	159.10	683.90	1.28E-05	4.76E-02	0.999
		1.00	90	326	125.30	515.30	7.55E-08	5.10E-02	1.0000
		0.90	81	441	108.90	376.70	3.37E-07	3.34E-02	1.0000
		0.83	75	665	103.90	213.00	4.67E-06	1.83E-02	0.9997
		0.83	75	807	73.44	199.20	4.57E-07	1.79E-02	0.9998
		0.75	68	815	85.71	202.70	2.89E-08	2.14E-02	1.0000
		0.71	64	3716	43.66	39.85	9.27E-12	6.60E-03	0.9995
		0.70	63	4265	49.74	30.30	2.48E-12	6.07E-03	0.9990
		0.70	63	1657	59.33	86.10	1.98E-12	1.61E-02	0.9998
		0.65	59	2754	59.04	55.19	4.76E-14	1.10E-02	0.9991
		0.60	54	6375	31.78	21.89	1.75E-11	3.70E-03	0.9990
		0.55	50	7035	39.67	18.96	1.05E-12	1.55E-03	0.9987
		0.55	50	15782	26.50	8.03	7.92E-15	1.97E-03	0.9980
		0.64	65	3128	56.47	36.88	4.87E-15	3.06E-03	0.9975
20	9.5-mm NMAS PG64-22	1.59	100						
		1.10	69	234	28.38	769.40	3.14E-07	5.93E-02	0.9999
		1.05	66	355	28.50	450.10	4.55E-08	4.48E-02	0.9999
		1.00	63	566	23.50	269.00	8.20E-14	5.21E-02	0.9995
		0.98	62	640	17.73	302.90	1.33E-11	3.77E-02	0.9999
		0.95	60	816	14.93	264.40	3.59E-16	4.22E-02	0.9948
		0.90	57	1167	19.97	138.60	6.38E-11	1.92E-02	0.9998
		0.60	55	4503	11.51	41.70	9.03E-13	5.82E-03	0.9965
		0.80	50	1343	18.49	108.30	2.79E-08	1.19E-02	0.9996
		0.75	47	2908	14.85	44.00	4.97E-13	9.21E-03	0.9998
		0.70	44	4882	13.25	30.93	7.15E-14	5.82E-03	0.9979
		0.65	41	1145	18.38	135.60	1.17E-09	1.68E-02	0.9997
		0.60	38	7588	8.64	19.20	1.75E-11	2.95E-03	0.9987
		0.54	34	28421	6.33	3.20	1.28E-13	9.42E-04	0.9906

Note: (1) a percentage to peak-load value of the monotonic test.

Temp	MIX	Load	Test Data	N_f	Released Energy Parameters				R^2
(°C)		(kN)	%(1)	(cycles)	R1 ($x10^{-03}$)	R2 ($x10^{-05}$)	R3	R4	
20	19-mm NMAS PG58-28	0.95	100						
		0.85	89	428	28.21	492.30	4.10E-09	4.45E-02	0.9999
		0.80	84	302	44.15	590.70	4.94E-07	4.89E-02	1.0000
		0.75	79	470	30.28	396.50	2.02E-09	4.18E-02	0.9999
		0.70	74	318	36.59	656.60	9.62E-10	6.47E-02	1.0000
		0.70	74	498	41.91	361.20	7.01E-13	5.61E-02	0.9854
		0.60	63	842	24.08	220.10	6.79E-10	2.42E-02	0.9999
		0.55	58	7260	12.61	15.96	5.28E-04	6.76E-04	0.9973
		0.55	58	1281	22.98	128.20	1.37E-13	2.26E-02	0.9999
		0.50	53	3952	11.00	48.80	2.28E-10	5.14E-03	0.9979
		0.50	53	1930	19.12	74.98	2.94E-15	1.70E-02	0.9993
		0.45	47	2112	14.80	107.10	1.34E-15	1.59E-02	0.9988
		0.45	47	19924	8.91	5.10	4.73E-10	9.56E-04	0.9986
		0.40	42	4177	10.16	43.37	4.18E-16	8.12E-03	0.9986
		0.30	32	9710	7.60	17.81	1.74E-14	3.09E-03	0.9988
20	9.5-mm NAMS RAS	1.30	100						
		1.05	81	181	34.24	891.60	3.07E-08	9.06E-02	0.9998
		0.85	65	385	18.83	375.70	1.60E-08	4.29E-02	0.9980
		0.85	65	337	18.22	500.10	4.27E-08	4.62E-02	0.9998
		0.80	62	612	22.93	301.80	1.31E-09	3.14E-02	0.9998
		0.75	58	1592	12.80	103.90	1.98E-12	1.59E-03	0.9998
		0.70	54	1187	12.25	153.00	2.20E-13	2.32E-02	0.9997
		0.65	50	5365	6.84	38.82	4.67E-16	6.22E-03	0.9970
		0.55	42	1317	7.77	133.50	6.97E-13	1.97E-02	0.9998
		0.55	42	3184	5.03	34.00	2.05E-13	8.81E-03	0.9963
		0.50	38	2394	6.20	90.82	3.25E-14	1.22E-02	0.9997
		0.45	35	7100	1.96	10.41	3.90E-19	2.32E-03	0.9973
20	19-mm NMAS FOAMED	1.60	100						
		1.24	78	147	49.31	1167.00	1.54E-06	8.97E-02	0.9999
		1.20	75	271	29.54	690.40	1.01E-09	2.95E-02	0.9977
		1.15	72	312	37.44	446.20	5.70E-09	5.86E-02	0.9999
		1.05	66	538	36.50	329.00	8.47E-11	4.22E-02	0.9999
		1.00	63	1144	28.52	135.00	1.34E-10	1.94E-02	0.9999
		0.90	56	1666	22.24	97.53	3.95E-11	1.36E-02	0.9997
		0.80	50	3822	17.40	40.11	1.83E-12	6.63E-03	0.9977
		0.65	41	6531	14.60	19.22	1.50E-09	2.83E-03	0.9979
		0.70	44	8249	13.43	16.96	7.90E-14	3.43E-03	0.9987
		0.70	44	8580	10.72	15.23	7.11E-18	4.33E-03	0.9941
		0.75	47	2845	15.09	79.36	1.20E-13	1.01E-02	0.9995

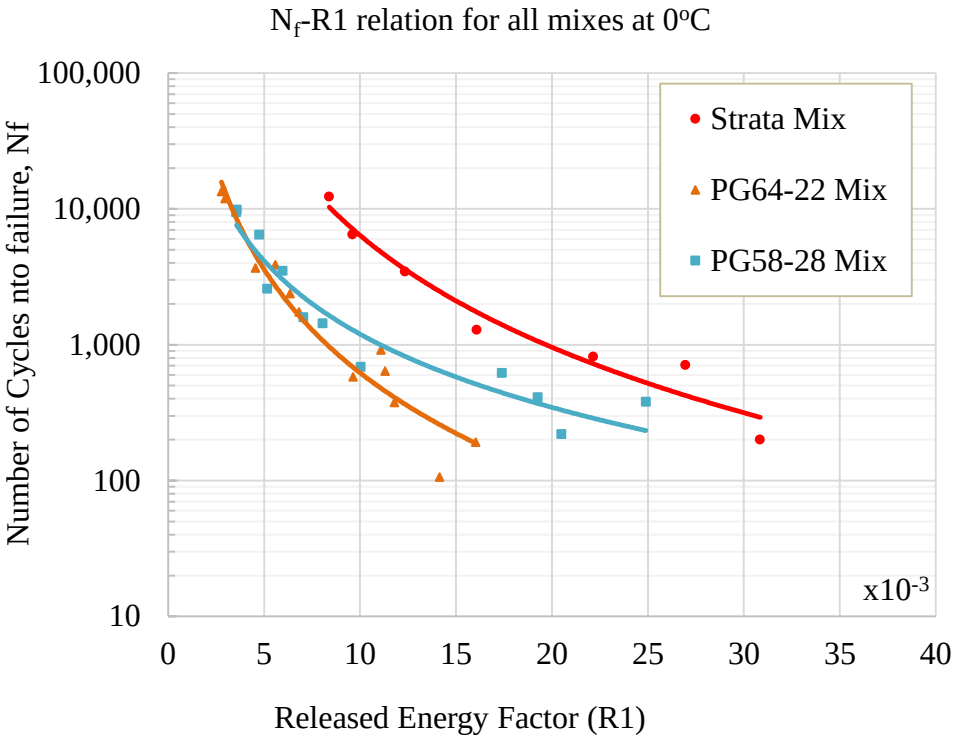

Figure B.1 N_f-R1 relation for all mixes at temperature of 0ºC.

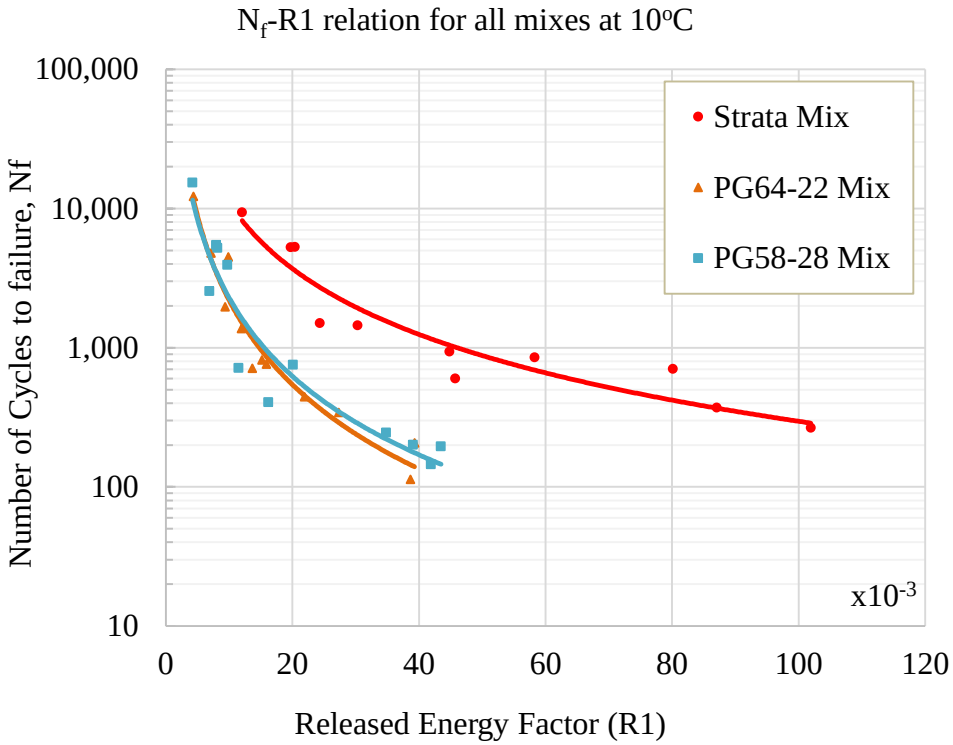

Figure B.2 N_f-R1 relation for all mixes at temperature of 10ºC.

Table B.2 Summary of C1, C2, and R^2 values for all test temperatures.

Temp (°C)	Mixture	C1	C2	R^2
-12°C	4.75-mm NMAS Strata	$1x10^7$	3.909	0.9336
	9.5-mm NMAS PG64-22	$8x10^6$	4.774	0.9329
	19-mm NMAS PG58-28	$7.1x10^5$	3.178	0.9125
	9.5-mm RAS with Eco-binder	$3.8x10^5$	3.326	0.8936
	19-mm NMAS Foamed mix	$2.7x10^5$	3.516	0.8685
0°C	4.75-mm NMAS Strata	$3x10^6$	2.738	0.9541
	9.5-mm NMAS PG64-22	$2.1x10^5$	2.531	0.9368
	19-mm NMAS PG58-28	$7.4x10^4$	1.793	0.9243
10°C	4.75-mm NMAS Strata	$4.1x10^5$	1.569	0.9005
	9.5-mm NMAS PG64-22	$2.2x10^5$	2.012	0.9477
	19-mm NMAS PG58-28	$1.7x10^5$	1.874	0.9024
20°C	4.75-mm NMAS Strata	$3x10^7$	2.354	0.9648
	9.5-mm NMAS PG64-22	$6x10^6$	2.944	0.9098
	19-mm NMAS PG58-28	$1x10^6$	2.195	0.9091
	9.5-mm RAS with Eco-binder	$2.7x10^4$	1.336	0.8448
	19-mm NMAS Foamed mix	$1x10^7$	2.902	0.9293

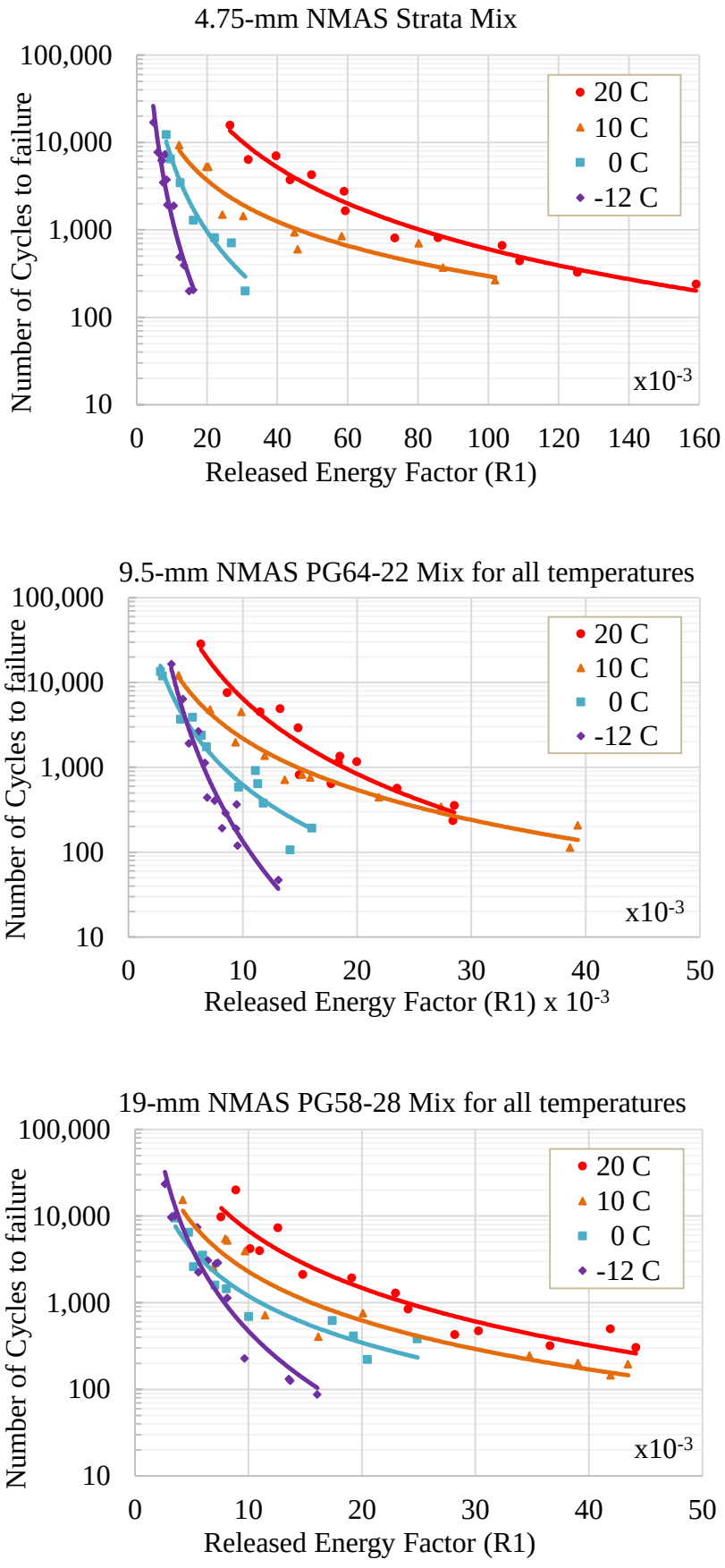

Figure B.3 Comparison of Nf-R1 curves of PG58-28 mix for all temperatures.

Appendix C

Supplemental plots and tables for chapter 5

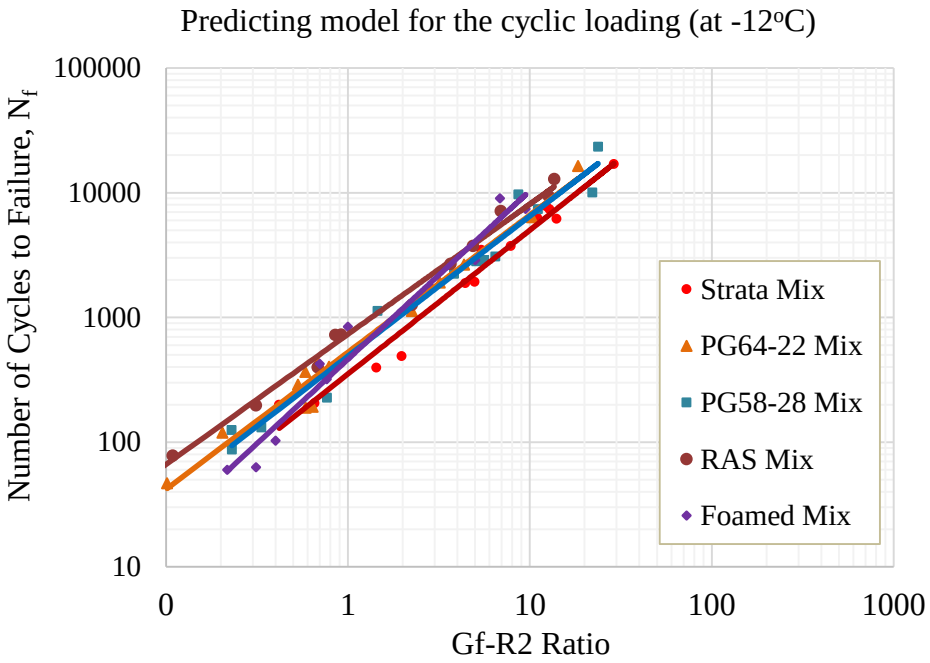

Figure C.1 Proposed model of cyclic loading test at -12ºC based on a relation between a ratio of fracture energy to R2 and numbers of cycles to failures, $N_{f.}$

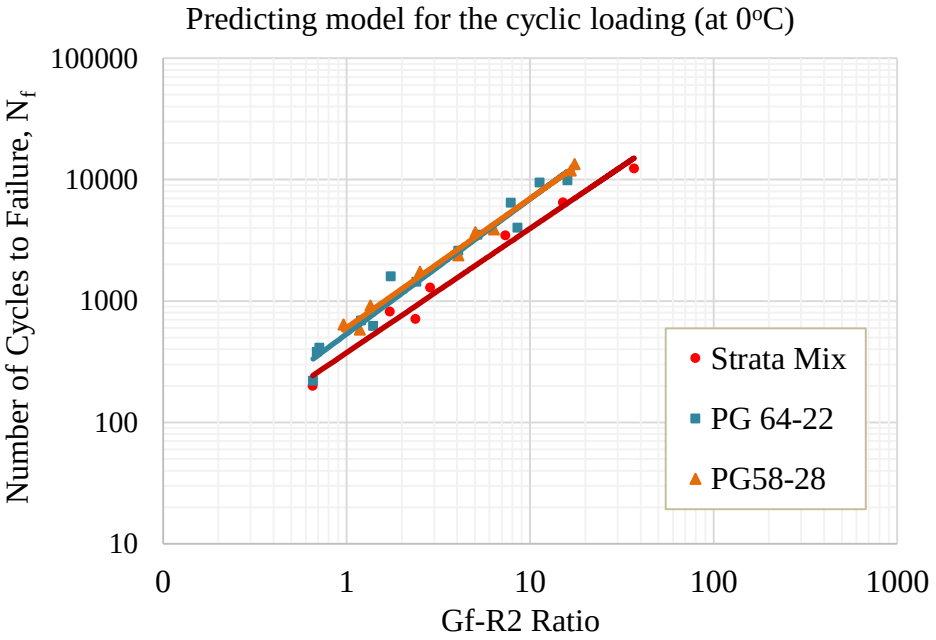

Figure C.2 Proposed model of cyclic loading test at 0ºC based on relation between ratio of fracture energy to R2 and numbers of cycles to failures, $N_{f.}$

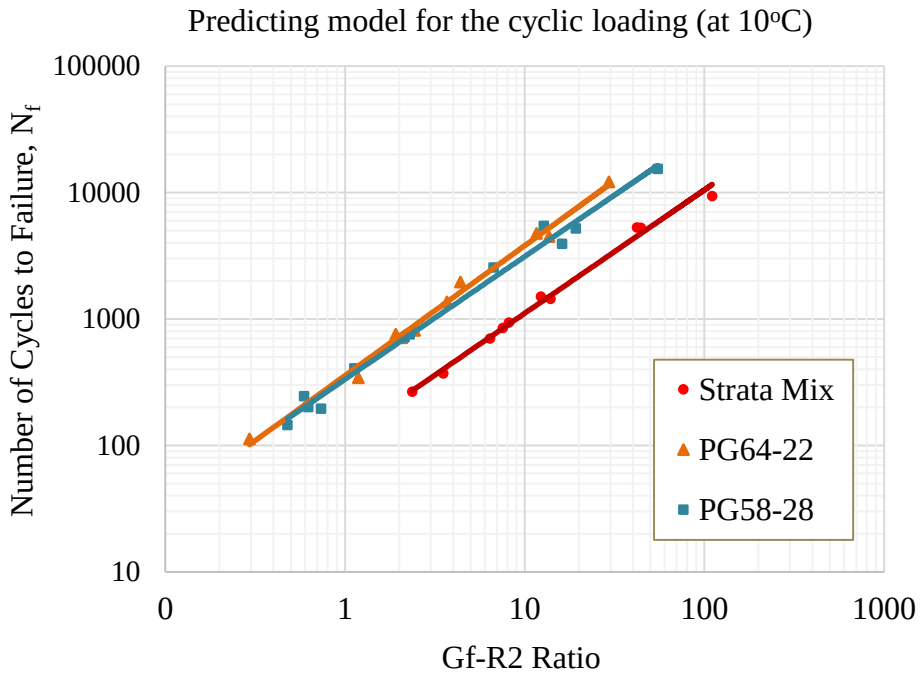

Figure C.3 Proposed model of cyclic loading test at 10°C based on relation between ratio of fracture energy to R2 and numbers of cycles to failures, N_f.

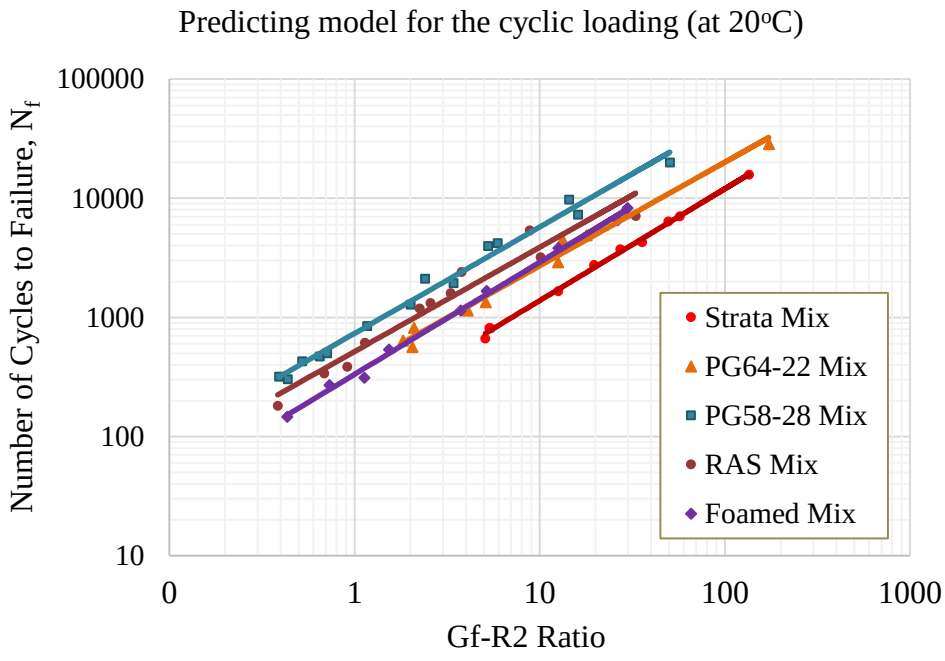

Figure C.4 Proposed model of cyclic loading test at 20°C based on relation between ratio of fracture energy to R2 and numbers of cycles to failures, N_f..

Table C.1 Summary of A and B coefficients based up limited numbers of specimens.

Temp	Mix	6 replicates			3 replicates		
		A	B	R^2	A	B	R^2
-12°C	Strata Mix	285.81	1.204	0.988	323.7	1.163	0.999
	PG64-22 Mix	475.86	1.169	0.982	383.45	1.296	0.999
	PG58-28 Mix	332.77	1.354	0.974	302.31	1.337	0.995
	RAS Mix	665.13	1.135	0.979	612.38	1.1605	0.998
	Foamed Mix	571.86	1.195	0.931	441.49	1.399	0.956
0°C	Strata Mix	347.86	1.047	0.984	343.27	1.034	0.9891
	PG64-22 Mix	667.58	0.989	0.982	768.98	0.964	0.998
	PG58-28 Mix	577.36	1.079	0.992	578.14	1.044	0.998
10°C	Strata Mix	125.74	0.948	0.993	129.5	0.922	0.996
	PG64-22 Mix	342.88	1.052	0.983	293.09	1.133	0.991
	PG58-28 Mix	344.72	0.968	0.985	306.08	0.957	0.998
20°C	Strata Mix	159.50	0.935	0.999	154.09	0.938	0.999
	PG64-22 Mix	346.69	0.881	0.996	332.91	0.880	0.997
	PG58-28 Mix	707.99	0.871	0.991	708.92	0.884	0.987
	RAS Mix	539.97	0.817	0.938	495.76	0.779	0.978
	Foamed Mix	367.92	0.899	0.999	365.17	0.906	0.999

Table C.2 Summary of A and B based on monotonic DC(T) results alone.

Temp	Mix	Model A			Model B		
		A	B	R^2	A	B	R^2
-12°C	Strata Mix	285.81	1.204	0.988	323.7	1.163	0.999
	PG64-22 Mix	475.86	1.169	0.982	383.45	1.296	0.999
	PG58-28 Mix	332.77	1.354	0.974	302.31	1.337	0.995
	RAS Mix	665.13	1.135	0.979	612.38	1.1605	0.998
	Foamed Mix	571.86	1.195	0.931	441.49	1.399	0.956
0°C	Strata Mix	347.86	1.047	0.984	343.27	1.034	0.9891
	PG64-22 Mix	667.58	0.989	0.982	768.98	0.964	0.998
	PG58-28 Mix	577.36	1.079	0.992	578.14	1.044	0.998
10°C	Strata Mix	125.74	0.948	0.993	129.5	0.922	0.996
	PG64-22 Mix	342.88	1.052	0.983	293.09	1.133	0.991
	PG58-28 Mix	344.72	0.968	0.985	306.08	0.957	0.998
20°C	Strata Mix	159.50	0.935	0.999	154.09	0.938	0.999
	PG64-22 Mix	346.69	0.881	0.996	332.91	0.880	0.997
	PG58-28 Mix	707.99	0.871	0.991	708.92	0.884	0.987
	RAS Mix	539.97	0.817	0.938	495.76	0.779	0.978
	Foamed Mix	367.92	0.899	0.999	365.17	0.906	0.999

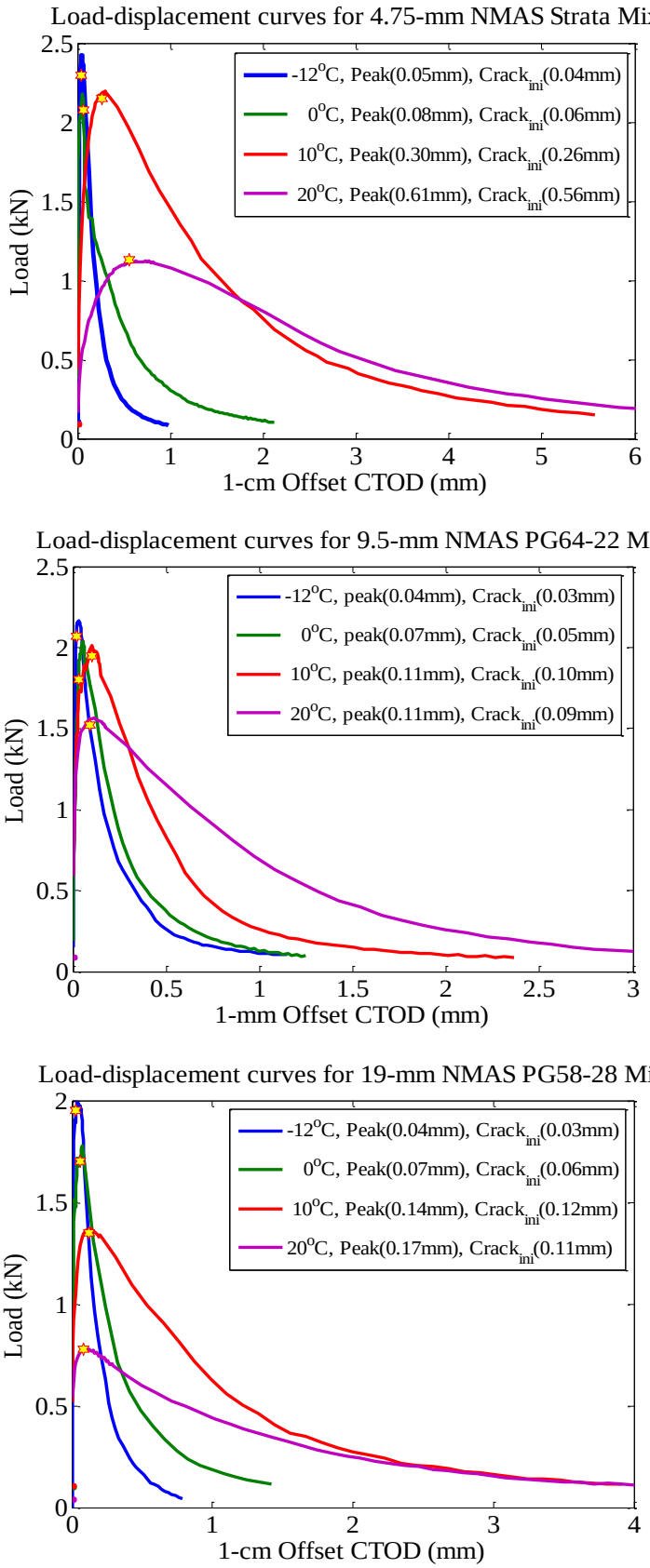

Figure C.5 Graphical presentation of crack initiation on load-displacement curves.

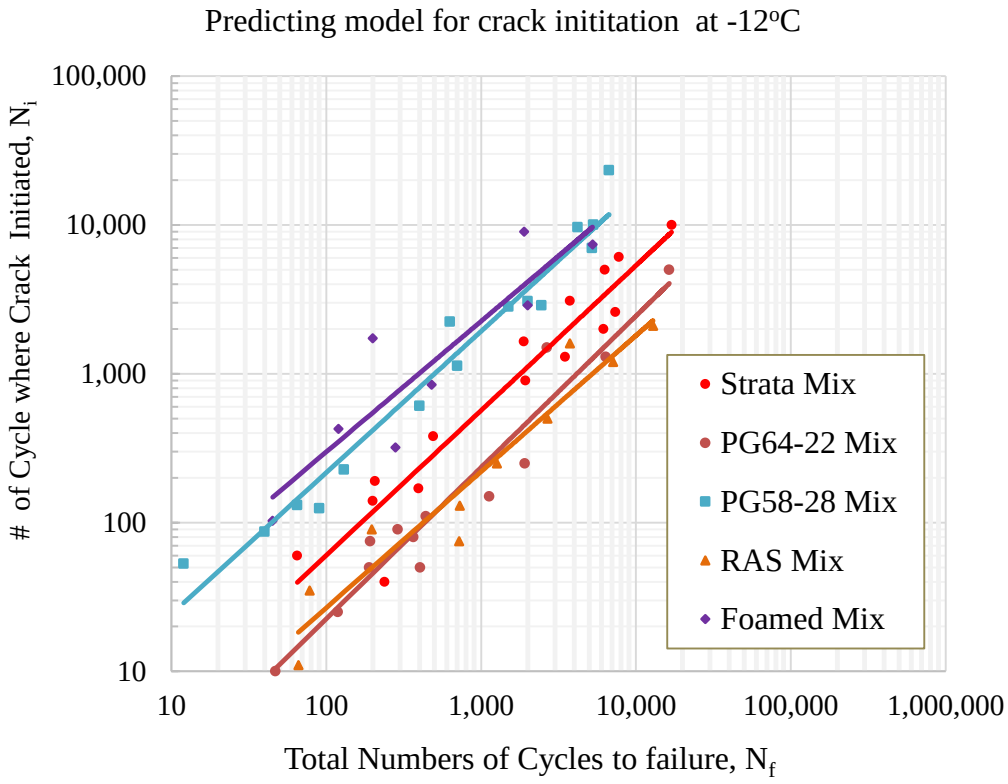

Figure C.6 N_i-N_f relation at test temperature of -12ºC.

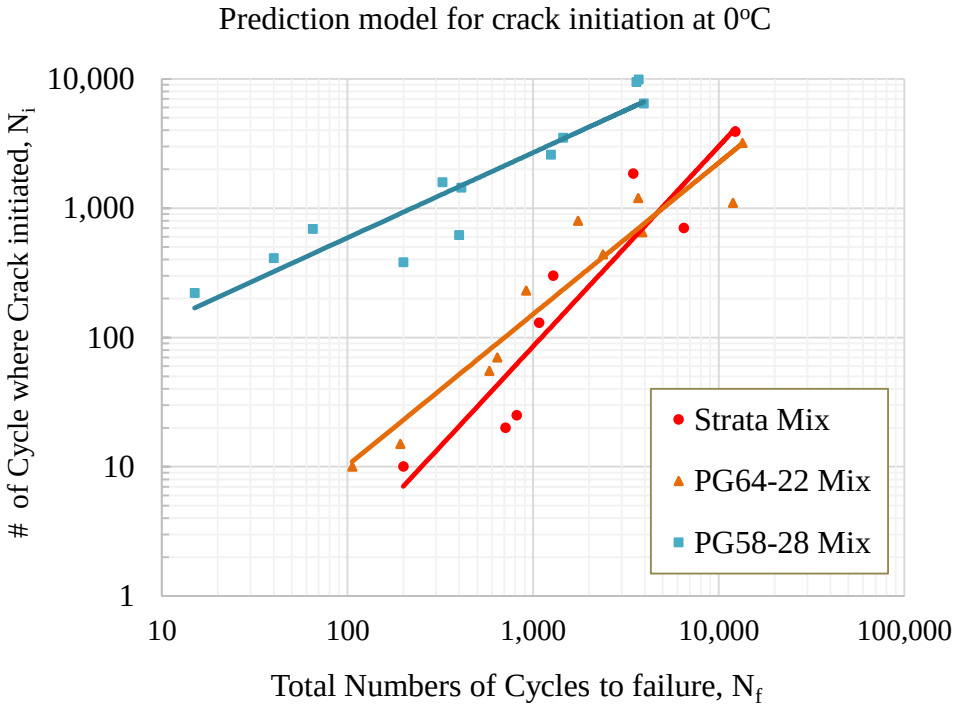

Figure C.7 N_i-N_f relation at test temperature of 0ºC.

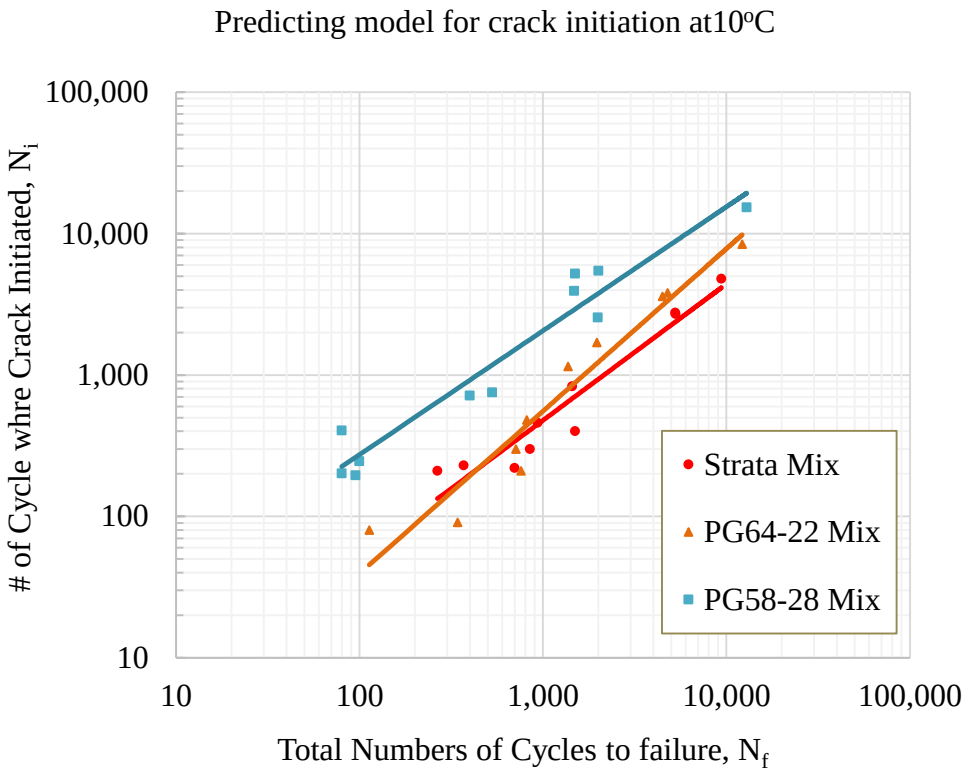

Figure C.8 N_i-N_f relation at test temperature of 10°C.

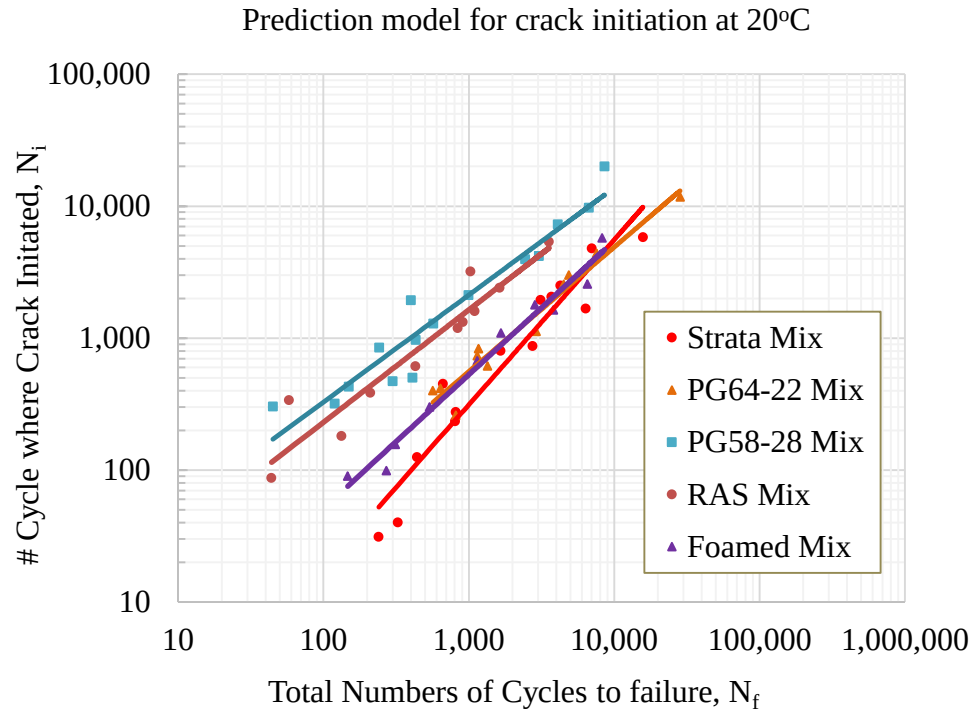

FigureC.9 N_i-N_f relation at test temperature of 20°C.

Table C.3 Summary of F1 and F2 for predicting model of crack initiation.

Temp (^{o}C)	Mixture	F1	F2	R^2
-12^{o}C	4.75-mm NMAS Strata	0.679	0.974	0.919
	9.5-mm NMAS PG64-22	0.396	0.915	0.921
	19-mm NMAS PG58-28	2.717	0.951	0.964
	9.5-mm RAS with Eco-binder	0.208	1.017	0.937
	19-mm NMAS Foamed mix	5.221	0.879	0.816
0^{o}C	4.75-mm NMAS Strata	0.002	1.547	0.865
	9.5-mm NMAS PG64-22	0.3956	0.915	0.921
	19-mm NMAS PG58-28	28.489	0.658	0.876
10^{o}C	4.75-mm NMAS Strata	0.614	0.964	0.924
	9.5-mm NMAS PG64-22	0.396	0.915	0.921
	19-mm NMAS PG58-28	4.835	0.876	0.937
20^{o}C	4.75-mm NMAS Strata	0.055	1.2651	0.924
	9.5-mm NMAS PG64-22	0.396	0.915	0.921
	19-mm NMAS PG58-28	7.780	1.812	0.920
	9.5-mm RAS with Eco-binder	4.563	0.851	0.901
	19-mm NMAS Foamed mix	0.478	1.014	0.976

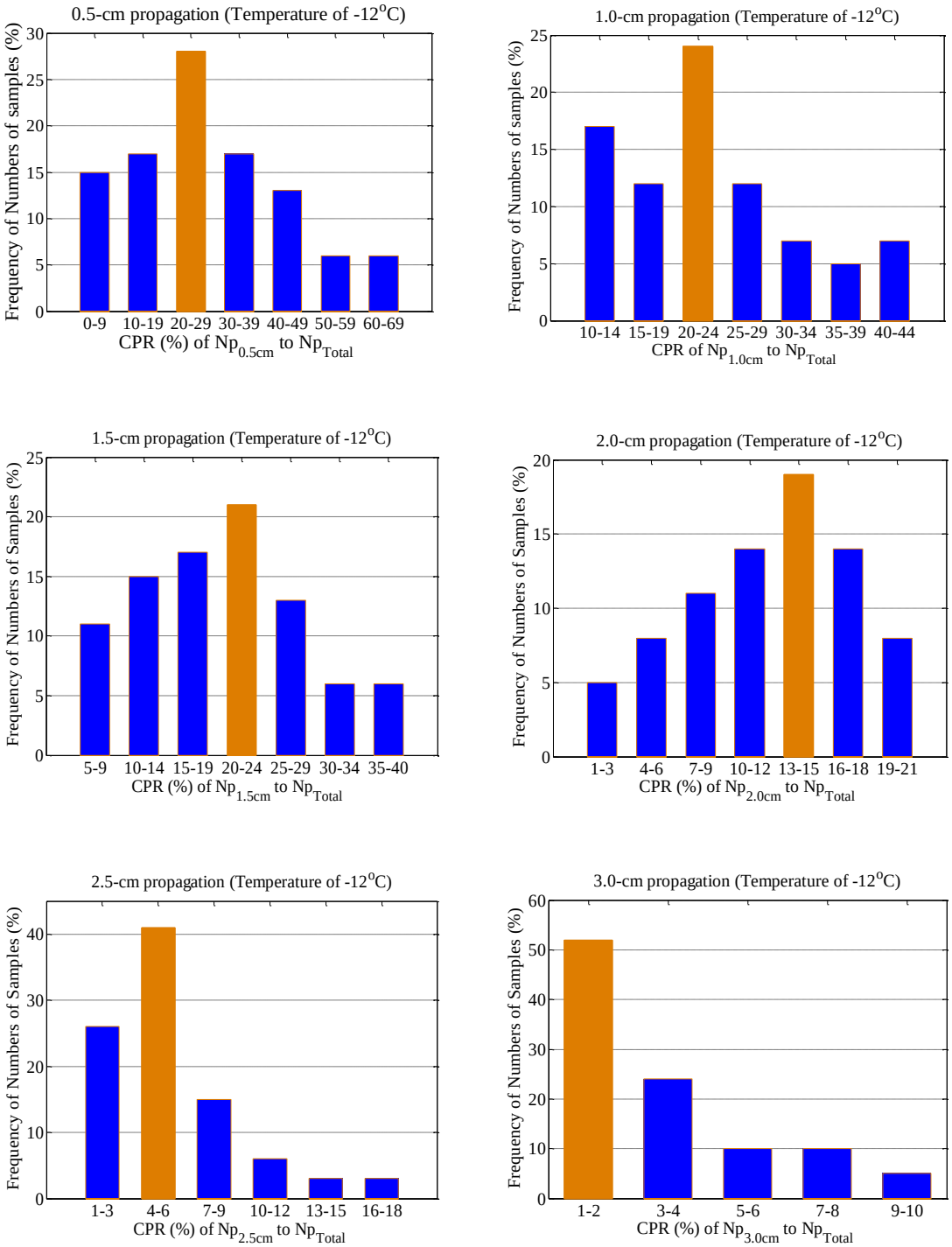

Figure C.10 Histograms of crack propagation ratio (CPR) at each crack length for all mixtures tested at -12°C.

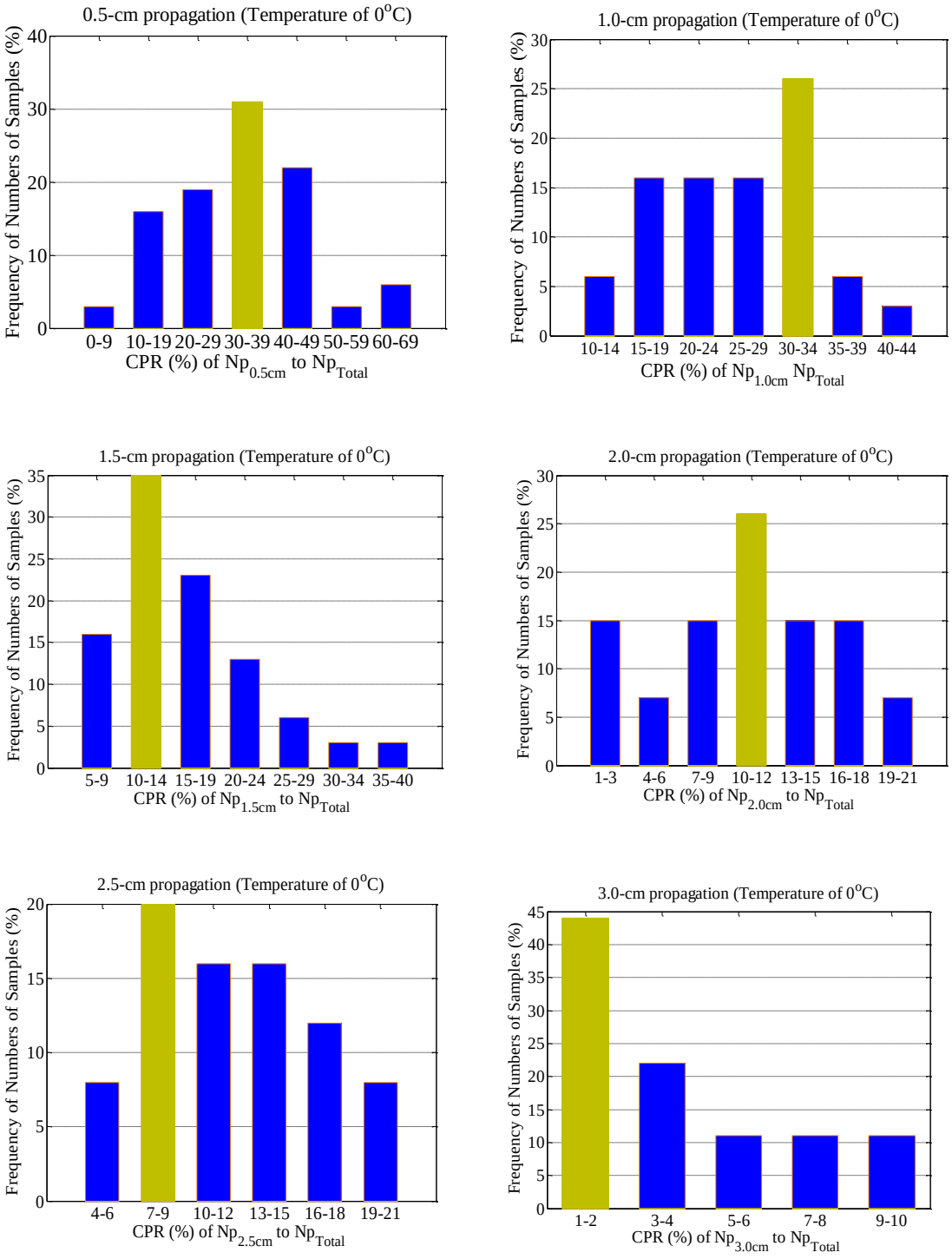

Figure C.11 Histograms of crack propagation ratio (CPR) at each crack length for all mixtures tested at 0°C.

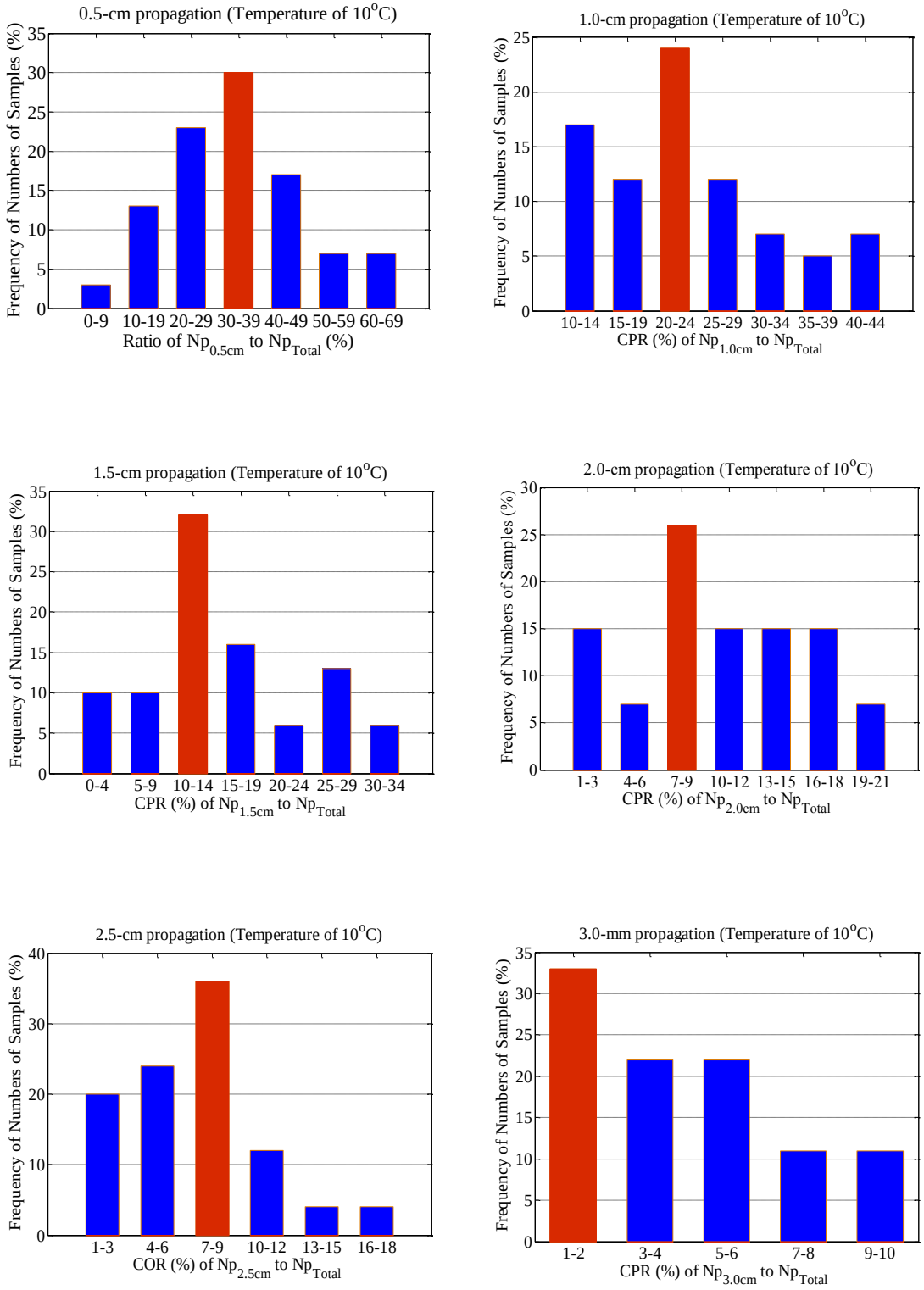

Figure C.12 Histograms of crack propagation ratio (CPR) at each crack length for all mixtures tested at 10°C.

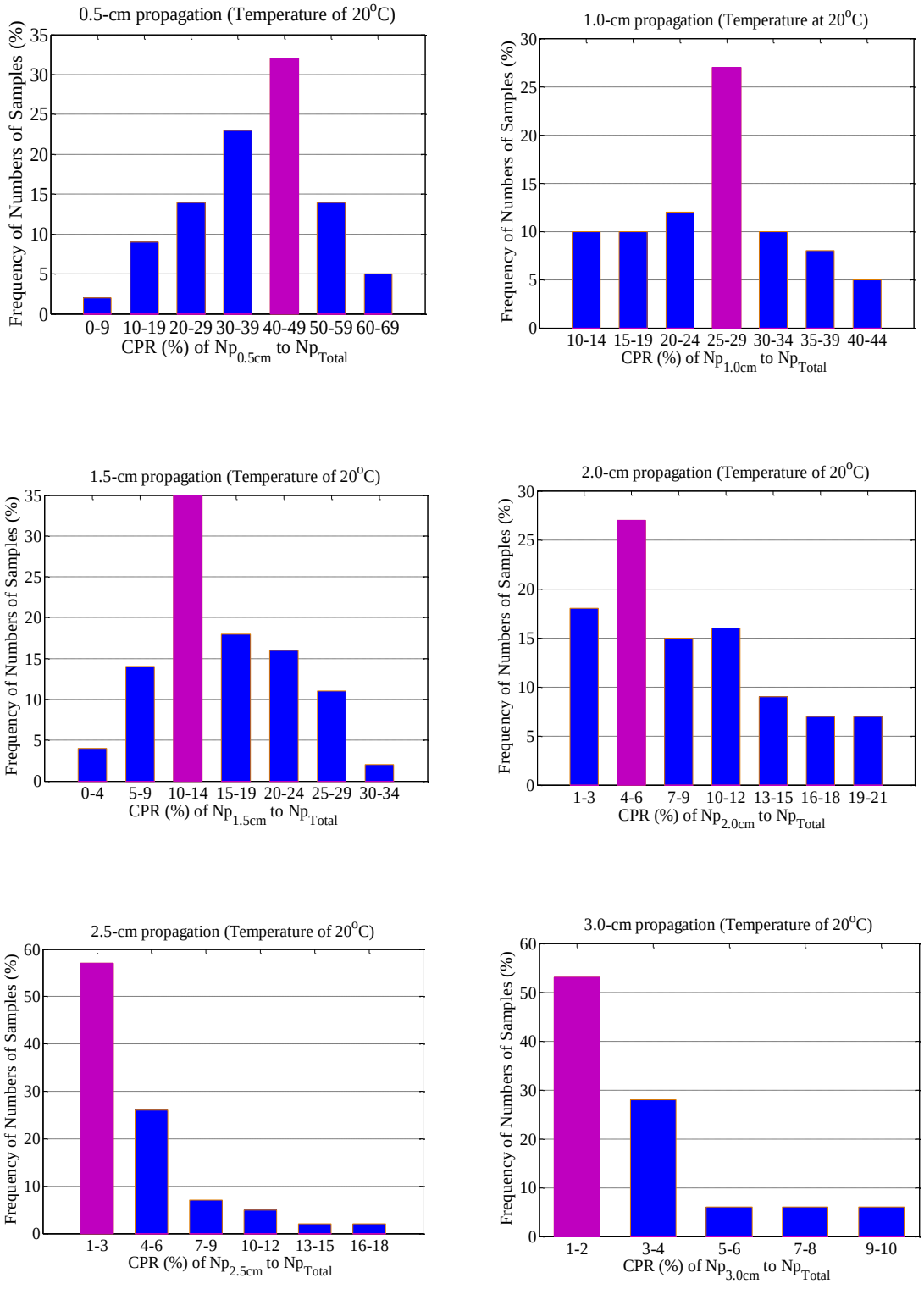

Figure C.13 Histograms of crack propagation ratio (CPR) at each crack length for all mixtures tested at 20°C.

Appendix D

Plots of load-displacement relations and RED models

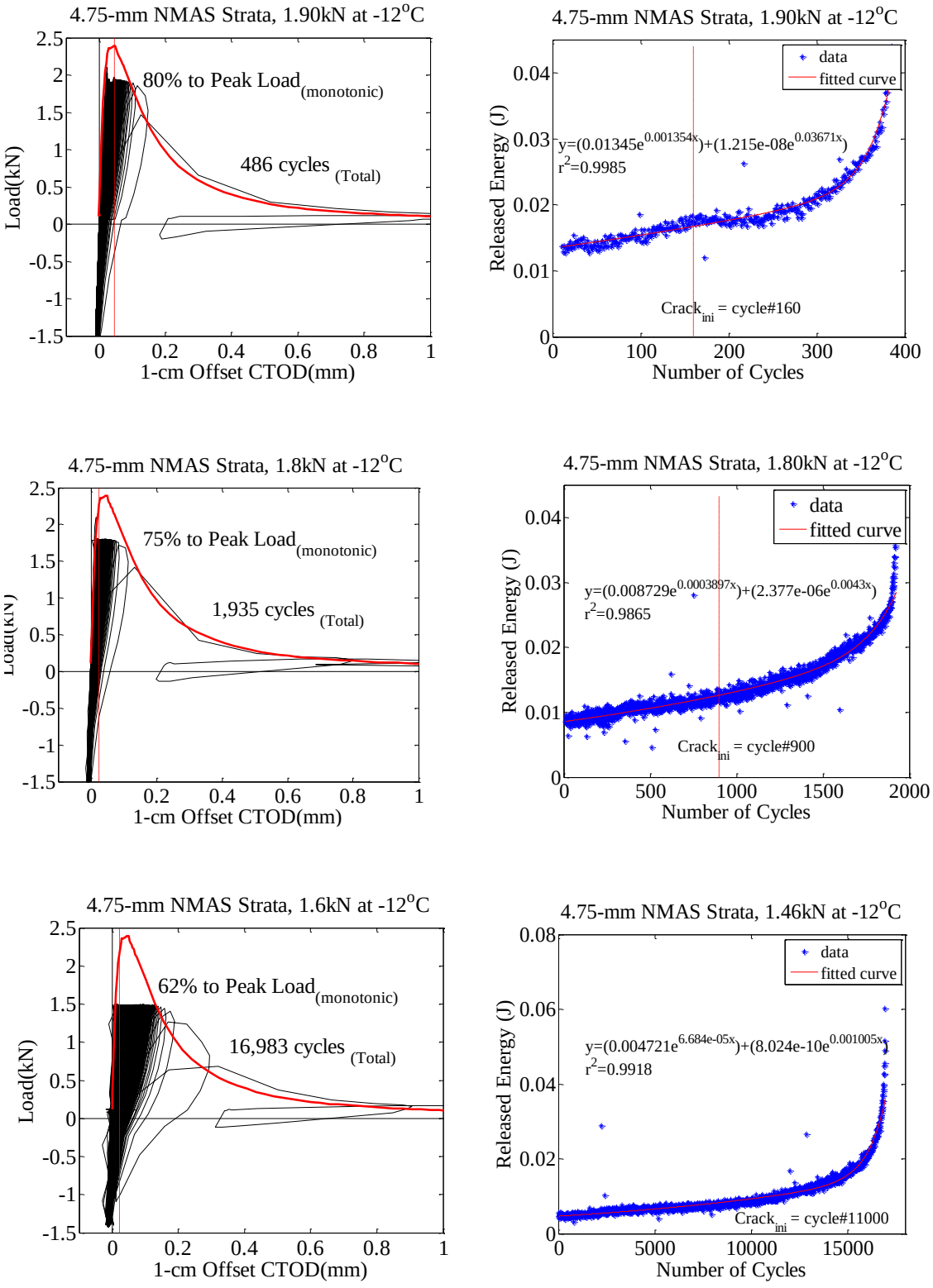

FigureD.1 Examples of load-displacement relations and RED models for Strata mix conducted at -12°C.

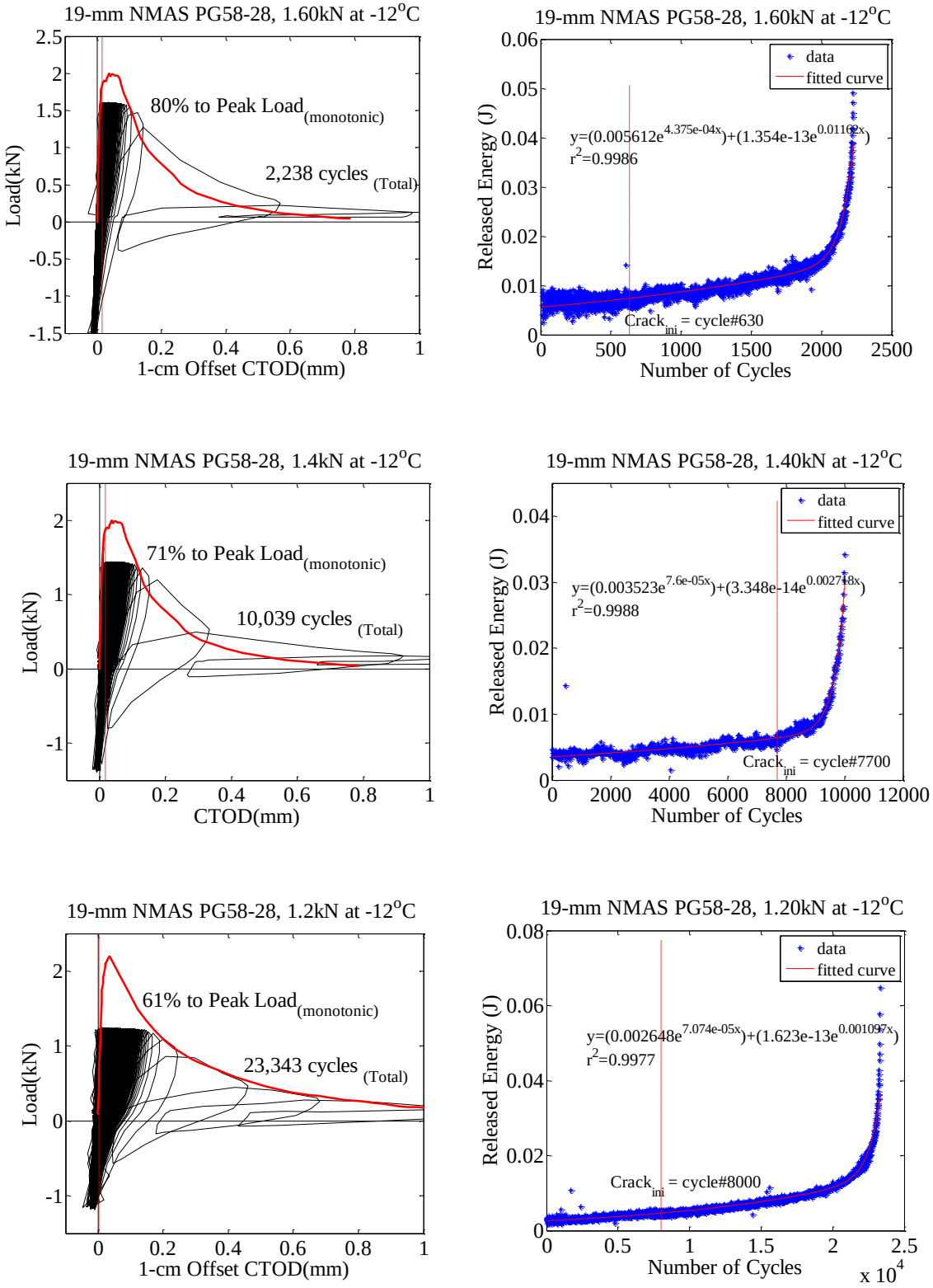

FigureD.2 Examples of load-displacement relations and RED models for PG58-28 mix conducted at -12°C.

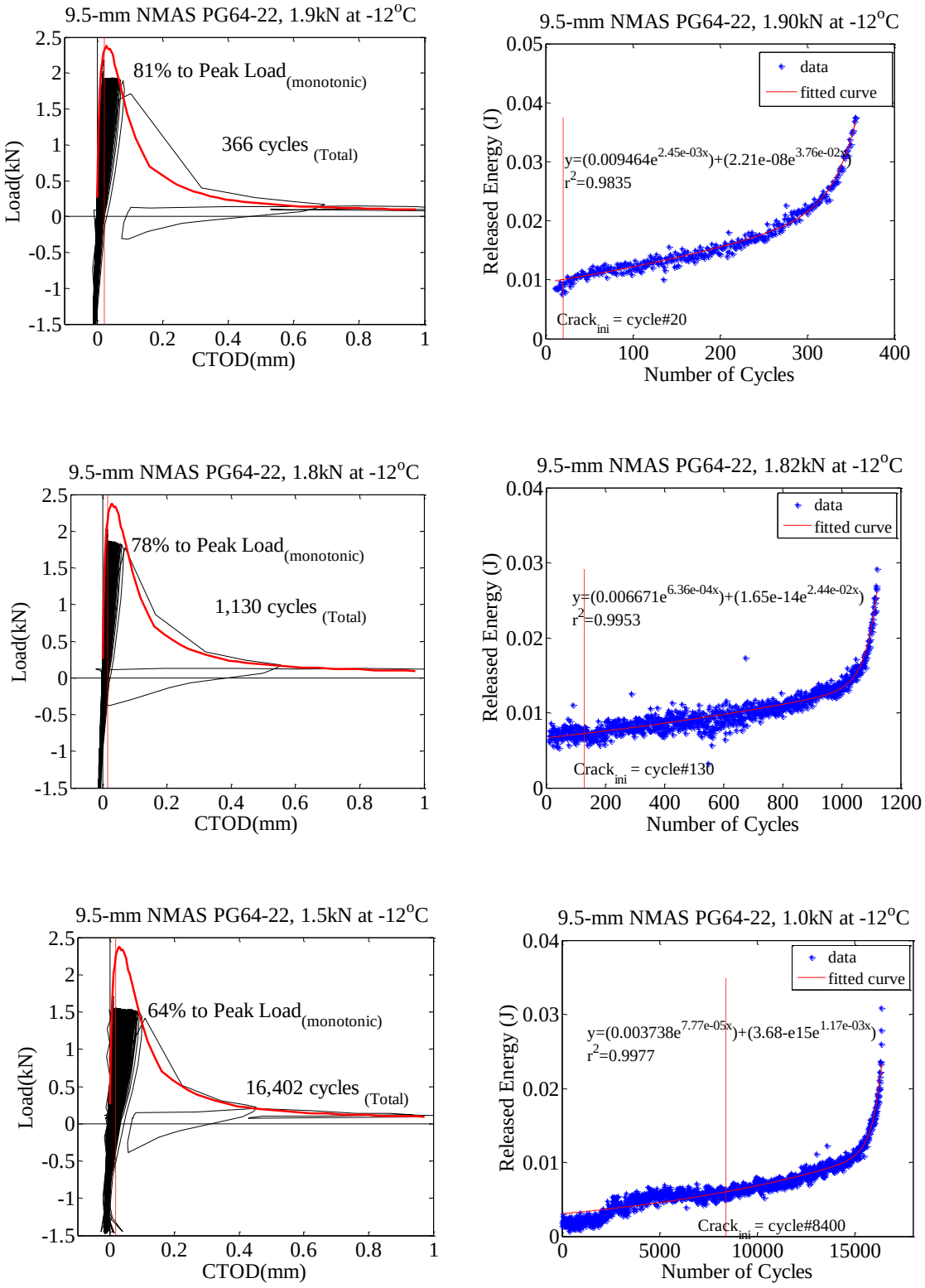

FigureD.3 Examples of load-displacement relations and RED models for PG64-22 mix conducted at -12°C.

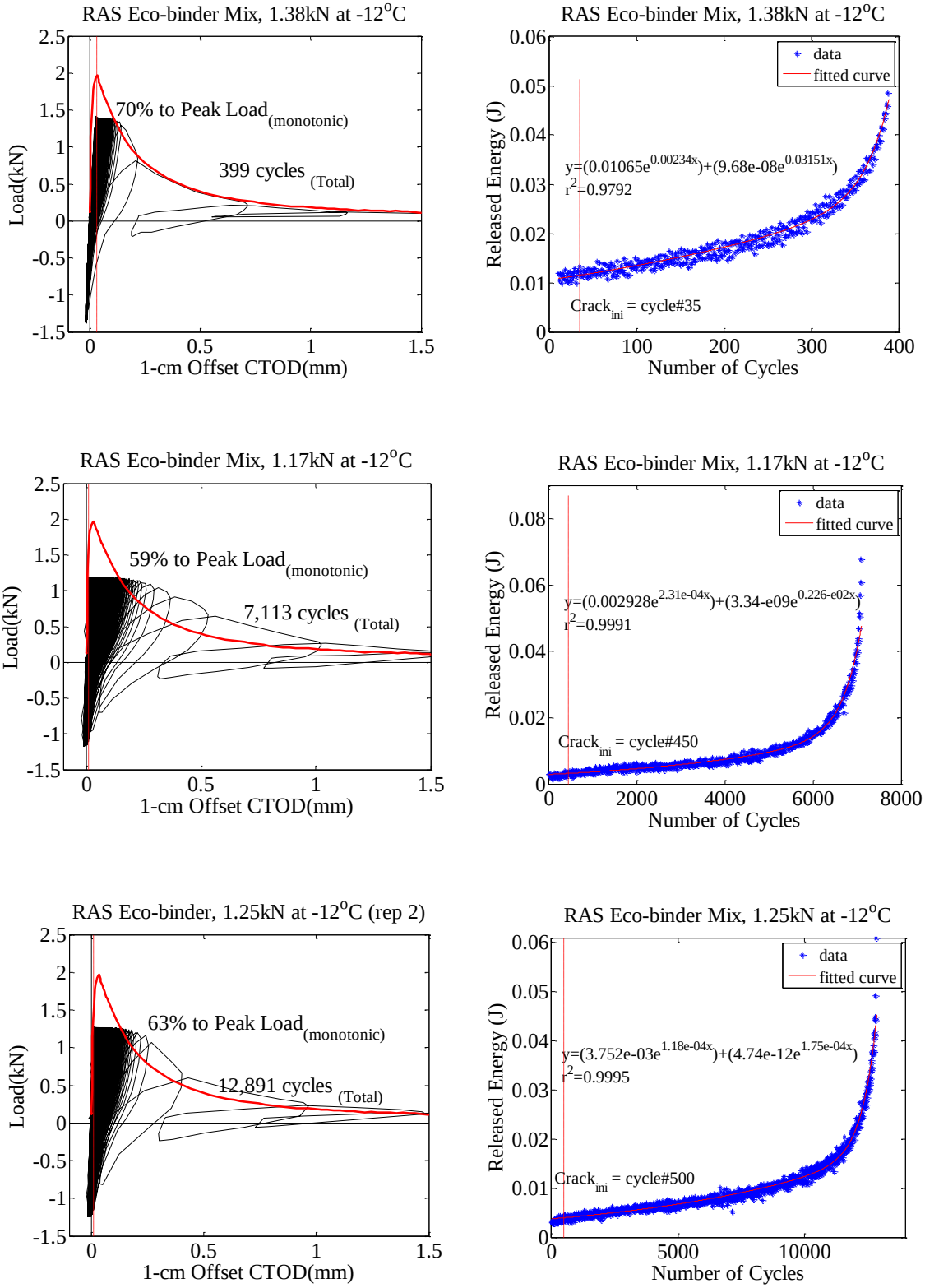

FigureD.4 Examples of load-displacement relations and RED models for RAS mix conducted at -12°C.

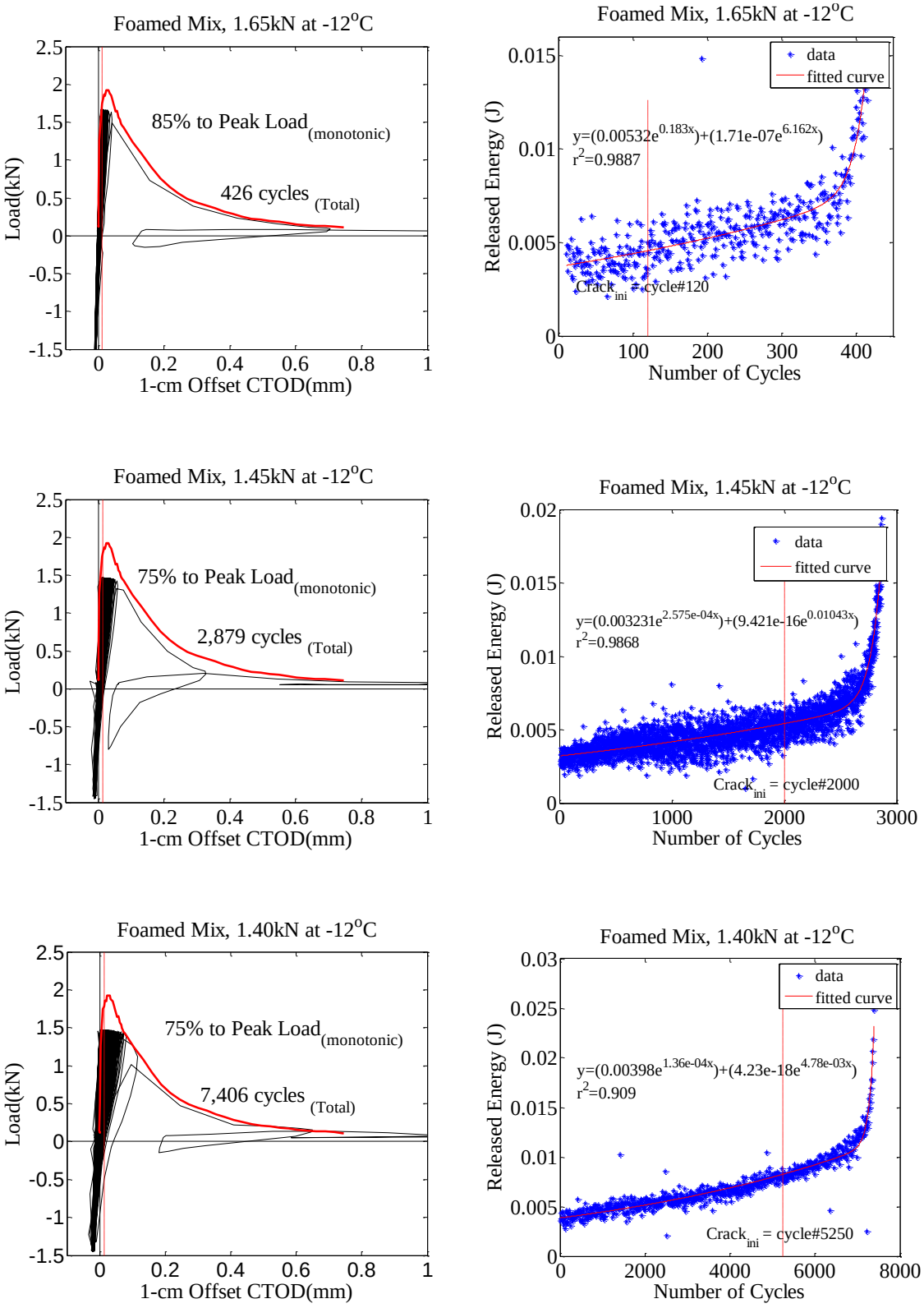

FigureD.5 Examples of load-displacement relations and RED models for foamed mix conducted at -12°C.

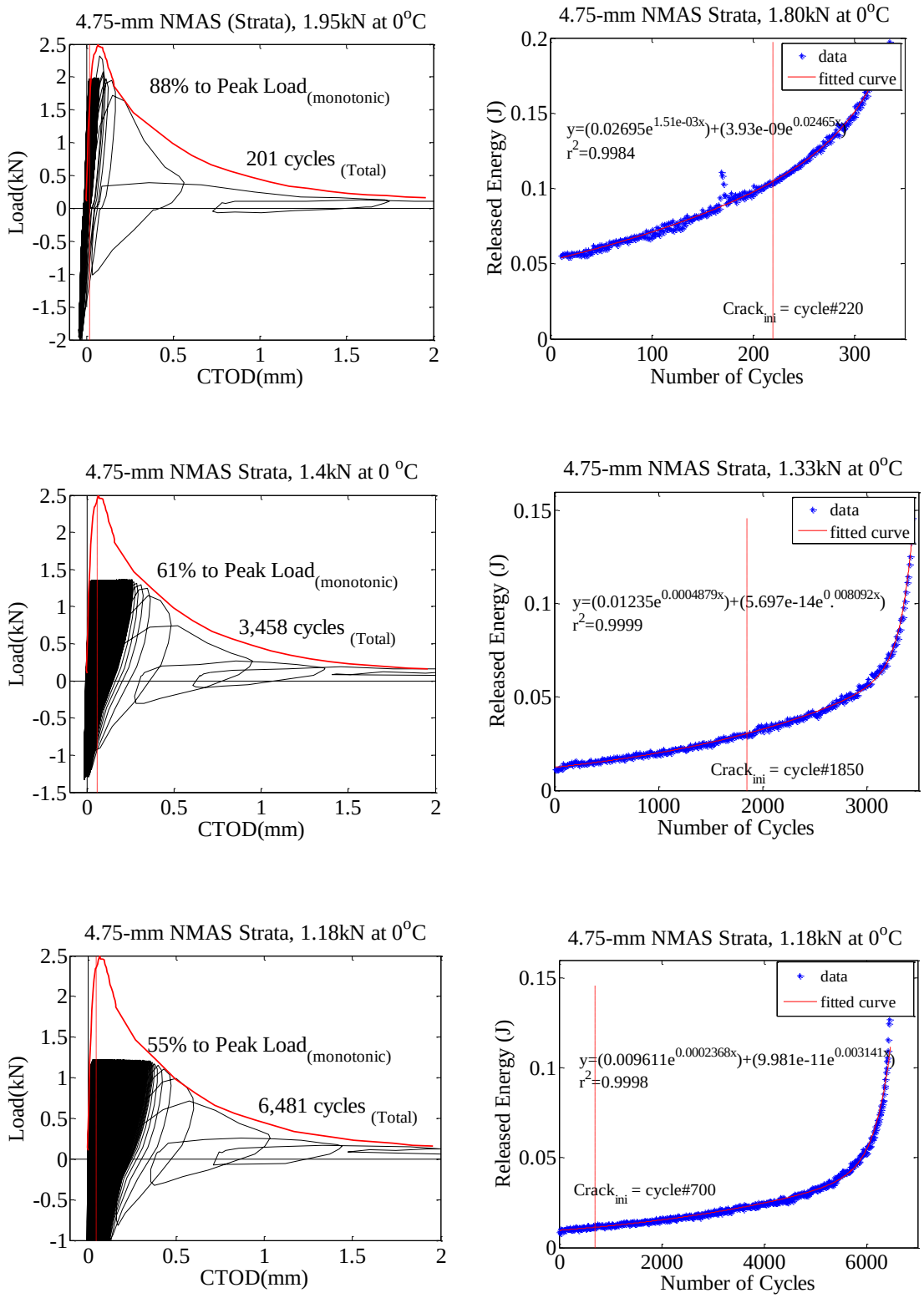

FigureD.6 Examples of load-displacement relations and RED models for Strata mix conducted at 0°C.

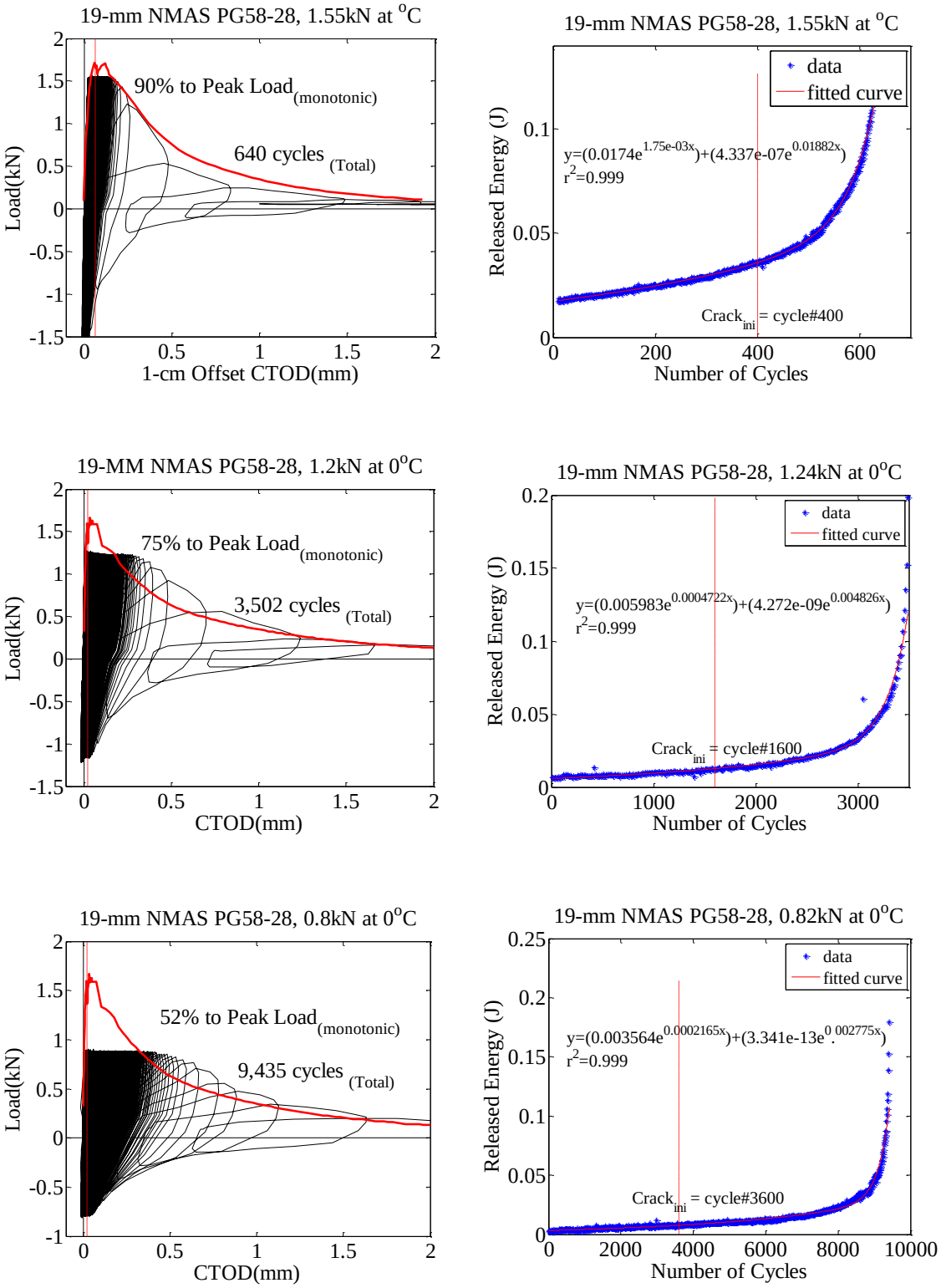

FigureD.7 Examples of load-displacement relations and RED models for PG58-28 mix conducted at 0°C.

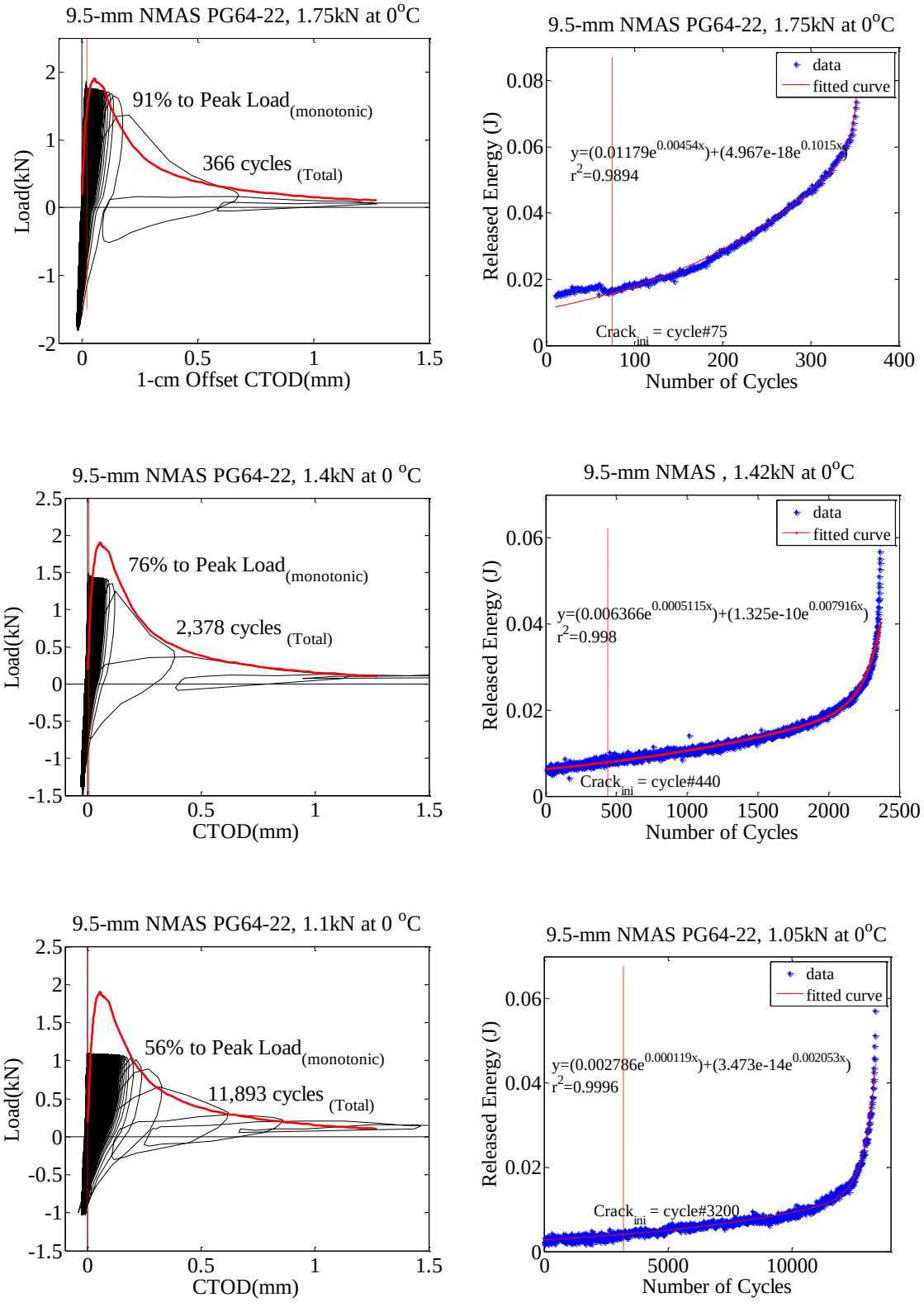

FigureD.8 Examples of load-displacement relations and RED models for PG64-22 mix conducted at 0°C.

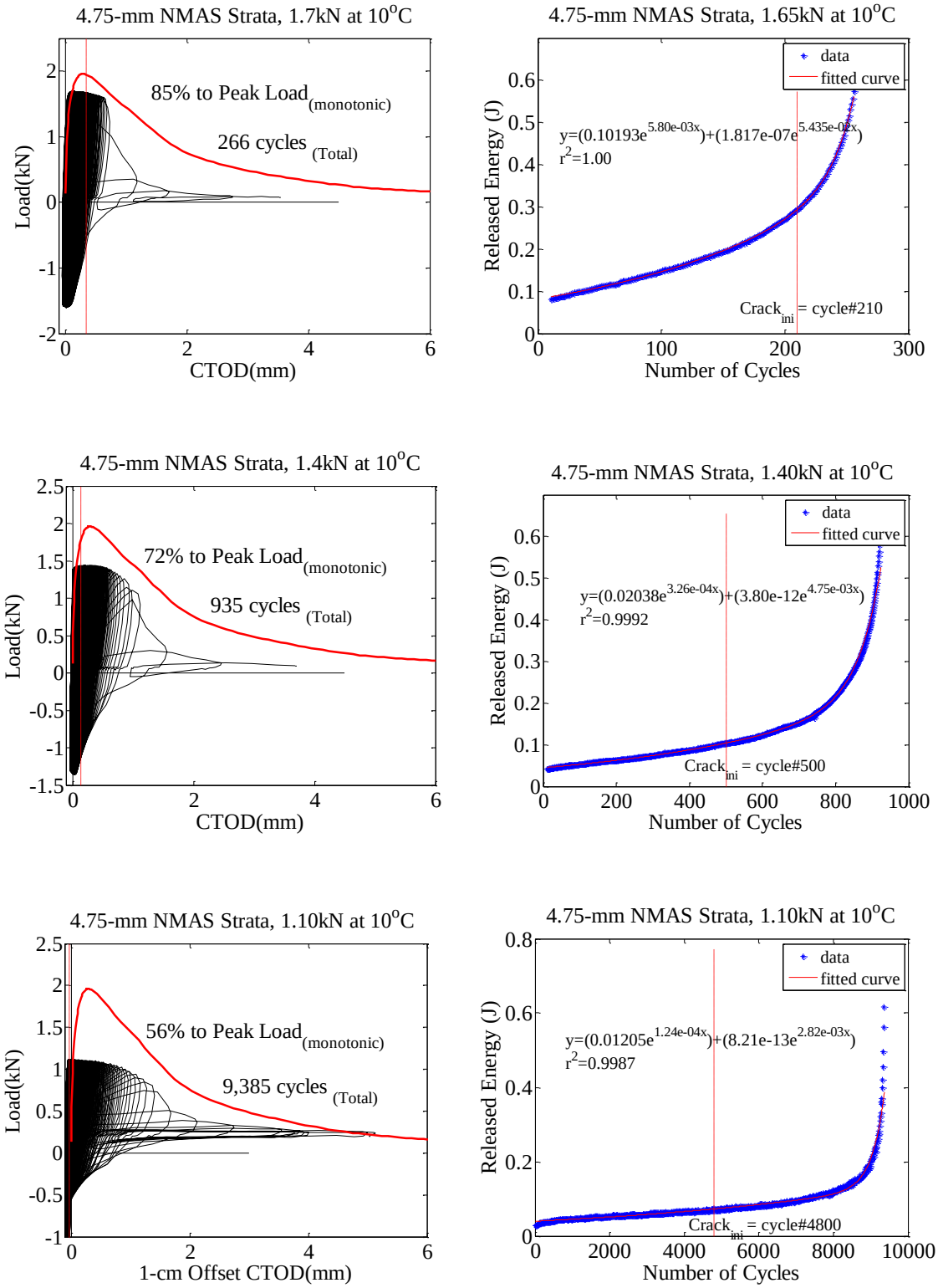

FigureD.9 Examples of load-displacement relations and RED models for Strata mix conducted at 10°C.

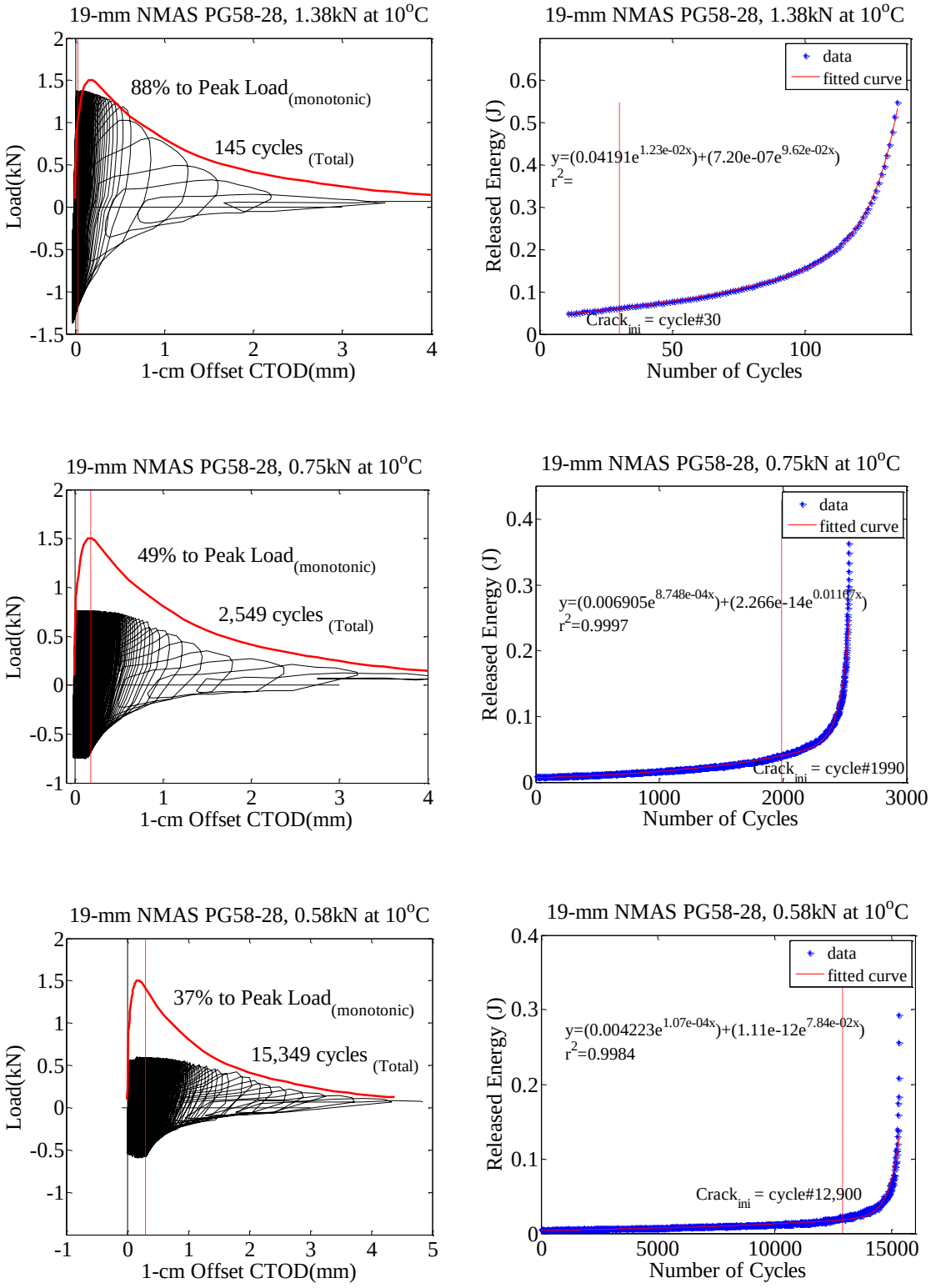

FigureD.10 Examples of load-displacement relations and RED models for PG58-28 mix conducted at 10°C.

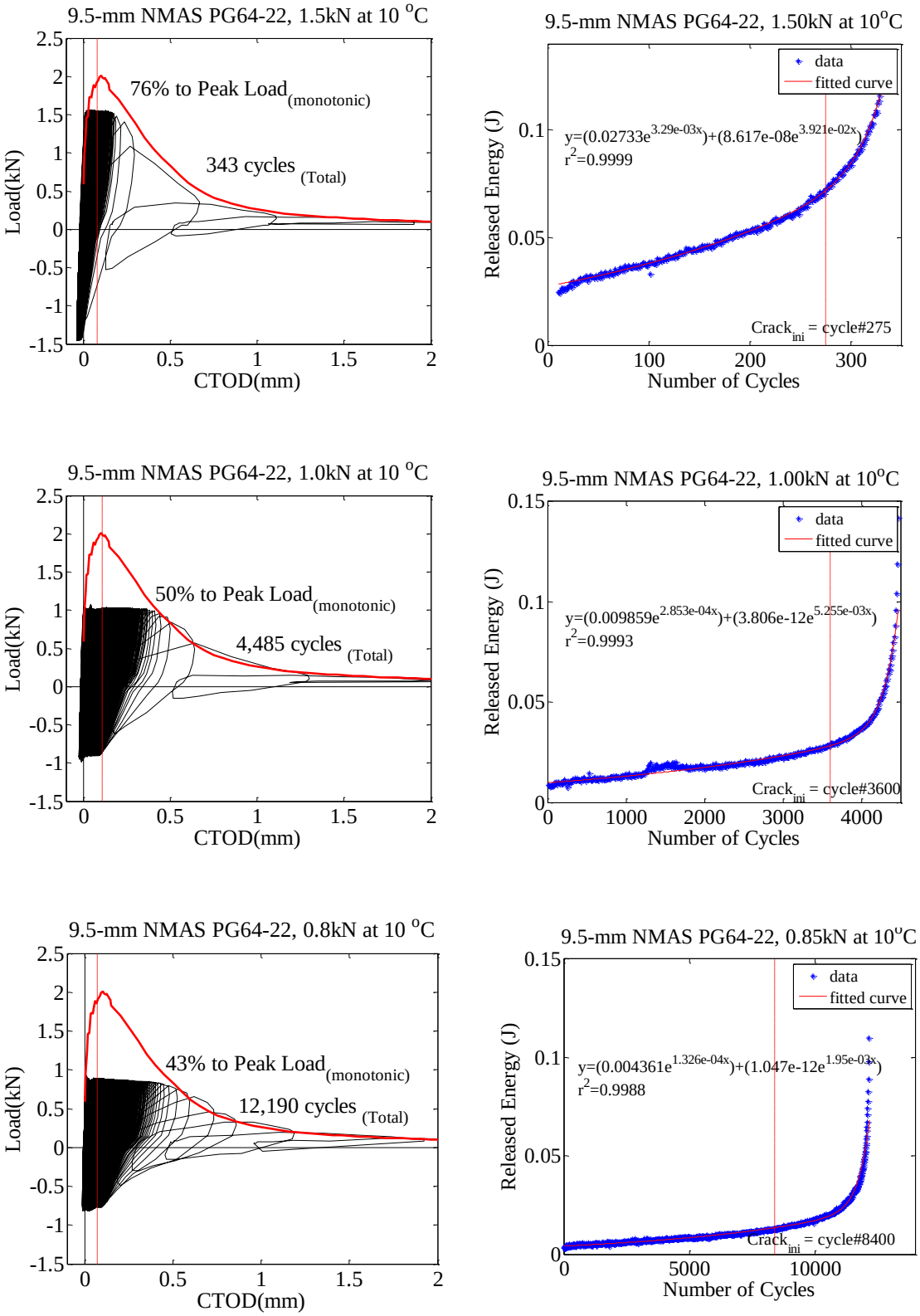

FigureD.11 Examples of load-displacement relations and RED models for PG64-22 mix conducted at 10ºC.

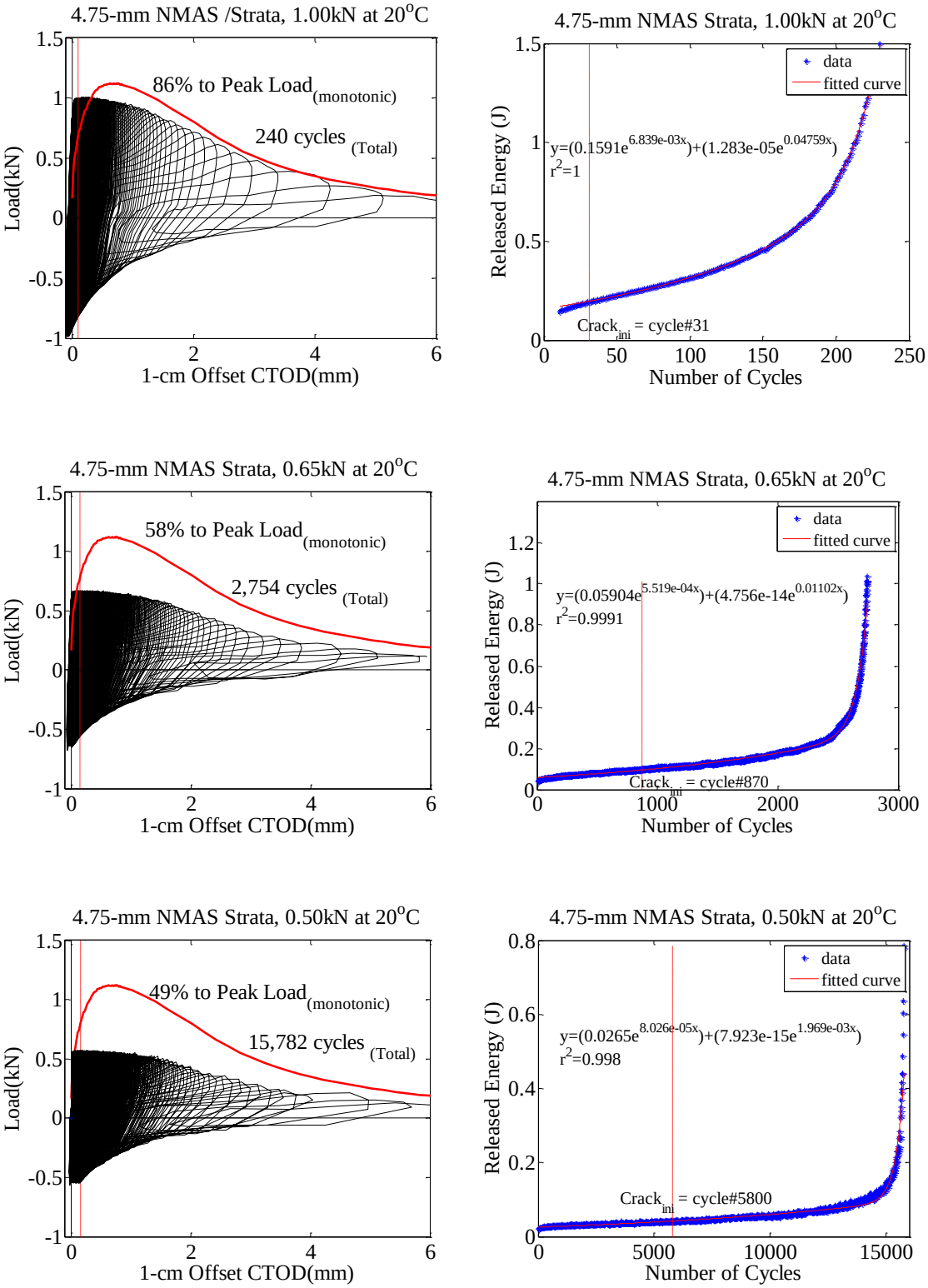

FigureD.12 Examples of load-displacement relations and RED models for Strata mix conducted at 20°C.

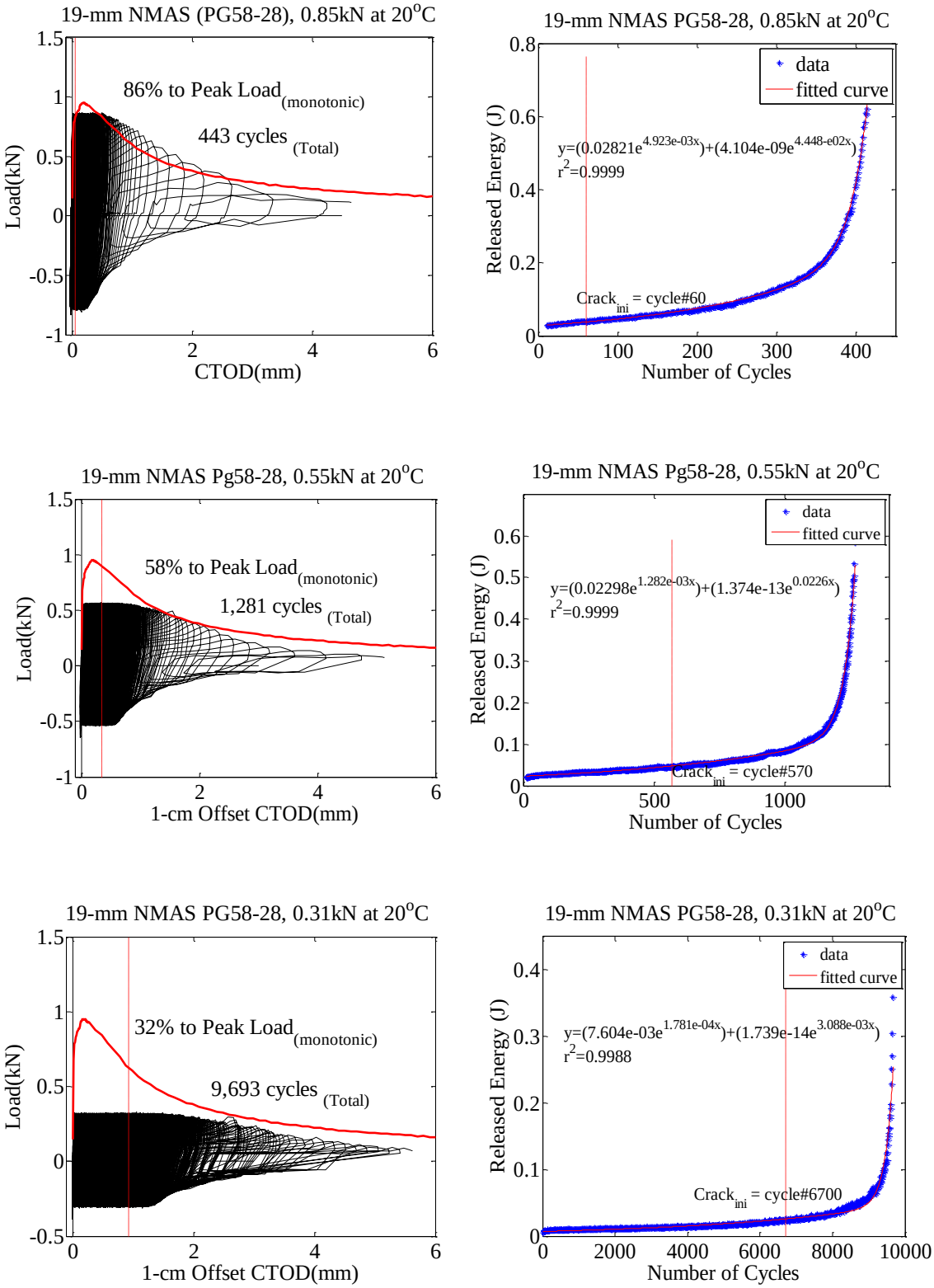

FigureD.13 Examples of load-displacement relations and RED models for PG58-28 mix conducted at 20°C.

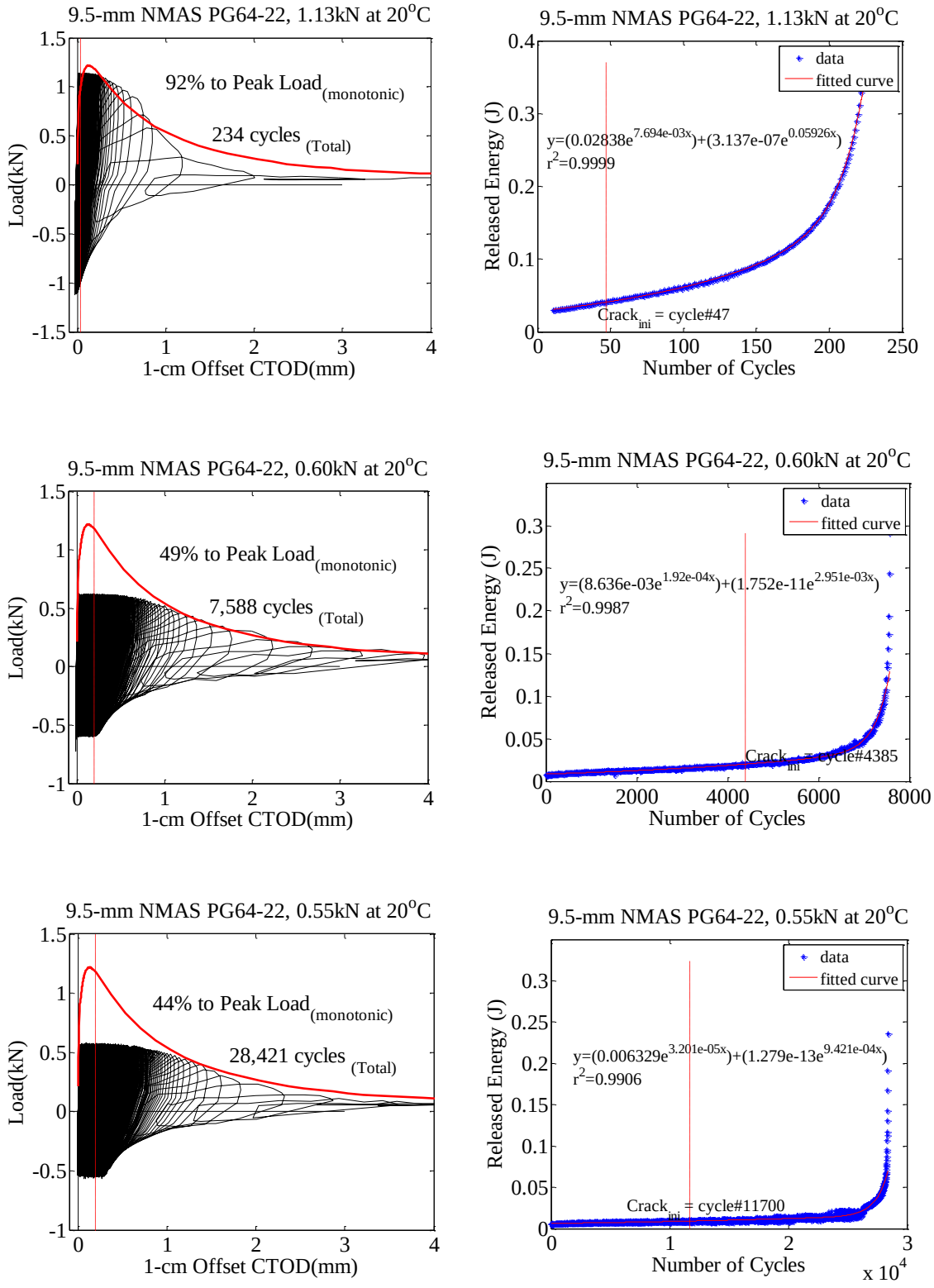

FigureD.14 Examples of load-displacement relations and RED models for PG64-22 mix conducted at 20°C.

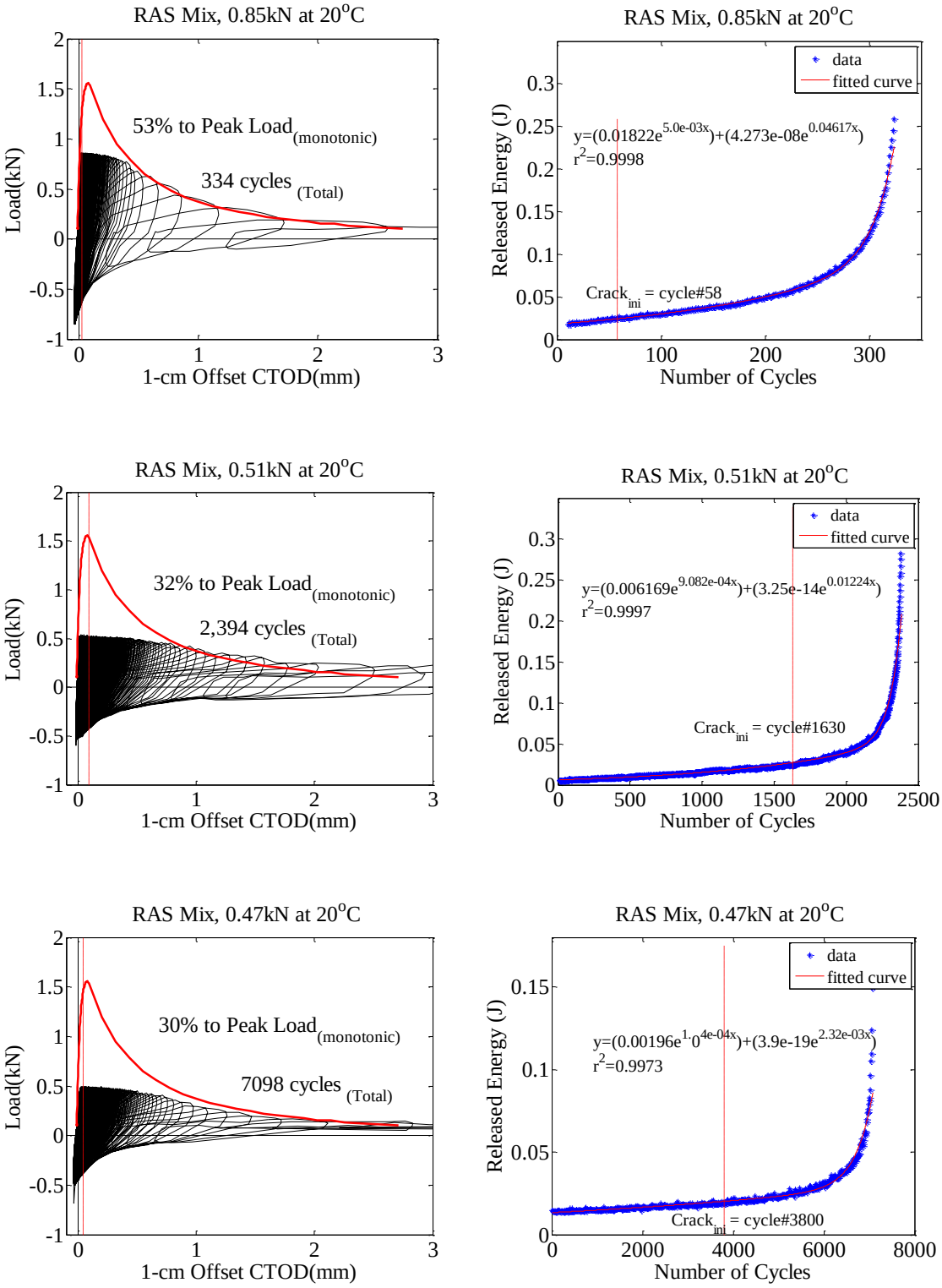

FigureD.15 Examples of load-displacement relations and RED models for RAS mix conducted at 20°C.

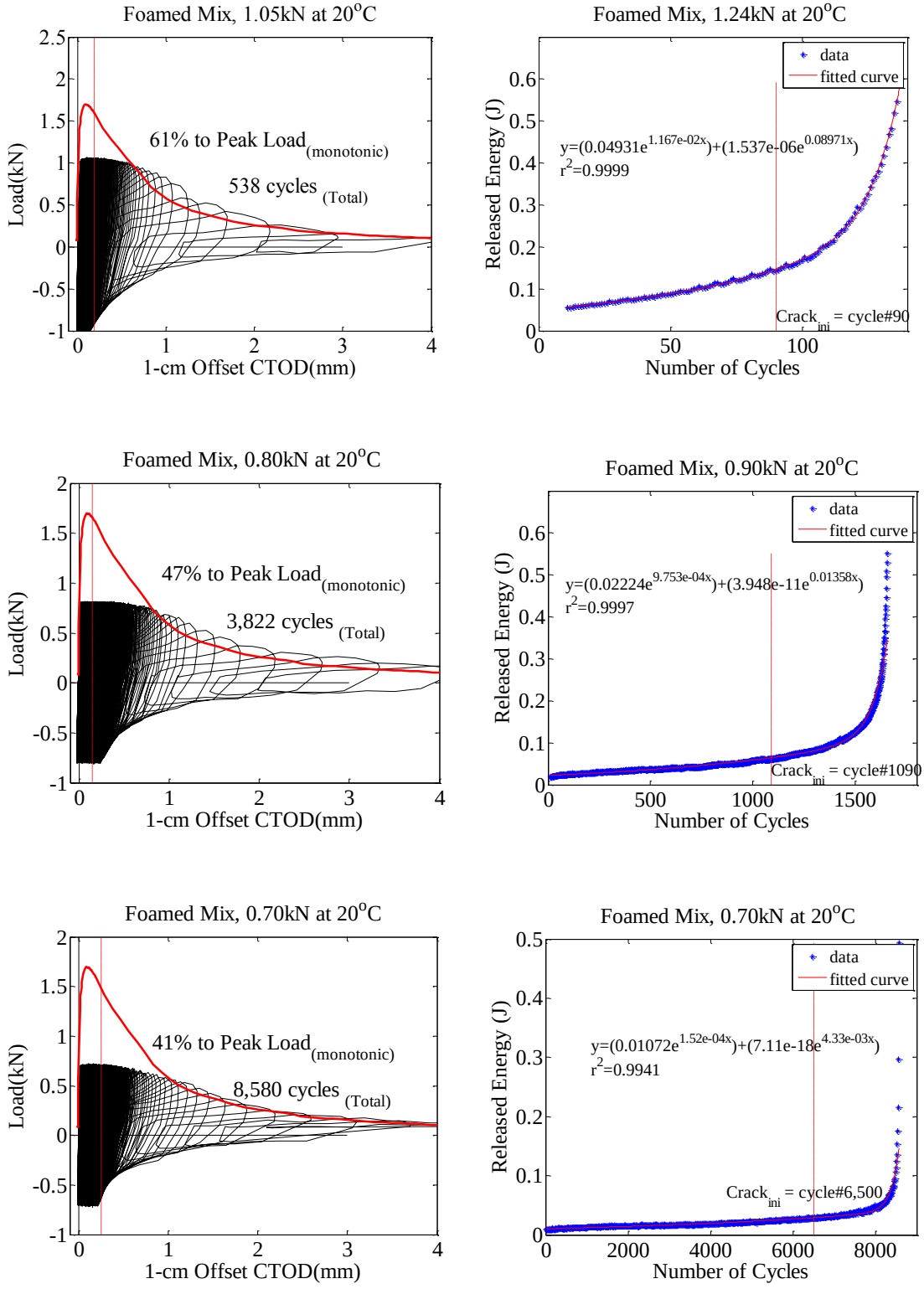

FigureD.16 Examples of load-displacement relations and RED models for foamed mix conducted at 20ºC.